ROCK MECHANICS IN JAPAN

VOLUME III

JAPANESE COMMITTEE FOR ISRM

1 9 7 9

ROCK MECHANICS IN JAPAN

VOLUME III

1979

BY JAPANESE COMMITTEE FOR ISRM
c/o JAPAN SOCIETY OF CIVIL ENGINEERS

CHAIRMAN; Tatsuo MIZUKOSHI

SOCIETIES CONCERNING JOINT COMMITTEE

JAPAN SOCIETY OF CIVIL ENGINEERS
Yotsuya 1-chome Shinjuku-ku Tokyo

THE JAPANESE SOCIETY OF SOIL MECHANICS AND FOUNDATION ENGINEERING
Sugayama-Building 23 Kanda Awaji-cho 2-chome Chiyoda-ku Tokyo

THE MINING AND METALLURGICAL INSTITUTE OF JAPAN
5-4 Ginza 8-chome Chuo-ku Tokyo

THE SOCIETY OF MATERIALS SCIENCE, JAPAN
1 Yoshida Izumidono-cho Sakyo-ku Kyoto

Printed in Japan

PREFACE

"Rock Mechanics in Japan, Volume III, 1979" was compiled by Japanese Committee for ISRM in order to introduce the research activities on rock mechanics in Japan from 1974 to 1978 to researchers and engineers concerning rock mechanics in the world. It consists of three parts. The first part is the brief comments on the activities on rock mechanics in the related societies. The second part is the summaries of selected papers, and the third part is the list of literatures appeared in sixteen kinds of journals in Japan.

It will be a great pleasure for me if this publication can be of any help in exchanging information between researchers and engineers concerning rock mechanics in the world, and can contribute to the development of rock mechanics.

Japanese Committee for ISRM was outgrown from the former "Joint Committee on Rock Mechanics, Japan" in June 1979, under the cooperation of four societies; Japan Society of Civil Engineers, The Japanese Society of Soil Mechanics and Foundation Engineering, The Mining and Metallurgical Institute of Japan and The Society of Materials Science, Japan. This Committee is a representative organization in Japan for ISRM, established with the object of attaining the smooth communication and coordination of mutual research activities in Japan and abroad, and consists of 130 personal members of ISRM and 70 supporting members.

Japanese Committee for ISRM is preparing to hold the International Rock Mechanics Symposium on Weak Rock in September, 1981 in Tokyo. The purpose of the Symposium is to exchange the recent knowledge on weak rock in the world and to discuss the engineering efforts to overcome the unfavorable geological conditions, which are often encountered in dam, underground opening, undersea tunnel, mining, large suspension bridge and transmission tower, excavated slope, and so on.

The Weak Rock is characterized especially in such rock mechanical aspects as swelling, slaking, disintegration, creep, consolidation, non linear deformation, and so on.

The following five items are now considered as main themes of the Symposium.

Themes (preliminary plan):

1) Engineering Property on the Weak Rock
2) In Situ Investigation of the Weak Rock
3) Specialized Theory and Analysis on the Weak Rock
4) Adequate Design and Construction Practice for the Weak Rock
5) Dynamics and Tectonics on the Weak Rock

In the Symposium, it is planned to make study tours to Japanese typical civil engineering structures under construction such as undersea tunnelling, underground power station cavern, offshore pillar of large suspension bridge and dams.

Japanese Committee for ISRM heartily invites you to the Symposium.

July 1979

Tatsuo Mizukoshi

Tatsuo MIZUKOSHI
Chairman of Japanese Committee
for ISRM

CONTENTS

I RECENT ACTIVITIES

ON

ROCK MECHANICS IN JAPAN

ACTIVITY ON ROCK MECHANICS IN THE JAPANESE SOCIETY OF SOIL MECHANICS AND FOUNDATION ENGINEERING

Toshikazu KAWAMOTO, Nagoya University

The Committee on Rock Mechanics in the Japanese Society of Soil Mechanics and Foundation Engineering has started in 1966 for the purpose of investigating consistently the mechanics of rocks and soils, whose activities are prescribed as follows: 1) examining the different and the common properties between rocks and soils, engineers in both field can improve in their knowledge mutually, 2) both rock and soil materials must be treated unifiedly as the foundation of structures. In the early stages it was discussed to pick up some material properties of rocks as engineering material, so that a classification model of rocks was proposed. Simultaneously an unification of technical terms and a standardization of rock tests were also discussed. The most useful results for members of the Committee may be the issues of "Terminologies of Rock Engineering" published in 1972 and of "Engineering Properties of Rock and Their Applications to Design and Execution" in 1974. The other roles are such that the office works of the International Society for Rock Mechanics and the preparation of the International Rock Mechanics Symposium on Weak Rock which will be held in 1981 as one member of the national group for rock mechanics in Japan, and so on.

The activities of the Committee after 1974 are mentioned here. In 1974 it was discussed whether or not the results in the report of the Japan Society of Civil Engineers for the bearing capacity, the deformation and shearing characteristics of rocks can be applied to soft rocks. Then the correlation between the classification of rocks, their Young's modulus and their strength were studied, using some results of granite in Mount Washu reported by the Honshu-Shikoku Bridge Authority. On that time it was questioned how the values measured in a field can be related to ones of laboratory tests. Designs of rock foundations were

also discussed. It was pointed out that the following topics must be investigated continuously: how the field tests can be used for the design of foundations effectively; soft rocks may be treated in a field of soil mechanics, so that several properties must be considered on the design of rock foundations, such as c, ϕ, creeping, anisotropy, nonhomogeneity, effect of water and so on; experimental datum of hard rocks must be collected much more, and material properties should be observed on the consistent view point of soil, soft rocks and hard rocks; the classification standard of soils may not be applicable to soft rocks, so that another one should be prepared. During these discussion there were reports of the Third International Conference on Rock Mechanics held at Denver (1974) and the Second International Congress of Engineering Geology held at Sao Paulo (1974) (reported by T. Kawamoto and M. Yamagata).

In 1975 some exploration methods for the design of rock foundations were discussed following the former policy. On that time explorations employed in the site of the Honshu-Shikoku Bridge Authority and developed in foreign countries were referred. Quoting "Report on the Creep Properties of Granite" (K. Akai et al), results of in-situ tests, laboratory tests and some analysis were compared, then it was discussed how these were used for practical designs and executions. The reports titled by "In Situ Tests of Creep for Granite at Tatara-Ohashi (one of the Honshu Shikoku bridges) (K. Ishikawa) and "Triaxial Compression and Creep Tests in Laboratory" (K. Akai) were submitted and discussed. Then it was concluded that the deformations caused by creep are approximated by $\varepsilon = a + b \log t$, and the laboratory tests tend to similar results.

In 1976 exploration and design methods for soft rocks were mainly discussed, so that field tatum of the Honshu-Shikoku Bridge Authority were examined referring several articles in Japan or from foreign countries such as "Lateral K-values of Clays in Osaka Layers" (K. Miki) and "An Application of Seismic Prospecting for Rock Mass Exploration and its Questions" (K. Zako). The following papers which were submitted to the Fifth Symposium on Rock Mechanics in Japan were reported and discussed; "Measurement and Prediction of Behaviour of Anisotropic Rock Masses during Underground Excavation Works" (S. Hibino), "Bearing Capacity of Weathered Rock Mass" (Y. Ohnishi) and "In Situ Creep Testing of Wea-

thered Granite" (K. Ishikawa). During then there was a report of the Second Conference on Numerical Methods in Geomechanics held at Blacksburg (S. Sakurai).

In 1977 the results of in-situ deformation tests for soft rocks were discussed, which was reported by Y. Ohnishi. There were reports and discussions on some papers from the International Symposium on Field Measurements in Rock Mechanics held at Zürich (S. Sakurai) and the International Symposium on Storage in Excavated Rock Caverns in Stockholm (Y. Kitahara).

In 1978 the Committee members visited the Okuyahagi underground power plant, which was under construction by Chubu Electric Power Company, then it was discussed how the excavation could be modeled and analyzed mathematically. Results of several measurements were also shown, so that there were subsequent discussions if the tests for soils are applicable to rock mass especially about the in-situ test of deformations in boring holes. Simultaneously there were talks about mechanical properties and effects by underground water or discontinuity for soft rocks which are not yet solidified completely or are weathered.

It must be pointed out that the Committee has made efforts to establish the Japanese branch of ISRM and its Symposium in Tokyo, participating in the national group on rock mechanics.

RECENT ACTIVITIES ON ROCK MECHANICS IN THE JAPAN SOCIETY OF CIVIL ENGINEERS

Tatsuo MIZUKOSHI, Chairman of
the Committee on Rock Mechanics

1. Introduction

The research activities on "Rock Mechanics" in Japan started with the investigations and studies of dam foundation rocks and tunnel bedrocks, in the early 1960s, and recently have become increasingly active in relation with the foundations of nuclear reactors, foundations of transmission towers, long slopes, cavities of large underground power stations, cavities of underground fuel storages, etc.

As for the contents of research work, at first, many researches were concerned with such investigations as the development of in-situ rock foundation test methods, the mechanical properties of rocks by those tests, and application of the results to design and execution of construction works. Later, the introduction of finite element method, consistent measurement of rock foundation covering the period from the design stage to and beyond the completion of structure and analyses of data thus obtained have remarkably enriched the contents of research works in light of theory regarding the behaviors of rocks. Those studies were at first made mainly on hard rocks related to high arch dams. But recently, large structures such as undersea tunnels and offshore pillars of large suspension bridges through or on weak rocks have become to be constructed. Therefore, research activities on weak rocks have necessarily increased.

2. The organization and activities of the Committee on Rock Mechanics

Research activities concerning rock mechanics of the Japan Society of Civil Engineers are mainly promoted by "The Committee on Rock Mechanics". This Committee was established in 1962, outgrowing from the Society for the Research of Bedrocks organized by the interested researchers of such research institutions as Central Research Institute of Electric Power Industry and Public Works Research

Institute of Ministry of Construction.

The Committee has the divisions and the subcommittee. The divisions are in charge of specialized investigations and studies, and at present, there are four divisions; the first division (dams), the second division (tunnels), the third division (theories and tests), and the fourth division (weak rocks).

The Committee has about two hundred members. There is a steering committee consisting of a chairman, vice-chairman, secretary-general, and the chairmen and secretaries of the respective divisions, for the purpose of management of the committee activities.

The main activities of the Committee wo to hold symposia on rock mechanics, study meetings and lecture meetings, and to publish technical books in field. The handbook titled as "Rock Mechanics for Civil Engineers" compiled and published by the Committee in recent years. As mentioned above, the divisions are engaged in specialized investigations and studies, and their respective activities and results are as follows:

The first division (dams)

Main activities: Researches and standardization on the geological investigation methods and grouting techniques for rock foundation of dam

Results of activities: Publication of "Standard for Grouting of Dam Foundation Rocks", "Collected Examples of Grouting of Dam Foundation Rocks", and "Geological Survey of Dams"

The second division (tunnels)

Main activities: Researches on the mechanized excavation of tunnels

Results of activities: Publication of "Tunnel Boring Machines in Japan, Their Results and Outlook"

The third division (theories and tests)

Main activities: Standardization of in-situ rock test, and the collection and analysis of the tests results

Results of activities: Publication of "Criteria for In-Situ Deformation Test Methods of Foundation Rocks by Plate Loading" and compilation of "Standard for In-Situ Shear Test of Foundation Rocks"

The fourth division (weak rock)

Main activities: Researches on weak rock

Results of activities: Study and compilation of "Simple Slaking Test Methods"

3. Trends of researches

The following themes are outstanding in the research papers published recently.

(A) Mechanical properties and engineering evaluation of weak rocks

(B) Development of rock test methods

(C) Behaviors of foundation rocks involved in underground excavation and slope excavation

(D) Execution cases of NATM construction method

(E) Seepage flow through bedrocks

(F) Others

According to the above classification, the themes of studies and reports in the domestic symposia on rock mechanics held in the past 5 years can be classified as shown in the following table.

Year	A	B	C	D	E	F	Total numbers
1975	2	9	5	0	1	9	26
1976	0	4	8	0	1	10	23
1977	5	7	8	0	1	19	40
1978	4	7	4	1	1	7	24
1979	7	4	3	3	1	7	25
Total numbers	18	31	28	4	5	52	138

4. Conclusion

It can be said that the research activities on rock mechanics in Japan started with the construction of Kurobe No.4 Dam which is a concrete arch dam, 186m high, and completed in 1964. Since then, rock mechanics has made a remarkable progress. However, the properties of bedrocks are quite complicated and there still remain many problems to be solved.

Therefore, the researchers of rock mechanics should make another effort to make further progress in this field keeping close contact with researchers in the related fields.

RECENT ACTIVITIES ON ROCK MECHANICS IN THE MINING AND METALLURGICAL INSTITUTE OF JAPAN

Yuichi NISHIMATSU, The University of Tokyo

The applications and research activities of rock mechanics in the mining have been increasing year by year during these five years, as represented by number of papers shown in Table. Many mining engineers have carried out various practical works concerning rock mechanics in the field of drilling, blasting, rock cutting, crushing and mine support. On the other hand, correlating with the practical works, the theoretical as well as experimental researches dealing with the mechanical properties of rock have been developed in the universities and other research institutes.

Table. Papers presented at the Spring Meetings of M.M.I.J., since 1974 until 1978.

Year	A Rock Mechanics	B Other Subjects	C Total	A/C %
1974	27	134	161	16.8
1975	28	128	156	17.9
1976	30	129	159	18.9
1977	50	146	196	25.5
1978	58	143	213	27.2

As a remarkable accomplishment of these research activities, the sampling of rock sample for rock mechanics tests[1] and the testing methods for compressive and tensile strengths of rock[2,3] are standardized in Japanese Industrial Standard, in 1975.

Many researchers have extended their studies related to the subjects introduced in Vol. 2, Rock Mechanics in Japan, 1973. On the other hand, they have developed other various subjects concerning the recent needs of technology, such as the utilization of geothermal energy, the prevention of rock burst and the development of rock store.

Accomplishments of their studies since 1974 up to 1978 appear in the list of literatures of this issue.

Conspicuous papers representing the recent tendency of rock mechanics in the field of mining may be summarized as follows.

One of the most important subject in mining is the rock pressure and strata control. Hence, many works are published concerning this subject.

Y. ISHIJIMA and his coworkers[4] have developed a moulded-gage-type stress-meter for the measurement of rock stress in the coal seam. This cylindrical shaped stress-meter consists of the wire strain gages moulded in the epoxy resin mixed with glass beas. S. KINOSHITA and his coworkers[5] have studied on the effect of stress-relief boring technique for preventing rock burst and/or mine gas outburst. They observed the volume of coal cuttings discharged from the borehole, frequency of occurence of rock noise, stress and gas pressure change in the coal seam accompanying the large diameter boring. T. NISHIDA and his coworkers[6] have studied on the mechanism of surface caving-in due to mining of coal seam at shallow depth, by means of model rock formation consisted of the piled-up glass and bumboo rods. They have discussed on the effect of groundwater level on caving-in. Y. OKA and his coworkers[7] have extended their works on the measurement of rock stress. They have theoretically developed and experimentally verified the observation equations to determine the three dimensional state of stress around the borehole from the strains at bottom of borehole which are measured by means of a door-stopper-type stress-meter. K. SUGAWARA and his coworkers[8] have studied on the core discing observed during boring in the highly stressed hard rock. They have estimated the state of stress near the bottom of borehole by means of Finite Element Method, and verified the result of theoretical analysis by the laboratory test. Y. NISHIMATSU and his coworkers[9] have discussed on the application of Linear Fracture Mechanics for estimating the rock stress at great depth by the hydraulic fracturing method. Z. HOKAO and his coworkers[10,11] have extended their works on the floor heave by means of the two-dimensional model roadway, and discussed on the effect of floor bolts for suppression of floor heave.

Y. TAKENAKA and his coworkers[12] have studied on the reinforcement of fractured rock formation near the coal face by injection of polyurethan. On the other hand, Y. TOMOSADA[13] have studied on the effect of rock bolts on the maintenance of underground roadway in the coal mine. Both of these studies were sponsored and cooperated by the Coal Mining Research Center, Japan.

In metal mine, N. NANKO and his coworkers[14] have tried to rationalize the roadway maintenance by means of various techniques such as the standardization of rock bolting, application of smooth blasting and the measurement of convergence.

Research activities for the prediction and prevention of rock burst have

become more and more active in these five years. Y. HIRAMATSU and his coworkers[15] have discussed on the mechanism of rock burst by considering the post-failure behaviour of rock and the stiffness of rock formation near the bursted rock mass. T. ISOBE and his coworkers[16-18] have observed the microseismic activity caused by coal mining by means of seismographs set on the surface and in the underground roadway. They have located the source of microseismic activity and correlated it with the extraction activities of coal seams. R. KOBAYASHI and his coworkers[19] have studied on the rock failure caused by rapid reduction of confining pressure in the triaxial compression test, and discussed on the mechanism of rock burst based on the test result. T. KONDO[20] has studied on the mechanism of gas outburst in the deep underground coal mine by means of the model test using the ice charged with high pressure carbon dioxide.

In the field of rock drilling and cutting, several remarkable works have been reported. T. HORIBE and his coworkers[21-23] have studied on the mechanism of crook of borehole. They drilled a model rock formation having the inclined boundary of two layers with different strengths, and have verified the deviation of borehole to the direction of up-dip side occured after shifting to the direction of down-dip side. Y. WATANABE and his coworkers[24] have developed a portable rock machinability tester, which weighs only 35 kg and consists of a rock bolt to fix the main part of tester to rock wall, the rotating disc provided with 3 model bits, and the handle to rotate manually the rotating disc. M. KURIYAGAWA and his coworkers[25,26] have studied on the mechanism of rock failure by wedge indentation. They have discussed on the failure process and the state of stress caused by wedge indentation by means of a hybrid method of photo-elasticity and Finite Element Method. The geometry of fracture crack estimated from the stress analysis has been verified by the indentation test with a model bit.

Concerning the development of utilization of geothermal energy, the temperature effect on the rock failure has been investigated. H. HAYAMIZU and his coworkers[27] have studied on the fracture of heated rock sample by a rapid cooling. They have rapidly cooled the rock sample, heated in an electric furnace, by passing water through a borehole, and discussed on the effect of temperature gradient on the crack generation around the borehole.

In the field of rock crushing, S. YASHIMA and his coworkers[28] have extended their works on the single particle crushing. They have observed the failure behaviour of rock sphere in the radial compression test, and discussed on the conversion of mechanical energy consumption to various types of energy.

In the field of basic rock mechanics, many works have been reported concerning the failure process of rock. A. FUKUSHIMA and his coworkers[29,30]

have studied on the dilatancy of rock sample under uniaxial compression by means of an improved Bridgeman's dilatometer and a stiff testing system. K. SATO and his coworkers[31] have studied on the dynamic failure process of rock by means of a split Hopkinson bar. They have discussed on the post-failure behaviour of rock under high strain rate in compression. R. KOBAYASHI and his coworkers[32] have studied on the post-failure behaviour of rock under confining pressure by means of a stiff loading system using the thermal contraction of stiffening columns. Y. HIRAMATSU and his coworkers[33,34] have studied on the deformation behaviour of rock under uniaxial tension and compression by means of a stiff testing machine, and suggested that the failure processes under tension as well as compression consist of accumulation of microfracturings. K. MATSUKI and his coworkers[35,36] have discussed on the failure process of rock under compression from the point of view of Linear Fracture Mechanics. They have developed a computer modelling system of progressive failure process of rock, considering the branching and coalescene of microfracturing cracks. Y. NISHIMATSU and his coworkers[37] have developed another computer modelling system of failure process of rock, which takes account of the heterogenety of rock texture by means of Finite Element Method. Using this computer modelling system, they have discussed on the effect of rock texture on post-failure behaviour of rocks. K. KANEKO and his coworkers[38,39] have studied on the effect of progressive failure of rock on elastic wave propagation. They have observed the change of velocity and amplitude attenuation of elastic wave, correlating the frequency of occurence of rock noise, and concluded that the change in attenuation of wave amplitude is more sensitive than that in propagation velocity to the progress of failure process.

In the field of in situ test, several works have been reported. T. KAWAGUCHI and his coworkers[40] have tried to estimate the in situ rock strength by the observation of dominent frequency of elastic wave caused by blasting. R. KOBAYASHI[41] have developed a testing system for the measurement of in situ shear strength of rock. In this testing system, the rock wall between two adjacent parallel boreholes is sheared by indentation of die piece.

Several works on the velocity of elastic wave in rock sample have been reported. T. SHIMOTANI and his coworkers[42] have observed the elastic wave velocity in the calcite single crystal and crystalline limestone cylinder, and discussed on the effect of grain size and anisotropy of calcite on mechanical properties of limestone. T. SAITO and his coworkers[43] have observed the elastic wave velocity of various rock samples, and discussed on the effect of rock texture and water content on elastic wave velocity.

Concerning the prevention of water polution with acidic mine water,

Y. NISHIMATSU and his coworkers[44] have studied on the failure and displacement of the concrete plug which is constructed in the mine roadway for water sealing of abondoned underground mine. On the other hand, Y. OKA and his coworkers[45,46] have studied on the effect of water sealing of mine roadway on seepage flow of mine water and groundwater level, by means of Finite Element Method. Both of these two works have been sponsored and cooperated by the Metal Mining Agency.

Literatures

1)-3) have been published as JIS M 0301, 0302 and 0303, respectively.
4)-46) except 18), 37) and 41) have been published as full papers in the Journal of the Mining and Metallurgical Institute of Japan, and these are appeared in the list of literatures at the end of this issue.
18), 37) and 41) are papers presented at the 5th National Symposium on Rock Mechanics held at Tokyo in 1977, and these are also appeared in the list of literatures at the end of this issue.

RECENT ACTIVITIES ON ROCK MECHANICS IN THE SOCIETY OF MATERIALS SCIENCE, JAPAN

Koichi AKAI
Professor, Department of Transportation Eng.,
Kyoto University, Kyoto

The commitee on Rock Mechanics in the Society of Materials Socience, Japan was organized in June, 1963. Since then, more than 80 regular meetings were held till Dec., 1978. In 1971, a sub-committee specialized in comminution was newly set up in the committee on rock mechanics and regular meeting has been held till now.

The committee now consists of about 60 authorized members, who are engaged in such fields as civil engineering, metallurgy, chemical engineering, geology, geophysics and seismology. One of the specific features of this committee is that the members who are specialized in many different fields can discuss the different aspects of the rock mechanics.

Activities by the committee are not confined to regular meetings, but involve public lecture meeting, symposium, short study course, field inspection and publication of special issue on rock mechanics and comminutions.

Those conducted under the auspices of the committee or in co-operation with the other society since 1974[1)] are as follows : one symposiums on rock mechanics, two field inspections, two releases of special issue on rock mechanics for the Journal of the Society of Materials Science, Japan [2)3)].

The regular meeting on rock mechanics has been carried out bi-monthly to deal with the following matters:

(1) Lectures on rock mechanics and discussion thereon.
(2) Selection of subjects on the public lecture, symposium, short study cource, etc. related to rock mechanics
(3) Discussion on managements of the committee
(4) Introduction among the committee members of information on activities by national and international societies for rock mechanics
(5) Other related topics.

The title of lectures and discussions at the regular meeting of the committee from 1975 to 1978 is as follows;

1. Magnetic Anomaly due to Stress Change in the Earth Crust of South-western Part of Japan, by N. Sumitomo.
2. Review of the Topics Presented to the 2nd Int'l Congress of the ISEG, by T. Kawamoto.
3. In-situ Stress Measurement in Selkan Tunnel, by Y. Oka.
4. Review of the Topics Presented to the 3rd Congress of ISRM in Denver, by Y. Oka, S Sakurai and K. Sassa.
5. Acoustic Emission, by S. Kobayashi.
6. Acoustic Emission in Rock Sample, by T. Yanagitani.
7. Application of Acoustic Emission to Reinforced Concrete Structure, by M. Ohtsu.
8. Measurement of Creep Deformation by Interference Fringe, by' H. Ito
9. Vibration of Ground and Underground Structures due to Blasting, by S. Sakurai.
10. Yielding and Creep Deformation of Soft Rock, by T. Adachi.
11. Review of the Topics Presented to the 2nd Int'l Conference on Numerical Methods in Geomechanics, by T. Kawamoto, S. Sakurai, S. Kobayashi and T. Adachi.
12. Failure of Teton Dam, by T. Niwa.
13. Review of the Topics Presented to the 25th Geomechanics Colloquy, by Y. Hiramatsu.
14. Rock Noise in Bessi Mine, by Y. Hiramatsu and Y. Oka.
15. Rock Burst and Water Induced Earthquake in Ikuni Mine, by Y. Tanaka and R. Nishida
16. Attenuation of Stress Wave in Rock and Rock Mass, by K. Kaneko and I. Ito.
17. Review of the Topics Presented to The Int'l Symposium on Field Measurement in Rock Mechanics, by S. Sakurai.
18. Geology and Earthquake in China, by K, Fujita and Y. Tanaka.
19. In-situ Stress Measurement in State of Ontario, Canada, by M. Hori.
20. Review of the Topics Presented to the Int'l Symposium on Recent Crustal Movements, by H. Ito
21. Review of the Topics Presented to the Int'l Symposium on " Rock Store '77", by Y. Hiramatsu.
22. Review of the Topics Presented to Int'l Symposium on Strata Control, Canada, by Y. Oka.

23. Geological Exploration at the Area of Land Slide, by Y. Kobayashi.
24. Remedial Measures to Land Slide or Rock Slide at Steep Slope, by T. Yasue.
25. In-situ Stress Measurement, by Y. Kameoka.
26. Monitoring the Stability of Rock Structures by Means of Acoustic Wave Attenuation, by K. Kaneko.

Recent activities of the committee on Rock Mechanics in the Society of Materials Science, Japan are known by the papers contained in the special issues, Rock Mechanics No. 4[2], published May, 1974 and Rock Mechanics No. 5[3], published Feb.,1978. The list of the original papers is as follows;

*** Rock Mechanics, No. 4 ***

1. The Maximum Pressure Acting on Tunnel Lining Installed in Visco-Elastic Orthotropic Underground Medium, by S. Sakurai and Y. Yoshimura
2. Transient Stresses Produced around Tunnels by Traveling Waves, by Y. Niwa, S. Kobayashi and T. Matsumoto.
3. Mechanical Properties of Soft Rock in Terms of Effective Stress, by K. Akai, T. Adachi and N. Tabushi.
4. The Failure Process of Rock in Compression, by Y. Nishimatsu, K. Matsuki and S. Koisumi.
5. The Correlation of the Rock Stress Measured In-situ and the Tectonic Stress Infered from Geological and Geophysical Studies, by Y. Hiramatsu, Y. Oka, H. Ito and Y. Tanaka.
6. Observations on Secular Changes of the Crustal Movements in a Tunnel at Otsu, by I. Ozawa.

*** Rock Mechanics, No. 5 ***

1. Experimental Study on Deformation Characteristics of Rock-like Materials, by T. Kawamoto and T. Ishii
2. The Fracture Behavior of the Granodiorite under Uniaxial Compression, by. T. Yanagidani, O. Sano, M. Terada and I. Ito.
3. Acoustic Emission and Failure Process of Rocks under Compression, by K. Matsuki, Y. Nishimatsu and S. Koizumi.
4. Deformation and Fracture of Rocks under General Triaxial Stress States- Anisotropic Dilatancy, by K. Mogi, K. Igarashi and H. Mochizuki.
5. Long-term Creep of Rocks (Results with Large Specimens Obtained in about 20 Years and Those with Small Specimens in about 3 Years), by N. Kumagai, S. Sasajima and H. Ito.

6. Bearing Capacity of Weathered Rock Mass Determined by Graphical Solution of Pole Trail Method, by K. Akai, Y. Ohnishi and H. Mizobe.

In addition to these original papers, the following reviews, technical notes are also included in these issues.

Review: Rock Fracture and Earthquake Prediction, by K. Mogi

Review: Rock Breakage Caused by Explosion of Explosives, by I.Ito

Tech. Note: Analysis and Measurements of Behaviors of Rock around Underground Cavity in the Process of Excavation, by M. Yoshida

Tech. Note: Stresses and Deformations around Two or More Pressure Tunnels in Elastic Rock Masses, by K. Hirashima and Y. Niwa

Review: Applications of Acoustic Emission to Rock Mechanics, by S. Kobayashi

REFERENCES

1) Rock Mechanics in Japan, Vol. 2, 1974, pp.13-16, in which the activities till March 1974 were described.
2) Special Issue on Rock Mechanics No. 4, Reprinted from Journal of the Society of Materials Science, Japan, Vol. 23, No. 248, May, 1974
3) Special Issue on Rock Mechanics No. 5, Reprinted from Journal of the Society of Materials Science, Japan, Vol.27, No. 293, Feb., 1978

II BRIEF SUMMARY OF RECENT STUDIES

ANALYSIS OF ACOUSTIC EMISSIONS IN COMPRESSION TEST OF GRANITE

Tomowo HIRASAWA, Kiyohiko YAMAMOTO, and Kinichiro KUSUNOSE, Tohoku University

1. Experiment

Cylindrical samples of granite, 4 cm in length and 2 cm in diameter, are tested under uniaxial compression to study the source process of acoustic emissions. Two kinds of granite are used in our experiment; one is coarse-grained granite whose grain sizes are between 0.5 mm and 5 mm, the other is fine-grained granite whose grain sizes are between 0.2 mm and 1.2 mm. Acoustic emissions are detected by a piezoelectric transducer of compressional mode attached not directly to the rock specimen but to the steel end-piece. By doing this, the same transducer can be used for experiments of different specimens. Signal amplitudes are recorded on three channels of an oscillograph through high- and low-gain amplifiers to cover a wide dynamic range of more than 40 dB. The predominant frequencies of observed wave-forms are found to range from a few hundreds KHz to a thousand KHz. The volumetric strain is measured by axial and circumferential strain gages attached directly to the rock sample.

2. Results

Fig. 1 exhibits a few examples of the frequency-amplitude relationship of acoustic emissions, where A indicates the case of coarse-grained granite at the axial stress of 1.4 kb, B and C the cases of fine-grained granite at 2.3 kb and 2.5 kb, respectively. It is found that the observed frequency distributions at law and moderate amplitudes of acoustic emissions obey the Ishimoto-Iida's formula, giving the m values as shown in the figure. We observe, however, that the number of larger events is fewer than would have been expected theoretically. There seems to exist a certain critical amplitude, and at amplitudes larger

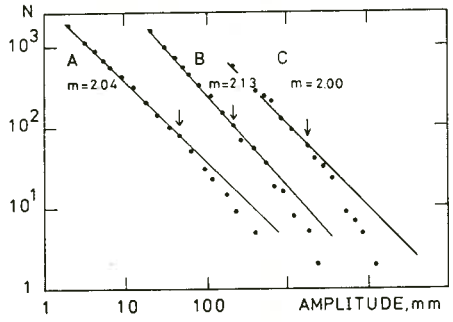

Fig. 1 Cumulative frequency of acoustic emissions vs. trace amplitudes. The data points for B and C are shifted toward the right for convenience.

than the critical one the observation deviates from the theory. This type of bending has frequently been found for the frequency distribution of acoustic emissions in literatures.

Acoustic emissions in a compression test of brittle rock are generally considered to be caused by sudden opening of tensile microcrack, because they are related closely to the dilatancy phenomenon. It is important to determine the size of microcrack which radiates elastic waves. The theoretical relation between the volume change due to cracking and the amplitude of radiated waves can be derived from the dynamic source model of tensile circular crack. Based on this theoretical relation, the size of microcrack, which radiates elastic waves, is estimated from the observation equations expressed in terms of the measured quantities of inelastic volumetric strain and statistical parameters in the Ishimoto-Iida's formula.

Depending on the amplitudes of events detected with piezoelectric transducer, the estimated sizes of microcracks range from 0.4 mm to 8 mm for coarse-grained granite and from 0.14 mm to 1.9 mm for fine-grained one. It is noted that this difference in crack size corresponds to the difference in grain size of the two rock types. The aspect rations of these tensile cracks are estimated at the order of 10^{-3}. The crack sizes of events having the critical amplitude in the observed frequency distributions are found to be about 3 mm for coarse-grained granite and about 0.7 mm for fine-grained one. These values agree approximately with the medium grain sizes of respective rock types. It is thus concluded that the source size of acoustic emission is related closely to the grain size distribution of individual rock type and that the insufficient number of larger events, as observed in our experiment, is explained by the limited number of larger grains.

CHANGE OF MECHANICAL PROPERTIES DURING SOLIDIFICATION OF SEDIMENTARY ROCKS

Kazuo HOSHINO, Geological Survey of Japan

As the results of a systematic laboratory work on high pressure experimentation of more than several hundreds specimens including most kinds of sandstones and mudstones in Japanese sedimentary basins, it was discovered that porosity is the most effective factor to control mechanical properties of the clastic sedimentary rocks. The experimentation was done at confining pressure up to 2,500 bars at room temperature, in strain rate of 10^{-4} to 10^{-6}/sec. Porosity n decreases as strength σ_s increases in semi-logarithm relation as follows

$$n = A\, e^{-b\sigma_s}$$

where A and b are constants. The above formula is similar to the following equation, well known as the equation of compaction,

$$n = n_0 e^{-ch}$$

where h is depth of burial, and n_0 and c are constants known as primary porosity and coefficient of compaction respectively. In comparision with the equation of compaction, b of the former formula is called strength coefficient.

Experimental results showed that strength coefficient is variable in different sedimentary basins as well as compaction coefficient is. The strength coefficient is an indication of somewhat softness of rocks against deformation and hence closely related to process of solidification or cementation of the matrix of natural rocks.

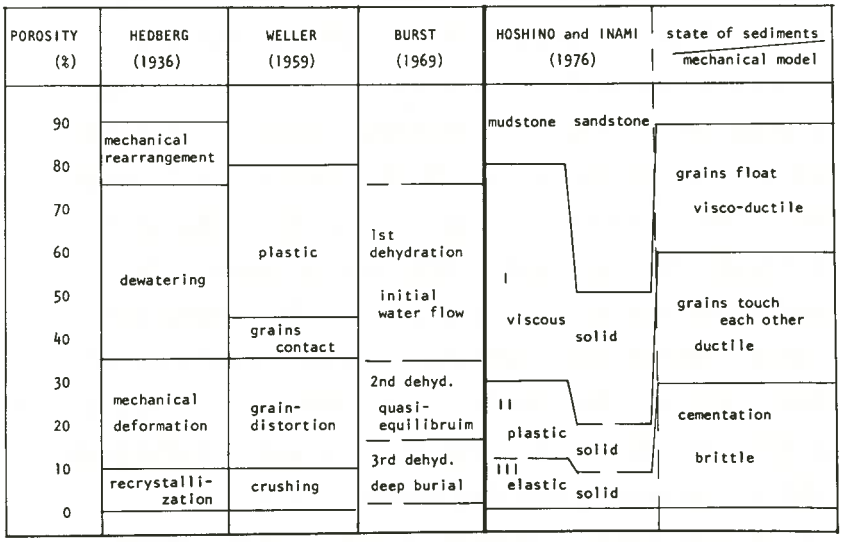

Fig. 1 Stages of compaction

Compaction coefficient, when it is transfered to coefficient of lithostatic pressure p, is equivalent to compressibility, and comparable to that obtained from short time experiment as shown in Fig.2. The former is 20 or 100 times larger than the latter. This difference is attributed to time effect on natural sedimentation for a long geological time under overburden pressure. Mechanical deformation during natural sedimentation is mostly non-elastic and compaction process is irreversible.

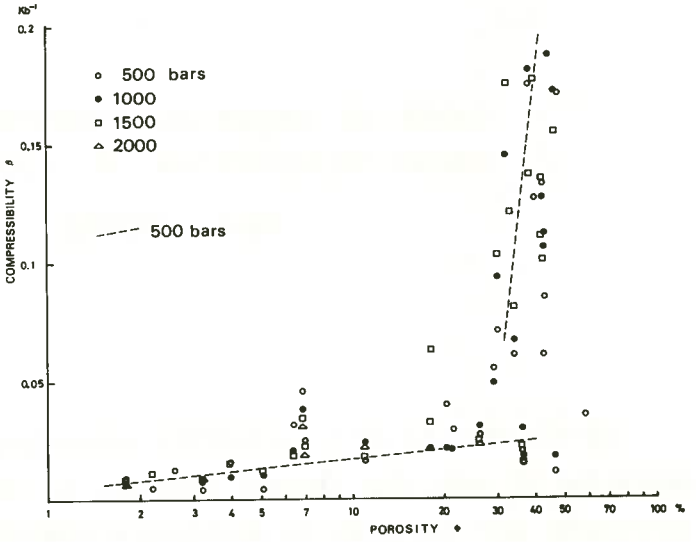

Fig. 2 Compressibility of argillaceous rocks at hydrostatic pressure up to 2000 bars. The abscissa is porosity in logarithmic scale.

Further analysis of the subsurface data in the oil-bearing basins as well as the results in laboratory showed an interesting results concerning mechanical evolution of the clastic rocks from the initial stage of surface sediments to final stage of perfect lithification. Compressibility increases moderately up to porosity around 30 %, however beyond that it goes up suddenly to value of liquid-like material (Fig.2). Equivalent viscosity and cohesive strength etc are strongly dependent on porosity (Fig. 3 and 4).

The above results have made it possible to materialize hypothetical model of compaction mechanism. From a viewpoint of mechanical evolution, process of compaction is divided into three stages as proposed in Fig.1. The first stage: The mineral grains within rocks are not touched each other yet. The rocks are viscous and behave like soil or fluid-like material. The second stage: The mineral grains come into contact. The rocks consist of mechanically stable framework built up of these grains. Physically, they are plastic solid or Bingham substance. The third stage: Authigenic minerals appear among the mineral grains, and cementation becomes common in every part within the rocks.

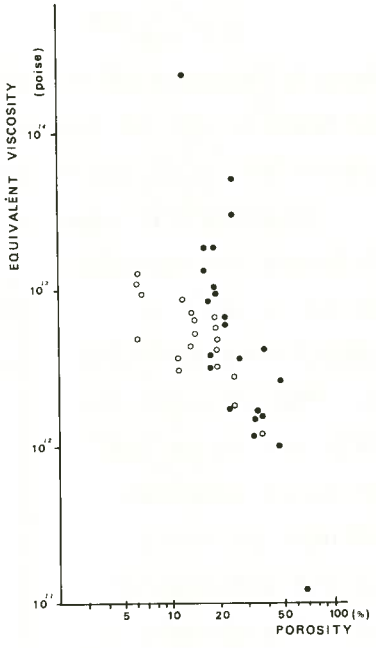

Fig. 3 Equivalent viscosity versus porosity. The both axes are in logarithmic scale. Close and open circles are argillaceous and arenaceous rocks respectively.

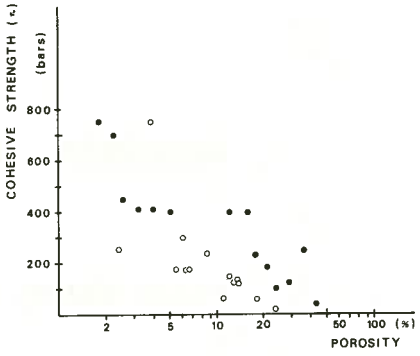

Fig. 4 (right) Cohesive strength versus porosity. Porosity is in logarithmic scale. Close and open circles are argillaceous and arenaceous rocks respectively.

REFERENCES

Hoshino, K., Koide, H., Inami, K., Iwamura, S., and Mitsui, S., 1972. Mechanical properties of Japanese Tertiary sedimentary rocks under high confininf pressure, Geol.Surv.Japan Special Report No.244, 200 p.

Hoshino, K., 1974. Effect of porosity on the strength of the clastic sedimentary rocks, Proc. 3rd ISRM, 2 A, p. 511-516.

Hoshino, K., and Inami, K., 1974. Comparative study on strength in sedimentary basins and it's bearing to petroleum geology, Jour.Jap.Assoc.Petro. Tech., vol. 39, p. 366-374 (*)

Hoshino, K., and Inami, K., 1975. Mechanical properties of rocks under high pressure and it's bearing to petroleum geology in Amakusa in northwestern Kyushu, Jour.Jap.Assoc.Petro.Tech., vol. 40, p. 236-245 (*)

Hoshino, K., and Mitsui, S., 1975. Mechanical properties of Palaeogene and Cretaceous rocks in Shikoku under high pressure, Jour.Jap.Assoc.Petro. Tech., vol. 40, p. 166-173 (*)

Hoshino, K., and Inami, K., 1977. Stages of compaction as defined from change of mechanical properties, Jour.Jap.Assoc.Petro.Tech., vol. 42, p. 90-99 (*)

Hoshino, K., 1978. Progressive stage and mechanism of compaction, Geol.Soc. Japan Memoir No.15 " Diagenesis ", p. 15-34 (*)

Hoshino, K., and Koide, H., 1978. Experimental rock deformation, Recent Progress of Natural Sciences in Japan, vol. 3, p. 55-61

Inami, K., and Hoshino, K., 1974. Compressibility and compaction of clastic sedimentary rocks, Jour.Jap.Assoc.Petro.Tech., vol. 39, p. 357-365 (*)

(*) written in Japanese with English abstract

MECHANICAL PROPERTIES OF CARBONATE ROCKS

Kazuo INAMI, Geological Survey of Japan

Porosity, permeability and ultrasonic wave velocity of 48 carbonate rocks were measured, among which 41 were taken in Japan and 7 were other countries.

1. Experimental technique

To measure the ultrasonic wave velocity, the ordinary pulse transmission method is used. The pulse of 300KHZ for P-wave, 40KHZ for S-wave, emitted and received by zirconate lead transducers. The ultrasonic signal detected is displayed on the oscilloscope with the received signal and 10μs quartz pulse.

Air permeability is measured by comparative method to compare the pressure-time curve between the samples and a standard sample, so that we measure state of low permeability, such as order of 10^{-3} md.

2. Samples

The samples collected at 12 places in Japan include 15 Paleozoic limestones, 9 Mesozoic Soma limestones and 14 crystalline limestones, (Fig. 1). The 7 samples from outside Japan are ranging from Mesozoic to Recent in geological age.

3. Density and Porosity

Fig. 1 shows the relationship between grain density and porosity. The grain density of the 14 crystalline limestones ranges between 2.69 and 2.73 g/cm^3 and mean value is 2.71 g/cm^3, while the 15 Paleozoic limestones has mean value of 2.71 g/cm^3.

This value shows good agreement with the density of calcite, which is 2.715 g/cm^3. The density of the 9 Mesozoic limestones, 2.70 g/cm^3 in mean, is smaller than that of the Paleozoic. This is possibly due to that chemical

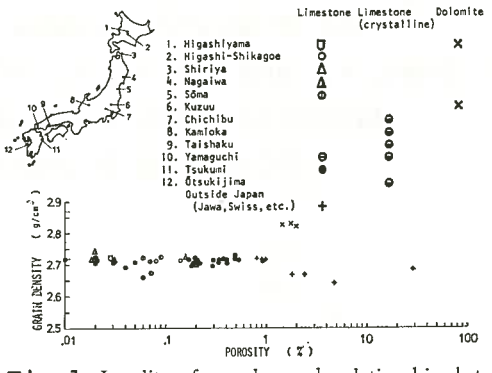

Fig.1 Locality of samples and relationship between grain density and porosity.

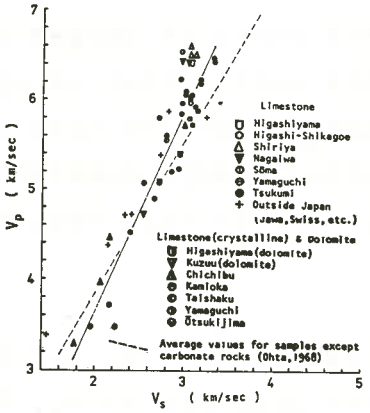

Relationship between P-wave and S-wave velocity. **Fig.2**

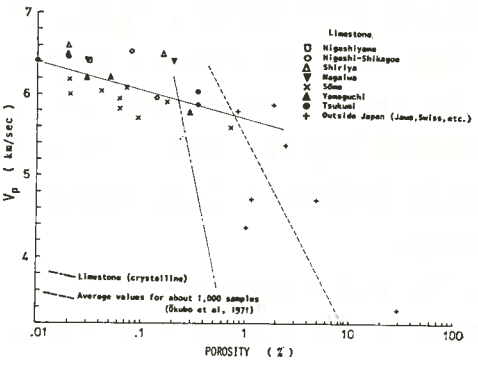

Relationship between porosity and P-wave velocity of limestones. **Fig.3**

content of SiO_2, Fe_2O_3, Al_2O_3 etc. The Mesozoic samples is more than that of the Paleozoic.

The porosity of the Paleozoic, Mesozoic and crystalline samples ranges respectably between around 0.01 and 0.04%, 0.02 and 0.1% and 0.2 and 0.6%.

4. Ultrasonic wave velocity

It seems that both ultrasonic wave velocity, V_p and V_s change according to geological age, that is, the Paleozoic samples the largest while the recent ones the smallest. V_p of the Paleozoic, and Mesozoic, is read respectively between 6.25 and 6.50, and 5.60 and 6.10 km/s, (Fig. 2).

This indicates that V_p is variable depending on such factors as overburden pressure, geological age and temperature. V_p of the crystalline limestones ranges from 3.30 to 5.80 km/s depending on grain size. V_p increases as grain size decreas.

The relation between Vp and V_s, as shown as the thick line in Fig. 2, is decided in the following equation.

$$V_p = 2.20V_s - 0.77$$

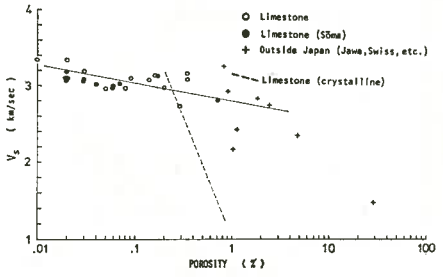

Relationship between porosity and S-wave velocity of limestones. **Fig.4**

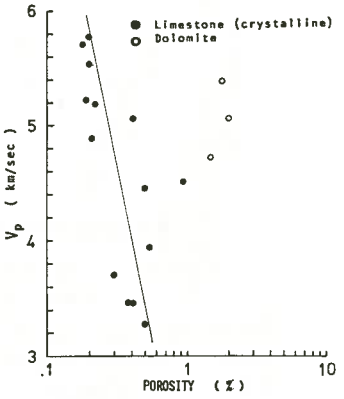

Relationship between porosity and P-wave velocity of crystalline limestones and dolomites. **Fig.5**

In Fig. 2, the dotted line is average V_p-V_s relation for Japanese mudstones and sand-stones. Both dotted and thick lines intersect at around 4.50 km/s of V_p.

Below this point, V_p/V_s of carbonate rocks is larger than that of the clastic rocks, while upper this point, that of clastic rocks is larger than that of the carbonate rocks. As that quartz and natural rubber are 0.68 and 0.08 respectively, generally, larger ratio indicate less ductile. In this points this result is interesting.

5. V_p, V_s and porosity

Fig. 3 to 6 show the relationship between V_p, V_s and porosity. V_p, V_s increase as porosity decrease. The gradient of V_p, V_s-porosity (n) curve, in the region of porosity down to 1%for V_p, 0.3% for V_s, is more gentle than that of up to that. In the region of porosity up to about 1%, the V_p-n curve may correspond to a dotted line, that is a average line for about 1,000 rock samples in Japan.

The V_p at 0% porosity may expect about 6.56 km/s, that is obtained from V_p of the polycrystalline model of calcite crystals. Both V_p and V_s are related with porosity as follows, (Ōkubo et al., 1971).

$$n = Ae^{BV}$$

where n is porosity (%), A and B are constants, V is P and S-wave velocity (km/s).

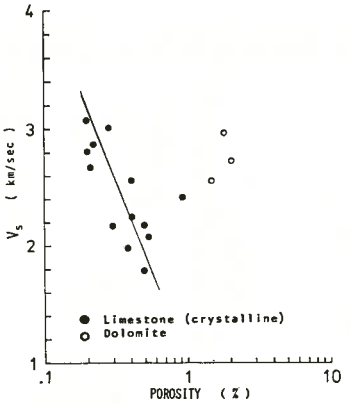

Relationship between porosity and S-wave velocity of crystalline limestones and dolomites. Fig.6

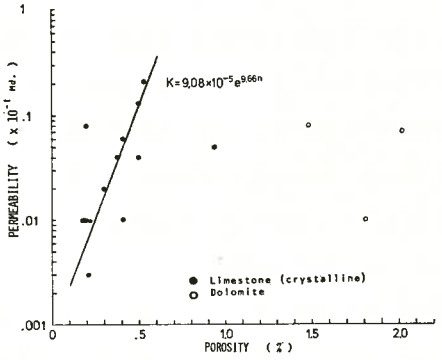

Relationship between porosity and permeability of crystalline limestones and dolomites. Fig.8

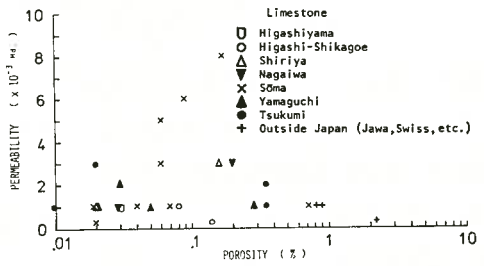

Relationship between porosity and permeability of limestones. Fig.7

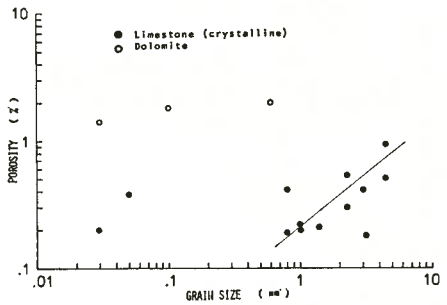

Fig.9
Relationship between porosity and grain size of crystalline limestones and dolomites.

STUDY ON THE PROPAGATION OF ULTRASONIC WAVE IN ROCK SPECIMEN UNDER UNIAXIAL PRESSURE

Masayasu INOUE, Michito OHOMI
KUMAMOTO University

1. Introduction

We have studied on the properties of rock specimen such as compressive strength, elastic constant,wave propagation relating water content, weathering degree and crack. In this paper we describe changes of propagation of compression and shear wave under uniaxial compression test.

2. Apparatus and Test Piece

Transducers(transmitter and receiver) are piezoelectric barium titanic ceramic and are placed in protector of steel box. Rectangular specimen (5 X 5 X 10 cm height) are prepared from rock mass and polished end surface with 200 mesh carborundum and smeared hand cream on the surfce. Specimen (dry condition in room) is placed on uniaxial compression test machin and velocity and amplitude are measured in direction parallel to stress. Specimens are marble (crystalline limestone), sandstone (mesozoic), tuff (tertiary), andesite and granite. Chief physical properties of the specimens are shown below.

rock type	density g/cm^3	velocity no loading P wave Km/s	S wave	compressive strength Kg/cm^2
marble	2.69-2.75	5.82-6.29	3.05-3.25	600-750
tuff	1.68-1.72	3.03-3.10	1.80-1.85	530-600
sandstone	2.48-2.53	4.54 4.72	2.48-2.57	1400-1650
granite	2.59-2.68	4.07-4.21	2.37-2.48	1300-1800
andesite	2.25-2.32	3.66-3.89	-------	510-680

3. Result and Discussion

Some foundamental problems concerning propagation phenomena under uniaxial pressure are examined at the first place.

Influence of smoothness of polishing surface on the ultrasonic wave propagation is examined. From Fig.1 it is clear that both specimens give almost equal amplitude for P wave but give considerable different value for S wave. Influence of smoothness of po-

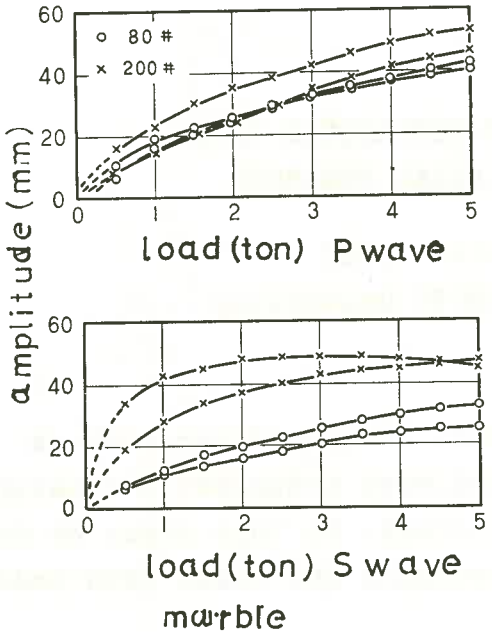

Fig.1 Influence of smoothness of end surface

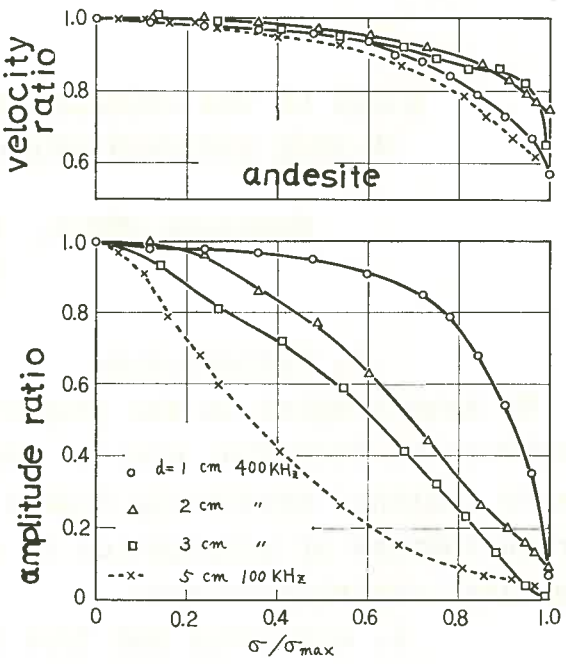

Fig.2 Influence of diameter

lishing surface on propagation velocity can be neglisible.

Difference of frequence of transducers has little influence on the velocity of P wave, we use 50 KHz transducer usually.

Influence of diameter of transducers on propagation wave is shown in Fig.2. As indicated in Fig.2, influence of diameter on propagation velocity is slight but influence on the amplitude is remarkable and is greater in rock having small Young's modulus.

As uniaxial pressure increases, contact of transducers to the end surface becomes close then energy transmittion between transducers and specimen can be improved.

After due consideration of preceding practical problems, we measure the change of propagation velocity and amplitude of rocks under increasing uniaxial pressure. Some of them shows Fig.3 and Fig.4. From Fig.3 the following became clear. As uniaxial pressuer increases, velocity and amplitude both P and S wave are increase also. At low pressure velocity and amplitude increase sharp and become constant curve until near the breaking stress but variation of the amplitude of S wave is distinguishable and the amplitude decreases rapidly at 70-90 % of the breaking stress. The reasons are (1) energy transmittion between transducer and specimen can be improved, (2) as pressure increases, numerous open cracks may be closed such as consolidation test of soil, (3) near

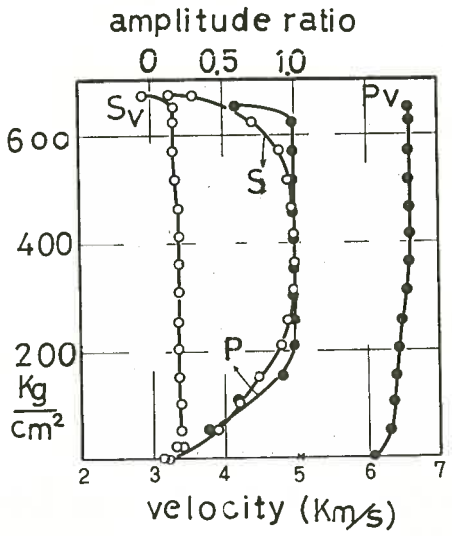

Fig.3 Result of marble

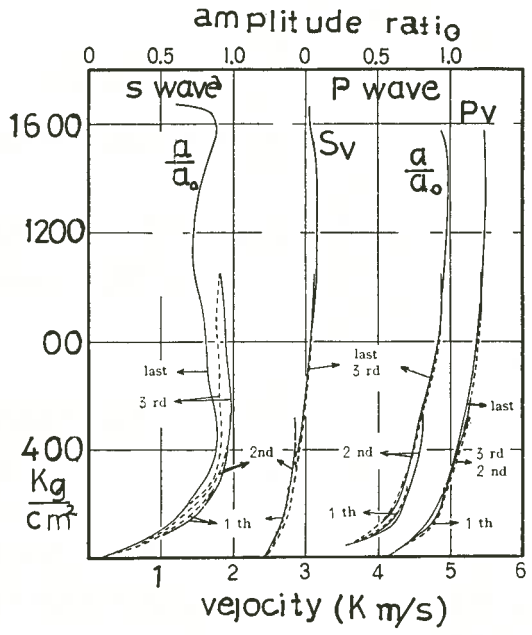

Fig.4 Result of granite

the breaking stress,microcracks develope rapidly then ultrasonic pulse can not transmit across microcracks without large loss of amplitude.

Fig.4 shows variation of propagation velocity and amplitude under repeated load. It is clear that variations present simillar tendency of preceding results in marble and sandstone but in tuff and granite hysteresis curves deform in amplitude of S wave.

5. Conclusion

From the data presented in this paper we may conclude following.

The end surface must be polished courteously with fine carborundum and painted with hand cream etc. Over 50 KHz, transducer is sufficient to measure velocity of propagation wave but diameter of transducer must be chosen suitable size compared with specimen to measure amplitude.

As uniaxial pressure increases, propagation velocity and amplitude increase also. The variation of amplitude of S wave is very remarkable so it is useful method to foresee the break of rock.

Reference

M. OHOMI, M.INOUE, Propagation properties of Elastic Wave In Rock under Uniaxial Compression, Technical Reports of the KUMAMOTO University. No.1, Vol.20,No.2,1971 No.2, Vol.20,No.3, 1971. No.3 Vol.21,No.2, 1972.

LONG-TERM CREEP EXPERIMENT OF ROCKS OBTAINED FOR 4 YEARS

Hidebumi ITÔ University of Osaka Prefecture
Sadao SASAJIMA Kyoto University

Since August 1974 the authors have carried out creep tests by bending three granite test-pieces, each 21×2.5×2.0 cm, and three gabbro test-pieces, 16×2.0×1.5 cm. The laboratory has occupied a vacant adit with 200 m depth below the ground surface in Kisenyama Underground Power Station of Kansai Electric Power Inc., Kyoto, where the constant room temperature (18°C) and humidity (nearly 100 %) are maintained naturally.

The fine-grained granite of test-piece is from Aji, Kagawa Prefecture, Japan and the fine-grained gabbro is from Sweden. The test-piece was shaped into a beam having a highly polished upper surface. The test-piece has been bent convex upwards as shown in Fig.1; each granite test-piece has undergone the maximum bending stress, 19.5 kg/cm^2 (ℓ=20.0 cm, ℓ_2=8.0 cm, W=5.25 kg, m=10.5 cm), for each gabbro test-piece, 20.4 kg/cm^2 (ℓ=14.9 cm, ℓ_2=6.0 cm, W=3.30 kg, m=10.8 cm). While measuring, an optical flat is set upon the polished surface to produce interference fringes with Na-D light (wavelength 0.5893 micron), its principle being based on Newton's rings. From an analysis of the interference

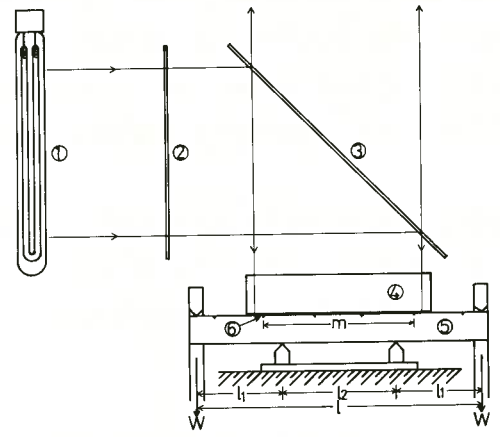

Fig.1 Schematic diagram showing a creep test by making use of interference fringes of light. 1:sodium lamp, 2:frosted glass, 3:plane parallel plate of glass, 4:optical flat, 5:test-piece, 6:reference marks carved on a polished surface of a test piece.

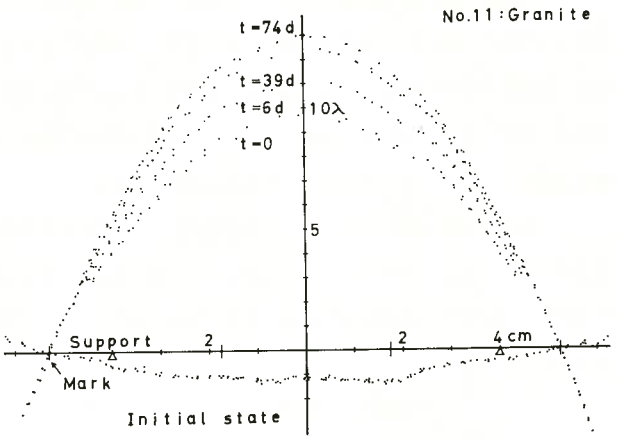

Fig.2 Time-dependent change of the profile of the upper surface of the granite test-piece No.11. t (in day) is the time of measurement and the ordinate is shown in a scale of Na-D ray's wavelength. Each mean curve through plotted points at respective measuring time gives the most probable profile.

fringes, we can determine the profile of the upper surface as shown in Fig.2, with an accuracy better than one-tenth of a wavelength. For further details concerning methods of determination of the profile, the reader is referred to Itô and Sasajima (in press).

A bending of the test-piece should be reduced to a difference between the profile at the time of measurement and the initial profile before loading (see Fig.2). At present let us represent the bending by a displacement $\delta(t)$ of a middle point of the beam relative to the two reference marks with the distance m (Fig.1). In Fig.3 the experimental results obtained over four years are shown. As seen in the figure the bending of each test-piece, granite or gabbro, does not show a monotone increase in creep, but a repeated 'turn back' with various periods, some of which are longer than one year. This strange phenomenon was first noticed by Kumagai and Itô (1970). When the creep has undergone the turn back, it is considered that the test-piece has worked against an external force. How does the test-piece get the energy ? In order to explain the creep accompanied by the turn backs, the present authors have proposed a hypothesis that an elastic constant of the test-piece varies with time during an advance of creep (Itô and Sasajima, in press).

For 22 years since 1957, Kumagai and Itô have carried out creep tests of two large granite beams each of 215×12.3×6.8 cm (Itô, 1979). The result obtained hitherto shows that the general trend of the creep, ignoring turn backs, has been linearly increasing, with a secondary creep of a viscosity, $3\text{-}6\times10^{20}$ poise. But they were not able to observe a primary creep clearly.

For the present result of granite, however, we may draw an general creep curve consisting of the primary and secondary creeps, as shown by a broken line in Fig.3. However, the secondary creep line is indicating a general trend only

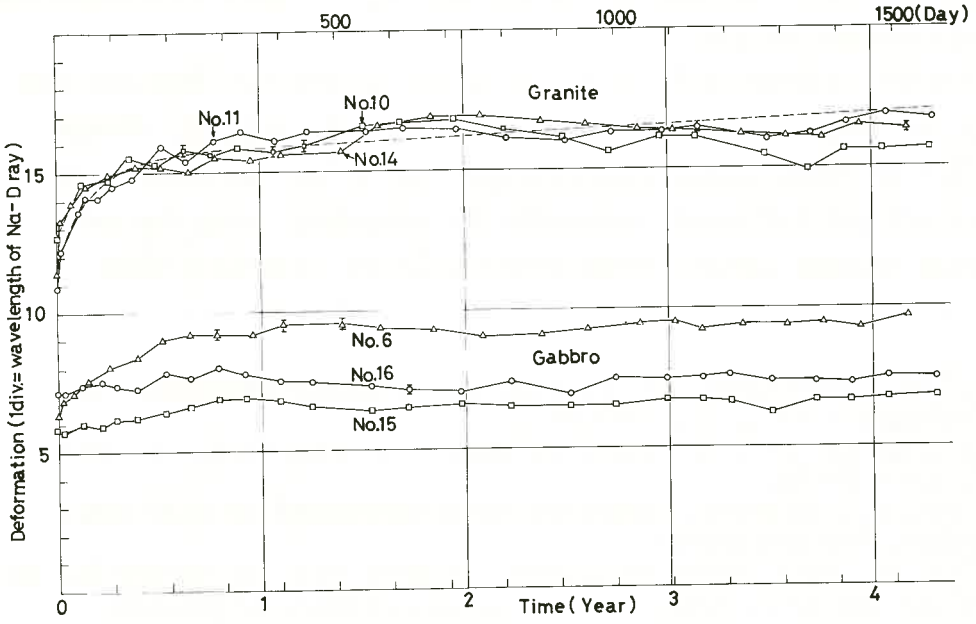

Fig.3 Experimental results obtained for 4 years. Nos.10, 11 and 14: granite test-pieces. Nos.6, 15 and 16: gabbro ones.

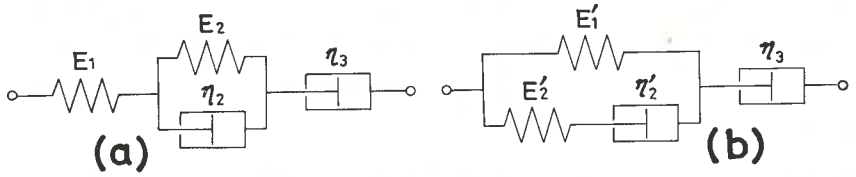

Fig.4 Two rheological models explaining the primary and secondary creeps.

for the current data and hence might be changed more or less depending on the future advance of creep. Two rheological models (Fig.4) are introduced to explain such creep curve mentioned above. The one (a) is the so-called Burgers model and in another one (b), if the dashpot with viscosity η_3 is lacking, it is the same as 'the standard linear solid' by Dieterich (1972), who has used it to account for aftershocks of the main earthquake.

The deflection curve of an elastic beam with Young's modulus E is given by a formula, $y = 1/E \cdot X(x)$. The deflection curve of a beam possessing the property modeled by Fig.4 (a) or (b) can be represented by a formula, $y = T(t) \cdot X(x)$ (Kumagai and Itô, 1970; Itô and Sasajima, in press). Here T(t) is given by

$$T(t) = 1/E_1 + 1/E_2 - 1/E_2 \cdot \exp(-E_2/3\eta_2 \cdot t) + t/3\eta_3 \qquad (1)$$

for the model (a) and

$$T(t) = 1/E_1' - E_2'/E_1'(E_1'+E_2') \cdot \exp\{-E_1'/(E_1'+E_2') \cdot E_2'/3\eta_2' \cdot t\} + t/3\eta_3 \qquad (2)$$

for the model (b), where these notations are the same as for Fig.4. The broken line in Fig.3 has been drawn according to Eqs. (1) and (2), and approximated by the formula

$$\delta(t) = 15.5 - 3.8 \exp(-t/60) + t/1000 \qquad (3)$$

where $\delta(t)$ is represented by wavelength unit and time t in day. Thus we can obtain the following quantities (c.g.s.): $E_1=3.8\times10^{11}$, $E_2=11.8\times10^{11}$, $\eta_2=2.0\times10^{18}$, $\eta_3=1.3\times10^{20}$ for the model (a), and $E_1'=2.9\times10^{11}$, $E_2'=0.94\times10^{11}$, $\eta_2'=1.2\times10^{17}$, $\eta_3=1.3\times10^{20}$ for the model (b). The quantity $3\eta_2/E_2=60$ days is the retardation time of the Kelvin (or Voigt) element of (a) and $3\eta_2'/E_2'=45$ days the relaxation time of the Maxwell element of (b).

For the gabbro test-pieces No.6, No.15 and No.16, we can not draw any common view of creep, although No.15 and No.16 undergo a nearly parallel change. After about 200 days it seems likely that No.6 also takes the similar change. At present, we can not yet definitely recognize the secondary creep for each test-piece, probably because gabbro creeps very slowly in comparison with granite.

References

Dieterich, J. H., 1972. Time-dependent friction as a possible mechanism for aftershocks. J. Geophys. Res., 77: 3771-3781.

Itô, H., 1979. Rheology of the crust based on long-term creep tests of rocks. Tectonophysics, 52: 629-641.

Itô, H. and Sasajima, S., in press. Long-term creep experiment on some rocks observed in 3 years. Tectonophysics.

Kumagai, N. and Itô, H., 1970. Creep of granite observed in a laboratory for 10 years. In: S. Onogi (Editor), Proc. 5th Int. Congr. Rheol., 2: 579-590.

ON THE VARIATION OF ELASTIC WAVE VELOCITY AND ENERGY SITUATION OF CONTAINED MOISTURE IN SOFT ROCKS

Munehiro KITAOKA, Gensuke ENDO,
Waseda University

1. Introduction

In the evaluation of mechanical properties of soft rocks, the influence of moisture is very important. Especially the investigation of physico-chemical influence of water is efficient to quantify simultaneously mechanical properties and energy situation of soft rocks. In this paper the variation of elastic wave velocity in soft rocks due to water adsorption is discussed with the change of energy situation of moisture, furthermore it is referred to softening due to water adsorption.

2. Characteristics of water adsorption

We used the method of water adsorption under vapour pressure, by which chemical potential in rock is overall equal in a state of equilibrum with water vapour pressure. Figure 1 shows the characteristics of water adsorption of several specimens with the change of relative humidity. The characteristics of water adsorption show the form of inverse S letter with the increase of vapour pressure, which means water adsorption swiches over from monomolecular to numerousmolecular layers. Therefore BET adsorption formula can be applied to these characteristics.

$$\frac{P}{V\,(Po - P)} = \frac{1}{Vm\ C} + \frac{C - 1}{Vm\ C}\left(\frac{P}{Po}\right) \qquad \cdots\cdots\cdots (1)$$

When specific surface area So is given as So = Vm / ro* , water content of monomolecular adsorption layer, relative humidity forming monomolecular layer and specific surface area are determined as shown in Table 1.

When Gibbs'adsorption formula is applied to these characteristics of water adsorption, free energy change of adsorpted water in a unit volume of specimen is expressed with formula (2) .

$$\Delta\gamma_v = -\frac{R\,T}{M}\int_p^P \frac{So\,\Gamma}{P}\,dP \qquad \cdots\cdots (2)$$

From the experimental results, we find the water adsorption is mainly a physical adsorption, which is dependent on van der Waals' power near the grain surface, and the quantity of adsorpted water is dependent on the specific surface area, which is the most important physical quantity in formula (2) .

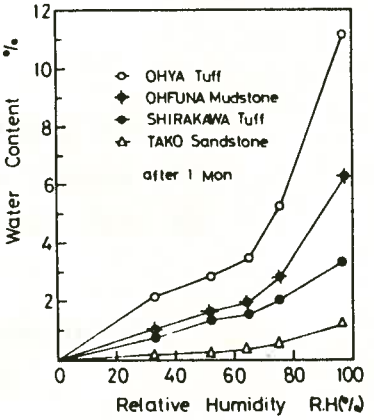

Fig. 1 Characteristics of isothermal water adsorption of soft rocks

3. Variation of elastic wave velocity with the change of the degree of water saturation

P-wave velocities (-o-) of soft rocks measured in the drying process after absorption under vacuum condition show without exception the lowest value during the change of the degree of water saturation ($\overline{Sr}(\%)$) as given in Figure 2. $\overline{Sr}(\%)$ is inherent in each sample, and this point correspondends with the sharply turning point of s-wave velocity and strength (Fig.3). The variation of elastic wave velocities (-●-) of water adsorbed samples under vapour pressure are shown also in Figure 2. In each sample the measured values are distributed in the region of $0(\%) \leqq Sr(\%) \leqq \overline{Sr}(\%)$. Especially Sr(%) in R.H. 96.5% almost correspondends with $\overline{Sr}(\%)$, that means $\overline{Sr}(\%)$ is dependent on specific surface area in formula (2).

Table 1 Water content and relative humidity by forming monomolecular adsorption layer and specific surface area determined by BET adsorption formula

Samples	Vm (g/cm^3)	R.H (%)	Se (cm^2/cm^3)
OHYA Tuff	0.0194	21.0	7.043×10^5
SHIRAKAWA Tuff	0.0107	22.0	3.880×10^5
OHFUNA Mudstone	0.0107	22.5	3.880×10^5
TAKO Sandstone	0.0032	33.0	1.141×10^5

To study the relation between p-wave velocity and the change of energy situation of adsorbed water in the region of $0(\%) \leqq Sr(\%) \leqq \overline{Sr}(\%)$, we show p-wave velocity in formula (3).

$$Vp = \sqrt{\frac{E\,(1-\nu)}{\rho^*(1+\nu)(1-2\nu)}} = \sqrt{E}\;\psi(\rho^*,\nu) \qquad \cdots\cdots\cdots (3)$$

From the experimental results, we gain $\psi(\rho^*,\nu) \approx Ko$ (const.) and a proportional relation between Young's Modulus and the quantity of free energy change, therefore following formula can be concluded.

$$Vp^2 = Vpo^2 + \beta\,\Delta\gamma_v \qquad \cdots\cdots\cdots\cdots (4)$$

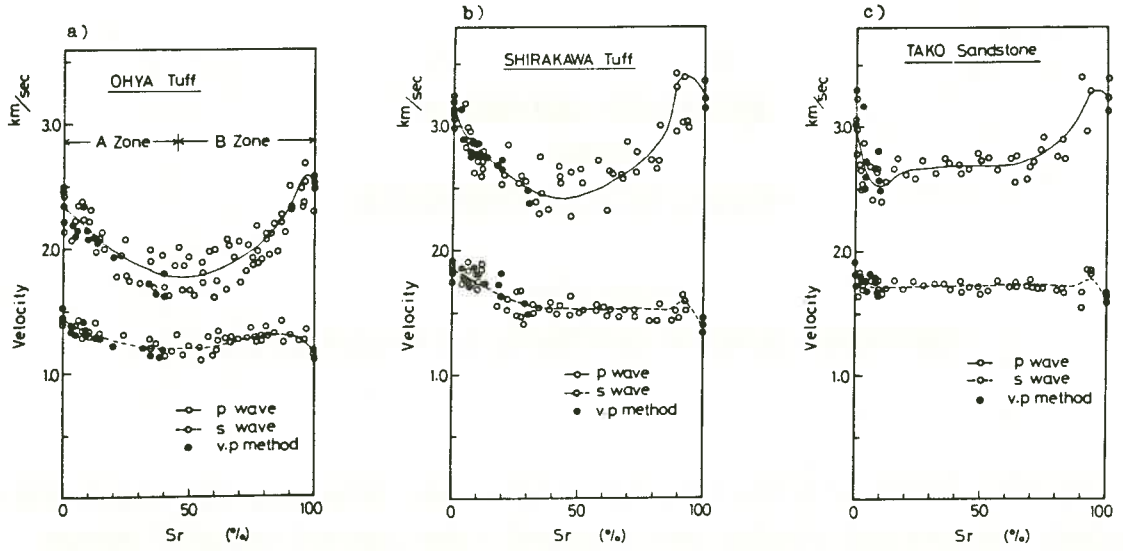

Fig. 2 The variation of elastic velocity due to the change of the degree of water saturation

As the experimental results furthermore give the relationship of $ß = K' Vpo^2$, formula (4) is changed into following formula.

$$\frac{Vp^2 - Vpo^2}{Vpo^2} = K' \Delta \gamma_v \qquad \cdots\cdots\cdots (5)$$

From the view of the swelling characteristic of rock, $(Vp^2 - Vpo^2)/ Vpo^2$ is interpreted as an Index expressing the softening potential.

On the other hand the theoretical formula by Biot-Geertsma is suitable to explain the increase of p-wave velocity in the region of $\overline{Sr}(\%) \leqq Sr(\%) \leqq 100(\%)$.

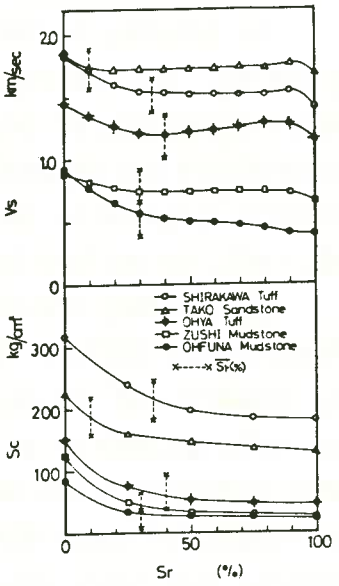

Fig. 3 Correlation of the change of shear wave velocities with uniaxial compressive strength for soft rocks as a function of the degree of water saturation

Symbols

C, Ko, ß, K' : const.
P : vapour pressure
Po: saturated vapour pressure
So: specific surface area
V : adsorptive water content
R : gas constant
T : absolute temperature
M : mol gravity
$\Delta\gamma$: free energy change
Γ : water content in a unit area
$ro^* = 2.76 \times 10^{-8}$ cm
E : Young's Modulus
ν : Poisson's ratio
ρ^*: apparent density
Vp: longitudinal wave velocity
Vm: water content of monomolecular adsorptive layer
Vpo: longitudinal wave velocity in $\overline{Sr}(\%)$

ANISOTROPIC DEFORMATION UNDER GENERAL TRIAXIAL COMPRESSION

Kiyoo MOGI
Earthquake Research Institute, University of Tokyo

By development of a new triaxial compression technique, all components of principal stresses and strains were measured under general triaxial stress states in which the intermediate compression is not always equal to the minimum or maximum compression.

In general, a state of stress is described by the principal stresses, σ_1, σ_2 and σ_3. The compressive stress is taken as positive and $\sigma_1 > \sigma_2 > \sigma_3$ in this paper. Directions of X-, Y- and Z- axis are taken as the directions of minimum, intermediate and maximum principal stresses at fracture. σ_X, σ_Y and σ_Z are compressive stresses in the directions of X, Y and Z, and ε_X, ε_Y and ε_Z are strains, which will be defined below, in the directions of X, Y and Z, respectively.

The loading system in this experiment is described in previous papers (Mogi, 1971a, 1971b). The minimum compression (σ_3) is applied by fluid confining pressure and the maximum compression (σ_1) and the intermediate compression (σ_2) were applied by solid pistons (Fig. 1). By this method, uniform true triaxial compression can be applied up to 7 kbars of the minimum compression (σ_3). The strains in three directions were measured by combinations of methods by electric resistance strain gage and differential transformer (Mogi, 1977).

In this experiment, the confining pressure (σ_X) was first applied, and the lateral load for σ_Y was increased to a constant value, then the axial load for σ_Z was increased at a nearly constant rate of $\varepsilon_Z (10^{-5}/\text{sec})$. Strains ε_X, ε_Y and ε_Z in the three directions are defined as the strains due to the increase of the axial stress ($\sigma_Z - \sigma_X$) under the constant σ_X and σ_Y. The volumetric strain due to the increase of the axial differential stress ($\sigma_Z - \sigma_X$) was calculated by the following equation:

$$\Delta V/V = \varepsilon_X + \varepsilon_Y + \varepsilon_Z$$

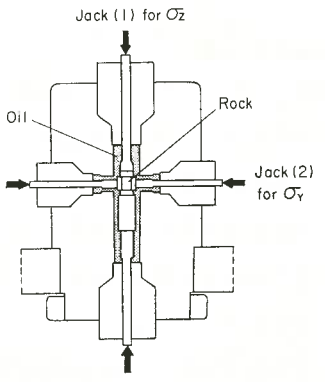

Fig. 1. High pressure vessel for the general triaxial compression.

In Fig. 2, the stress ($\sigma_Z - \sigma_X$) and the lateral strains ε_X and ε_y are shown as functions of the axial strain ε_Z. The minimum compression σ_3 (= σ_Z) is 0.60 kbar. The left figure shows the case of the axi-symmetric stress state ($\sigma_X = \sigma_y$). In this case, two principal lateral strains (ε_X and ε_y) are nearly equal. The right figure shows a typical case of the general triaxial stress state (σ_X= 0.60 kbar and σ_y=2.11 kbars). In this case, the ultimate strength ($\sigma_Z - \sigma_X$) is higher and the stress decrease after yielding is larger than those in the case of the axi-symmetric stress state, and ε_X is much greater than ε_y. It is noted that ε_X increases markedly before failure, but ε_y increases lenearly.

Fig. 3 shows the case of Inada granite which is a typical brittle crystalline rocks. In this case, the minimum compression is 0.70 kbar. The curves in the upper figures show the differential stress ($\sigma_Z - \sigma_X$) as functions of the axial strain ε_Z. In the lower figures, the lateral strain ε_X and ε_y are shown as functions of the axial strain ε_Z. The left figure shows the case of the nearly axi-symmetric stress state. In this case the strains ε_X and ε_y are nearly equal. The right figure shows the case in which σ_y is 2.53 kbars and σ_X is 0.70 kbar. In this case, ε_X increases markedly before fracture, but ε_y is nearly linear until fracture.

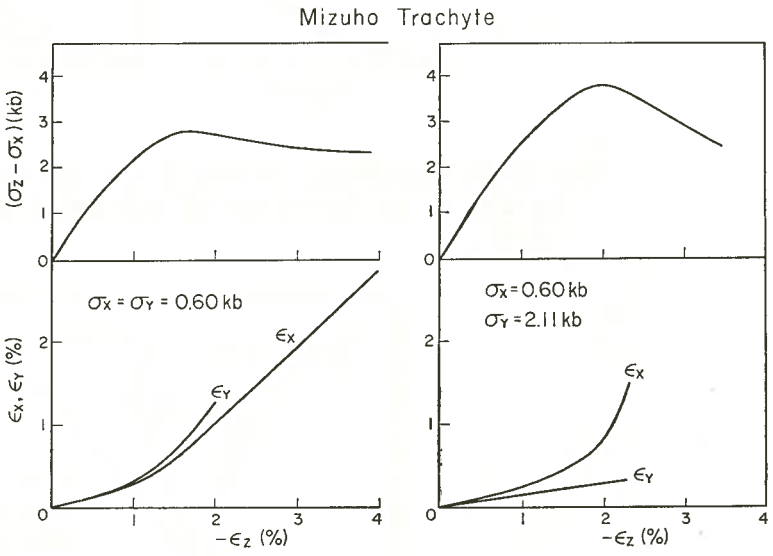

Fig. 2. Differential stress ($\sigma_Z - \sigma_X$) and lateral strains ε_X and ε_y as functions of the axial strain ε_Z in Mizuho trachyte. Left, axi-symmetric stress state; right, general triaxial stress state.

Fig. 4 shows the strains as a function of the differential stress in the case where σ_y=2.53 kbars and σ_X=0.70 kbar, in Inada granite. The vertical axis is stress and the horizontal axis is strain. The three principal strains and the volumetric strain are shown by solid curves. The dotted line corresponds to the elastic volumetric strain. The dilatancy curve is similar to the case of the axi-symmetric stress state, but the result shows that the dilatancy is mainly caused by the increase of ε_X.

The result in Yamaguchi marble is essentially similar to those in the trachyte and the granite. These results show that the dilatancy before fracture or yielding is caused by the inelastic deformation in the direction of the minimum compression. This anisotropic dilatancy is attributed to the crack opening

perpendicular to the minimum compression. This anisotropy markedly increases with increase of the intermediate compression.

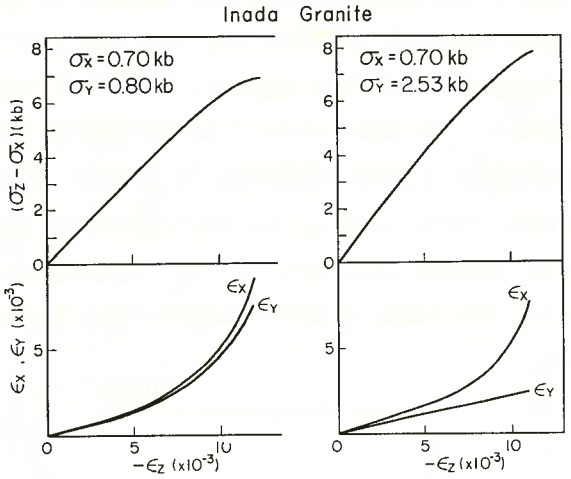

Fig. 3. Differential stress ($\sigma_Z - \sigma_X$) and lateral strains ε_x and ε_y as functions of the axial strain ε_z in Inada granite.

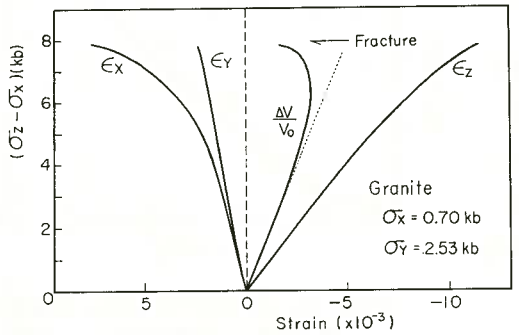

Fig. 4. Three principal strains (ε_x, ε_y and ε_z) and volumetric strain $\Delta V/V$ as functions of differential stress ($\sigma_Z - \sigma_X$) in Inada granite.

REFERENCES

Mogi, K., 1971a, Effect of the triaxial stress system on the failure of dolomite and limestone, Tectonophysics, 11, 111-127.

Mogi, K., 1971b, Fracture and flow of rocks under high triaxial compression, J. Geophys. Res., 76, 1255-1269.

Mogi, K., 1972, Effect of the triaxial stress system on fracture and flow of rocks, Phys. Earth Planet. Inter., 5, 318-324.

Mogi, K., 1977, Dilatancy of rocks under general triaxial stress states with special reference to earthquake precursors, J. Phys. Earth, 25, Suppl., S203-S217.

COMPUTER MODELLING OF ROCK FRACTURE IN UNIAXIAL COMPRESSION

Seisuke OKUBO and Yuichi NISHIMATSU
The University of Tokyo

INTRODUCTION

This study focuses on processes of fracture propagation and faulting in rock specimens under uniaxial compression. The FEM is applied to simulate failure of rock which is heterogeneous and consists of various materials and/or pores. The calculation is carried out well into the post-failure region.

MODEL OF ROCK SPECIMEN

Rock can be seen as a kind of composit material which contains a sufficient number of structural particles. Accordingly the rock specimen is divided into 252 triangular elements. Each element of model rock corresponds to each mineral particle or pore with its elastic constants and strength randomly distributed.

An incremental uniform displacement is applied at the upper end of the model rock. At each increment stress distribution is obtained for each element and tested by Mohr's criterion for failure. It must be noted that there are two modes of failure. One is compression failure,and the other is tensile failure.

Before failure each element is assumed to be isotropic. First, let's consider the stiffness matrix after compressive failure. We assumed that compressive failure caused by σv leads to a faulting plane at an angle of $\pi/4$ to the axis V. A stress matrix of a stratified or transversely-isotropic material in which a rotational symmetry exists within the plane of strata parallel to the faulting plane is applied. Such a material possesses five elastic constants $E1, \nu1, E2, G2$ and $\nu2$.The elastic constants $E1, \nu1$ are associated with the behavior in plane of the strata and $E2, G2$ and $\nu2$ with a direction normal to these. We assumed that the shear modulus of the failured element becomes 1/100 of the original value while the other elastic constants remained unchanged.

Next,let's consider the stiffness matrix after tensile fail-

ure caused by the maximum tensile stress σv. We assumed that a clean separation along the plane perpendicular to the V-axis appears,and the constants E2,G2 and $\nu 2$ associated with a V-direction become 1/100 of their original values.

After the tensile failure or rarely after the compression failure,the stress within the element may exceed the failure criterion again. In this case,we consider that the element is broken to small pieces,so that the elastic constants become 1/100 of their original values.

CALCULATION PROCESS

In Fig.1,a flow chart of the calculation is shown. In Part 1, elastic constants and strength are defined for each element. Two kinds of Young's moduli E_1 and E_s,either which is given randomly to each element,are considered. A pore is considered as an element whose Young's modulus is $(E_1+E_s)/100$. In Part 2,stress distribution of model rock is obtained by FEM. In Part 3,stress distribution is tested by the Mohr's failure criterion. The stress matrices of the elements which have failed are changed in accordance with failure mode for subsequent analysis. The process is returned to Part 2. The same calculation is repeated at the uniform displacement until no new element fails. This calculation is iterated at every incremental displacement.

The calculating processes were carried out well into the post-failure region.

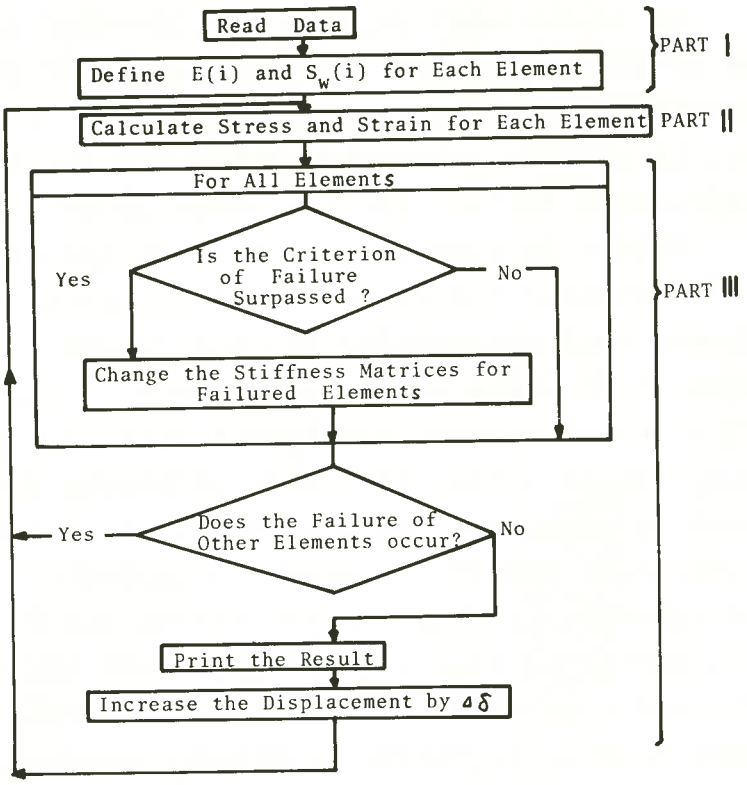

Fig.1 Flow chart of simulation

RESULT OF CALCULATION

Using the model rock, the processes before- and post-failure behavior of rocks are simulated. In the following discussion, the non-dimensional stress $\bar{\sigma}y$ and strain $\bar{\varepsilon}y$ are used to describe the results:

$$\bar{\sigma}y=\frac{F}{Fc}=\frac{\sigma y}{\sigma yc},\quad \bar{\varepsilon}y=\frac{\delta}{\delta c}=\frac{\varepsilon y}{\varepsilon yc}$$

where Fc, σyc are the external force and the averaged stress along the upper end, respectively when a homogeneous model rock fails, and δc, εyc are the applied displacement and the averaged strain, respectively at that time. Throughout the calculation, it was assumed that Poisson's ratio is 0.3 and ratio between compressive and tensile strengths is equal to 15.

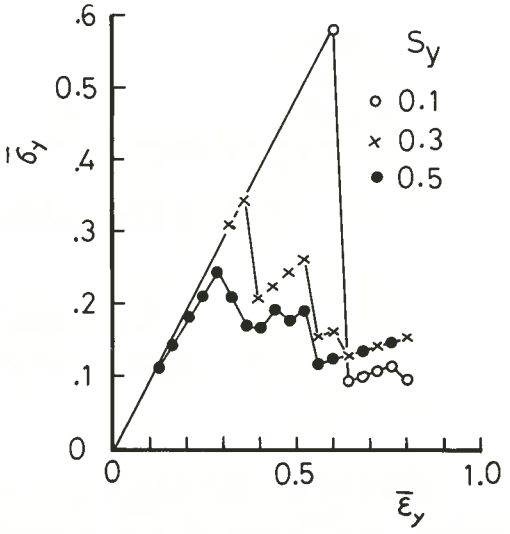

Fig.2 Stress-strain curves at different standard deviations Sy of strength

In Fig.2, stress-strain curves are shown when E_1/E_s= 1.2/0.8. A rock with a higher dispersed element-strength has lower strength and gentler negative slope in post-failure zone.

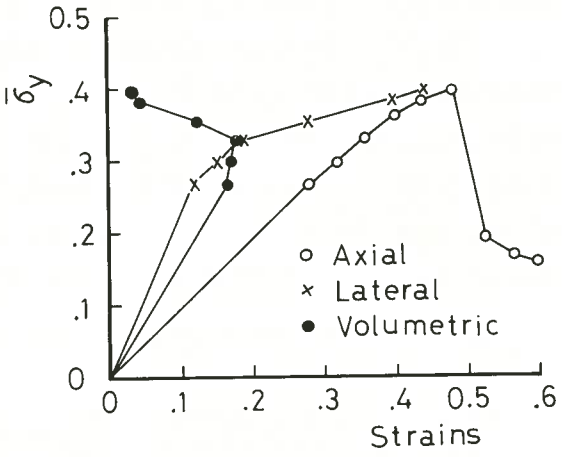

Fig.3 Variations of strains with axial stress: porosity= 3.6 %, $E_1=E_s$

In Fig.3, axial, lateral and volumetric strains are shown when the porosity is 3.6%. The volumetric strain increases rapidly when the stress is close to the strength. This phenomenon has been observed experimentally by many authors and is known as dilatancy. Dilatancy ascribed to the formation and extensions of axial cracks was well simulated.

The further results could be seen in the paper entitled "COMPUTER MODELLING OF ROCK FRACTURE IN UNIAXIAL COMPRESSION", 18th symposium on rock mechanics (1977) paper 3B3 by the same authors.

STUDY ON VARIATION OF LONGITUDINAL WAVE VELOCITY WITH SATURATION IN VARIOUS ROCK TYPES

Tokumi SAITO Iwate University
Mamoru ABE Tohoku University

Variation of longitudinal wave velocity with respect to water content was measured for various rock types by ultrasonic pulse method, and relation between rock texture and longitudinal wave velocity was investigated.

Rock types used in this investigation are five kinds of plutonic rocks, six kinds of volcanic rocks, eight kinds of sedimentary rocks, two kinds of clay ores and crystalline limestones. The size of rock specimen is $3 \times 3 \times 6$ cm.

200KHz barium titanite discs of 30mm in diameter and 6mm in thickness were used for both transmitter and receiver. The rock specimen was dried by the use of oven at 105°C and saturated with immerging in water after de-airated in vacumm. Crystalline limestone was dried by the use of desiccator, because the decrease in velocity was recognized when the specimen was oven-dried.

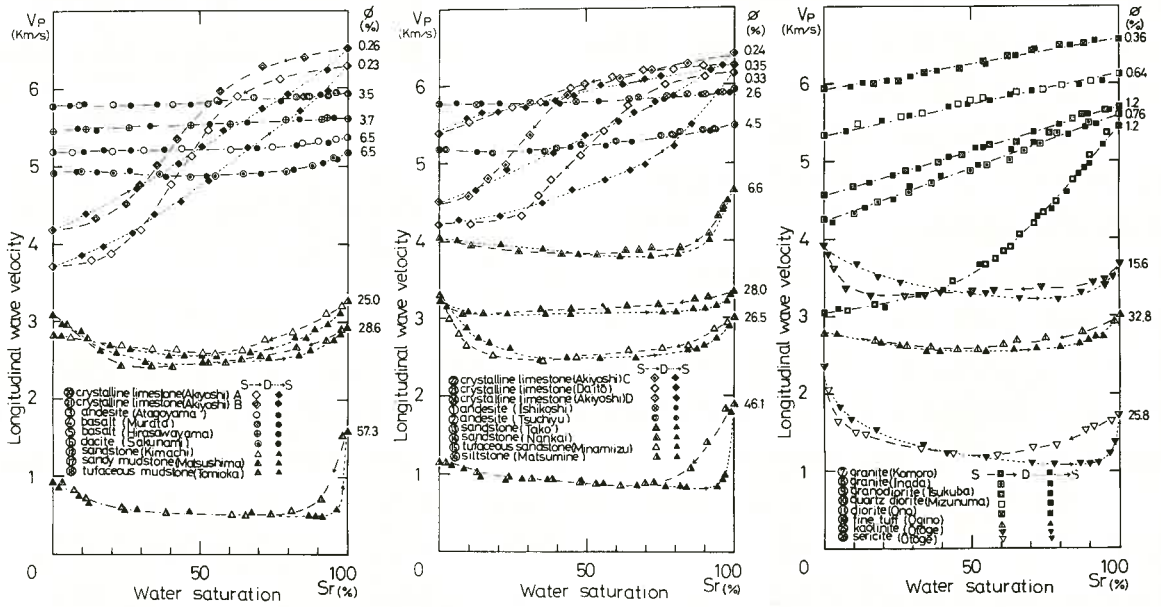

Fig.1 Longitudinal wave velocity as a function of water saturation. S:saturated state, D:dry state.

Velocity was measured in both evaporation and suction processes under room temperature and atomospheric pressure. In some cases the mesurements start from the evaporation process and end at the suction process, and the reverse way was also carried out in other case. But no difference due to the starting point was obsereved.

The graphs of longitudinal wave velocity versus the degree of water saturation for various rock types are shown in Fig. 1. The effective porosity(Ø) and the degree of saturation(Sr) are calculated by the following expressioms :

$$Ø = (Wh - Wd) / (Wh - Ws) \times 100 \quad (\%)$$

$$Sr = (Wi - Wd) / (Wh - Wd) \times 100 \quad (\%) \ .$$

Where Wd and Wh are the weight at dry and saturated states. Ws is the weight of specimen measured in water, and Wi is the weight at the state of measurement of longitudinal wave velocity. From Fig. 1, it is shown that the longitudinal wave velocity is strongly depend upon the rock texture and that the effect of water saturation on the longitudinal wave velocity is respectably larger for crystalline rocks than other types of rocks.

In order to investigate the velocity change due to a certain amount of water content, we introduce the following indices :

$$Is = (Vps - \bar{V}p) / Ø$$

$$Id = (Vpd - \bar{V}p) / Ø \ ,$$

where Vps, Vpd and $\bar{V}p$ indicate the velocities in saturated and dry states and the minimumm velocity obtained from the water saturation-velocity curve respectively. Id is applied to the case that the minimumm

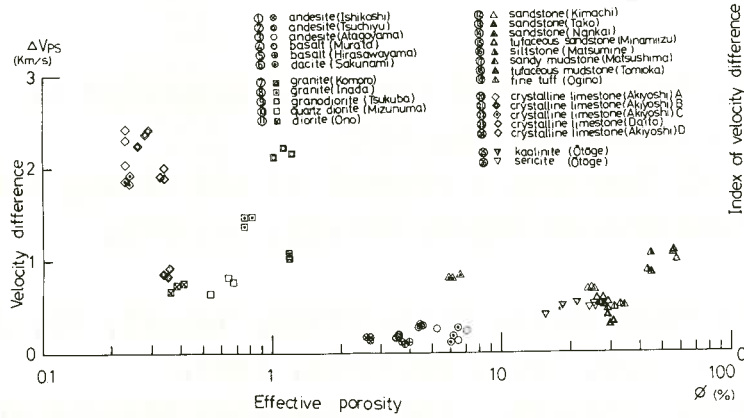

Fig.2 Velocity difference versus effective porosity. Velocity difference means here the difference between saturated and minimum velocities.

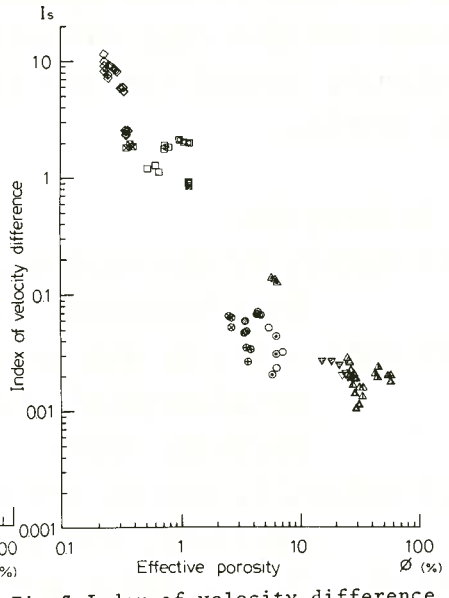

Fig.3 Index of velocity difference in saturated state as a function of effective porosity.

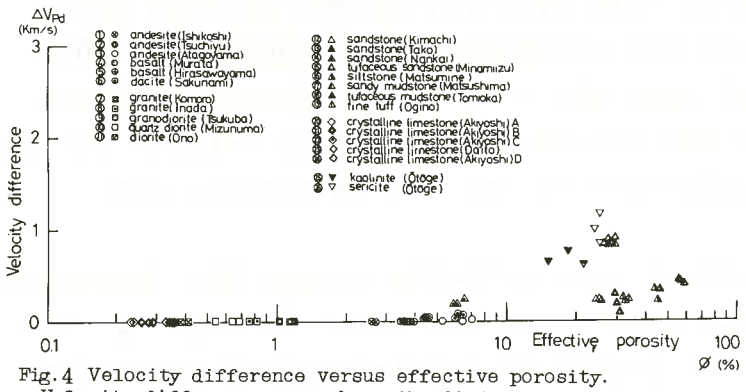

Fig. 4 Velocity difference versus effective porosity. Velocity difference means here the difference between dry and minimum velocities.

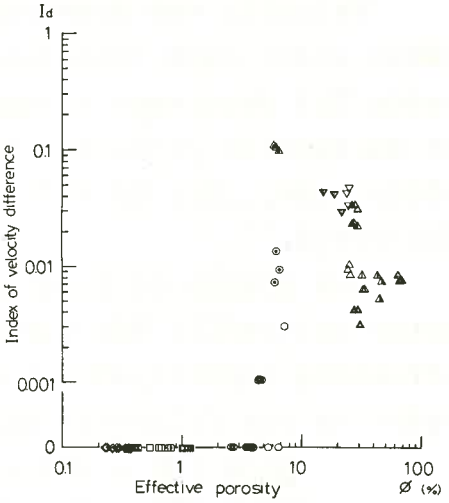

Fig. 5 Index of velocity difference in dry state as a function of effective porosity.

velocity is observed in partially saturated state. These indices mean the velocity change corresponding to 1% of effective porosity. The Is of crystalline rocks are extremely larger than those of other rock types, and the index of crystalline limestone increases with increasing grain size. This is mainly caused by the difference in rock texture, namely the shapes of pores in crystalline rocks are in the form of cracks. The large value of Id is obserbed in the case of rock specimen which contain clay minerals. This suggests that the increase in velocity toward the dry state is closely related to clay minerals in matrix.

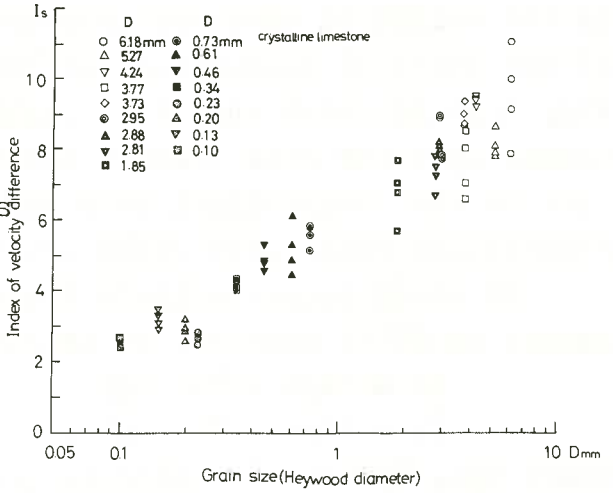

Fig. 6 Index of velocity difference in saturated state as a function of Heywood diameter. (crystalline limestone)

References

1) Saito, T. and M. Abe : Proceeding of the Fifth Symposium of Rock Mechanics in Japan, pp.1-6, 1977.

2) Saito, T., M. Abe and H. Yokoyama : Journal of the Mining and Metallurgical Institute of Japan, Vol.93, No.1072, pp.7-12, 1977.

3) Saito, T. and M. Abe : Geophysical Exploration, Vol.28, No. 3, pp.13-22, 1976, Vol.30, No.2, pp.14-24, 1977.

4) Abe, M., T. Saito and H. Yokoyama : The Technology Reports of the Tohoku University, Vol.42, No.1, pp.193-213, 1977.

MICRO-STRUCTURE DEPENDENCE OF THE MECHANICAL PROPERTIES OF MARBLE

Takakoto SHIMOTANI, Umetaro YAMAGUCHI, University of Tokyo

To study the dependence of mechanical properties of rock upon the micro-structure, marble is the most suitable rock. Because, it is composed of mono-mineral crystals, and has rather simple crystalline structure.

Experiment Uni-axial, bi-axial, and confined compression tests are performed on Akiyoshi marble. The experimental results are shown in Fig.1. As shown here, intermediate principal stress σ_2 influences undoubtedly to the strength failure point of marble, but not so much as hydro-static pressure. ($\sigma_1 \geq \sigma_2 \geq \sigma_3$, tension is positive.) And it is interesting that the curve of strength failure points are upword convex, having peak at $\sigma_2 \fallingdotseq -1.2\sigma_c$ (σ_c; uni-axial compressive strength).

Uni-axial compressive test on cored calcite specimens is also performed. The experimental results are shown in Fig.2 with the sample direction in relation to the optical axes of calcite. Calcite behaves anisotropically not only in elastic region[1], but also in post-failure region. In a-axis direction, it behaves as elasto-plastic having sharp yielding point, but in c-axis direction, it behaves as brittle.

Analysis To analyze the experimental results, elasto-plastic analysis[2] (EPA) is performed by using FEM, based on the following assumptions. 1) extended Von Mises yield criterion, 2) associate flow rule, 3) isotropic strain hardening and softening.

For the calculation, complicated behavior of the calcite is simplified as follows. 1) The distribution of yielding stress is homogeneous from 100 kg/cm^2 to 1,200 kg/cm^2. 2) The elements assigned yielding stress under 500 kg/cm^2 behave as the ideal elasto-plastic body, and the constitutive equation of other elements after yielding is

$$\bar{\sigma} = a_1 \exp(b_1 \bar{\varepsilon}_p) + a_2 \exp(b_2 \bar{\varepsilon}_p) \qquad \text{---------- (1)}$$

where $\bar{\sigma}$ is equivalent stress, $\bar{\varepsilon}_p$ is plastic strain, and a_1 etc. are constants. Eq. (1) can express strain hardening and softening characteristics of calcite.

The result of EPA is shown in Fig.3 with the experimental stress strain curve. The calculated curve well agrees to experimental one, except sharp stress drop after the strength failure.

Discussion As noted above, the yielding stress of calcite varies from 100 to

1,200 kg/cm^2, and calculation using eq. (1) results that strength failure point varies from 100 to 1,400 kg/cm^2. On the other hand, computed and experimental strength of marble is about 700 kg/cm^2. From these results, it can be considered that micro-factures of elements progress gradually with increase of external stress σ^{ex}, but at a given critical value of σ^{ex}, these micro-factures become unstable and progressive, and this critical σ^{ex} is strength failure stress.

The simplest model expressing above mechanism may be the parallel model composed of elements, strength of which varies homogeneously[3]. As shown in Fig.4, in the case that the constitutive element behaves as ideal elasto-plastic body, the relation between external stress σ_p^{ex} and internal stress σ is

$$\sigma_p^{ex} = (-\sigma^2 + \sigma_{max}\sigma - \sigma_{min})/2(\sigma_{max} - \sigma_{min}) \quad \text{---------- (2)}$$

where σ_{max} and σ_{min} is maximum and minimum strength of element respectively. And maximum of σ_p^{ex} is,

$$\sigma_p^{ex}{}_{max} = (\sigma_{max} + \sigma_{min})/2 \quad \text{---------- (3)}$$

On the other hand, in the brittle case shown in Fig.4,

$$\sigma_b^{ex} = \sigma(\sigma_{max} - \sigma)/(\sigma_{max} - \sigma_{min}) \quad \text{---------- (4)}$$

and maximum of σ_b^{ex} is,

$$\sigma_b^{ex}{}_{max} = \sigma^2{}_{max}/4(\sigma_{max} - \sigma_{min}) \quad \text{---------- (5)}$$

while, σ_{max} = 1,400, and σ_{min} = 100 kg/cm^2, so, $\sigma_p^{ex}{}_{max}$ = 750, and $\sigma_b^{ex}{}_{max}$ = 380 kg/cm^2. And because above two kinds of element are mixed in this case, it can be so considered that the strength failure occures at the intermediate value of above two extreme estimations. Therefore it can be said that this model can explain the strength failure mechanism, though it is simple.

On the other hand, the applicability of extended Von Mises failure criterion is examined[4]. Calculated curves of this criterion is shown in Fig.1 as solid lines. From these curves, it can be said that this criterion can well express the experimental results in the region of large σ_1 and σ_2, but fails in the region of small σ_1 and σ_2.

Conclusion 1, The result of EPA well agrees to experimental results. 2, The mechanism of strength failure under compression can be explained by the parallel model. 3, The extended Von Mises failure criterion can express the experimental results under poli-axial compression in the region of large σ_1 and σ_2.

— Reference —

1) Shimotani, T.; On the measurement of anisotropic elastic constants of rock-like materials by uni-axial compression, Jr. of Soc. of Material Scie., Japan, No.307, pp.326-331, 1979

2) Yamatomi, J., Shimotani, T.; An elasto-plastic analysis applicable to the strain softening materials, Jr. of MMIJ (under printing)

3) Shimotani, T.; Study on the strength failure of marble and calcite under

compression (1st Report), Jr. of MMIJ (under printing)

4) Shimotani, T.; Study on the strength failure of marble and calcite under compression (2nd Report), Jr. of MMIJ (under printing)

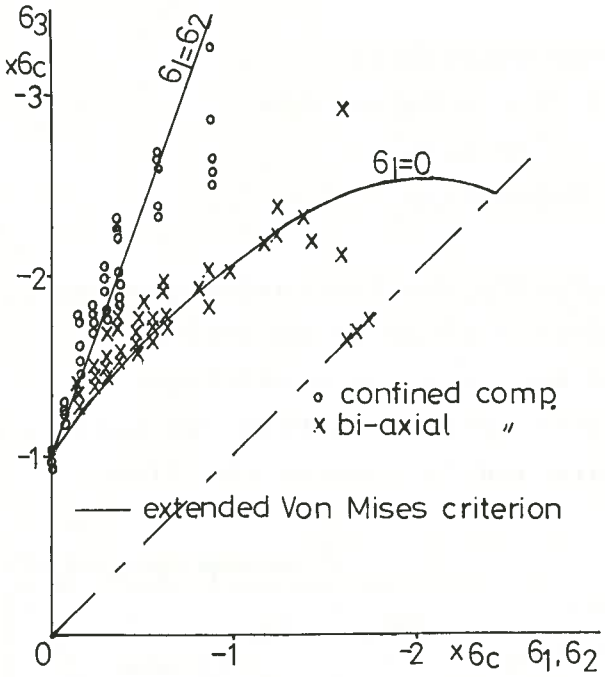

Fig.1 strenth failure of marble

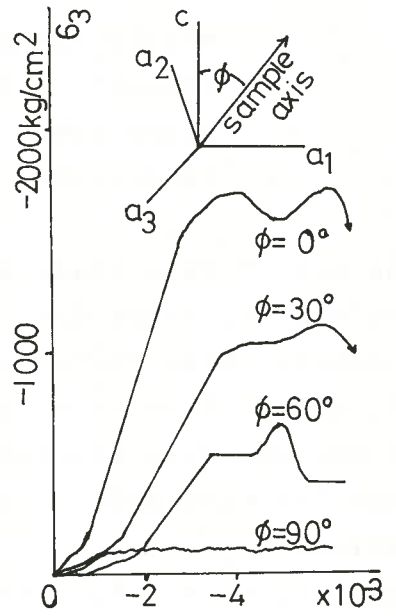

Fig.2 stress strain of calcite

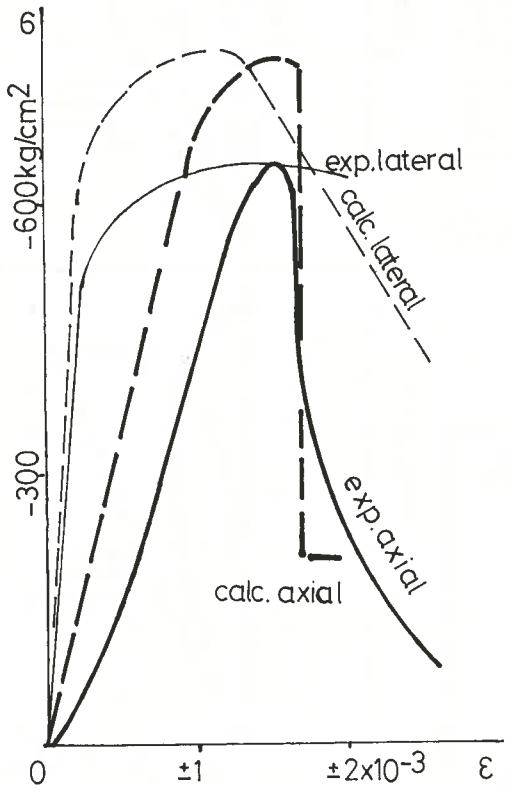

Fig.3 stress strain curve of marble

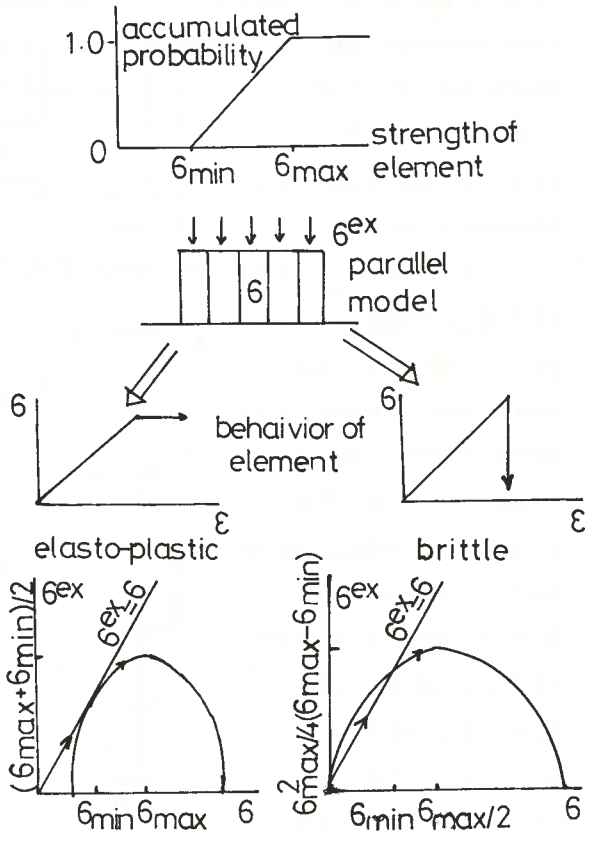

Fig.4 schematic diagram of parallel model

THE FRACTURE BEHAVIOR OF THE GRANODIORITE UNDER UNIAXIAL COMPRESSION

Makoto TERADA, Kyoto University
Takashi YANAGIDANI, Kyoto University
Osamu SANO, Kyoto University
Ichiro ITO, Kyoto University

The aim of this study is to clarify the fracturing process of granodiorite, known for its unstable behavior in situ at a tunnel construction spot, under various loading conditions. A stiff, closed-loop servo-controlled testing machine was used to control the unstable brittle failure and to observe the time dependent fracture under uniaxial compression.

Deformation and A.E.(acoustic emission) of the specimen (47.6 mm diameter, 95 mm length) during various tests were measured. The measuring system and an example of A.E. wave are illustrated in Fig. 1, respectively.

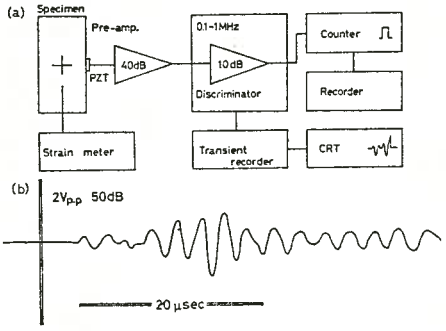

Fig. 1

(1) The uniaxial compression tests under the constant axial deformation rates, 1 mm/50 min and 1 mm/100 min, were carried out. These results are illustrated in Fig. 2, which demonstrate A.E. event begins to increase above

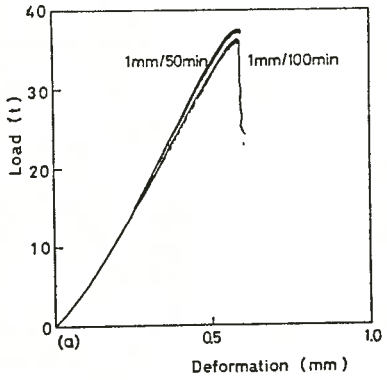

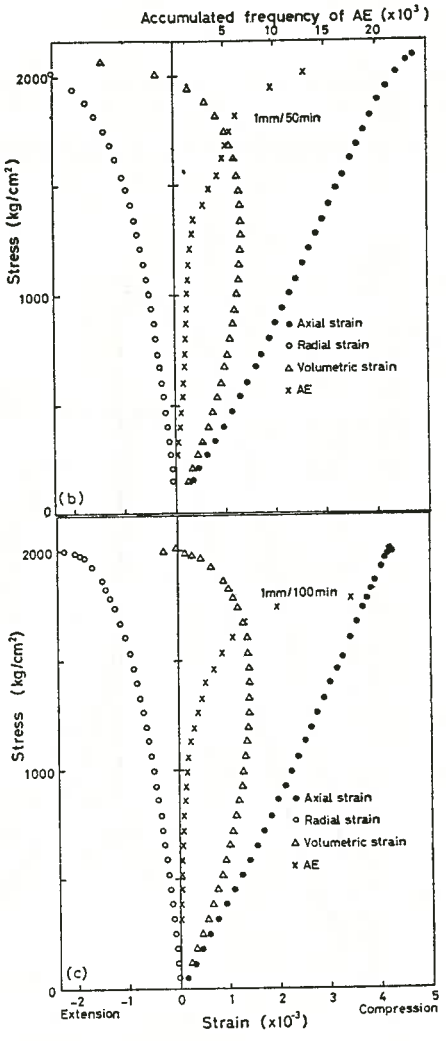

Fig. 2

1/3 level of the maximum stress and, at the same time, the volumetric strain begins to show inelastic change, namely dilatancy. It is concluded that the microfracturing is mainly tensile one that occurs along the axis of the applied load, from the fact that the inelastic deformation of radial strain, rather than that of axial strain, accounts for dilatancy.

(2) The stress relaxation tests under constant deformation were carried out at several levels below the strength. In this case, the axial strain relaxed slightly with time, while the radial strain increased gradually. The similar increase is observed in the accumulated events of A.E. curve. This result also shows that the increase of radial strain is due to the axial microfracturing. Another remarkable result is that the rock failed without the energy flux from the testing machine. The granodiorite is not stable even in the region below the load vs. axial deformation curve. On the other hand, when the stress level of the relaxation test is relatively low, the A.E. count rate decreases gradually, and the specimen has not shown any unstable behavior.

(3) The creep tests were carried out under several stress levels. The typical results are illustrated in Fig. 3. In the case of high stress level, small jumps of the change of axial strain and A.E. event were often observed. These jumps show that the local microfracturings occur somewhere within the specimen. In the case of the low stress level, the axial creep strain is very little. The pattern of the microfracture accumulation characterizes the inelastic behavior.

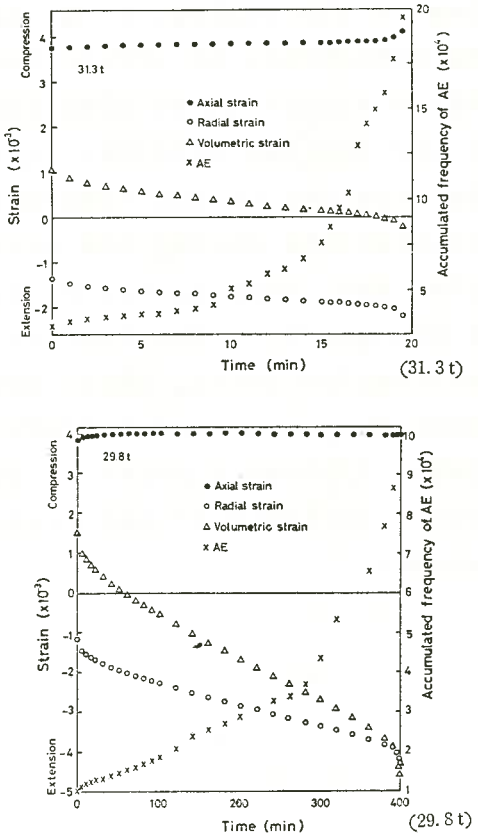

Fig. 3

(4) The cyclic loading tests were carried out and the hysteresis was observed in the stress-strain relationships, especially, in the radial strain. The dilatancy hysteresis and the absence of A.E. event on unloading cycle seem to

show that only tensile micro-fracturing contributes to the dilatancy hysteresis.

The main feature of these observations is supported by a lack of the shear-related microfracturing except those which might occur just under the platen. From this point of view, to obtain the complete load vs. axial deformation curve, the radial deformation instead of the axial deformation should be selected for the feedback signal of the servo-control system. The complete load vs. axial deformation curve of the granodiorite and its stress vs. volumetric strain curve, obtained by this way, are illustrated in Fig. 4. These curves seem to give the criterion of the failure of granodiorite. The vibrations of stress vs. volumetric strain curve show the response of the testing machine. Fig.5 shows the progress on the load-deformation relationship during the stress relaxation and creep tests, by replotting on the graph of the load vs. axial deformation curve, where symbol X shows the points of failure, and symbol O shows a point of stable state, in spite of the long loading period.

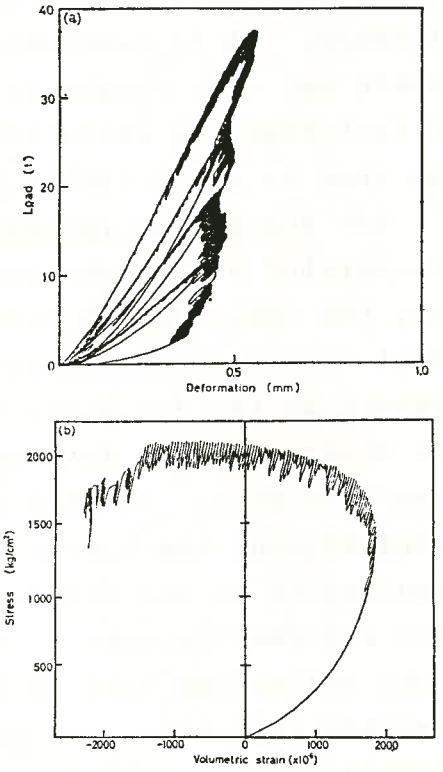

Fig. 4

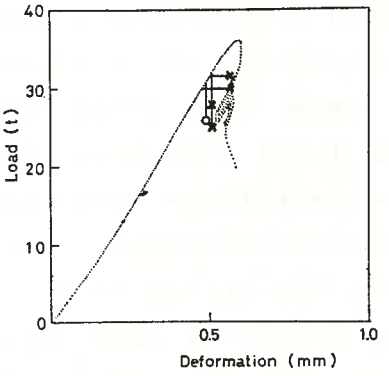

Fig. 5

PHYSICAL AND MECHANICAL PROPERTIES OF SOFT ROCKS AND ITS BEARING CAPACITY

Ryunoshin YOSHINAKA, Saitama University

1. Water retension and physical properties of mudstones[1)]

Water content under $_{p}F$ suction pressure can be a important index to physical and mechanical properties of mudstones such as shrinkage, swelling, residual friction angle, content of montmorillonite etc. Fig. 1 is one example of these relations.

2. Strength and deformation behaviour of soft rocks

2.1 Undisturbed decomposed granite[2)]: Deformation behaviour (axial and volmatric) and strength criterion have obtained from triaxial CD test. Some results are shown in Fig. 2, 3.

2.2 A strength criterion for soft and hard sedimentary rocks[3)]

$$\tau_m / \tau_{mo} = \alpha \left(\sigma'_m / \sigma'_{mo} \right)^{\beta} \quad \cdots\cdots\cdots \quad ①$$

where $\tau_m = \frac{1}{2} \left(\sigma_1 - \sigma_3 \right)$, $\sigma'_m = \frac{1}{3} \left(\sigma'_1 + 2\sigma'_3 \right)$, τ_{mo}, σ_{mo} are τ_m, σ'_m at $\sigma_3 = 0$ and α, β are constants. Eq. 1 is widely applicable. Some examples are shown in Fig. 4.

3. Bearing capacity of soft rock foundation[4),5)]

Model test used soft taffaceous rock with and without a vertical joint and FEM analysis have performed in two dimensional (plane strain) condition. The conditions introduced in analysis are: non-linear stress-strain relation from softening to hardening, a through-going joint by Goodman's joint element and bi-linear Coulomb-Mohr and non-linear (Eq. 1) failure criteria. Some results are shown in Fig. 5 and 6.

References

1. Yoshinaka, R. and Onodera, T. (1978), Water retention and physical properties of mudstones, Proc. 3rd Int. Cong. IAEG, Sec. 2, Vol. 2, p. 204-214.
2. -----, ----- (1977), Undisturbed sampling of decomposed granite soil and mechanical properties, Soil Sampling,

Specialty Session No. 2, 9th Int. Conf. of SMFE, p. 97-102.

3. -----, Yamabe, T. (1979), Strength criteria and scale effect of soft rocks, Proc. 12th Symps. Rock Mech., of JSCE, p. 31-35.

4. -----, Nishimaki, H. (1978), FEM analysis of bearing capacity and load-displacement behaviour of a foundation on soft rock, Proc. 11th Sympo. Rock Mech., of JSCE, p. 41-45.

5. -----, ----- (1979), Model test and numerical analysis of bearing capacity of soft rocks, Proc. 12th Sympo. Rock Mech., of JSCE, p. 26-30.

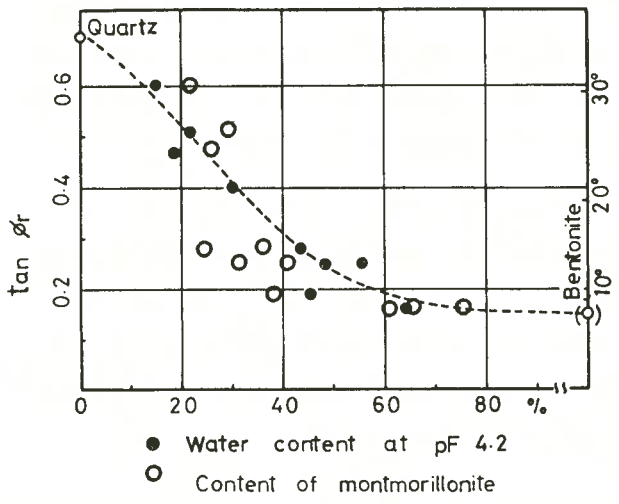

Fig.I Residual frictional angle and content (%) of montmorillonite determined by Methylen-blue method and water content at pF 4.2, of mudstone joints.

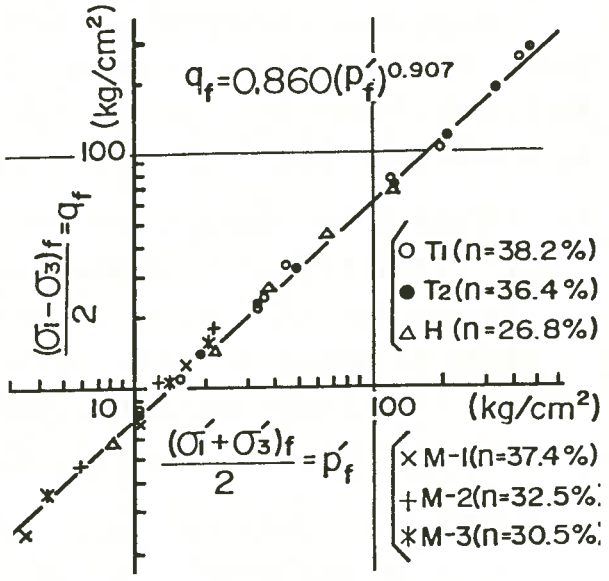

Fig.2 Logarithmic representation for failure stress

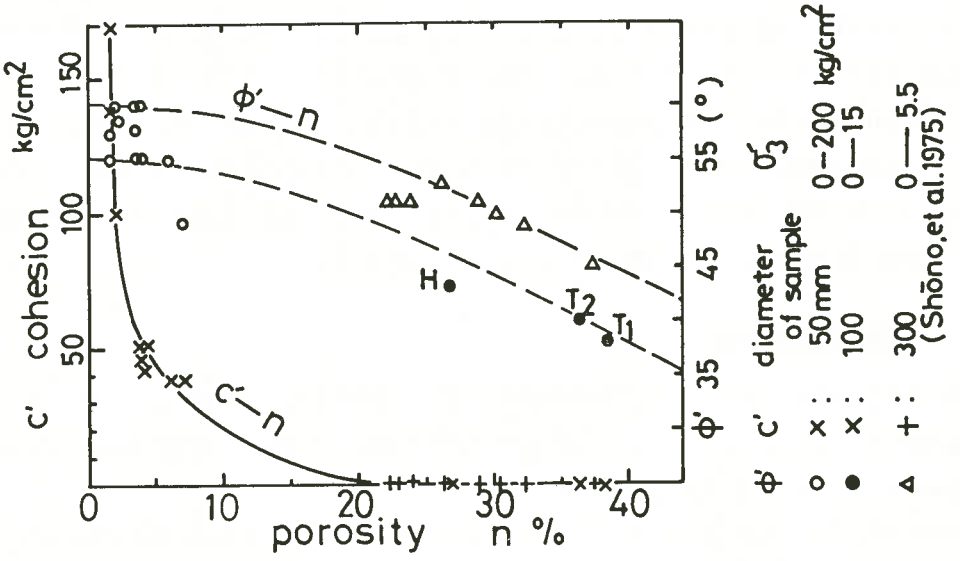

Fig.3 Degradation of strength with porosity (obtained by triaxial compression tests)

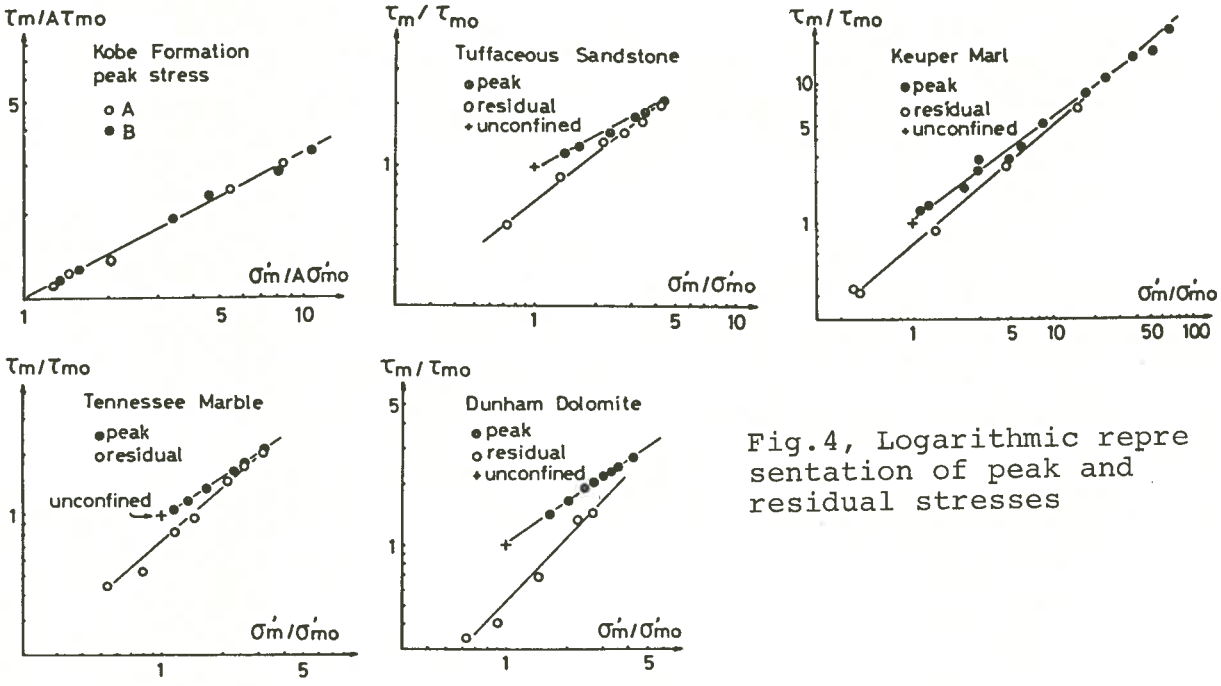

Fig.4, Logarithmic representation of peak and residual stresses

SAMPLE	qu (kg/cm²)	peak					residual			
		α	β = β'	A	N	r	α	β	N	r
London Clay[7]	2.10	1.096	0.647	1.296	15	0.996	0.413	0.798	6	0.997
Keuper Marl[8]	4.17	1.034	0.722	1.128	13	0.996	0.685	0.817	5	0.998
Kobe Formation A	72.0	1.230	0.518	1.539	12	0.994	0.687	0.573	12	0.950
Kobe Formation B	26.8									
Tuffaceous Sandstone	138.	0.959	0.527	0.916	6	0.994	0.681	0.774	6	0.997
Tennessee Marble[9]	1340.	0.976	0.651	0.934	7	0.998	0.762	0.864	7	0.998
Dunham Dolomite[5]	2670.	1.055	0.665	1.174	8	0.998	0.508	1.00	5	0.988
Ormond Siltstone[4]	558.	1.070	0.634	1.203	4	0.995				
Weathered Granite (T2)	0.23	0.937	0.907	0.497	8	0.998				

Table I, Constants of Equation I for soft and hard rocks

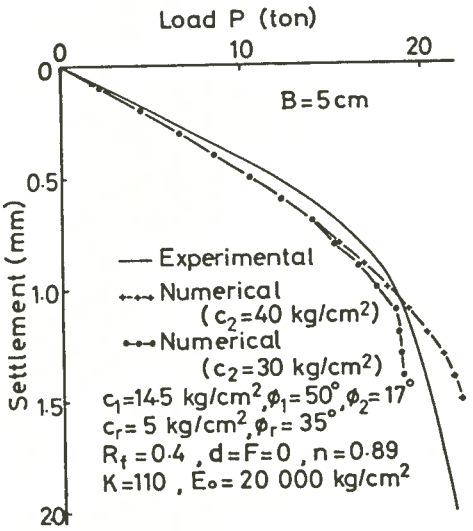

Fig.5, Load-settlement relation on soft taffaceous foundation (no-joint)

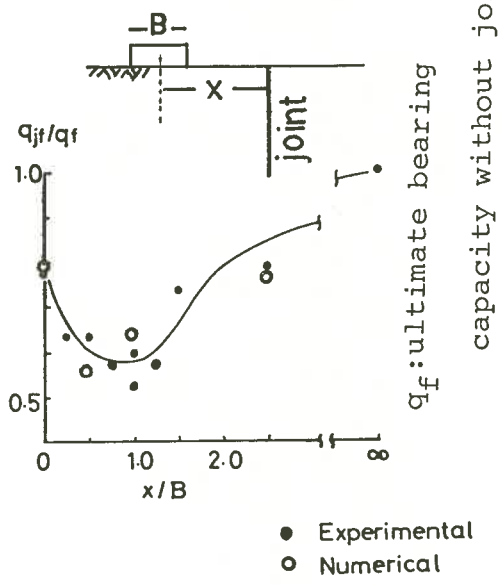

Fig.6, Decrease of bearing capacity caused by a joint

STRESSES AND DEFORMATIONS AROUND TWO OR MORE PRESSURE TUNNELS IN ELASTIC ROCK MASSES

Ken-ichi HIRASHIMA, Yamanashi University
Yoshiji NIWA, Kyoto University

The stability of rock masses around a pressure tunnel is influenced by many factors, *i.e.* the overburden load, the slope of ground surface and the shape of tunnel as well as mechanical characteristic such as strength, deformability and fissuration of the rock masses. When two or more neighbouring presure tunnels exist, their interactions should also be considered.

In this paper, the authors assume that the rock with circular tunnels is a homogeneous and anisotropic elastic body. The stresses and deformations in the neighbourhood of two or more parallel pressure tunnels are calculated by successive approximation using the point matching approach from the exact solution of anisotropic elastic body with a circular opening.

In order to obtain the stresses and deformations in an anisotropic elastic body, let us introduce the complex variables

$$z_k=x+\mu_k y\ , \quad (k=1,2) \qquad \cdots\cdots\cdots\cdots\cdots\cdots (1)$$

μ_k are the roots of characteristic equation for the anisotropic body under consideration. The stresses and displacements in rectangular Cartesian coordinates (x,y) are given in terms of two analytic functions

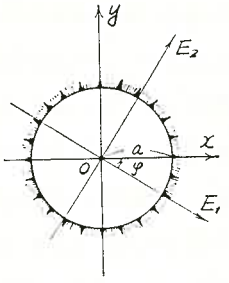

Fig. 1. Circular hole in an infinite anisotropic body.

$$\left.\begin{aligned}
\sigma_x&=2Re[\mu_1^2\phi_1'(z_1)+\mu_2^2\phi_2'(z_2)],\\
\sigma_y&=2Re[\phi_1'(z_1)+\phi_2'(z_2)],\\
\tau_{xy}&=-2Re[\mu_1\phi_1'(z_1)+\mu_2\phi_2'(z_2)].\\
u_x&=2Re\sum_{k=1}^{2}(a_{11}\mu_k^2+a_{12})\phi_k(z_k),\\
u_y&=2Re\sum_{k=1}^{2}\left(a_{12}\mu_k+\frac{a_{22}}{\mu_k}\right)\phi_k(z_k).
\end{aligned}\right\} \cdots\cdots\cdots\cdots (2)$$

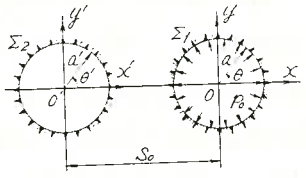

Fig. 2. Geometry of two equal circular openings Σ_1 and Σ_2.

We can seek the expressions for the functions $\phi_k(z_k)$ in the follows.

$$\phi_k(z_k)=\frac{1}{\mu_2-\mu_1}\sum_{m=1}^{\infty}\Gamma_{km}\zeta_k^{-m},\ (k=1,\ 2) \qquad \cdots\cdots\cdots (3)$$

The coefficients Γ_{km} are given as

$$\Gamma_{1m}=\mu_2\bar{a}_m-\bar{b}_m,\quad \Gamma_{2m}=-\mu_1\bar{a}_m+\bar{b}_m \qquad \cdots\cdots(4)$$

$$\left.\begin{aligned}&\bar{a}_1=\frac{1}{2}ap_0,\quad \bar{b}=\frac{1}{2}iap_0,\\&\bar{a}_m=\bar{b}_m=0,\quad (m\geqq 2)\end{aligned}\right\} \qquad \cdots\cdots(5)$$

where, p_0 is hydrostatic pressure acted on the contour of a circular tunnel as shown in Fig. 1 and 2.

From stresses and deformations around or near the opening in an infinite anisotropic elastic body obtained in above description, we can solve the problem of multi-connected region such as an infinite body with several tunnels utilizing the point matching technique. The method of analysis due to the point matching approach is repeating operations such that the boundary conditions with free surfaces of two or more tunnels are satisfied by the finite number of the boundary points of the tunnels. Obtaining stresses and deformations in the multi-connected body under consideration, the similar functions such as the ones defined by eq.(3) were used in these operations. The literatures [1～3] are to be refered for further details relating to this problem.

In order to check the accuracy of the results, the stress values σ_θ around two equal circular tunnels in an isotropic body were compared the results obtained by the present approach with the results by another methods. From the Table 1, it may be concluded that the present method is sufficientlly accurate for practical

Table I. Comparison of the results obtained by several methods of solution for the case of isotropic body containing two equal circular openings.

$\theta=\theta'$	Stress σ_θ around Σ_1			Stress $\sigma_{\theta'}$ around Σ_2		
	Bipolar[10] solution	Förster & Döring[7]	$\Delta\theta=2.5°$ $m=20$ $i=6$	Bipolar[10] solution	Förster & Döring[7]	$\Delta\theta=2.5°$ $m=20$ $i=6$
0°	0.994	0.994	0.994	1.110	1.110	1.108
15°	0.996	0.995	0.996	0.722	0.722	0.721
30°	1.000	1.000	1.000	−0.003	−0.003	−0.002
45°	1.009	1.009	1.009	−0.481	−0.481	−0.480
60°	1.024	1.025	1.025	−0.608	−0.609	−0.608
75°	1.050	1.051	1.051	−0.522	−0.522	−0.522
90°	1.092	1.092	1.092	−0.354	−0.353	−0.353
105°	1.152	1.152	1.152	−0.174	−0.174	−0.174
120°	1.225	1.225	1.224	−0.018	−0.017	−0.017
135°	1.269	1.268	1.268	0.106	0.106	0.106
150°	1.190	1.190	1.189	0.192	0.192	0.192
165°	0.943	0.943	0.943	0.244	0.244	0.244
180°	0.777	0.777	0.778	0.262	0.260	0.261

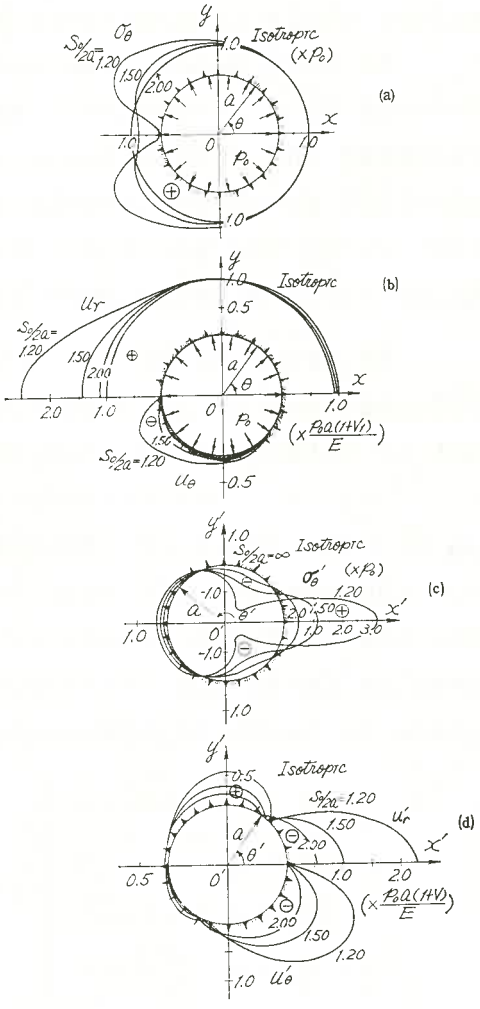

Fig. 3. Stresses and deformations around the openings Σ_1 and Σ_2 with equal circular cross sections in an isotropic elastic body, when the hydrostatic pressure p_0 applies at the inside of the right-side opening Σ_1.

usage.

Let us show some typical examples for circumferential stresses and deformations at the contours of the circular tunnels. Fig.3 shows the distributions of stress and deformation at the contours of the openings in an isotropic body containing two equal circular shapes with varing spaceing s_o. Fig.4 is in the case of orthotropic body. Fig.5 are the ditributions of σ_θ around the tunnels for the case of orthotropic body with inclined principal axes.

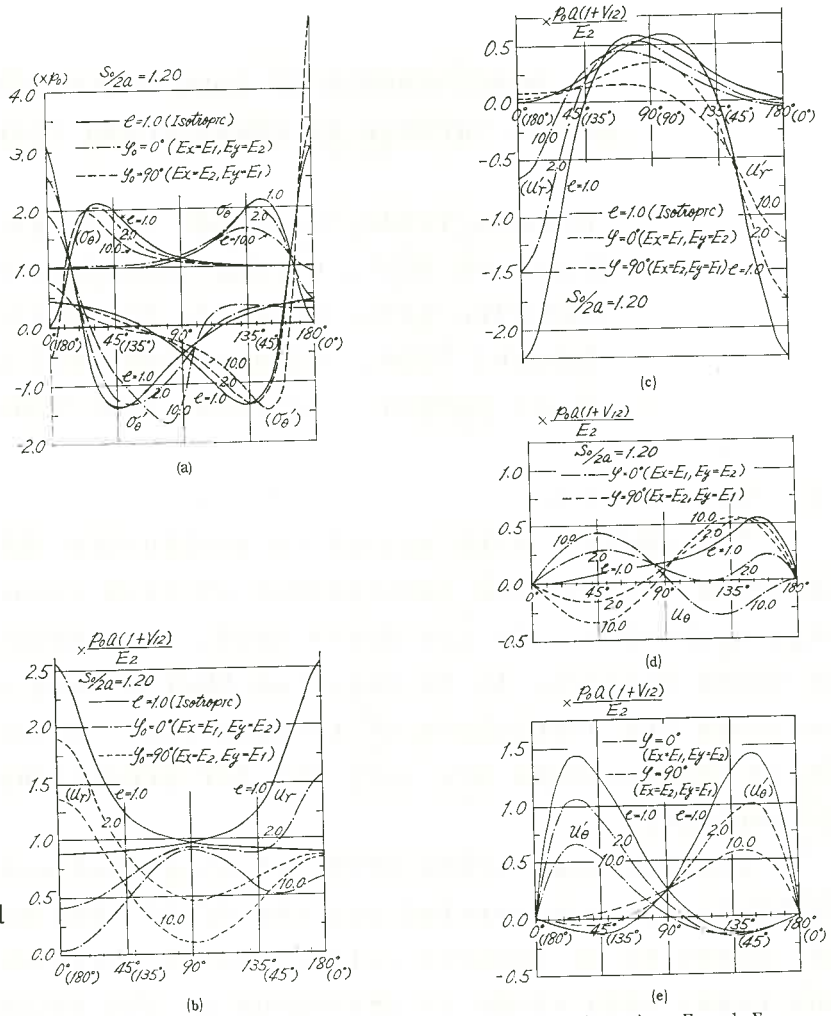

Fig. 4. Stresses and deformations around the two equal openings Σ_1 and Σ_2 with varing parameters $e=E_1/E_2$ and φ.

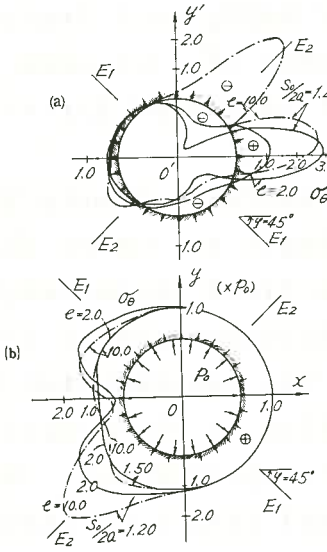

Fig. 5. Stresses around the two equal circular openings Σ_1 and Σ_2 for the case of orthotropic body with $e=2.0, 10.0$ and $\varphi=45°$.

REFERENCES:

1) Y. Niwa and K. Hirashima: Mem. Fac. Eng., Kyoto Univ., Vol.33(1971), pp.101-117

2) K. Hirashima: Proc. Japan Soc. Civil Eng., No.220(1973), pp.131-141

3) K. Hirashima: Proc. of the 22th Japan National Cogress for Applied Mechanics, (Theoretical and Applied Mechanics, Vol. 22), Univ. of Tokyo Press(1974), pp.211-220

MEASUREMENTS OF ROCK FRACTURING NOISES INDUCED BY UNDERGROUND COAL MINING

Toshiro ISOBE, Hokkaido University
Noriyasu MORI, Kitami Technical College
Kazuhiko SATO, Hokkaido University
Takashi GOTO, Kitami Technical College
Ikuro KAMEDA, Sumitomo Coal Mine Co.Ltd

1. Introduction

The factors with regard to rockbursts outbreaks have been put in order through the examination of them occured in this and foreign countries. On the other hand, in connection with the study of these factors, it is reported that mining method was changed to decrease the occurrance of rockbursts. Notwithstanding, the field observations are very few for predicting the occurrance of rockbursts.

The authors, since 1970, viewing rock noises as a precusor of rockbursts, have carried out the field observations of microseismic activity at several collieries in Hokkaido district. On the one hand, this study is analogous to the Accoustic Emission measuring of the rock test pieces in laboratory studies, and on the other hand, rock fracturing noise series which comes from extracting zone of coal seam is also analogous to the Earthquake Series as it is called foreshock-mainshock-aftershock in their observations.

In this report, it is described some features concerned to rockburst precusors that are obtained from the results of rock noise field measurements.

2. Measurements of rock fracturing noises

The system which has a function of real time processing possibility of the source location and energy of seismic events has been completed now. Wave forms monitored by the observations are divided into two classes. One is that the initial ground movement in each observation point has "downward pulling tendency" toward the destruction point. The other is that the initial ground movement in each observation point has "downward pulling and upward pushing tendencies" along the direction of destruction point. The phenomena "pull and push" are often recognized in the faulted zone.

3. The indexes of rockburst prediction

In this section, from the results of investigations obtained from the measurement in No.5 Section of Noborikawa Pit in Mitsui Sunagawa Colliery, the indexes which predict the probability of rockbursts will be described.

A. Source locations of rock failures

Fig.1 shows the source locations of seismic events induced by underground coal extractions. There are many seismic events homogeneously scattered in the figure. But, as shown by the letters A, B, etc. in fig.1, seismic events are accumulated on a certain area simultaneously as shown following items.

(1) High stress concentration zone such as coal mining edge.

(2) Isolated coal pillars.

B. Cumulative seismic energy released versus date

Fig.2 shows the released seismic energy as a function of time. In this figure, it is the most striking feature that this cumulative curve has a kind of revolution. When the seismic activity stops still and the tranquil condition continues for a long time, while the mining excavation proceeds regularly, attention must be paied to hazard of sudden and severe rock failures.

C. Frequency of occurrence of seismic events

A frequency distribution of maximum trace amplitude of rock noises, occurring in a certain time and a certain area, is fitable to Ishimoto and Iida's formula in seismology, that is, it can be indicated by a straight line on log-log coordinates whose slope is called as m-value. Fig.3 shows the variation of m-value accompanied with seismic events series. Hence, if m-value becomes smaller, the more increases the probability of occurrence of severe rock failures.

4. Conclusions

In short, the indexes in relation to rockburst prediction are following items.

(1) It is necessary to find out exact source locations of seismic events and its released seismic energy in the active area. And it is needed that from the blank space of source locations stored elastic strain energy will be estimated.

(2) Monitoring the variation of m-value and the variation of cumulative released seismic energy curve together, it is possible to predict the occurring time of rock failure as well as magnitude of it.

In order to make clear above mentioned matter, efforts must be piled on the field observations of rock noise measurement.

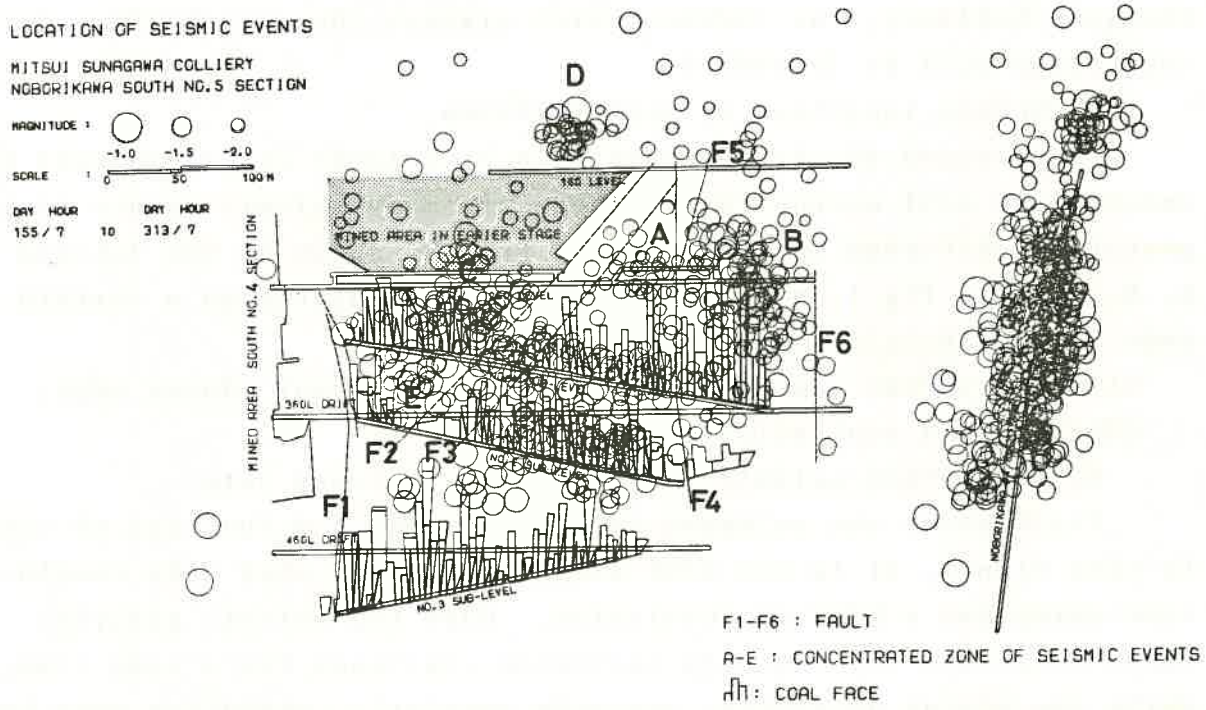

Fig.1 Distribution of seismic events in Block 5 during mining activity at Sunagawa Colliery(1976).

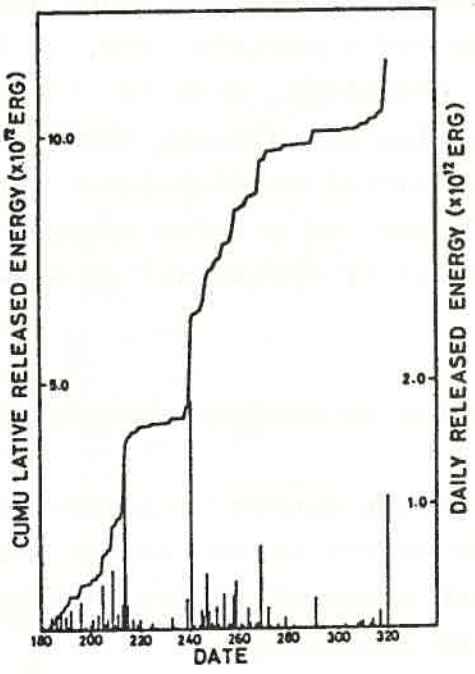

Fig.2 Cumulative seismic energy versus date of data occurred in Block 5 at Sunagawa Colliery(1976).

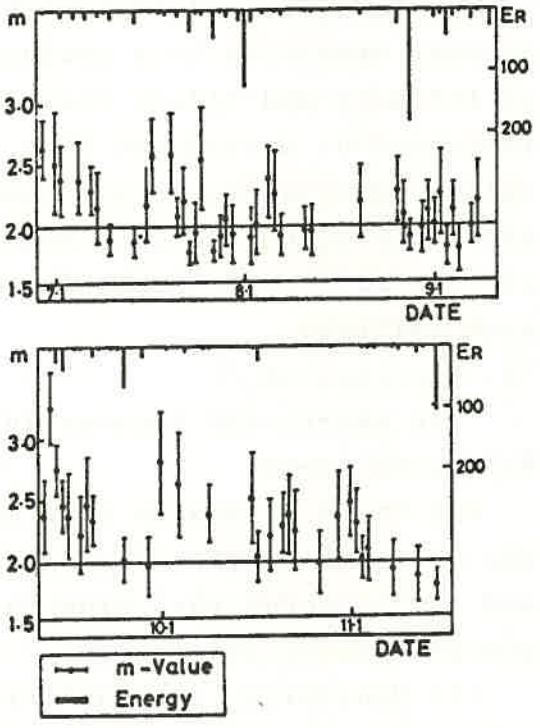

Fig.3 Corresponding m-value and released seismic energy of failures in Block 5 at Sunagawa Colliery(1976).

GEO-STRESS ESTIMATION USING ACOUSTIC EMISSION METHOD

Tadashi KANAGAWA, Masao HAYASHI and Yoshihiro KITAHARA
- Inst. of Electric Power Industry, Abiko

To investigate the geological activity of faults, or to construct underground electric power stations or deep tunnels and evaluate their stability, it is very important to estimate the geo-stress components of the surrounding rock.

Such a brittle material as rock, mortar and concrete omits acoustic signals due to its micro-fractures under an applied stress. The acoustic emission (AE) signals show the following characteristics:

(1) the emission rate increases gladually (1st stage), then remains almost unchanged (2nd stage) and finally increases exponentially (3rd stage) as the applied stress rises linearly up to the ultimate value of gross fractures.

(2) the 1st and 2nd stages display clearly an irreversible nature named the "Kaiser effect", that is, a solid material once stressed gives little or no emission during a subsequent loading up to the previous stress level. However, the 3rd stage does not clearly show the Kaiser effect because of the stress redistribution in the increased fracture regions.

A rock specimen sampled at various underground elevations has been loaded with the geo-stress for a long time. Therefore, it is expected to be able to estimate the geo-stress

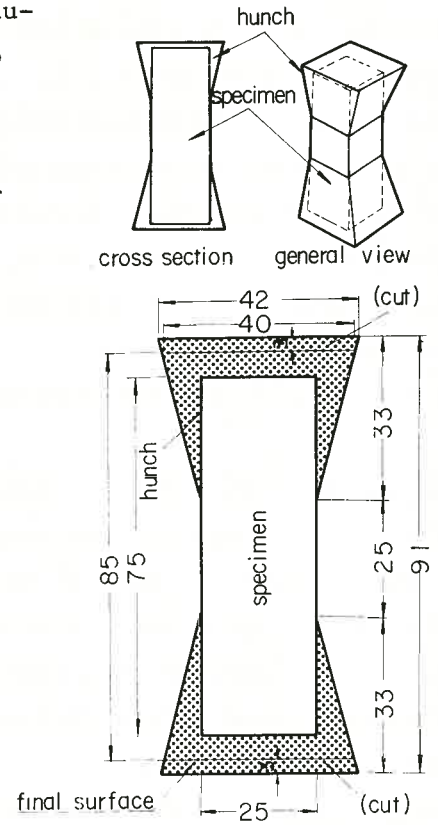

Fig. 1 Cross-section of the specimen.

by the Kaiser effect when the rock specimen is reloaded and the AE characteristics are measured.

In the application of the Kaiser effect to the estimation of the geo-stress in rock samples, one of the most difficult problems is how to eliminate the obstruction of erroneous AE signals caused by the strong stress concentration at the end corners of the rock specimen. A new technique to solve the problem has been developed, which utilizes a lowering of the corner stress with special hunches bonded on both pressed ends of the rock specimen as shown in Fig. 1. By means of a signal location technique using two AE transducers attached to both top and bottom faces of the rock specimen, it was confirmed that AE signals were not emitted at the end parts but expectedly emitted in the middle region of the sample.

At first, following test was carried out.

111 specimens of tuff were sampled with various direction components in several boring cores. Their size is 25 mm x 25 mm x 75 mm. After the processing of pasting of the hunches, the tuff specimen was compressed at a constant cross-head rate of 0.2 mm/min by the Instron testing machine.

The geo-stress component was determined from the load level where the AE summation curve showed the 1st knee-shape as shown in Fig. 2(a). Furthermore, the Kaiser effect was reconfirmed at the 2nd stage level of 2 tons as shown in Fig. 2(b).

The values of geo-stress components determined by AE were compared with the ones estimated by the in-situ over-coring method developed by Dr. Oka which utilizes strain

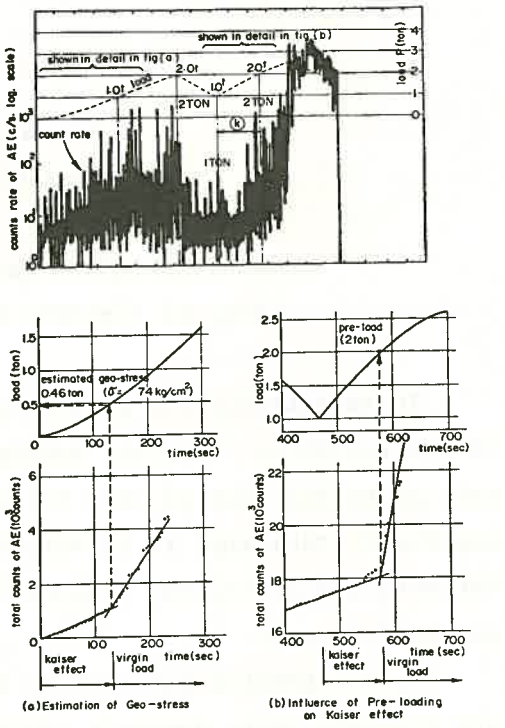

Fig. 2 Verification of the Kaiser effect and estimation of geo-stress in a tuff specimen.

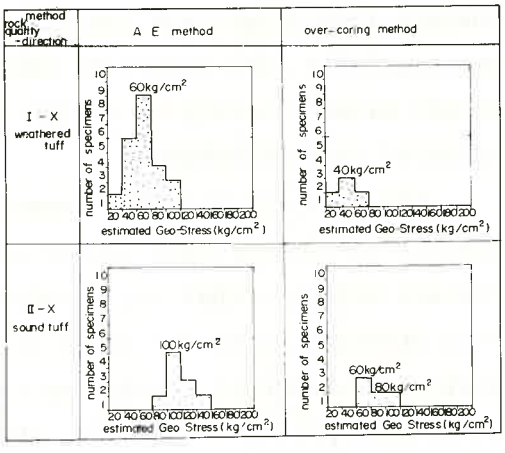

Fig. 3 Estimated geo-stress distributions in the X direction classified by the rock quality.

gauges bonded on the bottom of initial borehole with a small diameter and measures the stress released during boring of the overcore with a larger concentric diameter. In result, the values of AE method obtained larger value than that by overcoring method as shown in Fig. 3.

Fig. 4 shows the value of geo-stress determined by AE method and overcoring method after excavation of the ground. As the result of comparative analysis, we found that the value of AE method corresponds to historical maximum stress before excavation, the value of overcoring method developped by C.R.I.E.P.I. corresponds to actual stress in situ after excavation.

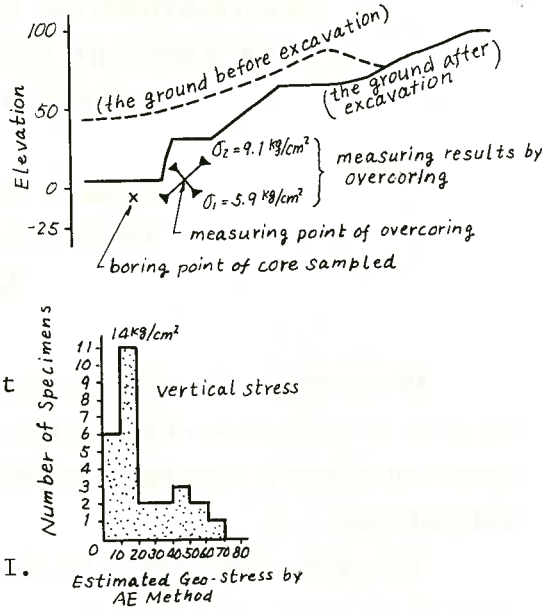

Fig. 4 The relation of measuring result between AE method and overcoring method.

Furthermore, Fig. 5 shows the value of geo-stress components determined by the AE method. On the other hand, maximum and minimum principal stress determined by overcoring method was in the range from 11 to 13 kg/cm^2. The result of the comparison indicates a good correlation between the geo-stress by the AE method and overcoring method.

The over-coring method takes long time and great man-power and cost, whereas the new AE method has a following merits:

(1) relatively inexpensive to use.

(2) convenience of rock-sampling to be able to use the usual boring core.

(3) ready adaptability to statistical estimation.

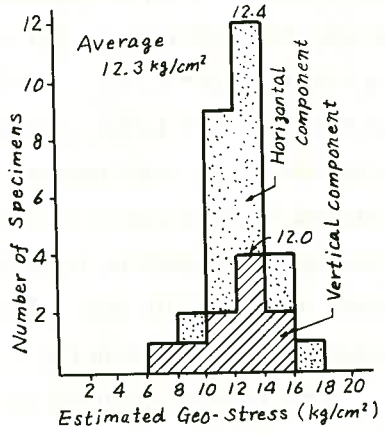

Fig. 5 Measuring result of AE method (mud stone)

Reference

(1) T. Kanagawa, M. Hayashi, H. Nakasa: Estimation of Spatial Geo-Stress Components in Rock Samples Using The Kaiser Effect of Acoustic Emission. CRIEPI E375004, December 1976

(2) T. Kanagawa, M. Hayashi, Y. Kitahara: Development for Measuring Geo-Stresses Soft Rock-Masses and Its Applications. CRIEPI E377004, May 1978

INVESTIGATIONS ON THE NEW METHOD OF DETERMINING ROCK STRESS BY THE STRESS RELIEF TECHNIQUE AND APPLICATIONS OF THIS METHOD

Yukitoshi OKA, Yoshitomo KAMEOKA
Toshiaki SAITO, Yoshio HIRAMATSU
Kyoto University

In determining the rock stress completely at a certain point by the technique of relieving the stress on the bottom of a borehole, it is considered that the measurement of strain must be carried out at least in three boreholes which are bored near the point and have different directions with each other.

The authors have studied on this method of stress measurement and have analyzed the stress on the bottom of a borehole by means of a finite element method applied to axisymmetric elastic bodies under asymmetric loads. It has found that rock stress can be determined by measuring at least six strain components on the bottom of a single borehole. Depending upon this principle, a strain cell with eight gages which are laid in it as shown in Fig. 1 has been developed. The relation between strain components on the bottom of a borehole $\epsilon_1, \epsilon_2, \ldots, \epsilon_8$ and the components of rock stress $\sigma_x, \sigma_y, \ldots, \tau_{xy}$ is represented by equation (1). The strain coefficients $a, b, \ldots, d'$ vary a little with Poisson's ratio ν. For ν=0.25, they take such values as following. As the values of $\{\epsilon\}$

$a = 0.487 \quad b = 1.712 \quad c = 0.305 \quad d = 1.223$

$a' = 0.511 \quad b' = 1.584 \quad c' = 0.425 \quad d' = 0.095$

are evaluated by the measurements, the rock stress can be determined by the equation (1). During the progress of overcoring, the variations in strain were measured at intervals of 5 to 10 mm. The results obtained at Yanahara Mine are shown in Fig. 1, as an example.

This method is applied to the measurements of rock stress in many mines where massive ore bodies were worked and many underground powerstations. The results of measurements present useful materials for interpreting earth pressure phenomena and for planning

$$\begin{Bmatrix} \epsilon_1 \\ \epsilon_2 \\ \epsilon_3 \\ \epsilon_4 \\ \epsilon_5 \\ \epsilon_6 \\ \epsilon_7 \\ \epsilon_8 \end{Bmatrix} = \frac{1}{E} \begin{bmatrix} a' & a' & -c' & -d' & d' & b' \\ -a & b & -c & d & 0 & 0 \\ a' & a' & -c' & -d' & -d' & -b' \\ b & -a & -c & 0 & d & 0 \\ a' & a' & -c' & d' & -d' & b' \\ -a & b & -c & -d & 0 & 0 \\ a' & a' & -c' & d' & d' & -b' \\ b & -a & -c & 0 & -d & 0 \end{bmatrix} \begin{Bmatrix} \sigma_x \\ \sigma_y \\ \sigma_z \\ \tau_{yz} \\ \tau_{zx} \\ \tau_{xy} \end{Bmatrix} \qquad (1)$$

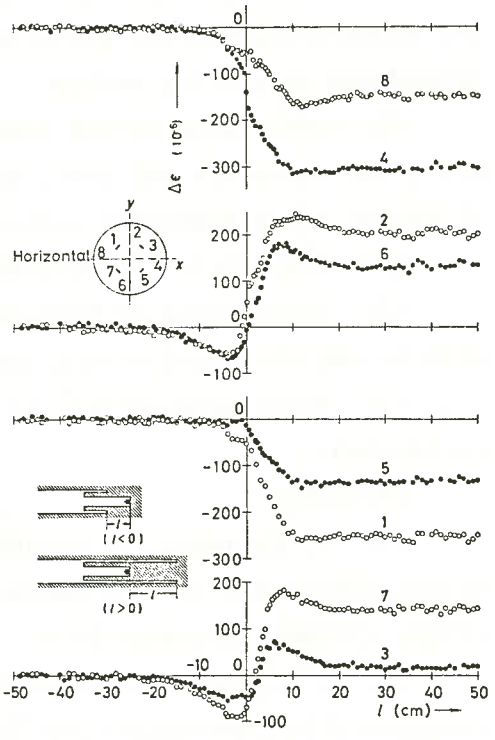

Fig. 1 An example of the variations in strain during the progress of overcoring

large underground excavations. As an example, the case of interpreting crack generation at the pilot drift of A powerstation is described as follows.

In this station, the initial rock stress has been determined as shown in Fig. 2, using this method. It was found that the maximum principal compressive stress is 85 kg/cm^2 and nearly vertical. The vertical normal stress is 72 kg/cm^2 and this value coincides with that determined by the analysis which makes use of a finite element method considering topography and gravity.

After the measurement of rock stress, the excavation work of the powerhouse was carried out from crown to floor. When this work progressed about 2/3, slight cracks were generated on the floor of pilot drift near the powerhouse, as shown in Fig. 3. Fig. 4 shows situation in the vicinity of the drift and position of cracks. To clarify this phenomenon, the stress around the drift is analyzed using a finite element method under the condition of the rock stress estimated above. Because of existence of the fault which crossed obliquely the drift, two simple models were considered as shown in Fig. 5. The first model has a fault on the opposite side of powerhouse regarding to drift, while the second model has a fault between drift and powerhouse. Dividing into 7 steps accompanied with the progress of excavation of powerhouse, the stress and deformation respectively was analyzed. Fig. 6 shows the distribution of the first principal stress around the pilot drift at the last step.

According to this analysis, it has been found that this initial rock stress generates the tensile stress at the left side on floor of pilot drift when the powerhouse is excavated about 1/2 and its magnitude in first model is more than that in the second model. These results can satisfactorily explain the fact observed on the spot.

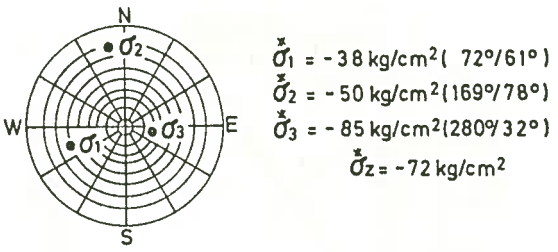

Fig. 2 Initial rock stress at A powerstation obtained using the new method.

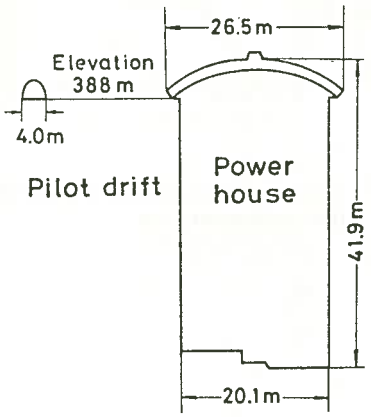

Fig. 3 Layout of pilot drift and powerhouse.

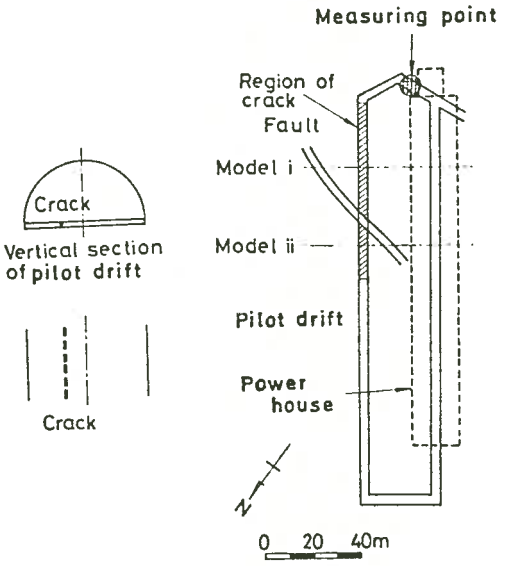

Fig. 4 Situation in the vicinity of the drift and position of cracks on the floor.

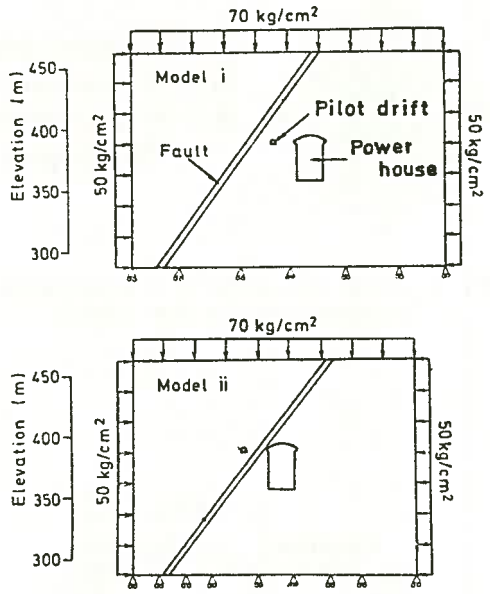

Fig. 5 Two analytical models for interpreting the crack generation.

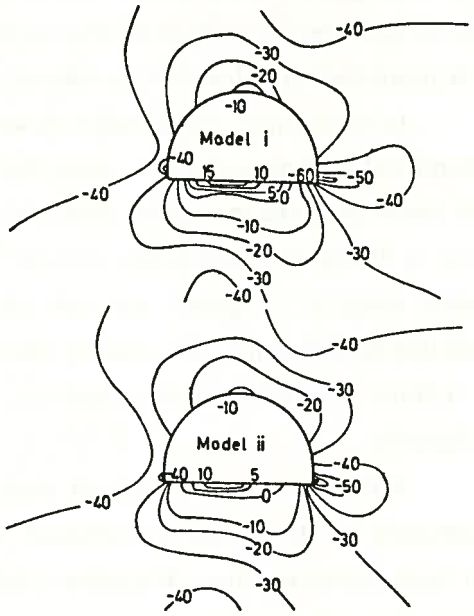

Fig. 6 The distribution of the first principal stress around the pilot drift at the last step.

GENERATION MECHANISM OF ROCK BURSTS AND WATER-INDUCED EARTHQUAKES UNDER THE TECTONIC STRESS FIELD

Yutaka TANAKA, Kyoto University
Yukitoshi OKA, Kyoto University

Recently in mining and civil engineering field the rock stress has become to be mesured by the stress relief technique, The results of in situ stress measurement in Japan are summarized in Table 1 and Fig.1. Numbers indicate each stress measuring site as follows: Undersea Tunnel; No.1-Seikan, Mines; No. 2-Kosaka, No.6-Hiraki, No.7-Yanahara, Underground Power Stations; No.3-Shintakasegawa, No.4-Okuyahagi, No.5-Okuyoshino, No.8-Okutataragi. Except Nos.3 and 8, stress measurements were carried out by the doorstopper method using strain cell with eight gauge developed by Oka et al.[1] σ_1, σ_2 and σ_3 in Tablel are three principal stresses, and their directions are shown in Fig.1 by stereographic projection on lower hemisphere. σ_v and $\overset{*}{\sigma}_v$ are vertical component of stress and theoretical overburden pressure respectively. Location of the site and azimuth of maximum compressive stress are shown with numbered thick arrows. Thin arrows show distribution of strain axes in the Japan Islands analyzed from data of the first order triangulation survey by Nakane.[3] Direction and length of the arrows indicate axis of maximum compressive strain and maximum shear strain velocity respectively.

It seems that the results of stress measurements connected closely with the tectonic stress inferred from Geodetic, Seismological and Geological studies.[2] The stress value, as for the vertical component, almost coincides with theoretical value ($\overset{*}{\sigma}_v$), therefore the other components can be expected to show a reasonable value. However, Nos.4,5 and 6 seem to have some topographic effect, especially No.6 is located near an active fault having microearthquake-occurrences and its depth is also shallower than the others. Thus, the stress state in the upper crust affected by topography, geological structure etc.. Nevertheless, the azimuth of σ_1 coincides with the direction of maximum compressive strain as seen in Fig.1.

In the northwestern district of Kinki including site Nos. 6 and 8, active faults, most of which are accompanied with microearthquakes, have developed as conjugate sets in NW-SE(left lateral) and NE-SW(right lateral) trend. The earthquakes in the district have an occurrence mechanism of strike slip type,

and their directions of compressive axis are nearly E-W (ref. Fig.2 upper left). It is conceivable that the tectonic stress field in the district takes E-W or NW-SE trajectory of crustal stress.

Rock bursts had begun to occur at the Ikuno mine in the district which is 10km south from Okutataragi(No.8) since January of 1970. Ground tremors caused by the rock bursts of large magnitude were observed by net of microearthquake observations. Souce mechanism of the rock bursts could be explained as a dip slip type. Namely, σ_1 estimated from seismic data were perpendicular to the vein-plane where the events occurred, and σ_3 was nearly vertical within that plane. It is interesting that the direction of principal stress of rock bursts coincided with that of tectonic stress in the vicinity. Besides, it is noticed that the frequent occurrence of rock burst and the active epoch of the seismic belt trending in the NE-SW direction near Ikuno coincide with each other.

In the beginning of 1973, mining operation has stopped and underground water began to be injected into the deep abandoned mine, at that time the lowest level had attained down to the depth of 1000m underground. Just after the water-injection small tremors occurred in succession. This activity seems to

Table 1

No.	depth	σ_1	σ_2	σ_3	σ_v	$\overline{\sigma}_v$	ref.
1	264m	147	93	84	86	65	1)
2	312	356	123	91	106	88	1)
3	235	140	48	5	-	-	2)
4	280	96	64	32	83	73	1)
5	560	85	50	38	72	69	1)
6	100	34	30	17	28	24	
7	370	331	172	9	147	110	1)
8	180	150	-	-	85	65~85	2)

unit: kg/cm²

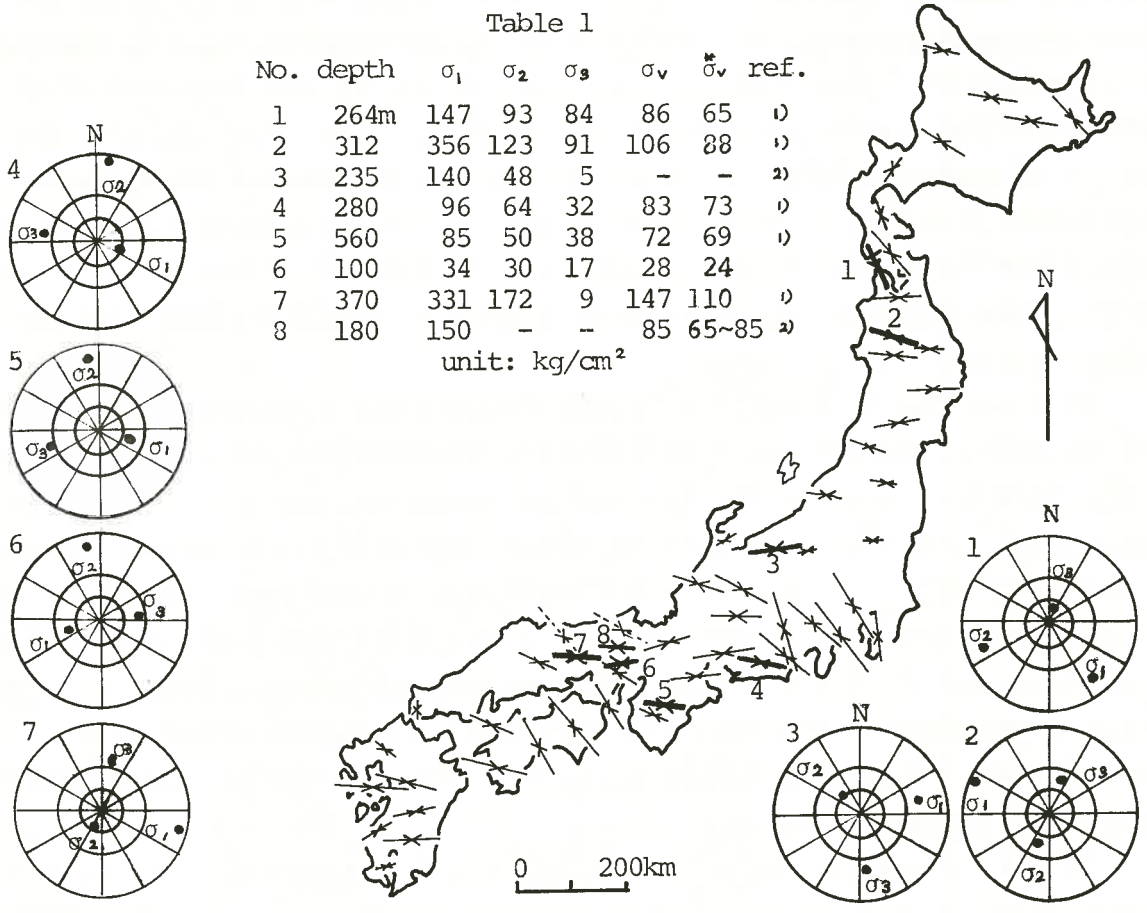

Fig.1 Azimuth of maximum compressive stress by in situ stress measurement and direction of maximum compressive strain by geodetic data. Direction of principal stress are shown on stereographic nets of the lower hemisphere.

be caused by disturbing the unstable equilibrium between tectonic stress and stress concentration around the mined-out area due to the water injection.

After a year cessation, in the biginning of 1975 water level reached the hight of 700m from the bottom of the mine, and since then, microtremors including two felt tremors in Feburuary and in March of 1976 have again occurred frequently. The large tremor(M=2.7) of March 30 has a focal mechanism of strike slip type differently from the former examples. One of the nodal plane of the event coincides with the strike of pre-exsting faults trending in the NW-SE direction. There are three systems of faults across the veins trending in the NW-SE, NE-SW and E-W directions respectively. The maximum compressive axis of the event is approximately horizontal and in the E-W direction, so that this felt tremor was caused by the slip on a pre-existing fault whose orientation is in conformity with the tectonic stress field, by increasing of the pore pressure in the fault due to rising of water level, i.e. high water pressure.

Rock burst occurred at a depth from 700 to 1000m underground. From S-P time(see Fig.2) origins of water-induced earthquakes can be expected from 2 to 5km depth, and hypocenters of microearthquakes are estimated to be at depth between 5 and 15km in the district. Insitu stress measurements are carried out at a depth of from 100 to 400m underground. It is important that the direction of maximum compressive stress estimated from the facts, regardless to the depth , takes the E-W direction.

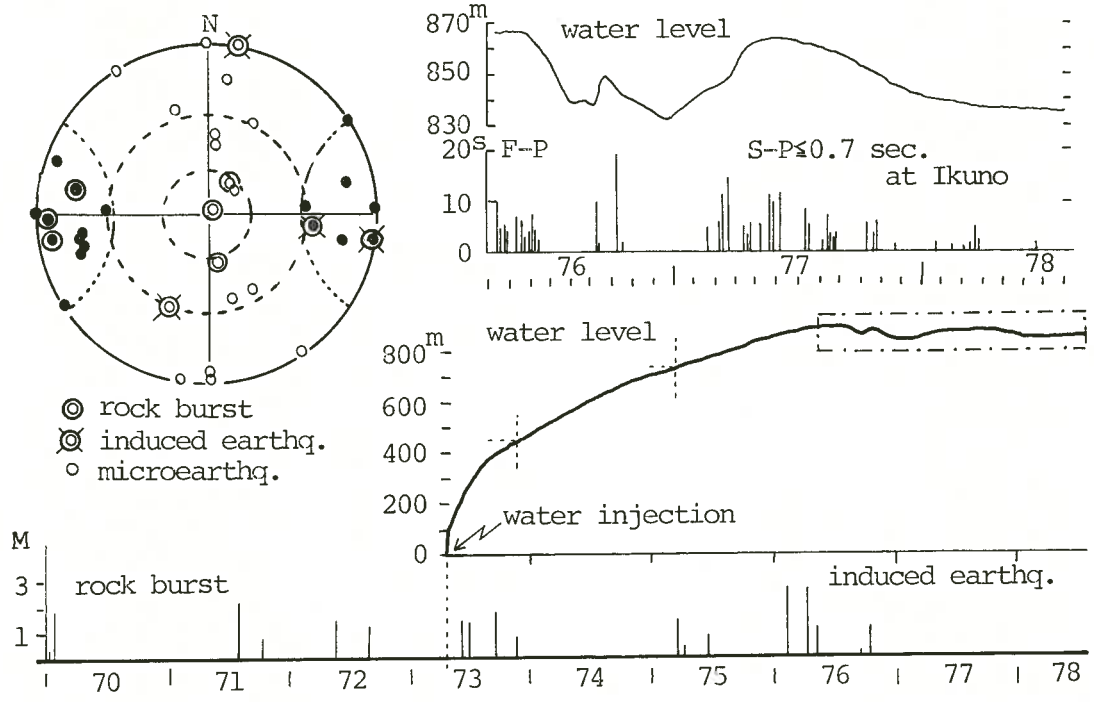

Fig.2 Water levels and tremors. Upper right:detailed figure of chain line part. Upper left:directional distribution of pressure(●) and tension(○) axes in focal mechanism (stereographic projection on lower hemisphere).

Reference 1)Oka et al.4)Tanaka et al.:5th National Symp. on Rock Mechanics,1977 2)Hiramatsu et al.:ib.4th,1973,3)Nakane:J Geodetic Soc. Japan, 19,1973.

CONSTITUTIVE EQUATIONS AND LONG TERM STRENGTH DEFORMATION CHARACTERISTICS OF SOFT SEDIMENTARY ROCKS

Toshihisa ADACHI, Kyoto University
Kouichi NISHI, Central Research Institute of Electric Power Industry
Kazuyoshi FUJIMOTO, Kajima Corporation

Now in our country, so-called soft rocks are distributed at the sites of such big civil engineering projects as Seikan undersea tunnel and Honshu-Shikoku bridge constructions. In order to efficiently and successfully proceed those projects, it is immediate necessity to derive the constitutive equations for such soft rocks as half solidified sedimentary rocks deposited in Miocene Epock of Tertiary Period and strongly weathered granite. The objective of this study is to serve data for obtaining more general stress-strain-time relation for the soft rocks. For the purpose various triaxial tests have been conducted to make clear the elasto-plastic and rate dependent behaviors of the materials by using Ohya-stone(porous tuff) deposited in Tertiary Period as an ideal soft rock.

Throughout this work, the following discussions and conclusions are obtained

(1) The elastic material constants are obtained in terms of effective stress.

(2) From the test results obtained by usual drained compression tests, elastic material constants are determined from the proportional regions of volumetric strain-mean effective stress and deviatoric strain-deviatoric stress relations.

(3) During shear deformation process the stress increases due to strain-hardening until attaining to the peak stress, thenceforth the stress turns to decrease with strain-softening and finally reaches the residual stress state. During this deformation process, the volume expantion mainly takes place. The residual stress state is the state under which only shear deformation continues without any changes in the effective stress and volumetric strain.

(4) In order to examine the method to determine the plastic yielding stress, the deviatoric stress-strain relation is plotted on log-log scale in Fig.1 where the loading-unloading path for this case is also given. A distinct broken point is clearly seen in the loading process between points 6 and 8. So that it may conclude that the broken point gives the stress value when the plastic deformation becomes to dominate. The stress value thus obtained is defined as the plastic yielding stress in this work.

(5) Fig.2 shows the effective stress paths, the plastic yield surfaces obtained by log-log plotting method, the failure surfaces defined by the maximum attained stress values and the residual strength. From the figure, it is concluded that (i) the plastic yield and failure surfaces are nonlinear with σ_m' under lower confining pressure range, (ii) both of the yielding and failure values for the drained tests are smaller than those of the undrained tests due to the rate effect, (iii) the residual strength is found to be expressed by a straight line, namely, by Mohr-Coulomb failure criterion.

(6) The yield function consistent with the plastic potential is determined by using the associated flow rule in the theory of plasticity and experimental results given in Fig.3. Namely, combining "normality rule" with the linear relation obtained in Fig.3 and integrating the derived differential equation, the yield function is determined as follows:

$$f = C^*\sigma_m'\{[C^*+(\alpha^*-1)(\sqrt{2J_2}/\sigma_m')]/\alpha^* C^{*\,\alpha^*/(\alpha^*-1)} = k^* \qquad (1)$$

where α^* and C^* are material constants and $\sqrt{2J_2}$ is the second invariant of deviatoric stress. In Fig.4, corresponding to the drained tests, we show the theoretical yield locus and experimentally obtained plastic incremental strain vectors. The normality condition on the yield locus is approximately satisfied. Namely, the yield function can well explain the volume expansion behaviors duri g plastic deformation.

(7) So far, the dis ussions have been made without taking account of rate effect but it is already found that the plastic yield and failure surfaces are rate sensitive. In order to make clear the long term deformation and strength properties of the material, drained triaxial creep tests were carried out. Isochronous stress-strain curves obtained from the tes s are shown in Fig.5. Exceeding the inflection point of the stress-strain curves, the plastic flow becomes dominant and drastic volume expansion takes place. Defining the inflection point as the static yield value of the material, the values are also plotted in Fig.2 as the creep test results. The minimum stress values under which the creep rupture occurs, are also given in Fig.2. These values may be considered as the long term strength of the material. It is noteworthy that these stress values are located near by the residual strength line.

(8) Taking account of the fact that the creep rupture may possibly occur for the stress state above the static yield value as seen in Fig.5, the material is idealized by elasto-viscoplastic body whose static stress-strain relation is defined by the elastic-perfectly plastic shape. Based on Perzyna's theory of elasto-viscoplasticity and by using the derived yield function as the static as well as dynamic yield function, the following constitutive equations for the material are derived.

$$\dot{\varepsilon}_{ij}^{VP} = \eta^*\Phi(F)f(\sqrt{2J_2}/\sigma_m')\{[(C^*-\sqrt{2J_2}/\sigma_m')\delta_{ij}/3\alpha^*] + S_{ij}/\sqrt{2J_2}\} \qquad (2)$$

where η^* is viscosity constant and F is excess stress function, and

$$f(\sqrt{2J_2}/\sigma_m') = \{[C^*+(\alpha^*-1)(\sqrt{2J_2}/\sigma_m')]/\alpha^*\}^{1/(\alpha^*-1)} \quad (3)$$

The functional form of $\Phi(F)$ is determined from also creep test results. The direction of strain rate vectors at the steady state creep deformation processes and the corresponding dynamic yield surfaces are shown in Fig.6. This concludes that the viscoplastic can well explain the behaviors of soft rocks.

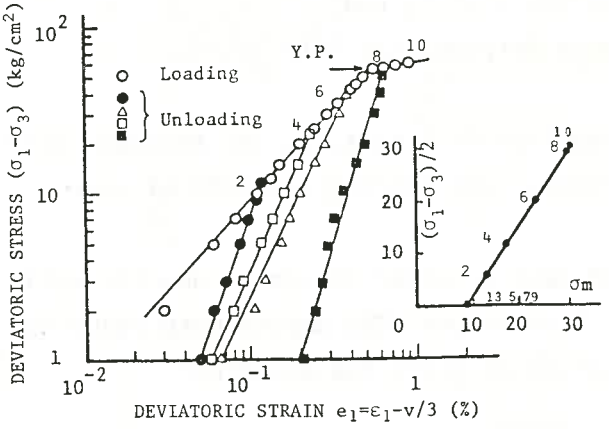

ADERF

Fig. 1 Deviatoric stress-strain relation

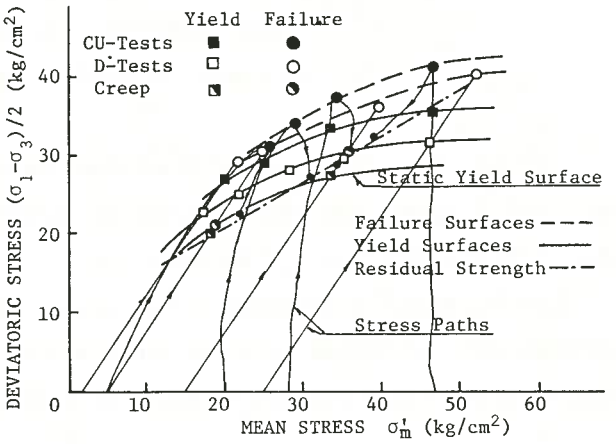

Fig. 2 Stress paths, plastic yield surfaces failure surfaces and residual strength

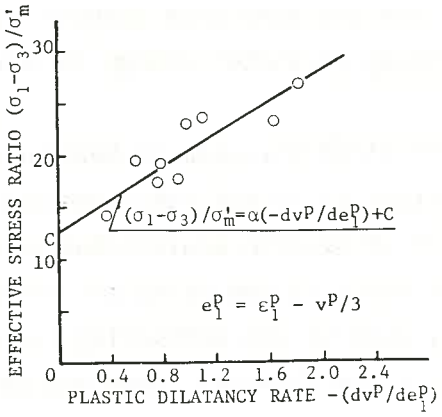

Fig. 3 Relationship between stress ratio and plastic dilatancy rate

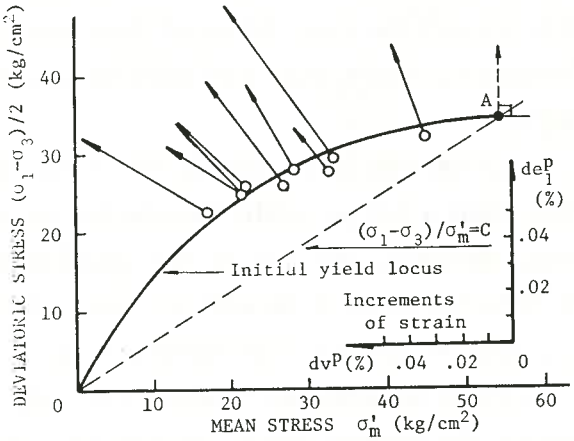

Fig. 4 Theoretical yield locus and plastic incremental strain vectors

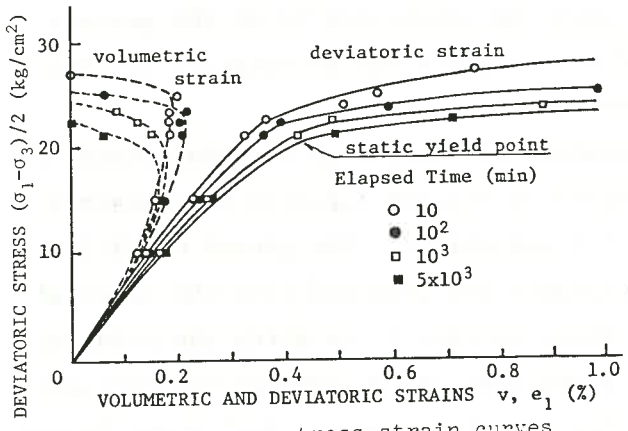

Fig. 5 Isochronous stress-strain curves obtained from draind creep tests

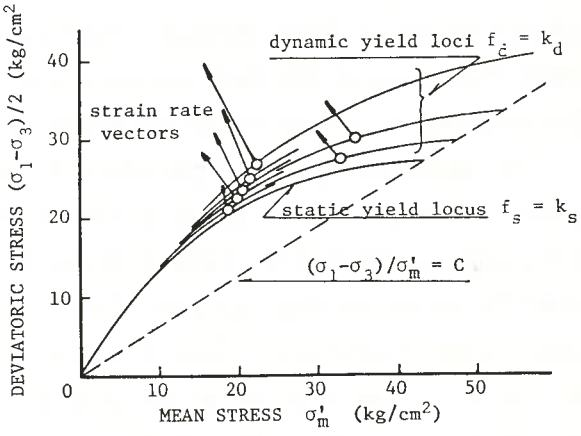

Fig. 6 Comparison of theoretical dynamic yield loci with creep strain rate vectors at steady state

BEARING CAPACITY OF WEATHERED ROCK MASS BY GRAPHICAL SOLUTION

Koichi AKAI, Kyoto University
Yuzo OHNISHI, Kyoto University, and
Hiroaki MIZOBE, Tokyo Metropolitan City

It has been recognized that the foundations of structures are becoming larger and larger, and the methods of determining the bearing capacity of such foundations are not established yet.

The Terzaghi's equation of bearing capacity is still in common use for estimating the ultimate bearing capacity of foundations. The approximate value of the bearing capacity for a shallow foundation is given the equation

$$q_a = cN_c + \frac{1}{2}\gamma B N_\gamma + \gamma D_f N_q$$

The Terzaghi's equation of bearing capacity is useful for the various types of foudation and various depth of footing, but it can not take into account the inhomogeneity such that the unit weight or strength parameter change in the ground.

It is extremely difficult to obtain the analytical solution of bearing capacity when a large scale foundation of a structure is on the inhomogeneous ground. However, the use of the graphical method of plastic equilibrium is often very effective. In this method, when the stress state of the close two points in the ground at the plastic equilibrium is known, that of the neibouring third point can be determined tracing the slip lines in the physical space and the poles in the stress space。At the same time, the stress circle at failure is drawn by the pole method for each point of the slip lines which has a different magnitude of failure strength depending upon the inhomogeneity of the ground. With this method the bearing capacity of a foundation can be obtained for the inhomogeneous ground whose strength is not uniform.

By means of strength parameters determined by laboratory triaxial tests, the graphical solution is applied to the problem of bearing capacity of weathered rock mass of Hiroshima type granite.($\phi = 0$ analysis). The ground condition used is shown in Fig. 1. The material constants are obtained from the triaxial consolidated undrained test results are shown in Fig. 2, in which the point of strength is taken to be at maximum pore water pressure because we now consider the short-term stability analysis only. Fig. 3 (a) is the physical space in the graphical method and Fig. 3 (b) is the corresponding stress space for a foun-

dation on the weathered rock mass.

Being subjected to vertical loading, the rock under OB and OA is in a state of plastic equilibrium. At any point along the base OB, σ_z and σ_x are a major and a minor principal stress respectively, and the rock mass immediately under the footing is in the active state. Therefore along the surface OB, θ is equal to zero and the slopes of the two families of slip lines (s_1 and s_2 lines) with respect to the Z-axis are $\pi/4$ and $-\pi/4$, respectively. In the region immediately below the surface along OA, the passive Rankine state, the constant normal stress (i.e., surcharge) at the boundary is a minor principal stress and the horzontal stress σ_x is a major. In this passive region, $\theta=\pi/2$ and the slopes of the two slip lines below the surface are $3\pi/4$ and $\pi/4$, respectively. From the boundary condition OA, the stresses in the region AOC are determined, taking into account

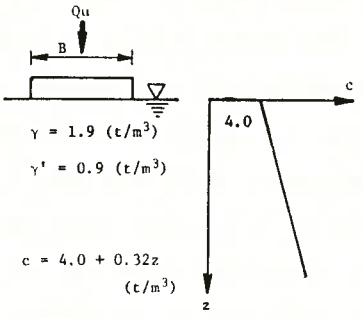

Fig. 1 Ground Condition for Weathered Rock Mass.

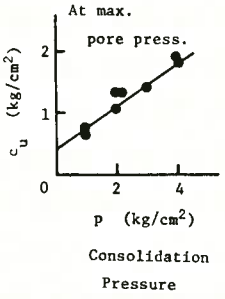

Fig. 2 Relationship between the Undrained Shear Strength and Consolidation Pressure.

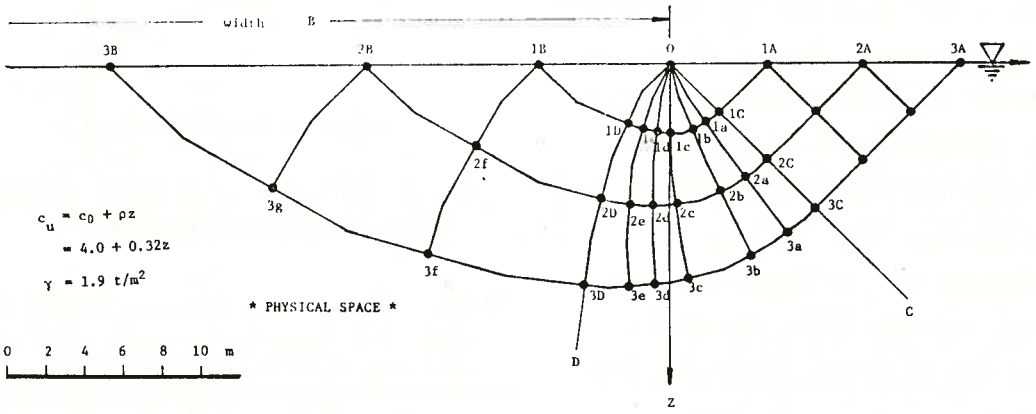

Fig. 3 (a) Physical Space.

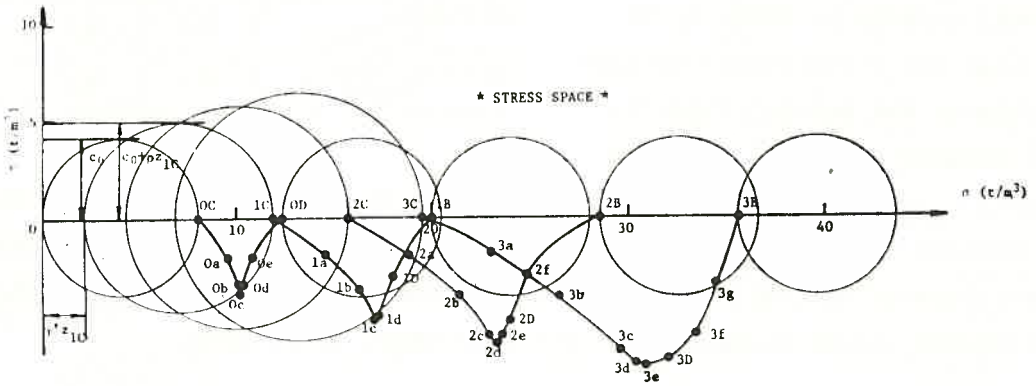

Fig. 3 (b) Stress Space.

the unit weight of soil or rock and the rate of strength increase.

The point O is a singular point in the region, representative of the stress discontinuity, and exists at the edge of the foundation and also all slip lines of the s_2 family between the lines OC and OD pass through the point O. The requirement that the two families of slip lines intersect each other at the angle of $\pi/2$ means that the slip lines of the s_1 family are curved in the region COD. Starting from the vicinity of the point O, the first step to construct a slip line net is to divide the angle COD into an adequate number of equal angle. Since the point O is close enough to the surface to neglect the weight and strength increase of rock mass, the locus of the pole along a slip line of the s_1 family in the vicinity of the point O is easily obtained according to the pole trail method and the result is shown in Fig. 3(b) as the trace of the pole from OC to OD through Oc. Following the straight-line portion in the region AOC and based on the locus of the pole obtained as stated above, a slip line of the s_1 family is extended through a point nC (n=1,2,...) to intersect the s_2 slip lines Oa at a point na, or at a point nb,....., along the curve nCnD in the area COD to the point nD, and finally the s_2 lines reach the negative X-axis in a point nB along another curve nDnB.

By suitable choice of the point nA, the loaded portion OnB is extended to the negative X-axis direction. Repetition of this procedure results in the determination of the slip-line field with a desired degree of approximation. Fig. 4 shows the distribution of the major principal stresses calculated by the above method. The bearing capacity determined by the pole trail method was compared with the ones by the conventional methods in Table 1. It shows that the conventional methods overestimate the bearing capacity 10-20% greater than the graphical solution. From the distribution of the major normal principal stresses in Fig.4, it is noticed that the larger the width of foundation is, the greater the discrepancy between Method(1) and Method(2) becomes, and Method(3) gives the most overestimated values of bearing capacity as shown in Table 1.

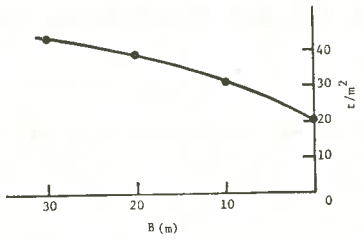

Fig. 4 Distribution of Major Principal Stress along Foundation Base.

Table 1 Comparison between Bearing Capacities Calculated by Conventional Methods and Graphical Pole Trial Method.

B (m)	10	20	30
(1) Graphical Solution of Plastic Equilibrium	26.0	30.9	34.7
(2) Terzaghi $q_d=5.14c_u$	26.1	31.5	37.0
(3) ϕ=0-Slip Circle Analysis	29.2	35.2	40.0

t/m²

A STUDY OF ROADWAY CLOSURE
— Linear analysis by the FEM —

Makoto IHARA, Prof.,Dr.Eng., Kyushu University
Kikuo MATSUI, Kyushu University

1. Introduction

There have been many studies on maintenance of roadway excavated in a homogeneous rock mass. The effect, however,due to the presence of non-homogeneities in a rock mass results in a change of the general stress distribution expected from the corresponding solution for the homogeneous rock mass.

In this report, the authors take up a coal mine roadway with a weak floor. And the influence of the thickness of the weak floor and the roadway shape on the distribution of the stress and displacement around roadway was studied by the finite element method.

2. Method of solution

An analyzed model and the roadway shape are shown in Fig.1. The depth of the roadway,H, and the half of the roadway height or width,a, are 400m and 2.5m respectively.

Since the model is symmetrical with respect to the vertical axis through the center of the roadway, only half of it was analyzed in consideration of the gravity loading and plane strain conditions. In addition, the upper and lower boundaries of the model are located at a distance $10a$, from the center of the roadway and $16a$ for the side boundary.

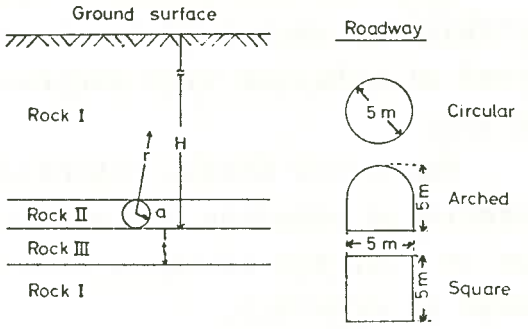

Fig.1 Analyzed model and roadway shape

Table 1 Values of physical properties used in model

Rock	Young's modulus E:(t/m^2)	Poisson's ratio ν	Specific weight γ:(t/m^3)
I	1.0×10^6	0.25 0.4	2.5
II	1.0×10^5	0.25 0.4	1.5
III	1.0×10^4	0.25 0.4	3.0

The physical properties of each rock are shown in Table 1. Each rock is homogeneous, isotropic and elastic body and is bonded so that no slip and separation occur at the interface. Rock I,II and III correspond to a hard rock, a coal seam and a weak floor respectively.

The stress and displacement fields about each roadway were determined for each value of the thickness of a weak floor, t, varying from 0 to $7a$.

3. Results and discussion

The tangential stresses, σ, at the roof, sidewall and floor of the roadway — all normalized to the vertical stress, γH — are plotted in Fig.2 for different values of t/a, ν= 0.25 and 0.4. The positive value means compressive stress. They changed significantly at the low values of t/a and for $t/a>3$, they reach constant values.

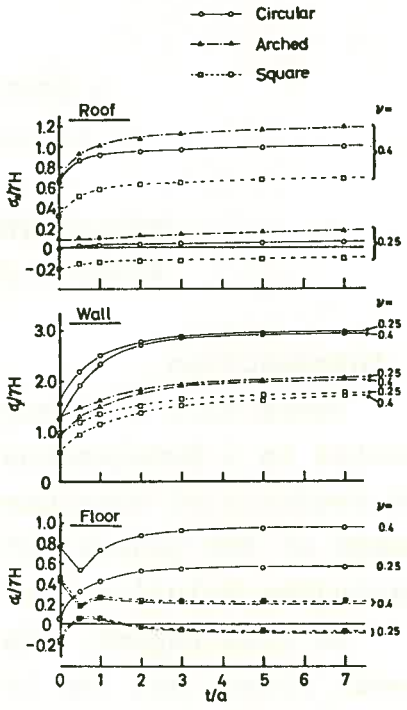

Fig.2 Tangential stress at the various values of a weak floor

The roof and sidewall stresses exhibit for each roadway shape a similar trend of behavior with increasing values of t/a.

The floor stress exhibits a characteristic behavior for each roadway. For ν= 0.4, the stresses show a minimum value at t/a= 0.5.

Figs.3 and 4 illustrate the distribution of the horizontal and vertical stresses for the circular roadway.

In Fig.3 the horizontal stress is plotted for ν= 0.25. These curves show that the effect of the presence of a weak floor is significant for $r/a<4$, where r is the distance from the center of the roadway. For $r/a\geqq4$, they reach the initial stress values. The horizontal stress at the floor decreases at

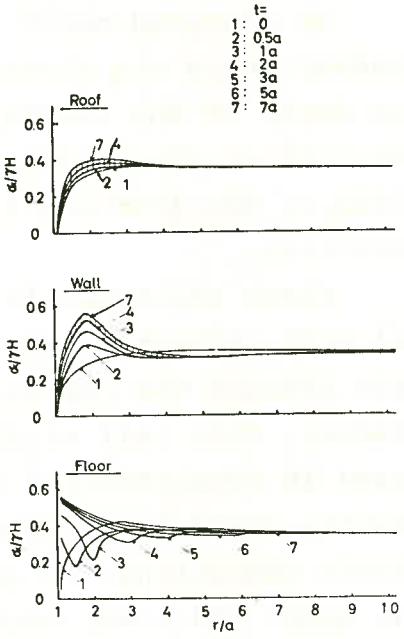

Fig.3 Distribution of the horizontal stress for the circular roadway (ν= 0.25)

the interface between the "weak" Rock III and the lower "hard" Rock I. This decrease at the interface is almost neglected for $t/a>5$.

It is shown in Fig.4 that the vertical stress is also affected by the thickness of the weak floor for $r/a<4$, but the rapid change of the stress does not occur at the interface of the floor.

Similar trends as shown in Figs. 3 and 4 are observed for the arched and square roadways and $\nu = 0.4$.

In Fig.5 the amount of the roof lowering and floor lift are plotted for the different thicknesses of the weak floor. These curves show that the thicker the weak floor becomes, the greater the roadways deform. These results coincide with experimental result qualitatively. It is also observed that the circular roadway deforms with less amount than the arched and square roadways. So the circular form is suitable for the roadway shape.

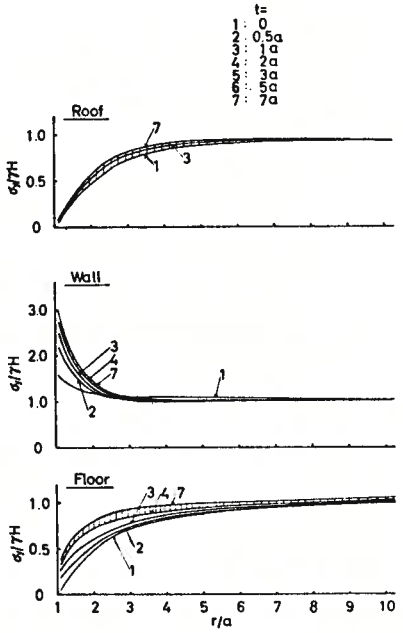

Fig.4 Distribution of the vertical stress for the circular roadway ($\nu = 0.25$)

4. Conclusion

The influence of the thickness of a weak floor and the roadway shape on the distribution of the stress and displacement around roadway was studied by the finite element method.

It is found that the stresses and displacements depend on the thickness of the weak floor, the roadway shape and the physical properties of rocks.

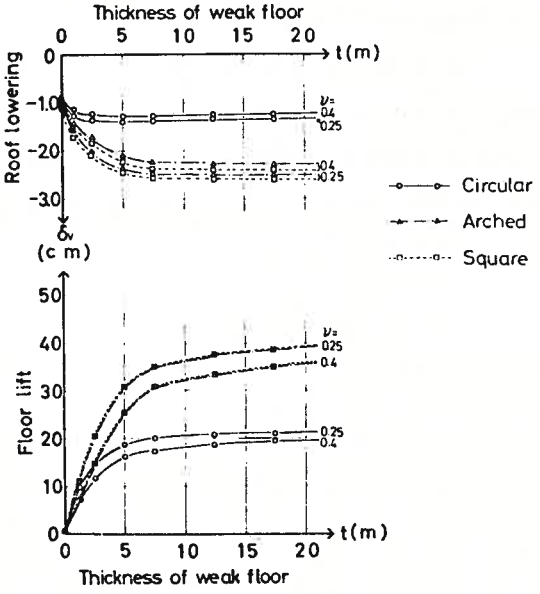

Fig.5 Roadway closure at the various values of a weak floor

IN SITU JACKING TESTS AND CHARACTERISTICS OF STRAIN DISTRIBUTION IN ROCKMASSES

Ryuichi IIDA, Isao SHIBATA, Tadashi NISHIOKA, Kozo SAITO,
Public Work Research Institute the Ministry, of Construction

Rockmasses in general contain cracks, joints and other discontinuities. Such discontinuities have much influence on mechanical characteristics of rockmasses. Strain distributions in rockmasses measured in an in situ jacking test can be utilized to interprete these characteristics of rockmasses. The new type of device to measure continuous strain distributions were developed and used by embedding them into rockmasses. They consist of 11 cm long gauges overlapped each other in epoxy resin and can measure strain distributions in a 1 m long drill core hole.

In situ jacking tests were carried out and geological conditions and the properties of rockmasses obtained at these sites are shown in Table 1. A typical load-displacement curve and load-strain curves both near the surface and in the deeper location of rockmasses at the site of Kawaji Dam are shown in Fig. 1 to 3.

Table 1

Name of Test Site	Kawaji Dam		Takizawa Dam		Okawa Dam	
	A	B	No. 1	No. 2	No.301	No.303
Kind of Rock	Diorite	Diorite	Slate	Slate	Rhyolite	Rhyolite
Number of Cracks/m	6	6	20	19	-	-
Fillings of Cracks	No	No	Soil	Soil	Soil	Soil
Loading Plate	Flat Jack	Flat Jack	Rigid Jack	Rigid Jack	Rigid Jack	Rigid Jack
Dia. of Plate	80 cm	80 cm	30 cm	30 cm	30 cm	30 cm
Modu.of Elas. of Core (E_c)	212,000 kg/cm^2	292,000 kg/cm^2	174,000 kg/cm^2	320,000 kg/cm^2	-	-
Modu.of Def. (D)	71,000 kg/cm^2	51,000 kg/cm^2	31,000 kg/cm^2	26,000 kg/cm^2	7,800 kg/cm^2	11,700 kg/cm^2
Modu.of Elas. (E_R)	145,000 kg/cm^2	122,000 kg/cm^2	44,000 kg/cm^2	40,000 kg/cm^2	18,700 kg/cm^2	22,000 kg/cm^2
D/E_R	0.490	0.419	0.705	0.650	0.42	0.53
E_R/E_C	0.683	0.418	0.253	0.125	-	-

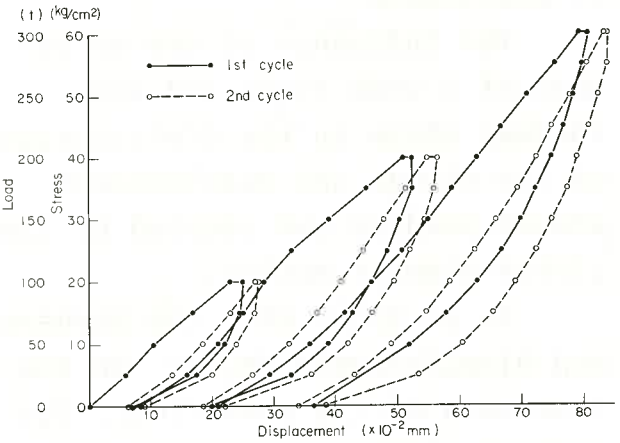

Fig. 1 Load-displacement Curve at Site B of Kawaji Dam

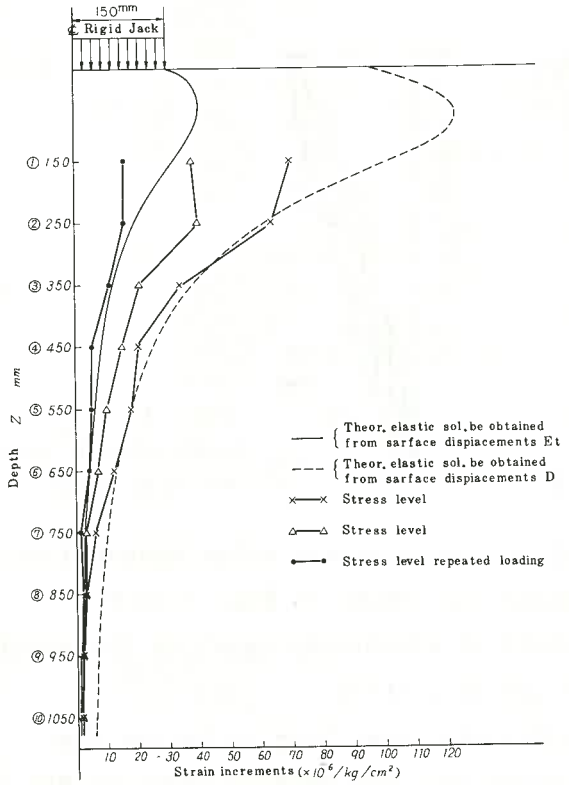

Fig. 6 Distribution of the Strain Increments in the Rockmass at Site No.301 of Okawa Dam

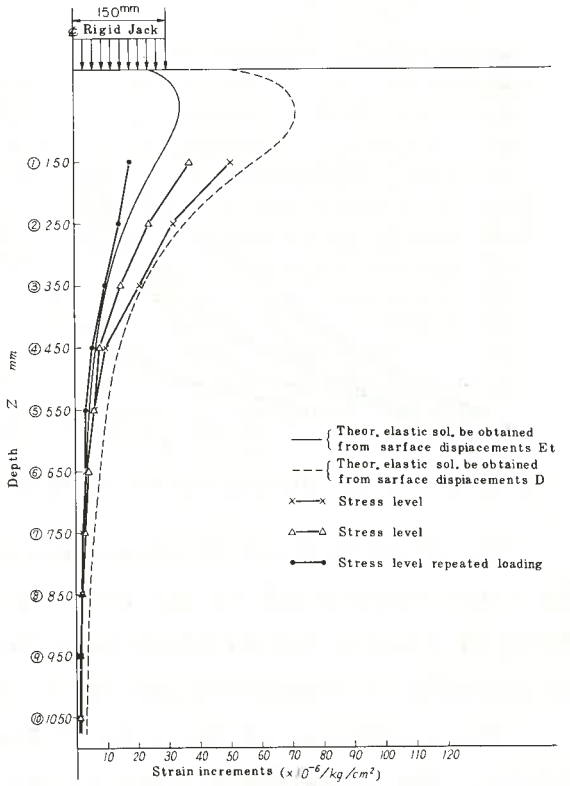

Fig. 7 Distribution of the Strain Increments in the Rockmass at Site No.302 of Okawa Dam

surface ($Z < 30$~50 cm) show much larger value than those of elastic bodies having the moduli of elasticity equal to those of rockmasses and those of their cores, and they decrease according as the loads are applied. But strain increments in the depth are approximately equal to those of elastic bodies and irrelevant to load increments. These indicate that surface loosenesses caused by the excavation of adits are compacted by loading.

The rockmasses at the site of Takizawa Dam are Paleozoic Slate having many joints with fillings of clay. Results of tests show that the larger the loads are applied the larger strain increments are in the location deeper than 30 cm. According to the examination of drill cores and rockmasses, this part of rockmasses has many joints with filling of clay. This indicates that the fillings of clay yield and cause large strain when the applied load increase.

The rockmasses at the site of Okawa Dam are very weathered Rhyorite having many cracks and joints with fillings of clay. Surface loosenesses at the test sites caused by the excavation of adits were carefully removed, especially surface loosenesses at site No.303 removed to 50 cm deeper than those at site No.301. Strain distributions are affected by cracks and joints. But the larger the loads are applied the smaller strain increments are and compaction can be observed. Rockmasses of which surface loosenesses are removed have about one and a half times larger moduli of elasticity and smaller strain near the surface than loosened rockmasses. This indicates that the excavation of adits causes surface looseness of rockmasses even though rockmasses are not

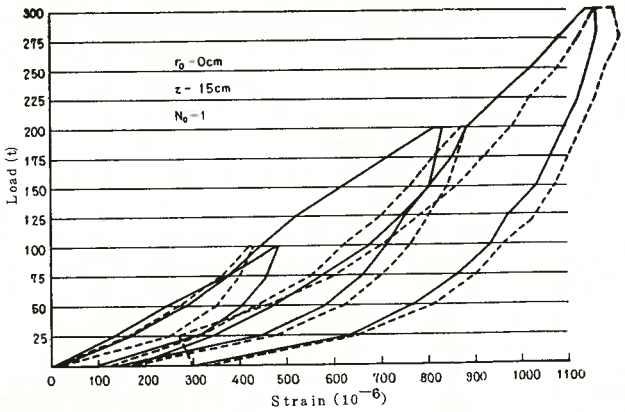

Fig. 2 Load-strain Curve at site No.B

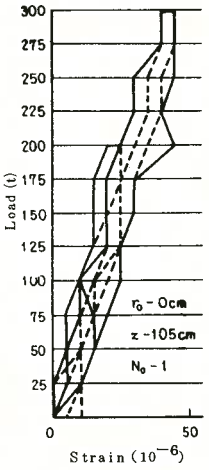

Fig. 3 Load-strain Curve at site No.B

The distributions of strain increments per unit stress value measured at the first loading and at the repeated loadings are shown in Fig. 4 to 7. Those of elastic bodies which have the moduli of elasticity equal to the moduli of elastity of rockmasses and their cores are also shown.

The rockmasses at the site of Kawaji Dam are sound Diorite having few joints. The load-strain curve at the location near the surface shown in Fig.2 are inelastic simular to the load-displacement curve shown in Fig. 1, but rock-masses in the depth indicate the same behavior as those of the elastic bodies. The same tendency are also observed in Fig. 4. Strain increments near the

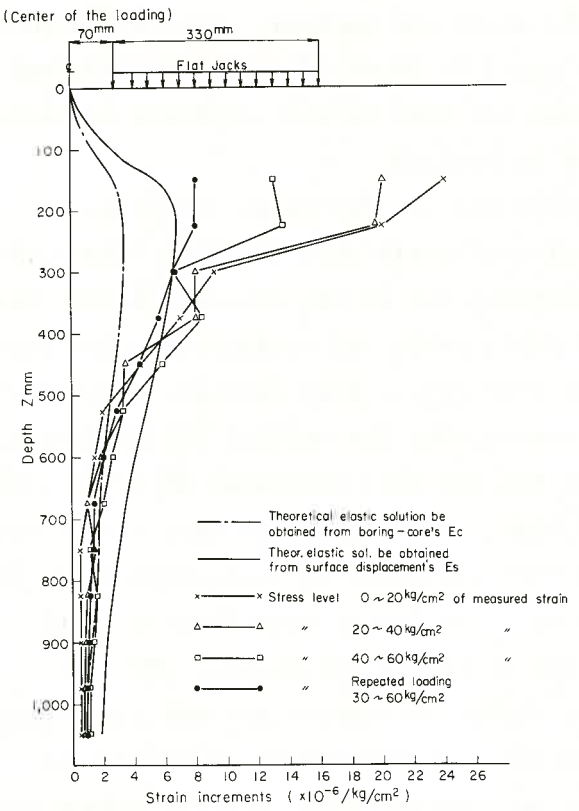

Fig. 4 Distribution of the Strain Increments in the Rockmass at Site B of Kawaji Dam

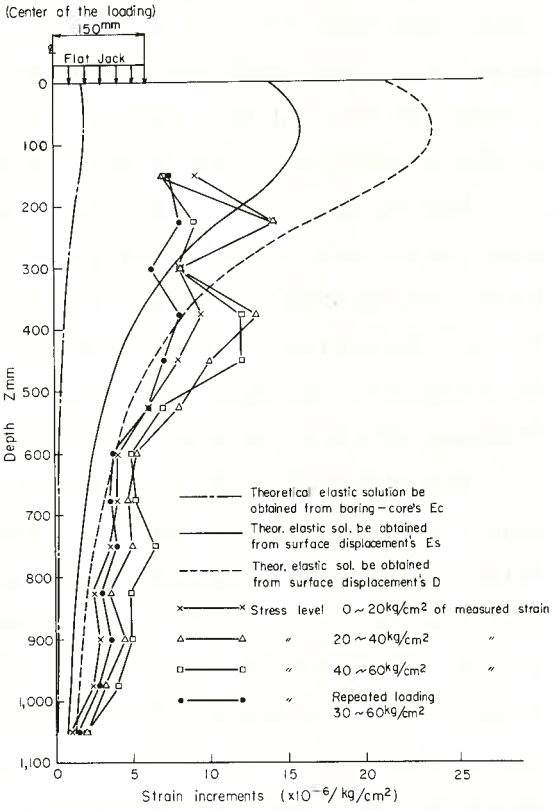

Fig. 5 Distribution of the Strain Increments in the Rockmass at Site No.2 of Takizawa Dam

sound and were blasted carefully.

From these studies the followings are concluded with regard to loosenesses in rockmasses caused by the excavation of adits.

(1) Rockmasses which have small deformability and large moduli of elasticity ($E_R > 100{,}000$ kg/cm^2) have different properties between in the location near the surface ($Z < 30$~50 cm) and in the depth. Strain increments near the surface show much larger value than those of elastic bodies having the moduli of elasticity equal to those rockpieces. But strain increments in the depth are approximately equal to those of elastic bodies. These indicate that surface loosenesses by the excavation of adits emphasize the difference between the moduli of deformability and the moduli of elasticity and make the moduli of elasticity smaller.

(2) Rockmasses of which surface loosenesses are removed have smaller strain increments near the surface than loosened rockmasses.

Surface loosenesses to 30~50 cm from the surface should be removed carefully to avoid the influence of excavation.

Rockmasses have following characteristics with regard to the nature of discontinuities.

(1) Rockmasses which are sound and have no loosenesses and no fillings indicate the same strain distribution as those of elastic bodies having the moduli of elasticity equal to those of rockpieces.

(2) Rockmasses which are sound but have loosenesses indicate a tendency that the larger the loads are applied the smaller strain increments are. The moduli of elasticity of these types of rockmasses are smaller than those of their cores.

(3) Rockmasses which have fillings but no loosenesses are inelastic and strain increments are complicated and not consistent. There is a case where the larger the loads are applied the larger strain increments are.

(4) Rockmasses which have fillings and loosenesses are inelastic and have the small moduli of elasticity. These types of rockmasses indicate a tendency that the larger the loads applied the smaller strain increment are.

Therefore, rockmasses can be devided into four types according to the nature of discontinuities.

(1) rockmasses with no loosenesses and no fillings
(2) rockmasses with loosenesses and no fillings
(3) rockmasses with no loosenesses and fillings
(4) rockmasses with loosenesses and fillings

The rockmasses which belong to (1) can be assumed as elastic bodies. The rockmasses which belong to (2) indicate inelastic behavior and can be analyzed using the method proposed by the author.

MEASUREMENTS OF DISTURBANCE IN ROCK MASS INDUCED BY THE EXCAVATION OF A STEEP COAL SEAM

A case study on Noborikawa Pit

Yoji ISHIJIMA and Shigenori KINOSHITA, Hokkaido University

1. Introduction

Rock mass movements due to the mining activity around the gate road (or panel entry) usually driven in the footwall at a distance of 7 to 15 m below the coal seam were monitored in the several mining panels at Noborikawa Pit of Sunagawa Coal Mine in Hokkaido. Under the circumstances that the depth of the mining area below surface was approximately 750 m, and that coal measure strata was mainly composed of massive sandstone having a mean uniaxial compressive strength of 130 Mpa, danger of rockburst was anticipated. In this mine, only a single coal seam of 2.5 m in thickness and 78 degrees in inclination was excavated by the hydraulic mining method, which did not require for miners to enter into the mining front. Therefore, only the gate road was in need of attention for its maintenance and safety.

The measurements presented in this paper were concerned with the monitoring the deformation by single and multi-extensometers and the monitoring the stress change by means of the hydraulic capsules . In addition, survey traverses were conducted to assess the absolute movements of the rock mass.

2. Convergence of the panel entry

Six rod-type extensometers of 6 m in length were established with an arrangement of Schuermann's proposal.[1] According to this arrangement, we can obtain not only the information on the mutual convergence of roof and floor or sidewalls, that is inner convergence of the road, but also the information on the outer-convergence defined as a relative displacement between the two opposite ankers fixed at 6 m depth from each wall of the road. The outer-convergence can give a more qualified information on the stress change in the rock mass, because it suffers less influence of the relaxation created around the opening than the inner-

convergence.

A typical results concerning on the outer-convergence is shown in Fig. 1. It indicates that when the mining front advanced to the measuring point some 40 m in front of it, convergence commenced under the influence of the front abutment pressure. An excessive change occured when the face just passed over the point, accompanying a large amount of extension of the displacement D_{1-2} perpendicular to the seam. This will be owing to the stress relief induced under the excavated area. The change of deformation, thereafter, ceased when the measuring point was about 60 m behind the mining front, indicating that the area has been stabilized.

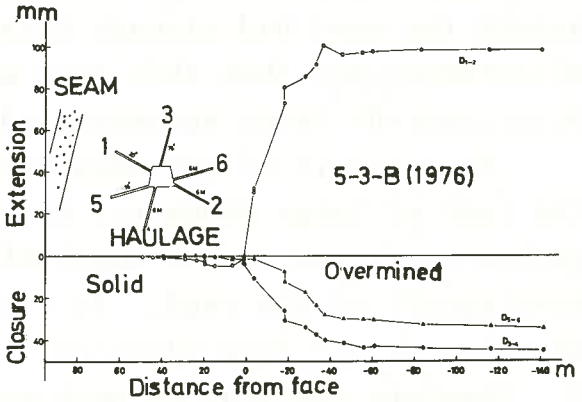

Fig. 1 Change in outer-convergence relative to distance from face

The measurements were conducted at eight different stations in seven different mining panels. It would be interesting to investigate whether there could be any local differences among the measured values. For this purpose, the strain (e), the ratio of the final outer-convergence to the distance between the two opposite ankers, was plotted against the span of the footwall across the entry (l) in Fig. 2. Data fit well to the regression line, which indicated that the convergence was mainly related to the span of the footwall and that the influence of the regional difference was small. Thus it is possible to consider that the rock mass was homogeneous in behavior.

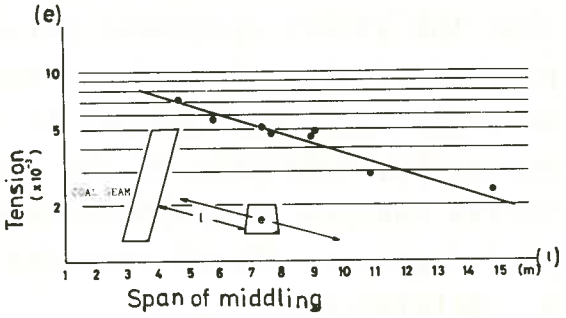

Fig. 2 Relationship between the strain (e) and the span of the footwall (l)

On the other hand, the results on the inner-convergence showed that the road continued closing throughout the measuring period in every direction,

although a remarkable change was found when the face passed over the measuring point. This should indicate that the relaxed zone around the road had already existed before the start of the measurement and that this zone was enlarged and/or more heavily deteriorated being accomapanied by the mining activity.

As a result of the measurement by using multi-extensometers, the zone of large movement, thus, probably the relaxed zone, was proved to extend to the depth of approximately 3 m from the hangingwall of the road. It was also cleared that the coal seam shrinked as the face advanced.

3. Absolute movement of rock mass and stress change

Based on the traverse surveying conducted twice before and after mining, on the same network of the panel entries, the tendency of the rock mass movement towards the excavated area was recognized. It is interesting to note that the local disturbance was detected in the vicinity of a particular fault zone, which showed that the fault was activated and slipped by the mining.

Hydraulic capsules burried at the points of 6 m depth from the wall with the three different directions showed that the stresses increased at first as the mining front approached, then they relieved subsequently as it passed over the measuring station.

4. Interpretation of the measurements

Three dimensional elastic stress analysis based on the displacement discontinuity method developed by Crouch[2] was conducted. In this analysis the existance of the road was neglected and attention was directed towards obtaining the general idea of the rock mass movement in the footwall, under the assumption that the rock mass was homogeneous and elastic. Mining sequence was simulated using the elastic model. Main result was that the stress component perpendicular to the seam was preferentially released and the rock mass movement towards the excavated area was induced by the overmining. Results of surveying, behaviors of the outer-convergence and the measured stress changes were approximately coincident with the anticipations, though some differences were recognized in details.

5. References

1) Schuermann F: Das Messen von Gebirgsbewegungen mit Langemessankern, Glückauf 1975 Nr.13 pp 625-631

2) Crouch S.L. and Fairhurst C: The Mechanism of Coal Mine Bumps, USBM Contact Report H0101778, 1973

EXPERIMENTAL STUDY ON DEFORMATION CHARACTERISTICS OF ROCK-LIKE MATERIALS

Toshikazu KAWAMOTO, Nagoya University
Toshiaki ISHII, Yokohama City

The deformation characteristics of rock-like materials with different porosities are studied experimentally using the specimens of cement mortar and tuff under triaxial compression states. The stress and strain are dealt with respectively by dividing into their isostatic and deviatoric components, and the deformation characteristics are considered under several stress states standing on continuum mechanics. Furthermore, it is studied how the porosity and the microscopic structure have influence on their properties of deformation on loading.

The specimens of cement mortar are made from usual Portland cement mixed by the following ratio: water / cement / sand = 0.65 / 1 / 2. They are formed into cube with edges of 10.8 cm using steel forms, then after thirty five days the experiments are undergone. Their physical and mechanical constants are shown in Table 1.

Table 1. Physical and mechanical constants of specimens.

	α_c kg/cm^2	ε_c %	E kg/cm^2	ν	e_0	γ g/cm^3
mortar	424	0.63	1.2×10^5	0.10	0.38	2.13
tuff	915	0.995	8.25×10^4	0.11	0.06	2.71

The specimens of tuff are formed into cube with edges of 5.4 $\pm$ 0.15 cm. They seem to be homogeneous macroscopically, whose physical and mechanical constants are also shown in Table 1. Their initial porosity e_0 is 0.06, which is considerably less than the cement mortar's.

Using triaxial shear testing machine which loads specimens by oil jacks in three directions through three pairs of plates, the specimens are loaded in the following states:

Test A ; unconfined compression test ($\sigma_1 > \sigma_2 = \sigma_3 = 0$),

Test B ; test under hydrostatic pressure (isotropic compression test) ($\sigma_1 = \sigma_2 = \sigma_3$),

Test C ; test under constant mean stress (deviatoric stress test) (σ_m = const., $\lambda = \pm 1$), where σ_m is the mean stress and λ the Lode's parameter, which designates the magnitude of the intermediate principal stress given by $\lambda = (2\sigma_2 - \sigma_1 - \sigma_3) / (\sigma_1 - \sigma_3)$. Note that $\lambda = 1$ shows the state of tension, and $\lambda = -1$ the compression.

Test D ; test under constant mean stress for the materials with isotropic stress history (σ_m = const., $\lambda = \pm 1$; first they are stressed under the isotropic stress history σ_{hi}, then undergo Test C). Materials which have experiences of higher stresses compared with ones on experiment are called over-compressed materials, so that Test D is called a deviatoric stress test under over-compression.

We control the mean stress σ_m and the octahedral shear stress τ_{oct} independently, thus the subsequent response of strains, say the mean strain ε_m (or the octahedral normal strain ε_{oct}) and the octahedral shear strain γ_{oct} are analyzed respectively.

The mean stress-strain relationships and the variations of elastic component ε_m^e and plastic component ε_m^p of strain are shown in Figs. 1 and 2 for mortar and tuff, respectively. Moreover, these figures give the variations of porosity and plastic energy loss which is defined by $W_h^p = \int 3\sigma_m d\varepsilon_m^p$. Figures 3 and 4 show the stress-strain relationships of tuff without and with the isotropic stress history under the deviatoric stress test with various mean stresses.

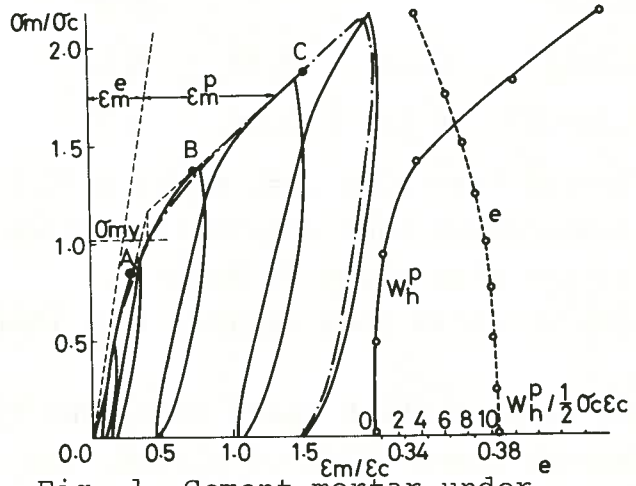

Fig. 1. Cement mortar under hydrostatic compression

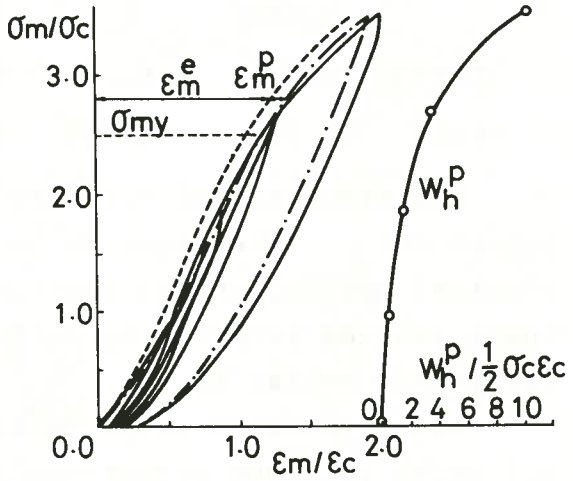

Fig. 2. Tuff under hydrostatic compression

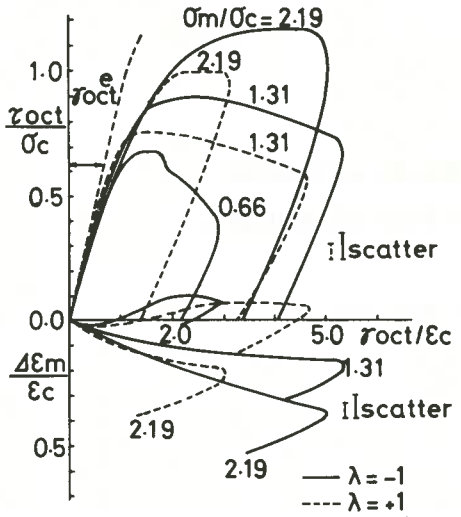

Fig. 3. Tuff under deviatoric stress test (σ_{hi}/σ_c=0.0)

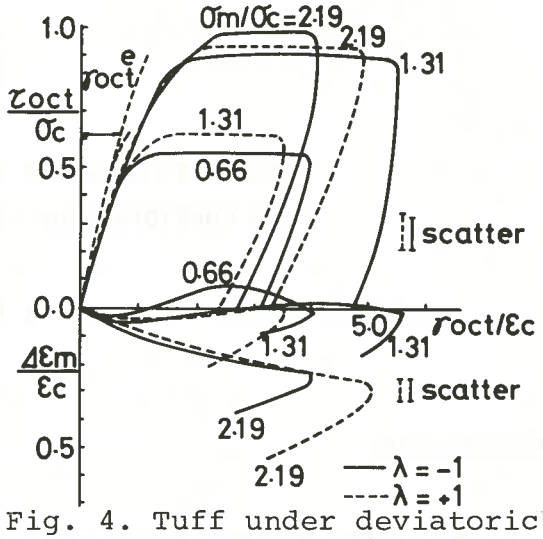

Fig. 4. Tuff under deviatoric stress test (σ_{hi}/σ_c=3.50)

The followings becomes clear for the deformation characteristics of isotropic rock-like materials with the homogeneous distribution of porosity.

(1) The deformation characteristics of the porous rock-like materials depend essentially upon the variation of form of microscopic structure with the stress history.

(2) The stress-strain relationships of these materials under the isostatic stress are represented approximately by a bi-linear curve and its bending point may be considered as the yield point for the hydrostatic pressure.

(3) In the state of normal compression, the amount of recoverable shearing strain γ_{oct} varies in proportion to τ_{oct} up to the yield point and its rate of variation does not depend on the mean stress σ_m.

(4) In the state of normal compression, the contractancy arises with the increase of shearing strain under the constant mean stress and its magnitude increases with the mean stress.

(5) In the state of over compression, the slope of τ_{oct} - γ_{oct} curve up to the yield point is steeper than one in the state of normal compression, and the slope does not depend upon the normal stress.

(6) In the state of over compression, the contractancy is smaller than one in the normal compression and the dilatancy arises when the mean stress is relatively small.

The deformation characteristics of rock-like materials mentioned above may be explained reasonably by assuming the end cap-shaped yield surface in hardening for the yield condition of materials.

STABILITY ANALYSIS OF A SUBMERGED CUT SLOPE WITH CONSIDERATION FOR STRESS-PATH DEPENDENCE

Yoshimasa KOBAYASHI, Tadashi HASHIMOTO and Yasuaki ICHIKAWA

INTRODUCTION

The finite element analysis of stresses in soils requires data of stress-strain relationship of the element soils which generally exhibit a non-linear character. This property used to be taken into consideration in stress analyses in soils yielding useful results, however a more realistic approach would be that which takes also the stress-path dependence into account. In this paper a series of finite-element analyses of behaviors of a sea-bottom ground during excavation for a bridge foundation reaching 30 m below the sea bottom are presented, where the stress-path dependence of soil characteristics is introduced in the analyses.

SOIL PROFILE AND STATEMENT OF THE PROBLEM

The site is situated I5 m below the sea level and composed of diluvial sediments, which are classified into SIII-S, SIII-C, SII-SG, SI-C and SI-S from the sea bottom downwards, about 30 m in thickness underlain by a fairly to waekly weathered base rock of granodiorite. Two cases of excavation of 30 m depth at an inclination of either I/I.5 or I/2.0 are studied. The excavation is assumed to be executed layer by layer of I0 m thickness, thus after three steps reaching the bedrock surface 30 m below the sea bottom, and the stress states at every stage of excavation are analysed.

TRIAXIAL TESTS OF SOIL SPECIMENS

A series of triaxial tests including unloading of soil materials from SIIIS to SI-S were conducted on either undisturbed specimens for cohesive soil or fine sand, or specimens mould at an appropriate density for medium to coase sand. Specimens of every soil type are subjected to the following four types of stress path after having been consolidated isotropically under the pressures corresponding to their original overburden stresses: I)σ_1 is increased while

σ_3 is kept constant, 2)σ_I is increased while σ_3 is decreased, 3) σ_I is sustained constant while σ_3 is decreased and 4)both σ_I and σ_3 are decreased, where σ_I and σ_3 represent axial and lateral pressures, respectively. All the tests were carried out with a strain rate of 0.25 to I.0 %/hr.

As a result of the tests it revealed that the Poisson's ratio ν and Young's modulus E, which are employed in the computaions may be approximated by

$$\nu=(b\sigma_I-a\sigma_3)/[a(\sigma_I+\sigma_3)+2b\sigma_3] \quad \text{and} \quad E=(\sigma_I-2\nu\sigma_3)/[I-c(\sigma_I-\sigma_3)]/a(\sigma_I-\sigma_3)$$

where a,b and c are constants depending on the type of soil and the stress path. The stress path is represented by a parameter angle α measured counterclockwise from the upward vertical in the σ_I-σ_3 plane. The constants a, b and c determined from the test results are illustrated in Fig.I.

Summarizing the test results, failure occurs under a smaller strain by unloading than in loading.The ultimate strains and the factors of safety for I % strain for every type of soil are given in Table I.

PROCEDURE OF ANALYSIS AND RESULTS

For solving a problem a solution in

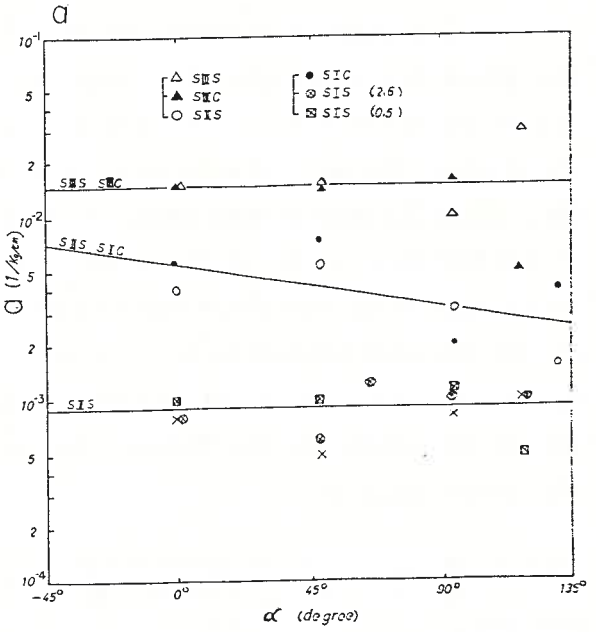

Fig.I Constants of Deformation Properties of Soils

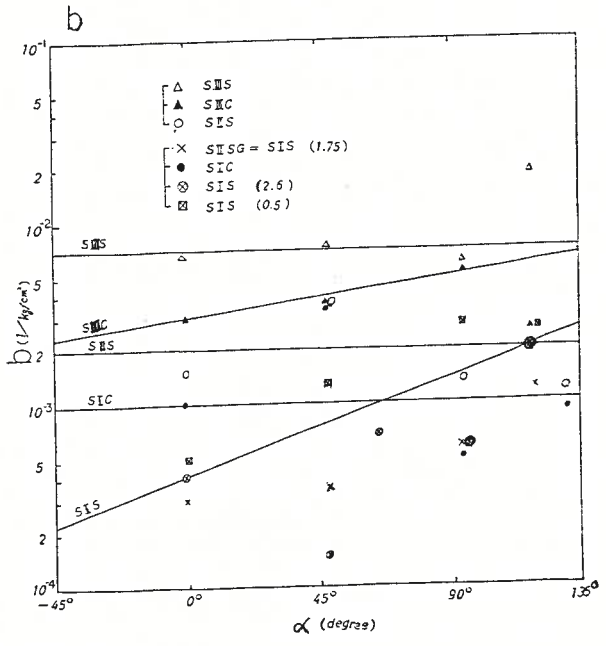

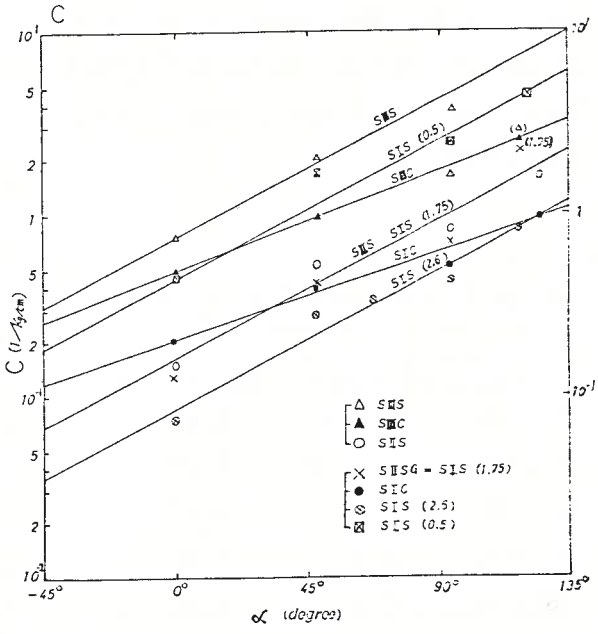

respect to both stress or strain and stress path must be seeked after iteratively, because the deformation properties are functions of the both factors. A stress path is represented by the angle of the straight line in the σ_I-σ_3 plane connecting the stress-state points prior and after individual loading or unloading. On each stage of approximation in respect to stress path a secant-modulus iteration is carried out to reach a solution in nonlinear material. Every provisory solution enables to define a new stress path which is in general of higher degree of approximation than in the preceding stage. New constants a, b and c are selected on the basis of the new stress path, and again a secant-modulus iteration is repeated. Thus, in order to solve a problem two-fold loops of iteration for stress or strain as well as for stress path must be carried out.

As a result of analyses it revealed that in case of slope inclination I/I.5 the shear strain at the slope end within the SI-C layer exceeds I.0 % and the region of strains higher than 0.5 % appears on the sea bottom at I5 m behind the slope shoulder and extends shallow along the slope surface as far as the slope end, where it penetrates especially deep(50 m !)into the SI-C layer. In case of inclination of I/2.0 the strain higher than I.0 % does not appear and only a small region at the slope end within the SI-C layer attains 0.9 % strain. One of the regions exceeding 0.5 % strain extends into the SI-C layer as long as 50 m, and another appears at the slope shoulder. The results show a marginal factor of safety in the former case in contrast to a substantial stability in the latter (Fig.2).

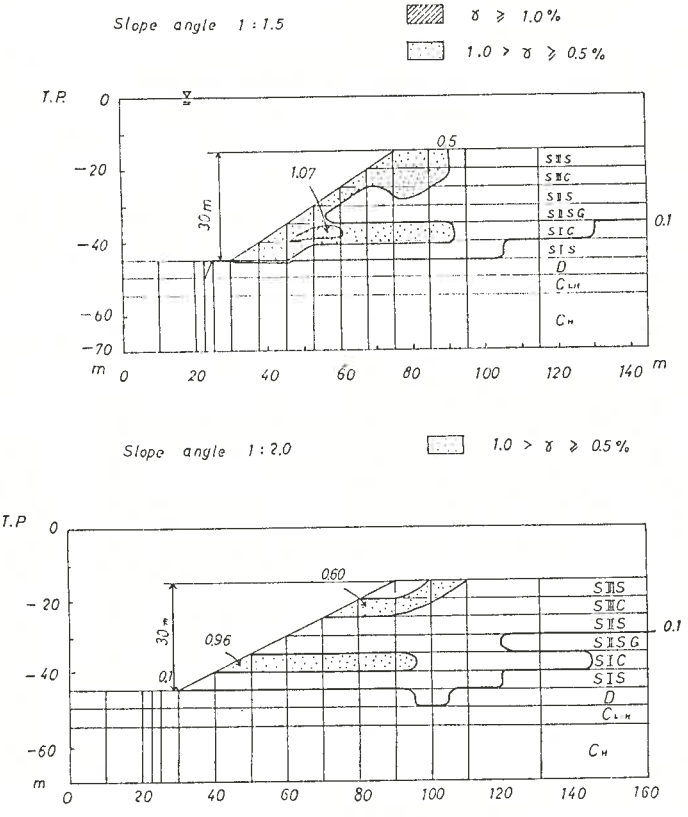

Fig.2 Shear-Strain Distribution after 30 m Excavation →

Table I Ultimate Strain and Factor of Safety for I % Strain

Layer	ult.str.	fac.of saf.
SIII-S	4.0 %	I.45
SIII-C	7.5	I.78
SII-SG	2.0	I.07
SI - C	2.5	I.20
SI - S	2.5	I.22

REFERENCE

Duncan,J.M.: Nonlinear Analysis of Stress and Strain in Soils. J.Soil Mech. and Found.Div., Proc. ASCE, Sept.I970, SM 5.

EVALUATION OF DEFORMABILITY OF SOFT ROCK MASS CONSIDERING SWELLING AND SLAKING CHARACTERISTICS

Keiji KOJIMA, Yasusuke SAITO, The University of Tokyo
and Hiroto OCHI, Honshu-Shikoku Bridge Authority

With respect to the sharp decrease in the modulus of deformation accompanying the swelling and slaking, here from stand point of estimating the modulus of deformation (Esp) of a rock mass from the core test values (Es), the decreasing deformability in the core test values as related to the swelling and slaking factors will be examined through correlation analysis.

1. Simple and rapid test for swelling and slaking: For simple and rapid test of the swelling and slaking, practical applicability is observed in testing the change in repeated cycles of drying and wetting of the intact rock (proportion to the moisture content in the first cycle, WSL_1) and simple water absorption test of the powdered rock with solidification removed by pulverization (moisture content, WA). While for the swelling strain ($\Delta V/Vo$), typical values were taken through the conventional one dimensional swelling strain test with no axial pressure. The samples used for swelling test were of artificially compacted mud stone according to the method of Nakano (1966).

Rod penetration test is a kind of point loading tests. RP is the slope of load to deformation when the rod ($2mm^2$ in cross sectional area) is penetrated into rock fragments of several centimeters.

2. The meaning of the test values: The WSL_1 represents the extent of slaking and is considered to be a quantum associated with the fragility of intact rock, and the WA represents the latent possibility of swelling of the constituent particles upon removal of the cementation of rock fragments. Fig. 1 illustrates the meaning of cross plotting of these two factors.

The mud stone provided by artificially compacting the pulverized rock fragments into the original density corresponds to the intact rock without cementation and is thus considered to give a maximum swelling strain at such density. In Fig. 2 are plotted the maximum swelling strains of "artificial mud stones" prepared from some samples of different WA values with the dry density changed.

RP is considered to represent the strength of cementation or fablic of the grain particles. The RP is usable as an index of the degree of solidification

preventing the swelling and slaking.

3. Composite scores of swelling and slaking: However, the aptitude to swelling and slaking of a rock mass is hardly expressed by a single factor among such factors. It will then be convenient if there is any simplified characteristic value (or composite score) available for examination of the distribution of swelling and slaking or correlationship with any other quantum. Here such a simplified characteristic value will be sought upon the concept of principal component analysis (a kind of multivariate statictical analyses). Here, using, as the factors of swelling and slaking, WSL_1, RP and $\Delta V/Vo$ described in the foregoing, a composite score is considered.With respect to the data of the Kobe Group, the first and second principal components Z_1 and Z_2 are calculated.

4. Evaluation of deformability considering swelling and slaking: Primarily, in a soft rock area, it has been found that core test values are nearly in agreement with the values of insitu test in a logarithmic relationship. While in the mud stone of the Kobe Group which has swelling characteristics, both are not in agreement as shown in Fig. 3. Esp is measured generally under a wet condition immediately after drilling so that it is scarcely subjected to the influence of swelling and slaking. Then, it is considered that the extent of swelling and slaking of Es can be expressed by log Es/log Esp, (RLE).

When the correlation of RLE and the principal component Z of swelling and slaking is sought, there obtained an estimated RLE according to the multiple regression equation with respect to the factors of Z, and estimated RLE is correlated to the values of measurement as shown in Fig. 4. The multiple regression equation is expressed by

$$\log Es/\log Esp = 0.742 - 0.297Z_1 + 0.133Z_2 \quad \text{---------- (1)}$$

And the multiple correlation corefficient r is 0.76. It is considered to be closely related with the factors of swelling and slaking. The equation (1) is transformed as

$$\hat{Esp} = Es^{1/EST(Z_1,Z_2)} \quad \text{---------- (2)}$$

$$EST(Z_1,Z_2) = 0.742 - 0.297Z_1 + 0.133Z_2$$

with respect to estimate the modulus of deformation from the composite scores. The relationship between the values of test in bore hole of the modulus of deformation (Esp) and the estimated ones ($\hat{Esp}$) obtained from the equation (2) is illustrated in Fig. 5.

This figure makes a suggestion that the deformability of soft rock mass can be properly evaluated, if the core test values (Es) are corrected with swelling and slaking characteristics. But in the relation of Fig. 5, the correlation coefficient is rather small (r = 0.46). This may be the reason why large amount of scatter is originally found in measured values of rock mass and measured points of Es and Esp were not always the same in the depth of bore hole. In

addition to the reason, considering that the correlation coefficient between Es and Esp was very small value of 0.03 before correction, such correction is considered to be rather effective.

REFERENCE

NAKANO, R. (1966); The Bulletin of the Agricultural Eng. Research Station, Ministry of Agriculture and Forestry, No.4,Jan.,pp.143-169.

KOJIMA,K. (1978); Proc. 3rd International Congress of IAEG, Madrid, Spain, Sec. II, Vol. 1, pp.218-227.

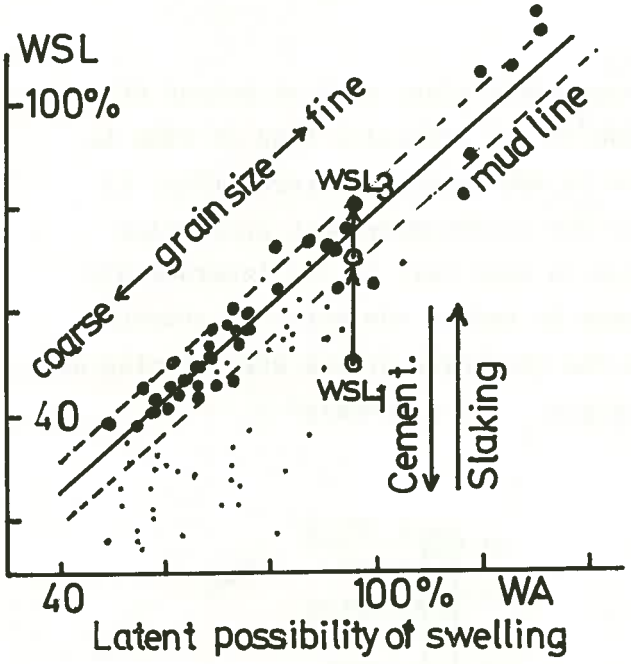

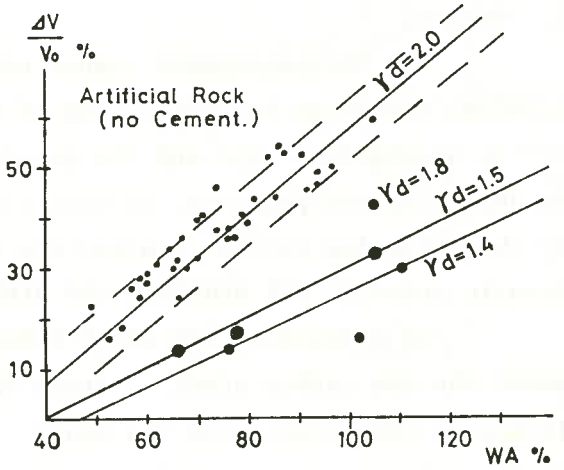

Fig. 2 Relation between WA and ΔV/Vo of artificial rocks compacted in various dry density (γd).

Fig. 1 Meaning of WA-WSL diagram (● completely disintegrated, ○ not completely).

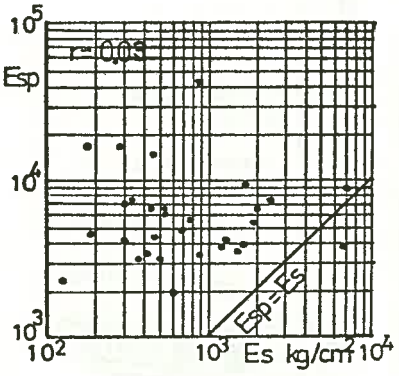

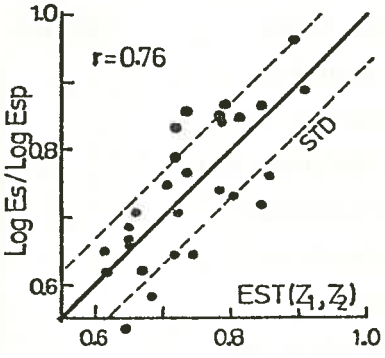

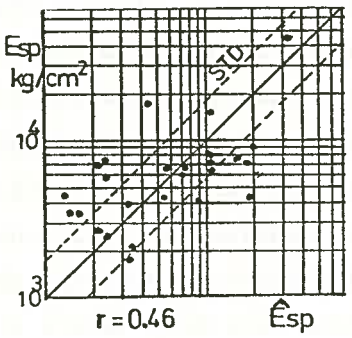

Fig. 3 (left) Relation between Es and Esp of the expansive soft rock mass in the Kobe Group of Miocene age.

Fig. 4 (center) Relation between the test values of RLE and the estimated ones calculated from the composite scores of swelling and slaking.

Fig. 5 (right) Relation between the test values of Esp and the estimated ones ($\hat{E}sp$) obtained from the measured Es corrected by the composite scores.

THE SHINTAKASEGAWA EMBEDDED PENSTOCK DESIGN

Youichi MIMAKI, Tokyo Electric Power Co., Inc.
Shouzou KATANO, Tokyo Electric Power Co., Inc.
Minoru KAMIJYO, Tokyo Electric Power Co., Inc.

1. General

The Shintakasegawa pumped storage power plant with an output of 1,280MW, discharge for generating of 644m^3/S and effective head of 230m is of the underground type and the penstock is embedded in bedrock. (Fig. 1) In designing the penstock, we made clear the surrounding rock properties by the following method to allow the rock to bear part of the internal hydraulic pressure and provided the drainage to reduce the external pressure.

As a result, we could reduce the thickness of the steel lining and adopt the low carbon steel (Break Strength 5.8 x 10^5KN/m^2) lining in comparison with the usual design and ensure good weldability under the severe condition in the shaft.

2. Design for internal pressure

The stress of the steel lining and the surrounding rock for internal pressure was obtained from the multiple thick-walled cylinder analysis based on the theory of elasticity assuming that the visco-plastic deformation is in proportion to the elastic deformation and the surrounding rock is isotropic and homogeneous. But the bedrock at this penstock site was granite and there were many joints at the site, so before the design, the inelastic characteristic of the rock and the properties of gap were investigated from the in site chamber test and we verified the deformation equation applied to the surrounding rock. The

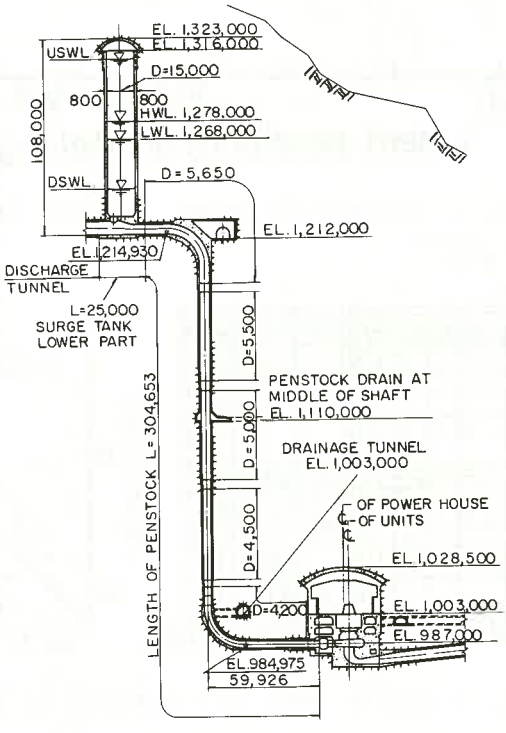

PENSTOCK	UNIT	NOTE
TYPE		4- EMBEDED IN TUNNEL LINING
INSIDE DIAMETER	M	5.65 ~ 3.30
LENGTH	"	NO.1, NO.3 322, NO.2, NO.4 339
BRANCH	"	WYE BRANCH INSIDE DIAMETER 8.0~5.65
DESIGN INSIDE PRESSURE	"	120 ~ 380

Fig. 1 Shintakasegawa Penstock

chamber was about half scale of the real size. (Fig. 2) Maximum pressure was 3000KN/m^2 in which the strain level is equivalent to the real penstock, and the displacements of the steel lining, the concrete backfilling and the surrounding rock were measured continuously. An anisotropy of the secant elastic modulus (Table 1), (E max/E min), was about 1.1 ~ 1.2. As for the design analysis for internal pressure, it was assumed that the rock was isotropic and homogeneous, and the smallest elastic modulus (E min) was adopted.

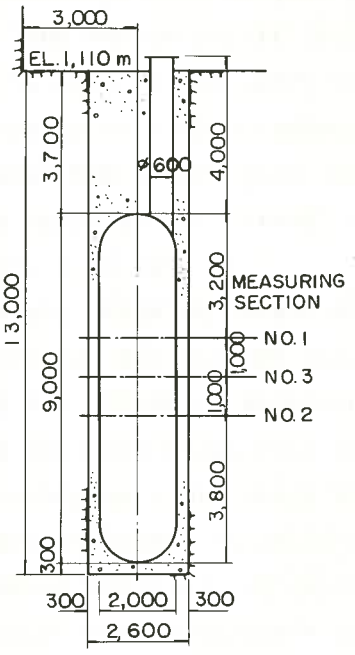

Fig. 2 Test chamber

The result shows that the plastic displacements of rock including the gap between the concrete and the rock is large at even low stress level before grouting, but after grouting, the plastic displacement is in proportion to the elastic displacements, as a results, the steel lining stress after grouting can be reduced remarkably. (Table 1, Fig. 3)

The entire length of the penstock was subjected to consolidation grouting (P = 1000 ~ 1500KN/m^2) in order to ensure the adequacy of the design.

The rock properties along the entire length of the penstock were grasped by the sonic logging and the elastic modulus along the penstock was obtained from the relationship between the dynamic elastic modulus at the chamber test site and the static one obtained from the chamber test. As a result, the elastic modulus of the rock was larger than 1.2 x 10^{7}KN/m^2, but the elastic modulus of the rock applied to the design analysis was uniformly determined 6 x 10^{6}KN/m^2 and the plastic displacements of the rock including the creep was regarded as 50% of the elastic displacement.

As a limit of bearing part of the rock of the internal pressure,

	CHAMBER TEST		JACK TEST	SONIC LOG	CORE TEST
	VALUES BEFORE CONSOLIDATION GROUTING	VALUES AFTER CONSOLIDATION GROUTING			
ELASTIC MODULUS (x10^{6}kN/m^2)	20.2	23.1	10.8	30.7	28.8
THE RATIO VERSUS SONIC LOG	0.66	0.75	0.35	1.00	0.94
PLASTIC DIPLACEMENT (mm)	0.05 δ_e + 0.029	0.23δ_e + 0.001	—	—	—
CREEP COEFFICIENT α (%)	12.2	18.8	16.0	—	—
CREEP COEFFICIENT β (1/hr)	1.02	1.09	1.65		
POISSON'S RATIO ν	—	—	—	0.34	0.13
LEGEND	MEAN VALUE OF FOUR MEASURING POINTS		MEAN VALUE OF EIGHT POINTS	ø 56 BORING	

Table 1 Chamber test results

we adopted such a condition that the steel lining stress must not exceed the yield stress even if the boundary condition of outerpart of the steel lining was free.

3. Design for external pressure

In case of a usual method, the design external pressure is very large because the penstock is installed in shaft, and if we design for this large external pressure, the steel plate to prevent the buckling of the steel pipe must be thick, so the effectiveness that the surrounding rock sustains hoop tension based on internal hydraulic pressure is lessened.

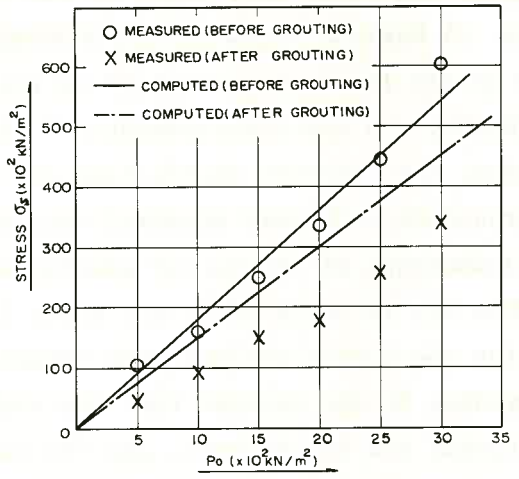

Fig. 3 Steel lining stress (σs) versus pressure (Po)

So we examined the means of decreasing ground water pressure by the electrical analogy. The electrical analogy results shows that, owing to the drainage effect of the tunnel which is installed in the upper, middle and lower parts of the penstock, the external hydraulic pressure for the penstock becomes less than about 60% of hydrostatic pressure, assuming that a static water level is equal to the seepage line. In case of providing the four drain holes (ϕ 50mm) parallel to the steel lining (diameter 6m), the external hydraulic pressure was reduced to 50% of that in case of no drainage, and in case of six drain holes, it was reduced to 30%.

Judging from the economical point of view including the internal hydraulic pressure, six drain holes (ϕ 100mm) were provided parallel to the steel lining for the purpose of reducing the external hydraulic pressure to 30% of hydrostatic pressure.

The coefficient of bearing part of the rock of the internal hydraulic pressure became 58 ~ 67%, as a result, the weight of steel lining was reduced to about 35% in comparison with the usual design.

THE METHOD OF ELASTO-PLASTIC ANALYSIS FOR UNDERGROUND EXCAVATIONS IN CONSIDERATION OF THE POST-FAILURE PROPERTIES OF ROCKS

Yoshiaki Mizuta, Shoji Ogino ; Yamaguchi University
Hikeun Lee ; Seoul National University, Korea
Yukitoshi Oka, Yoshio Hiramatsu ; Kyoto University

1. Introduction

The authors have developed a method of elasto-plastic analysis of rock stress and deformation around underground excavations laying emphasis on the fact that the strength of rock changes irreversibly depending on the three dimensional stress and strain state. The applicability of this method has been investigated by comparing the result of analysis of the deformation around a circular tunnel with those of a model experiment.

2. Post-failure behavior of rocks

The authors have used an extention of the Von Mises yield criterion to represent failure thus,

$$\left(\frac{\tau_{oct}}{Y_0}\right)^2 = a\left(\frac{I_1}{3Y_0} + b\right) \qquad (1)$$

$$I_1 = \sigma_1 + \sigma_2 + \sigma_3 = 3\sigma_m$$

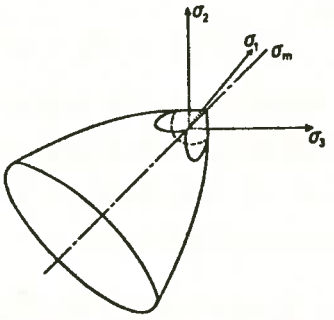

Fig.1 The yield surface expressed by equation(2) and (3).

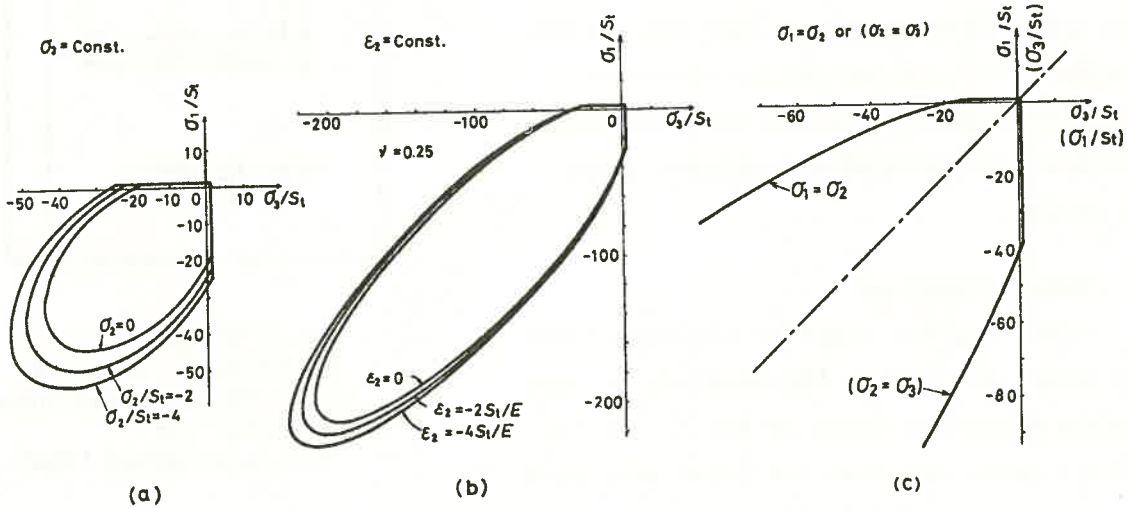

Fig.2 Failure criteria for several conditions for marble with the parameters $\alpha / S_t = 6.907$ and $K / S_t^2 = -4.865$.

$$\tau_{oct} = \frac{1}{3}\left[(\sigma_1-\sigma_2)^2+(\sigma_2-\sigma_3)^2+(\sigma_3-\sigma_1)^2\right]^{\frac{1}{2}}$$

σ_i ; Principal stresses
Y_0 ; Yield stress under uniaxial compression
a, b ; Material constants obtained from triaxial test

The general representation of equation(1) using stress invariants is

$$F = \alpha I_1 + J_2 - K = 0 \qquad (2)$$

$$J_2 = \frac{3}{2}\tau_{oct}^2, \quad \alpha = -\frac{1}{2}aY_0, \quad K = \frac{3}{2}abY_0^2$$

However, in the case where the maximum principal stress is equal to S_t(yield stress under uniaxial tention), the failure criterion becomes

$$F = \sigma_1 - S_t = 0 \qquad (3)$$

These conditions are represented graphically in Fig.1 and Fig.2. The value of Y_0 was assumed to be given by the empirical expression :

$$Y_0 = \overset{*}{Y}_0 \exp\left[-\beta\left(\varepsilon_1-\varepsilon_3-\frac{\sigma_1-\sigma_3}{2G}\right)^{\lambda+\mu\sigma_1}\right] \qquad (4)$$

$\overset{*}{Y}_0$; Uniaxial compressive strength
G ; Shear modulus
β, λ, μ ; Material constants
ε_i ; Principal strains

The solid lines in Fig.3 show the stress-strain curves calculated by equation(4), the dashed lines show the experimental results for confined compression tests on marble.

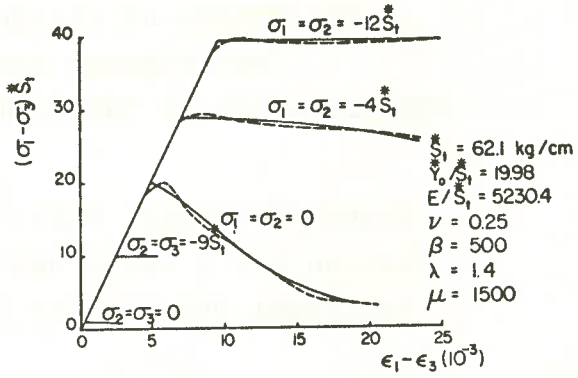

Fig.3 Stress-strain curves for uniaxial tension, uniaxial compression and confined compression tests.

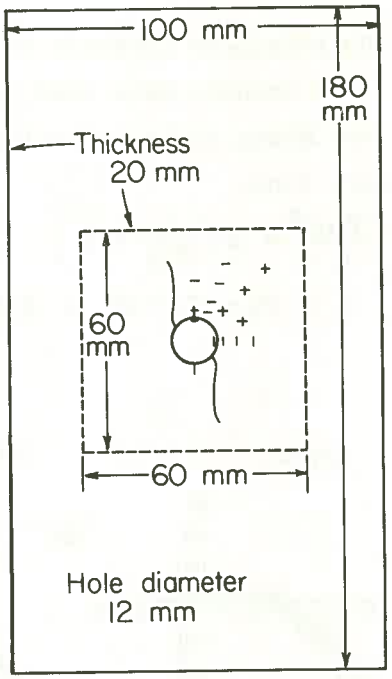

Fig.4 Models for experiments compared with the size and shape of model for analyses(dashed line).

3. Model experiment

The size and shape of the experimental model as well as the location of wire strain gages are shown in Fig.4. Both single gages and rosettes gages were used.

It was observed that tensile fractures were initiated first on the roof

and floor of tunnel, but these ceased to propagate and a second set of fractures as shown in Fig.4 were developed. The dashed arrows in Fig.5 show the measured strain at a later stage of the observations.

4. Analysis

The authors calculated the strains in the rock around a circular tunnel by the Initial Stress Finite Element Method assuming that every element behaved as a St. Venant body at each step in the calculation, but with a reduction in strength and increase in plastic-following the rule indicated by equation(4) during the next calculation step. Computation were carried out using the parameters shown in Fig.3. The model used in the analysis is shown in Fig.4. The calculated strains are shown by solid arrows in Fig.5 and, the development of tensile failure is shown by the cross-hatched regions in Fig.6. It is shown on these figures that the agreement between analytical results and experiment is fairly good.

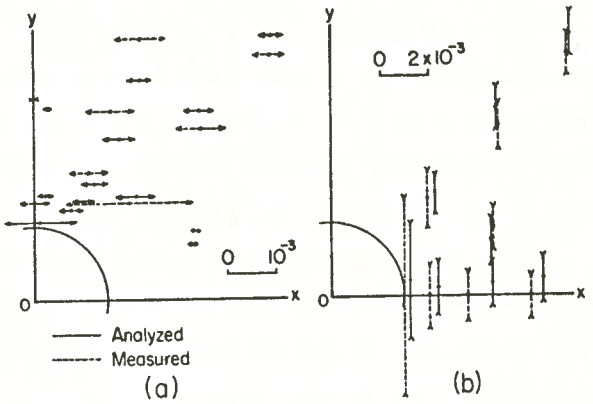

Fig.5 Comparison of the measured strains with the analyzed.

Reference
O.C.Zienkiewicz;The Finite Element Method in Engineering Science

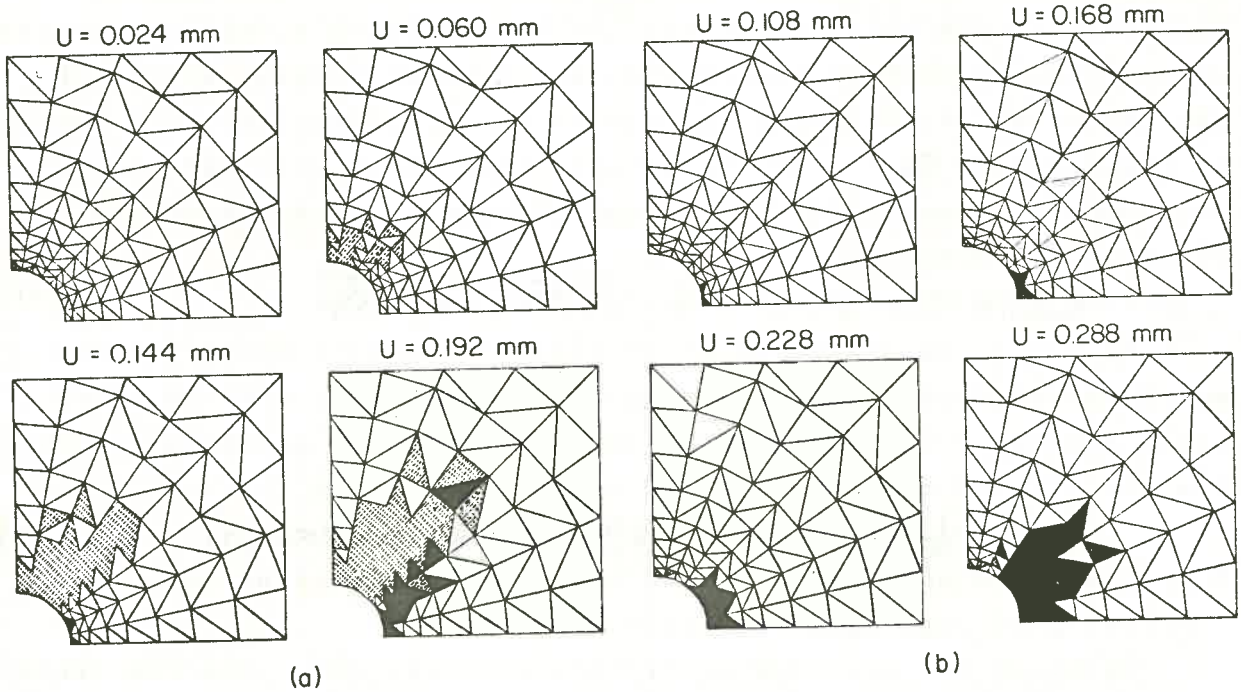

Fig.6 Initiation and development of failure under uniaxial(a) and biaxial(b) compression supposed by analysis.

ON THE FRACTURE CONDITION OF ROCK-LIKE MATERIALS IN COMPRESSION

Koji NAKAGAWA, Yamaguchi University

1 Introduction

In the study of fracture of rock-like materials one of the most interesting problem may be to make clear the fracture process of the specimen. It is known that the failure of a specimen of rock-like material occurs after a complicated fracture process that is crack initiation or propagation.

In this study the original and modified (by McClintock and Walsh) Griffith's failure criteria were discussed in explaining the fracture initiation and the strength failure of the specimen of rock-like materials.

2 Original and modified Griffith's failure criteria

In the two dimensional stress plane, Griffith related the concentrated stress at the tip of elliptic flaw to the failure condition of the brittle material. The Griffith's failure criterion means that the failure occurs when the maximum tensile stress at the tip of an initial flaw reaches at the thoretical tensile strength of the material σ_c. For the ellptic flaw which oriented at the angle ψ with respect to the maximum principal stress direction the condition is given by

$$\xi_0 \sigma_c \geq \sigma_1 \sin^2\psi + \sigma_2 \cos^2\psi - \sqrt{\sigma_1^2 \sin^2\psi + \sigma_2^2 \cos^2\psi} \qquad \cdots (1)$$

By McClitock and Walsh the Griffith's failure criterion was added an assumption that the flaws in the material tend to close under stress. The modified failure criterion is given as follows for an elliptic flaw which close under zero stress

$$\xi_0 \sigma_c \geq -\frac{1}{2}\left[(\sigma_1 - \sigma_2)\sin 2\psi - \mu\{(\sigma_1 + \sigma_2) - (\sigma_1 - \sigma_2)\cos 2\psi\}\right] \qquad \cdots (2)$$

3 Original and modified Griffith's failure criteria as failure criteria of rock-like materials

Original and modified Griffith's criteria only give the crack initiation conditions from the tip of the flaw in the material. However, these criteria are sometimes used as the failure (strength

failure) conditions of the specimen of rock-like materials because they give good strength failure conditions of the specimen. It will be interesting to discuss this relation because we know the complicated fracture process exists between the crack initiation and final failure of rock-like materials.

If we consider a single elliptic flaw of fixed eccentricity and orientation ψ, the crack initiation condition is given by Eq. (1). It means that the crack initiation conditions for flaws with different values of ψ are given by different curves in stress plane. When a stress point travels through a stress path, some internal flaws oriented at ψ will initiate branching cracks through a finite distance as soon as the stress condition satisfy Eq.(1) or Eq.(2). However, an insufficient amount of cracking will have taken place to cause a gross failure. Thus some additional "loading" will be required to produce further fractures. With an addition of loading, other flaws initiate cracks from their tips one after another. Ultimately, a sufficient intermeshed network of cracks will be formed so that macroscopic failure does occur and no further loading will be possible.

We assume an uniform distribution of open elliptic flaws and give the crack initiation condition by Eq.(1). The strength of the material and the eccentricity are taken to be kept constants. For a given stress point, some flaws satisfy Eq.(1) and some do not. If the loading path is fixed, the ratio of the number of the cracked flaws to the number of the total flaws is given for any stress point. Generally this ratio increases with the increase of the load. To get the ratio for every stress point, 100 flaws(open elliptic flaws) were assumed in the specimen. The value of ψ of each initial flaws was assumed to distribute uniformly between $0°$ and $90°$. With a fixed value of $\frac{3}{2}\sigma_c (=2\sigma_t)$, the number of flaws which satisfy Eq.(1) are shown in Fig.1 for each stress point.

Griffith's criterion in two-dimensional stress plane is given as an envelope for the crack initiation curves from the tips of elliptic flaws with any inclination to the principal stress direction. In Fig.1, the condition is given as the boundary between zero area and non-zero area (broken lines). But, as mentioned above, Griffith's criterion does not mean the failure condition of the specimen but means the crack initiation condition of rock-like materials. We assume that the strength failure of the specimen occurs when the fracture ratio (the ratio of the number of

the cracked flaws to the number of total flaws) reaches to a fixed value. If we take the ratio as 50%, the strength failure condition is given by solid lines.

Now we assume that the distributed initial flaws are closed elliptic ones and their crack initiation conditions are given by Eq.(2). The coefficient of friction between the flaw faces is taken to be 0.4. 100 initial flaws with uniformly distributed directions were assumed. The fracture ratio in stress plane is given in Fig.2.

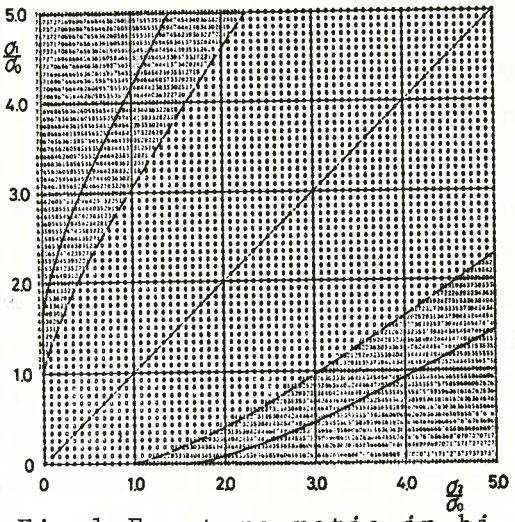

Fig.1 Fracture ratio in biaxial compressive stress. Griffith's criterion (in %)

In the actual rock-like materials the strength of flaw tips and the friction coefficients at flaw faces may not be constants. A Gaussian distribution of $\Sigma\sigma_c$ in Eq.(1) was assumed for 400 uniformly distributed initial flaws. The standard deviation from the average value is 25%. The fracture ratio is shown in Fig.3. The fracture initiation for this material occurs at lower stress level than that in Fig.2. When the strength failure conditions are given as 50%, the conditions in both materials are coincide because the distribution is normal.

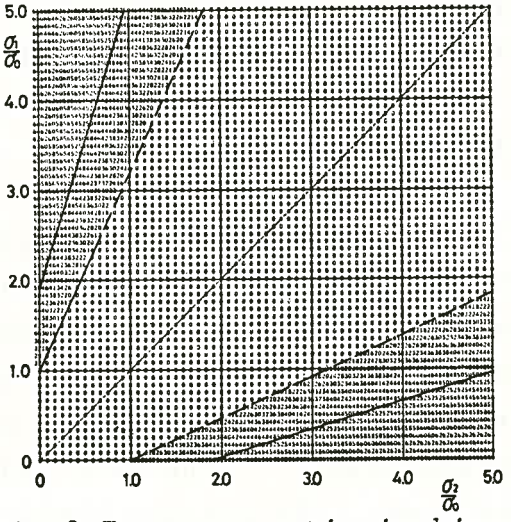

Fig.2 Fracture ratio in biaxial compressive stress. Modified Griffith's criterion

When the values of μ and $\Sigma\sigma_c$ are distributed normally, the fracture initiation condition is not straight lines, but strength failure condition remains as straight lines.

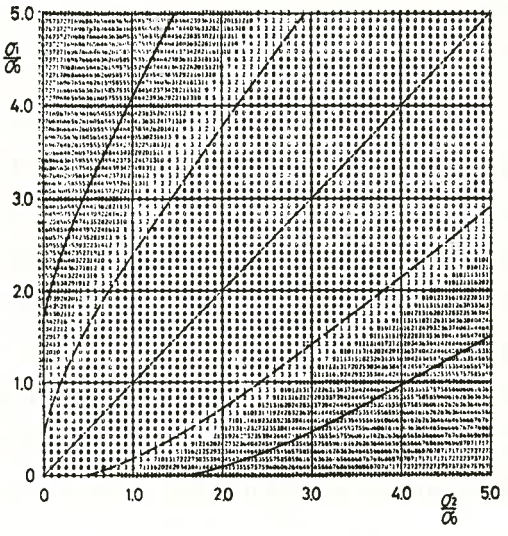

Fig.3 Fracture ratio in biaxial compressive stress. Griffith's criterion with normally distributed

CAVE-IN DUE TO MINING AT SHALLOW DEPTHS

Tadashi NISHIDA, Kyusyu university

Nobuhiro KAMEDA, Kyusyu university

Due to mining at shallow depths, it often happens that the roof of a cavity falls in and that the surface above a cavity caves in. This cave-in is different from general surface subsidence. That is, in case of cave-in, the structures on the ground suddenly collapse but the extent of the damage on the surface is small. Experimentally, it is known that when a cavity exists within a depth of 30 m, cave-in occurs and the extent of the damage is within about 3 m in diameter.

The authors have studied the mechanism of cave-in theoretically by incremental load procedure of the finite element method, on the assumption that the ground is an elasto-plastic material in which a bi-linear stress-stain relationship is established. In this analysis, we applied the Mohr-Coulomb condition of failure, where the tensile strength is half the cohesion. If it is judged from this condition that an element becomes to fail, its Young's modulus and Poisson's ratio are changed respectively to $E'=E/100$ and to $\nu'=1.5\nu$ as shown in Fig.1(where E and ν are Young's modulus and Poisson's ratio respectively in an element which does not fail).

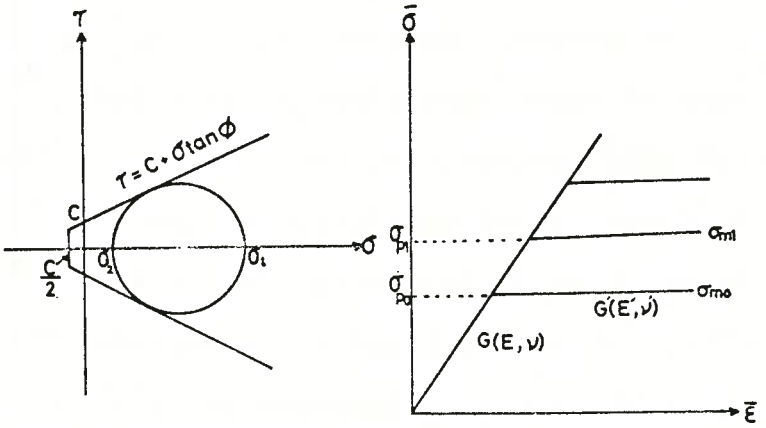

Fig.1 Mechanical properties of ground

Whether cave-in occurs or not, is determined by the development of the plastic zone, its geometrical shape and deformation around the cavity. Fig.2 shows the relationship of the critical depth of cavity(Hc) to the width of cavity(2b) for different cohesions of the ground(c). Here the internal friction angle(ϕ) and the specific weight(γ) of the ground are taken as 40° and 2.5 t/m^3 respectively. As indicated in this figure, in the case of 2b=10 m, c=5 t/m^2 and a depth of cavity less than 16 m, cave-in occurs. Fig.3 shows the relationship of the critical depth of cavity to the cohesion for different internal friction angles. Here the width of cavity is taken as 10 m and the specific weight as 2.5 t/m^3. When the cohesion is over 11 t/m^2 approximately, the effect of the internal friction angle can be neglected and cave-in does not occur.

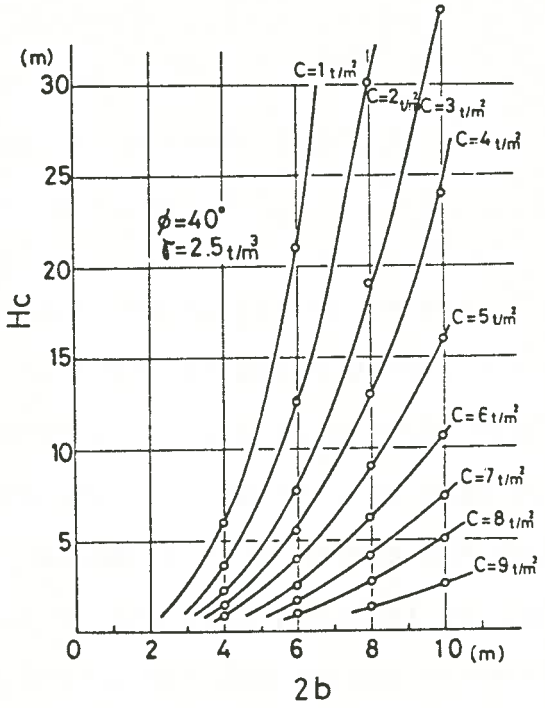

Fig.2 Relationship between Hc and 2b with parameter c

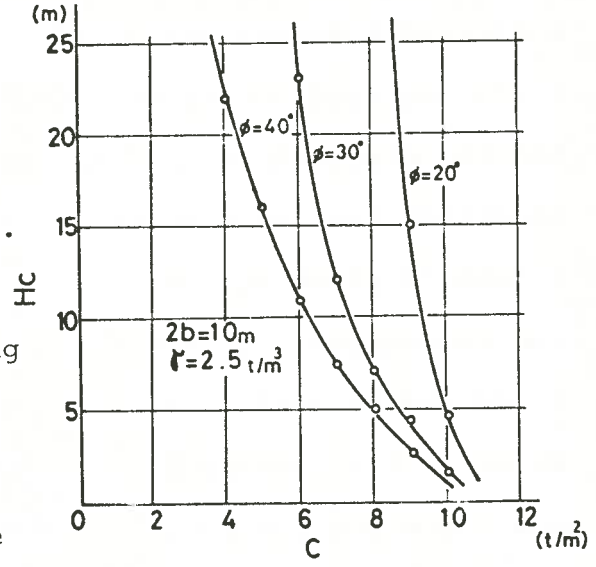

Fig.3 Relationship between Hc and c with parameter ϕ

In general, cave-in has a tendency to occur very often after a long and heavy rainfall or when a cavity is drained, and especially in the latter case. This cave-in due to the effect of rainfall and drain depends on three factors : increase of specific weight, decrease of shearing

resistance and decrease of strength of the ground.

Loading on the surface above a cavity also has an important effect on the occurence of cave-in. As the effective factors, the width of loading(2B), the depth(H) and width of the cavity and the internal friction angle must be considered. Consequently the width of loading(2Bs) which is given by Eq.(1) and Eq.(2) develops mostly the plastic zone.

in case of a rectangular cavity

$$2Bs=2b+2H\cot(45^{\circ}+\phi/2) \qquad (1)$$

in case of an arched cavity

$$2Bs=2H\cot(45^{\circ}+\phi/2) \qquad (2)$$

Fig.4 shows the relationship of the ratio of the width of loading to the width of cavity to the magnitude of loading for different depths of cavity when the plastic zone develops to the surface in the case of a rectangular cavity, 2b=8 m, c=1 t/m^2, $\phi=40^{\circ}$ and $\gamma=0$. In Fig.4 the values in parentheses show the ratios of 2Bs/2b which are derived from Eq.(1).

As described above, it becomes clear that the occurence of cave-in is related to the width and depth of the cavity, the mechanical properties of the ground, the existence of water and the loading on the surface.

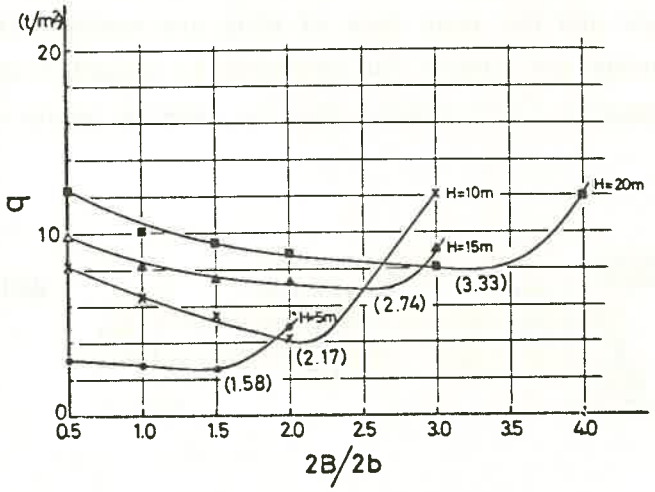

Fig.4 Relationship between q and 2B/2b with parameter H

THE FAILURE AND DISPLACEMENT OF CONCRETE PLUG FOR SEALING IN THE PIT MOUTH OF CLOSED MINE

Yuichi NISHIMATSU, The University of Tokyo
Yukitoshi OKA, Kyoto University
Yoneji NISHIDA, Metal Mining Agency of Japan

1. Introduction.

The mine water flowing out from the closed mine must be chemically treated or the pit mouth has to be sealed to prevent the water pollution, because the mine water is frequently acidic and contains a small amount of metallic ions. The latter is better than the former, because the operating cost is not needed for the sealing, but for the chemical treatment.

Thus, many concrete plugs for sealing are constructed and planned for construction in the pit mouth of closed mine. These plugs and the rock mass around the plug must be completely water-tight and strong enough to support the hydrostatic pressure of dammed up mine water.

This paper reports the model tests to find the design criteria of concrete plug for sealing.

2. Model test in the hard rock.

A borehole of ca.77 mm in diameter is bored through the massive block of rock sample, as a model roadway. A model plug made of cement mortar is constructed in this model roadway (see Fig.1). The mechanical properties of rock sample and plug materials are shown in Table 1. After the rock wall of borehole and the rear face of plug are coated with the water-tight paint, the mechanical packer for grouting is inserted into the borehole. The hydrostatic pressure is increased step by step by means of a grouting pump. Two types of

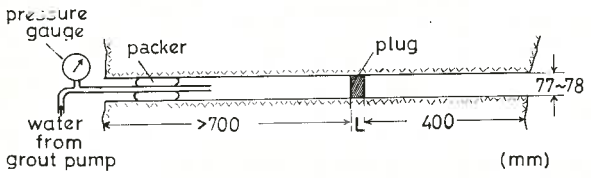

Fig.1. Schematic Illustration of Model Test.

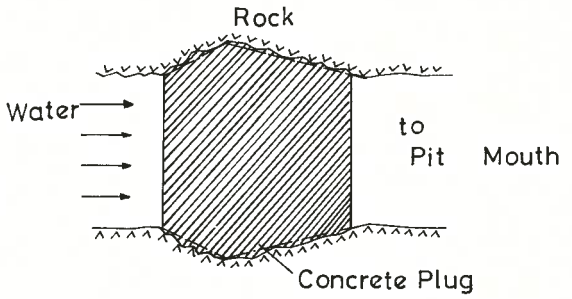

Fig.2. Conventional Type of Concrete Plug.

Table 1. Mechanical Properties of Rock Mass and Plug.

	Test in Hard Rock		Test in Weak Rock	
	Rock Sample	Model Plug	Model Rock	Model Plug
Compressive strength	1,298 kg/cm^2	369	82	999
Tensile strength	72 kg/cm^2	35	11	43
Shear strength	167 kg/cm^2	67	19	94
Young's modulus	7.9×10^5 kg/cm^2	1.6×10^5	2.4×10^5	18.0×10^5
Poisson's ratio	0.32	0.20	0.09	0.19

model plug are tested. One of them is a cylindrical plug and another type is a conical plug, which needs reaming of the rock wall to be constructed and models the conventional type of concrete plug constructed in practice, as shown in Fig.2.

The test results are summarized as follows:

(1) The cylindrical plug without reaming of rock wall is very weak and easy to slip out by the hydrostatic pressure which gives a mean shear stress smaller than the shear strength of plug materials. The mean shear stress is defined as $\tau_m = P \cdot A/(L \cdot l)$, where P is the hydrostatic pressure, A is the cross section of roadway, L is the axial length of plug, and l is the mean cincumferential length of roadway.

(2) The conical plug with reaming of rock wall is sufficiently strong and supports the hydrostatic pressure which gives a mean shear stress greater than the shear strength of plug materials. This result is not explained by the theory of elasticity, and suggests the local yielding of rock and/or plug, because the elastic stress analysis gives an extremely sharp stress concentration near the rear face of plug.

3. Model test in weak rock.

In some cases, the rock wall of roadway is so fractured or soft that it is weaker than plug materials. In order to investigate such a difficult case, the weak rock is modelled by the cement mortar of a poor mixing proportion. The model plug is prepared with another hard cement mortar, the mechanical properties of which are shown in Table 1. The model roadway of 140 mm in diameter with a model plug is prepared by molding of model rock mass. The hydrostatic pressure is applied by means of a gummy capsule connected to a grouting pump, because it is afraid that the permeation of water would cause swelling of the model rock.

The test results are summarized as follows:

(1) The mean shear stress at which the yield and failure of rock wall takes place to cause the slip of model plug is greater than the shear strength of model rock materials.

(2) The model rock mass is longitudinally cut into half cylinders to observe the failure crack as well as slip lines around the model plug (see Fig.3). Three types of crack has been observed, which are radial tension cracks, conical tension crack extending from the perimeter of plug to the front free surface, and circular shear cracks in the rock wall near the front face of plug.

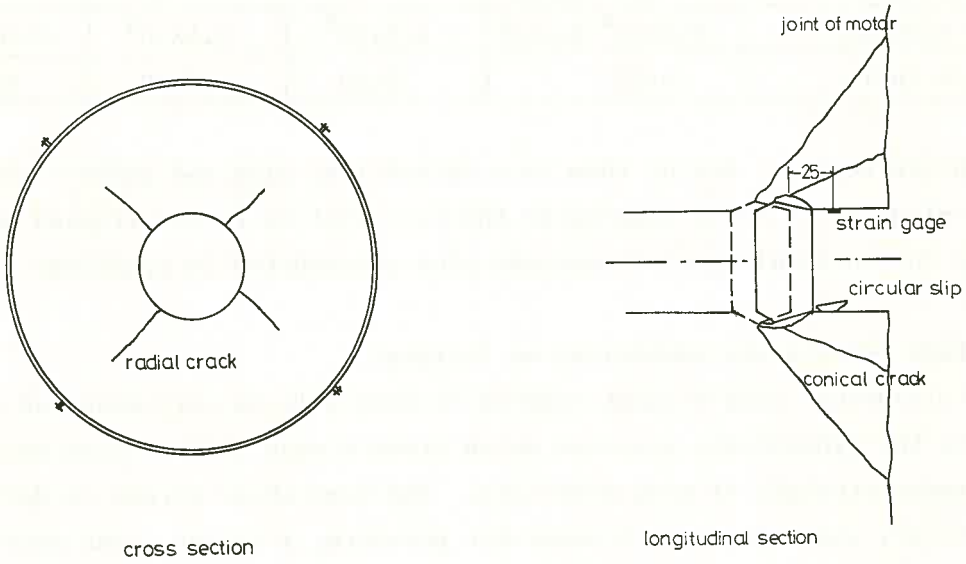

Fig.3. Failure Cracks and Slip Lines in the Weak Rock.

In order to explain these test results, the elasto-plastic stress analysis and computor modelling of the progressive failure of rock are carried out by means of F.E.M., considering the mechanical properties of model rock.

The results of theoretical analysis are summarized as follows:

(1) The conical tension crack would be generated at the lowest hydrostatic pressure, next the radial tension crack would be generated and finally the yielding of rock wall near the front face of plug would occur.

(2) The mean shear stress around the plug needed for the yielding of rock wall near the front face of plug is nearly 10% greater than the test result.

4. Conclusion.

Based on the theoretical analysis and the test result, it's concluded that:

(1) The cylindrical plug without reaming of rock wall is easy to slip out.

(2) The resistance against the slip of conical plug is greater than the estimation based on the mean shear stress hypothesis.

(3) The theoretical analysis shows that the tension crack occurs in the weak rock near the rear face of plug at a relatively low hydrostatic pressure. This tension crack would increase the water permeation which would accelerate the progress of failure process in turn.

STRUCTURAL BEHAVIOR OF THE KUROBE DAM AND DEFORMATION OF ITS FOUNDATION ROCK

Takehiko NIWA The Kansai Electric Power Co., Inc.

The Kurobe dam was completed in 1963. Water which started to fill up the reservoir in earlier years had reached to an intermediate level in 1960 and the level was raised in successive years with careful reservoir operation and by planned stages before it came to a maximum water level in 1969.

Type: Center over-flow type arch dam
Structural height: 186 meters
Crest length: 492 meters
Volume of dam: 1,608,000 cubic meters
Reservoir capacity: 199,285,000 cubic meters

The structural behavior of the dam and its foundation rock has been and is being observed over a long time with various measuring devices which are arranged in the extraordinary large number and over wide areas of the dam and the foundation rock. This paper is to deal with the records obtained by the rock deformeters which were placed directly to measure the inner deformation of the foundation rock.

1. Deformation of Foundation Rock

In 1964 rock deformaters were placed and have since been in service. The reservoir water level was then 1415 meters. Shown in Fig. 1 are some examples of horizontal deformation measured by the rock deformeters placed in two horizontal planes of both banks. What these rock deformaters showed is the elastic deformation of the rock foundation but residual deformation is also recognized to some extent. It is observed that even in case the comparatively large residual deformation was recorded the foundation rock showed elastic deformation and its residual deformation became smaller after the maximum water level was reached. Ratio of Er1 (modulus of rock deformation during virgin loading) to Er2 (modulus of rock deformation during repeated loading) obtained in Fig. 1 is

0.26 - 0.48. The value of Er1 over Er2 obtained by rock test in site is in the range of 0.30 - 0.62. The average value is 0.46. Strain values as obtained by rock deformeters are as shown in Table-1 below:

Table - 1 Strain of Foundation Rock

		RIGHT BANK		LEFT BANK		TOTAL AVERAGE
		1370m	1340m	1365m	1320m	
Total strain	Average	71×10^{-6}	49×10^{-6}	69×10^{-6}	68×10^{-6}	60×10^{-6}
	Near by dam	101×10^{-6}	79×10^{-6}	111×10^{-6}	104×10^{-6}	-
	Far away from dam	54×10^{-6}	34×10^{-6}	38×10^{-6}	46×10^{-6}	-
Residual strain	Average	21×10^{-6}	26×10^{-6}	49×10^{-6}	50×10^{-6}	37×10^{-6}
	Near by dam	28×10^{-6}	36×10^{-6}	70×10^{-6}	68×10^{-6}	-
	Far away from dam	17×10^{-6}	22×10^{-6}	34×10^{-6}	39×10^{-6}	-
Elastic strain	Average	50×10^{-6}	23×10^{-6}	20×10^{-6}	18×10^{-6}	23×10^{-6}
	Near by dam	70×10^{-6}	43×10^{-6}	41×10^{-6}	36×10^{-6}	-
	Far away from dam	37×10^{-6}	12×10^{-6}	4×10^{-6}	7×10^{-6}	-

Average strain obtained by the rock deformeter network is $49 \times 10^{-6} \sim 71 \times 10^{-6}$.

2. Stress Analysis of Dam by the Load History

For the purpose of examining the results of observation on the present state of the dam and the foundation rock, additional analytical studies have been conducted. The method employed for the analysis is the stress analysis of complete adjustment or S.A.C.A. as abbreviated. Two kinds of module of deformation were obtained by field tests as shown in Fig. 2 and they were taken into account as the load history. The radial deflection at the crest of the dam crown obtained by S.A.C.A. and measured by pendulum is shown in Fig. 3. While the reservoir level was raising up, the slope of the load and deflection curve obtained by the analysis is nearly identical with the one measured by pendulum. The annual increase of residual deformation as measured is larger than that as calculated by the analysis. After the maximum high water level was reached, residual deformation as measured by pendulum was found to be remarkably small.

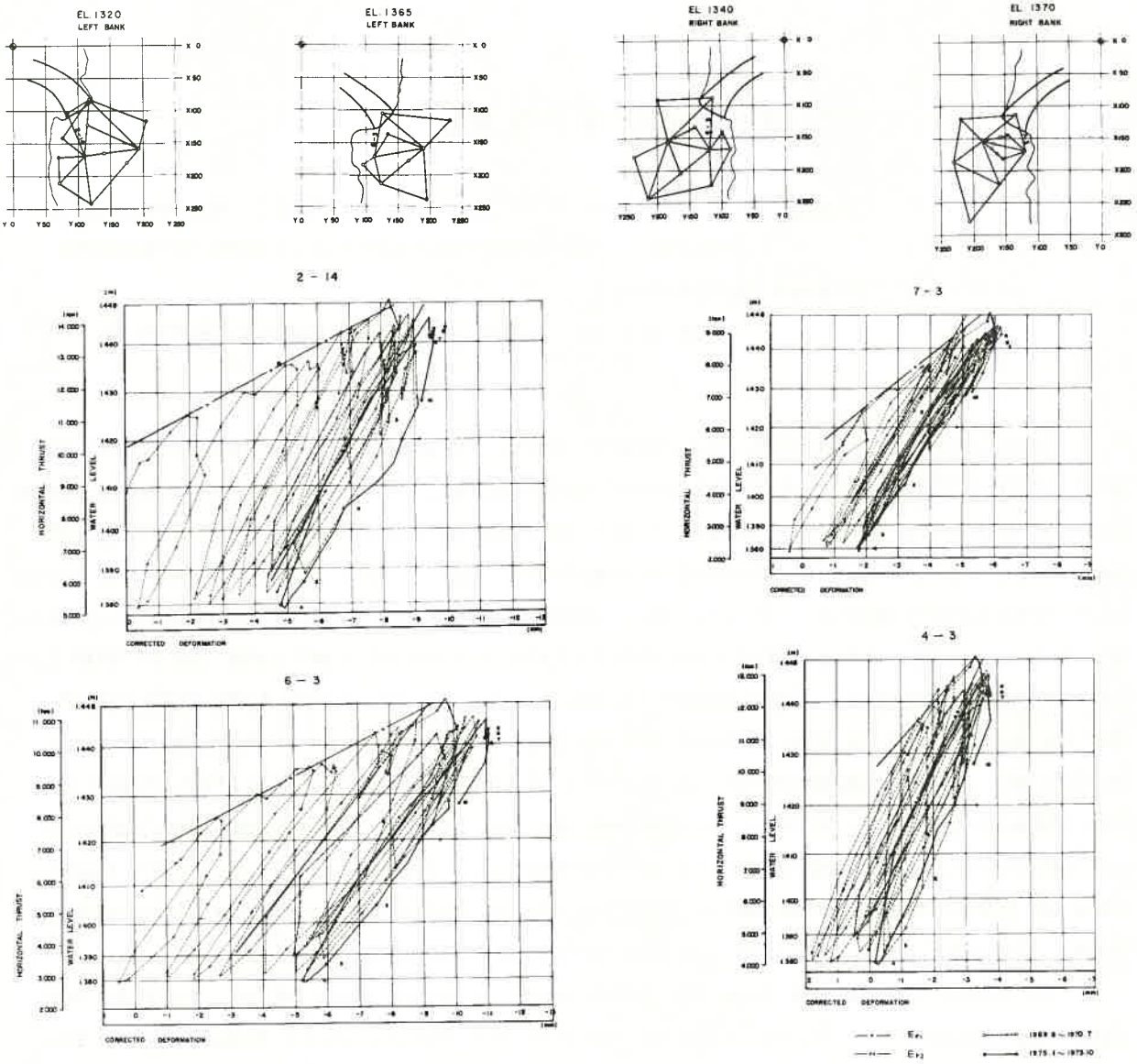

Fig.1 Water Level-Deformation Diagram of Rock Mass

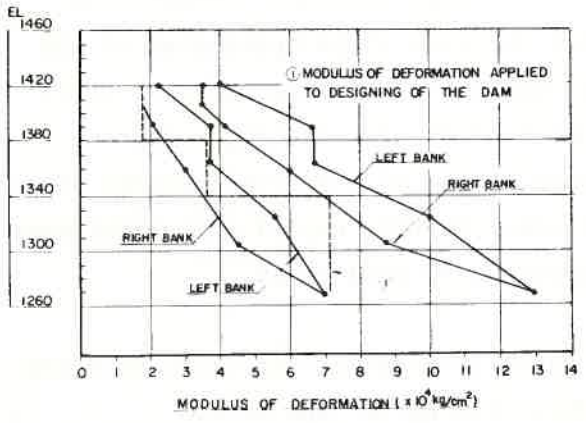

Fig.2 Modulus Deformation of Rock Mass

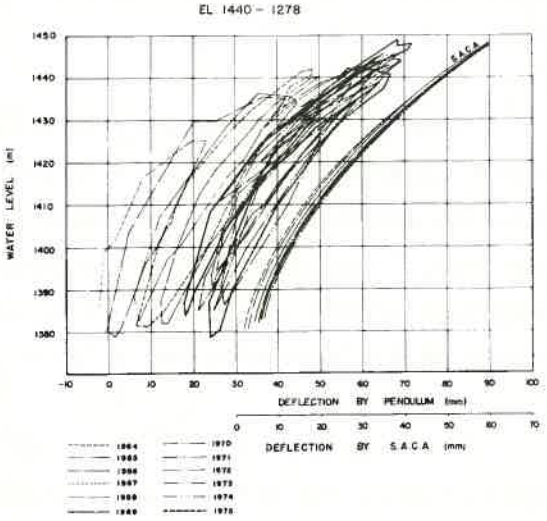

Fig.3 Dam Deflection due to Hydrostatic Pressure

A STUDY OF MECHANISM OF ROCK BURST

Yosiji NIWA, Shoichi KOBAYASHI, Takuo FUKUI, Masayasu OTSU
Department of Civil Engineering, Kyoto University
Minoru SHIMOKAWACHI
Japan Railway Construction Public Coorporation

Rock burst is a sudden and violent local failure from its surrounding medium induced by mining or underground excavations. The mechanism of rock burst has not been clarified yet, but in the persuit of researches of it mechanical behaviors of rock and structural characteristics of rock masses liable to burst have been investigated. It has been observed that rock burst occurred in general on the surface of a tunnel excavated into a zone of hard rock and of high initial earth pressure. From these facts, it may be concluded that rock burst may be influenced by the initial stress states of the surrounding, geological structures, rock characteristics such as strength and deformability, shape of the tunnel(opening), stress concentrations and deformations, and also methods of excavation including blasting or fracturing. We have not sufficient knowledge at present to decide which of them are of primary importance and how they work. In reality, these factors may be interrelated in a complex way.

In order to prevent from the occurrence of rock burst or at least to reduce the violence of it and also to predict the burst, it is necessary to investigate rock burst phenomena in detail and analyse them based on appropriate experimental or mathematical models, and then to apply the results to excavation and construction procedures.

This paper is a summary of a paper (of the same title) presented to the fifth internal congress of rock mechanics, Tokyo, 1977, which consists of 1) in-situ observations at the Daishimizu tunnel of the Johetsu super express railway, 2) laboratory model studies of rock burst, 3) three-dimensional stress analysis around an advancing face of a circular tunnel, and 4) some considerations on the mechanism and triggering conditions of rock burst.

The rock mass in the region of rock burst consists of quartz-diorite and subjected to the initial earth pressure about 180 kg/cm^2 and more.

Uniaxial compressive strength of the specimen shaped from a cored sample at the bursted site is about 2130 kg/cm^2 and tensile strength obtained by the

split test is about 110 kg/cm^2. Thus the brittleness index is about 20. The Poisson's ratio is about 0.21.

Small size rock bursts are observed and recorded by the use of apparatus for acoustic emission detection with frequency range 10 kHz - 1 MHz (PZ-5) and 1 kHz - 20 kHz (accelerometer 4344, B&K). In-situ records of events from 30 min. to 180 min. after blasting are shown in Fig.1. The counts of events decay as a whole exponentially with an increase of elapsed time after blasting. The close examinations of the records reveal that events continually occurred violently for a few seconds and that they decayed as a whole with the elapsed time. The arrival time decay of the P-S waves also increased with an increase of the elapsed time after blasting. This fact suggests that fractures occurred at first near the surface of a tunnel and gradually moved further deep into fresh zone until the stable some conditions were satisfied.

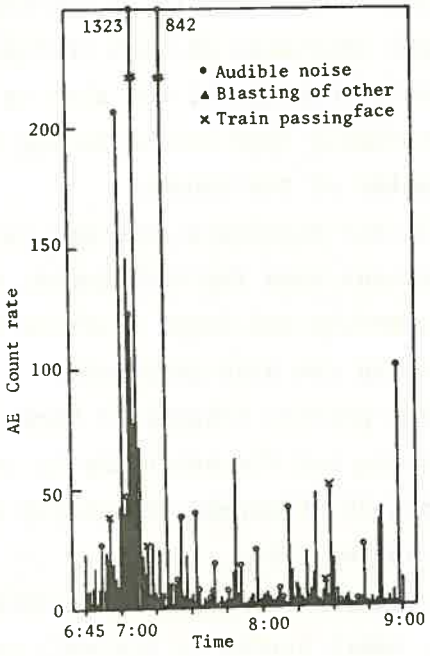

Fig.1 Events-Time record of rock burst

In the laboratory small size model tests of a tunnel, events of acoustic emission were also detected. They decreased with some periodical fluctuations with an increase of loaded time, even under constant load. These results are quite similar to those of in-situ observations. The very small fragments from the surface of a hole bored in the model were observed. These phenomena, so to speak of a small burst, are more distinguished in the more brittle models. These phenomena were observed when the model subjected to hydrostatic pressure about 40 - 60 percents of the uniaxial strength of the model material. The region of the phenomena occurred were the outside from the end face about a diameter of the hole.

The complete three-dimensional stress states around an advancing face of a circular tunnel are analysed by the use of the boundary integral equation method with an assumption of linear elasticity. The typical results are shown in Fig.2.

The maximum circumferential stress on the surface when subjected to an initial hydrostatic pressure p increases from 1.0p to 1.8p as going away from the

advancing face by a diameter of the tunnel. The regions beyond a diameter of the tunnel may apt to suffer from rock burst. The analytical results are in good agreement with the observed results both in the field and laboratory.

Knowledge about mechanisms and conditions of rock burst obtained from the research may be summarized as follows;

1) Rock burst occures on the surface of a tunnel excavated in high initial pressure zones of hard rock, and also in the outside region from the advancing face by a diameter of the tunnel.

2) Stress concentrations may play the most important role for rock burst, while inhomogeneity and local fracture due to blasting are also important.

3) The primary trigger to burst may be blasting and the secondary is increase of magnitude of stress due to the advance of the tunnel face.

4) The pre-burst phenomena such as discing, small bursts on the wall of a bore hole and audible or subaudible noise are useful informations to predict a burst.

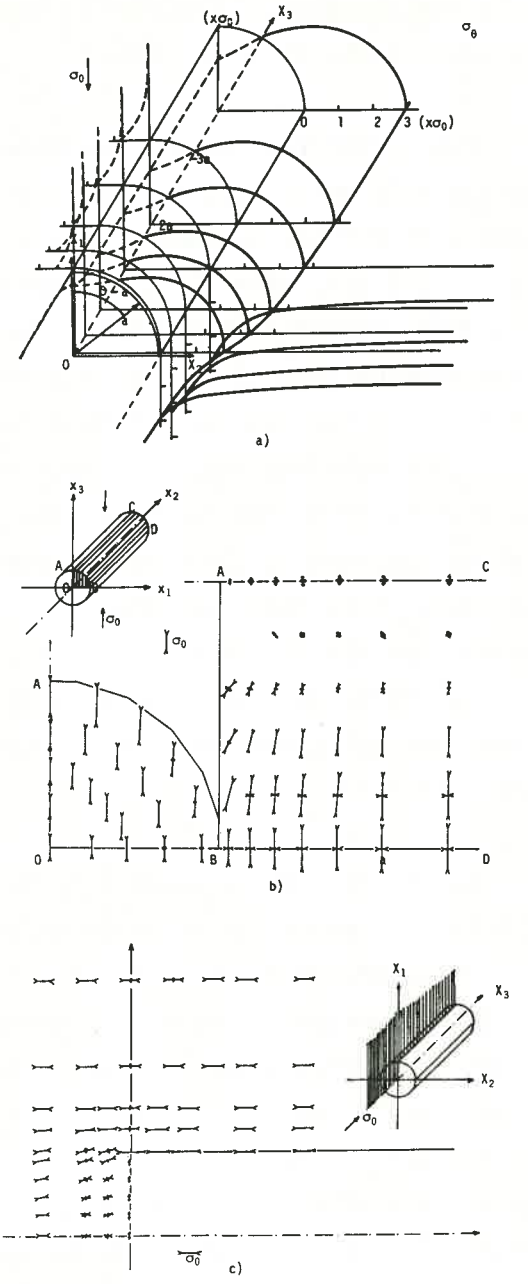

Fig.2 Stresses around an advancing face

It may be also concluded that rock burst on the surface of a tunnel may be predicted by the afore-mentioned pre-burst phenomena and that the strengthening of the surface by shot concrete or rock bolts, for instance, may be very effective to prevent or reduce the violence of rock burst.

As a matter of fact, rock bolts and metal net are effectively used at the Daishimizu tunnel so as to circumvent rock burst as well as a protective guards.

IN-SITU CREEP TEST OF WEATHERED GRANITE

Hisashi OHSHIMA, Yukikazu YANAKA,
Honshyu-Shikoku Bridge Authority

1. Introduction

It is traditional to consider that the amount of creep deformation of heavily weathered granite is smoller than that of elastic deformation. The amount of creep settlements of stuructures on weathered granite can be predicted by a simple stress-strain-time function such as logarithmic approximation, in short-time in-situ loading tests.

Prior to the designing the long-span Bridges foundations, long-time creep deformation tests in site was performed in order to grasp the creep deformation characterristics of heavily weathered granite. And that test results have been utilized for the design.

2. Test conditions and procedure

The plate loading tests were performed at the pier site of Tatara Bridge in Onomichi-Imabari Route. Prior to the loading tests, preboring were carried out in order to know the mechanical properties of the rock. Then, the tunnel with $2^m \times 2^m$ was excavated for 180m.

The material characteristics of rock which was used the creep tests were as follows;

The modulus of deformation (E_b); 100~1,500kg/cm^2,
The effective porosity (n); 18~25%,
The density (ρ); 2.1~2.2g/cm^3.

Loading was applied for a period of about 30 days in each loading stage using rigid circular loading plates of 40~60cm diameter. And grand strains under the plate were measured by triaxial and monoaxial strain-maters (capacity; 3,000~30,000x10^{-6}) for some case. The loading pattern is shown in Fig.1.

3. Creep test results

3.1. Creep deformation

The relation between the deformation of loading plate and the time is plotted in semi-log scale, as shown in Fig.2,

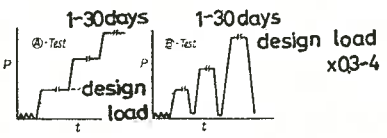

Fig.1. Loading pattern

and in log-log scale, as shown in Fig.3. The logarithmic approximation is applicable for a low loads ($P<10kg/cm^2$) and short durations (about 100~1,000 hours). Therefore, prediction by exterpolation of the amount of future settlement varies widely with which model to approximate.

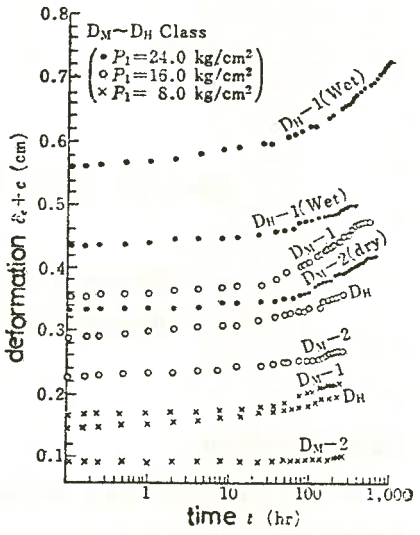

Fig.2. Deformation - Time Relationship

3.2. Behavior of underground strains

The relation between the vertical component of strain and the sustained creep load intensity is shown in Fig.4. The strains at shallow point are tend to flow in tensile side. This inclination was considered that the case of the instantaneous loading the elastic deformation occures under undrain condition, but the case of the sustained creep loading the inflence of natural ground occures. The relation between the volume compressive strain ($\varepsilon_V = \varepsilon_x + \varepsilon_y + \varepsilon_z$) and the deviator strain ($\varepsilon_r = \varepsilon_{max} - \varepsilon_{min}$) which were obtained by the results of measurement of the underground strains is shown in Fig.5.

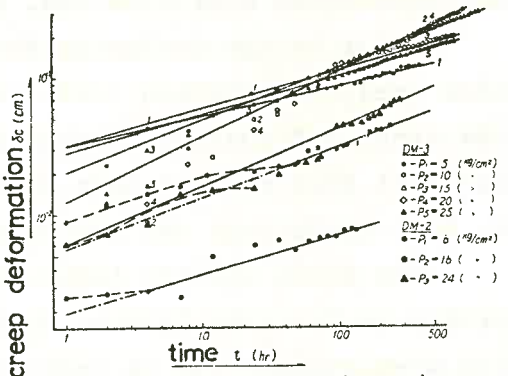

Fig.3. Creep deformation—Time Relationship

In case of instantaneous loading, the deviator strain generally tend to increase, but the volume compressive strain tend to increase remarkably in sustained creep loading (especially the intensity of load is less than $10kg/cm^2$). In other words, the greater part of the creep deformation is caused by the volume compressive strain. Therefore, the creep deformation characteristics of the weathered granite is effected by compaction. And creep shear strain under sustain loading does not tend to increase.

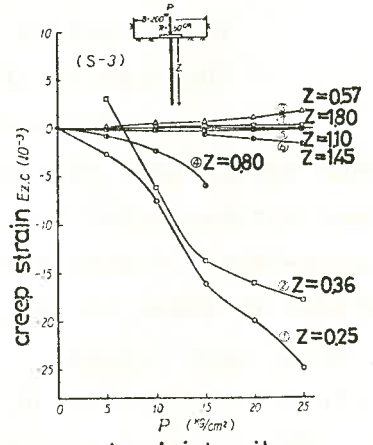

load intensity
Fig.4. Creep strain—Load intensity Relationship

The creep deformation of the weathered granite is considerably immense and complicated because of its geological origin and

mineral ingredients. In order to estimate the complex creep behavior of geologic materials for use in practice, a rheological models approach and an empirical relationship method have been proposed. Here, we applied 5-element Voigt model as shown in Fig.6, and the calculated material constants are listed in Table.1.

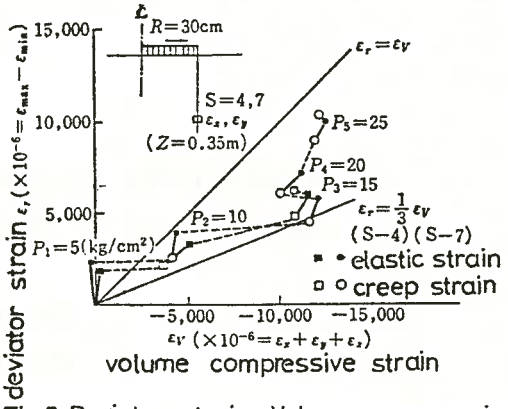

Fig.5. Deviator strain–Volume compressive strain Relationship

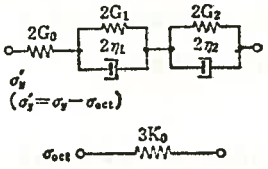

Fig.6. Rheological model

Table.1. Material constants of rheological model

	P (kg/cm²)	G_0 (kg/cm²)	G_1 (kg/cm²)	G_2 (kg/cm²)	G^* (kg/cm²)	η_1 (kg·min/cm²)	η_2 (kg·min/cm²)	G^*/G_2
B_{CW}-2	8	1.25×10^3	2.0×10^3	1.06×10^3	6.52×10^2	1.0×10^7	9.1×10^7	0.62
B_{CW}-1	5	8.3×10^2	1.3×10^3	1.6×10^3	5.1×10^2	7.8×10^6	5.3×10^7	0.32
	10	3.07×10^3	1.4×10^3	9.4×10^2	9.6×10^2	1.5×10^7	9.6×10^7	1.02
	15	6.7×10^3	1.7×10^3	1.6×10^3	1.4×10^3	1.4×10^7	1.5×10^8	0.88
	20	1.2×10^4	2.2×10^3	4.7×10^3	1.9×10^3	2.3×10^7	2.5×10^8	0.41
	25	1.4×10^4	2.2×10^3	5.4×10^3	1.9×10^3	2.4×10^7	4.5×10^8	0.35

$$G^*=\frac{G_0G_1}{G_0+G_1}$$

PROBABILISTIC CONSIDERATION ON THE INITIATION AND PROGRESS OF FRACTURE IN ROCK-LIKE MATERIALS

Masao SATAKE, Tohoku University
Hisataka TANO, Nihon University

1. Introduction This paper proposes a probabilistic consideration on the relation between the stress of fracture initiation and the final strength in rock-like materials, using a bundle model composed of a large number of elements with statistically distributed strengths.

2. Proposed model for fracture

It is well-known that on the uniaxial compression test an evident differnce is observed between the stress of fracture initiation and the final strength. From the above fact it may be suggested that the strength of rock-like materials can be considered using a model composed of a large number of elements with statistically distributed strengths.

Denoting the probability distribution function of the strength of elements by $F(\sigma)$, we have

$$F(\sigma) = \int_0^{\sigma} f(\sigma)d(\sigma) \qquad (1)$$

where $f(\sigma)$ is the probability density function of the strength of elements as shown in Fig. 1.

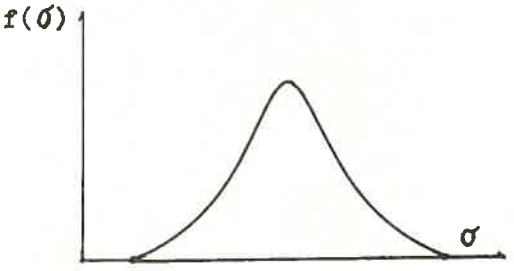

Fig. 1

Suppose a bundle model[1] as shown in Fig. 2 , with cross section of unit area and subjected to increasing load with constant rate. At first stage the load is distributed equally over total N elements. If the average stress reaches the minimum value of strength of elements, some of elements fail and the load is redistributed among the remaining elements. As the load increases, some of elements will fail successively.

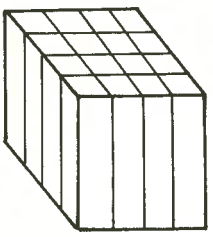

Fig. 2

Denoting the apparent stress which is measured with respect to the total area of the bundle model by σ and the average stress of remaining parts by σr, the relation between σ and σr may be given, using $F(\sigma)$ defined by Eq.(1), as

$$\sigma = \sigma r \left\{1 - F(\sigma r)\right\} \quad (2)$$ [2)]

Consequently, denoting the maximum value of σ, ie the final strength, by σf, we can write as

$$\sigma f = \left[\sigma r\left\{1 - F(\sigma r)\right\}\right]_{max} \quad (3)$$

Further, for our consideration, let us introduce a ratio α is written as [3)]

$$\alpha = \sigma f / \sigma i \quad (4)$$

where σi denotes the stress of fracture initiation. It is considered that this ratio α may express a fracture toughness of the bundle model.

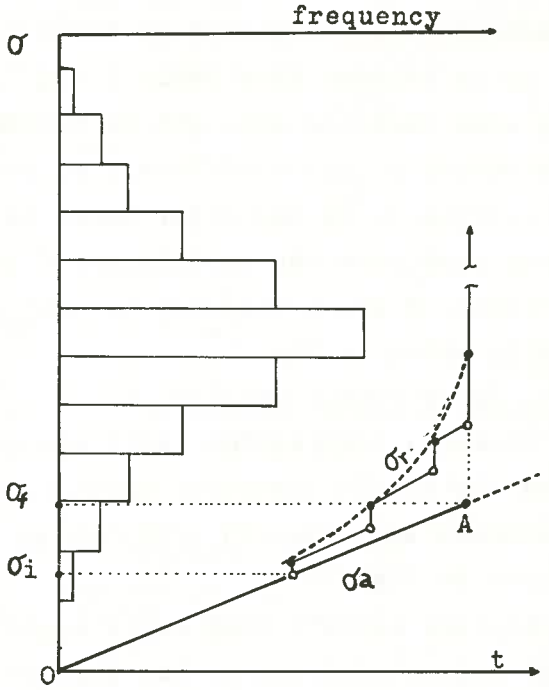

Fig. 3

3. Numerical calculation

The strength σf and the ratio α can be obtained if the distribution function $F(\sigma r)$ of the constituent elements is known, which, however, may be considered to be difficult in practice.

From this reason, the graphical analysis is required to determine the value of σf, using the relative frequency, as is shown in Fig. 3. In this figure, the straight line OA shows apparent applied stress σa with a constant rate and the zig-zag line shows the stress σr on the remaining elements. Used values of relative frequency distributions listed in Table 1 are assumed from some appropriate distributions. C values listed in the table denotes the coefficient of variation of strength. To make the comparison simple, the mean value of normal type distribution 1 and 2 are put as same to the value of the uniform one, and also they are defined at the same range.

probability distribution	strength (kg/cm²)			C (%)
	mean value	max.	min.	
normal (1)	155	280	35	24.5
normal (2)	155	280	35	33.9
uniform (3)	155	280	35	46.5
exponential (4)	108	280	35	59.0
impulse (5)	155			0
experimental (normal type)	155.4	208	95	13.3

Table 1. Distribution of the strength of of elements.

probability distribution	strength (kg/cm²)	α
normal (1)	94	2.7
normal (2)	76	2.0
uniform (3)	52	1.5
exponetial (4)	39	1.1
impulse (5)	155	1.0

Table 2. Strength of the bundle model (estimation).

Calculated results on basis of these

distribution are listed in Table 2.

As is evident from Table 1 and 2, it is seen that the strength of models decreases as the coefficient of variation C increases. On the other hand, it is seen that when the coefficient C increases, α has a tendency to decrease, as is shown in Fig. 4.[4)]

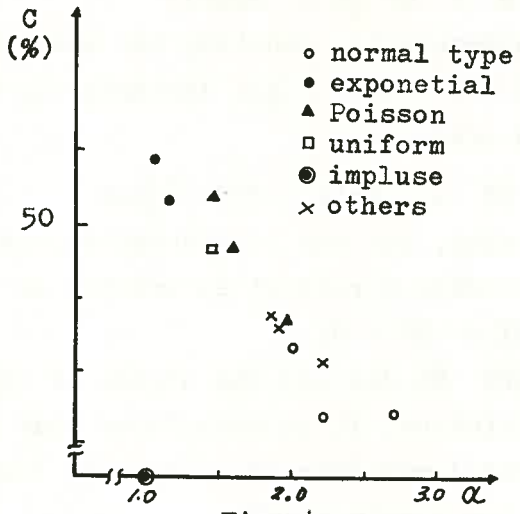

Fig. 4

4. Experimental results

Uniaxial compression tests are carried out for bundle elements compsed of 100 columner specimens (1 × 1 × 20 cm) shown in Fig. 1.

Obtained results from experiments and the estimated value of the strength of a bundle model are shown in Table 3. It is seen that the experimental value and the calculated one shows a comparatively good agreement.

estimation	experiment
118	123

Table 3. Strength of the bundle model(kg/cm^2).

5. Conclusion

The summary is as follows;

(1) It is obviously recognized that α defined as the ratio of the fracture initiation to the final strength is closely related with the inhomogeneity of the strength of constituent elements.

(2) When the coefficient of variation C of elements increases, the strength of the bundle model and the ratio α decreas.

(3) Therefore, it is considered that the larger the coefficient C is, the weaker the material is and the faster the progress of fracture is respctively.

References

1) Daniels, H.E.: The statistical theory of the strength of bundles of threads. 1 ,Proc. Roy. Soc., A, 183, 405-435 (1945).

2) Tano, H. and Satake, M.: Consideration on the mechanism of fracture initiation and propagation of brittle materials, Proc. 5th Nat. Symp. Rock Mech., 55-59 (1977).

3) Satake, M. and Tano, H.: Consideration on the modes and strength of rocks under compression test, Rock Mechanics in Japan, Vol.2 ,52-54(1974).

4) Tano, H. , Satake, M. and Shirota, S.: A study on the mechanism of brittle fracture and deformation using a model., Proc. 32th Annual Meeting of JSCE, Part 3, 343-344 (1977).

AN INVESTIGATION FROM ROCK-BURST PHENOMENA IN DAI-SHIMIZU TUNNEL

Minoru SHIMOKAWAUCHI Japan Railway Construction Public Corporation.
Tsuneo KIZAWA Taisei Corporation

1. Introduction

Dai-Shimizu Tunnel of Joetsu Shinkansensen a long mountain railway tunnel with the length of about 22 km passing under the mountains mostly of hard quartz diorite.(1)

Rock-burst frequently occured when overburden were 500m ∿1,200m, without regard to the overburden of the tunnel. (see Fig.2.)

Fig. 1. The location of Dai-Shimizu Tunnel

2. Observed rock-bursts

Rock-bursts where overburdens were relatively small are shown as points No. 1, 2, 3 and 4. in Fig. 2. and Table 1.

In the vicinity of these, have many joints and rifts, and in some cases interlayeared clay and fractured zones accompanied with spring water, were observed.

The locations of rock-bursts are of monolithic rocks

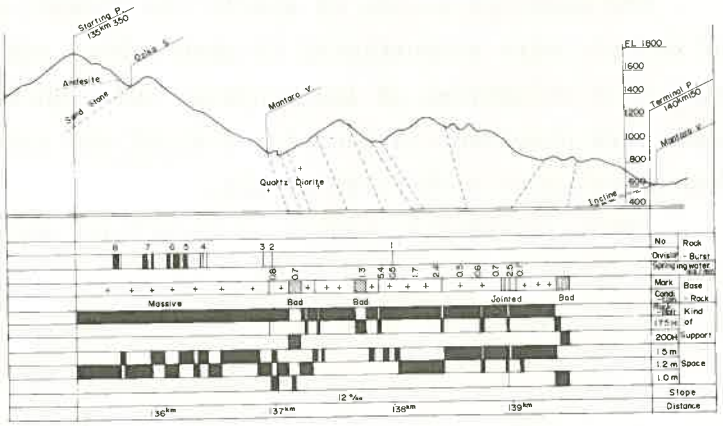

Fig. 2. Construction data of central portion of Dai-Shimizu Tunnel(full face excavation)

Table 1. Observation of rock-burst

NO	1	2	3	4	5	6	7	8
Position and net distance	138,012m ~ 137,999m	136,993m ~ 136,927m	136,927m ~ 136,912m	136,464m ~ 136,454m 136,439m ~ 136,427m 136,417m ~ 136,401m	136,272m ~ 136,257m	136,229m ~ 136,163m 136,139m ~ 136,115m	136,049m ~ 136,025m 136,001m ~ 135,978m	135,803m ~ 135,979m 135,781m ~
Ground depth from the tunnel	650m	470m	510m	750m	850m	1,000m	1150m	1150m
Ground condition	Massive strure, There is a jointed rayer with accompanying springing water on this side.	Two Vertical joints in the face, and side walls are massive structure.	The horizontal joints have been developed under the arch shoulder At end of the division the fractured clay vein appeard	The upper half portion of right ore massive, and the same of left has springing water. The fractured clay layer appeares at top and	massive	massive	There are few joint and and almost composed of massive structure There are vertical fissure parallel to the facing at 136.9km.	There is springing water of about 0.3m³/min from the right shoulder at 135.8 km Massive
Occurring point	Left and right Side walls	The right shoulde of arch to the face and full facing.	The right shoulder of arch	The right shoulder of arch	The right side wall	The right shoulder of arch	Crown and right shoulder of arch. One part of face	The left and right shoulder of arch.
Duration (hour)	72 ~ 240	14 ~ 21	48 ~ 120	48 ~ 120	24 ~ 48	24 ~ 240	24 ~ 240	24 ~ 280
Rock scale (m²)	1.0 x 1.0 ~ 1.0	1.0 x 0.5	0.02 x 0.05 ~ 0.03 x 0.3	0.3 x 0.5 ~ 0.5 x 1.0	1.0 x 1.0	0.3 x 0.5 ~ 0.5 x 1.0	0.3 x 0.5	0.2 x 0.5 ~ 0.5 x 1.0
Occurring condition	Occurs at about 20m back word from the face. Afterward occurs at the tunnel for storage.	Occurs at the right shoulder during 4m advanced chopping of face, and spreads to the face.	Occurs at about 10m backward from the facing. Occurs continuously after net replacing due to full deposite of rock fragments in the netting support	Occurs at the right shoulder during excavating work of the facing. Occures continously after about two hours of blasting and slips out through to the fractured clay layer	Occurs at the lower portion bf rock volt construction of about 10m back word from the face	The thin rock fragments are deposited in the lock-net support (after completing excavation)	Occurs partially during the excavation of face and occurs continuously after excavation	Occurs shoulder portion of about 10m backword from the face
Sketch	area of face = 80 m²	Granit Vein Joint	Clay Cracky	Clay massive cracky				

without such defects. Rock-bursts where overburdens were large are shown as points No. 5, 6, 7, and 8, where rocks are seemed to be in almost perfect conditions.

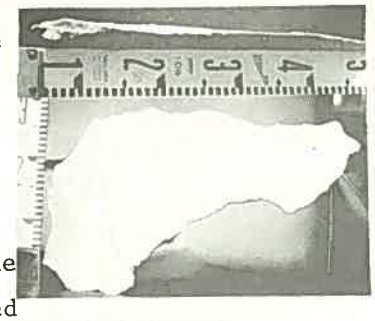

Fig. 3. The rock-burst fragment at 136Km P.

3. Rock conditions around rock-bursts

The stresses in the rock near 138 km point where the indication of rock-burst was first observed were measured by using the borehole deformation method.(2)

The initial vertical stress(a measured minimum stress) was 260 kg/cm^2, while the maximum vertical stress due to stress concentration caused by excavation was 644 kg/cm^2. (Fig. 6.)

The three-dimensional analysis by using three bore holes' measurements were performed.

Principal stresses were obtained by using these values and assuming the rocks were homogeneous and isotropic. An example is shown in Fig 7.

The measured values of static and dynamic moduli of elastic were proportional to each other, and the ratios of velocities of longitudinal and transverse wave were observed constant for both of the rocks which had experienced rock-burst or not.

Fig. 4. The rock-burst at 138Km P.

After rock-burst, moduli of elasticity and the

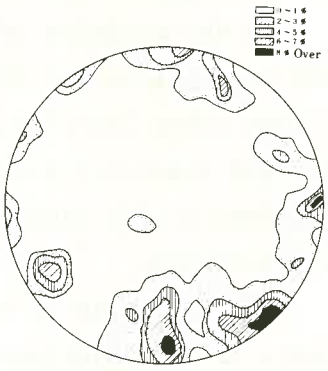

Fig. 5.→ Diagram of joint direction near 138Km P.

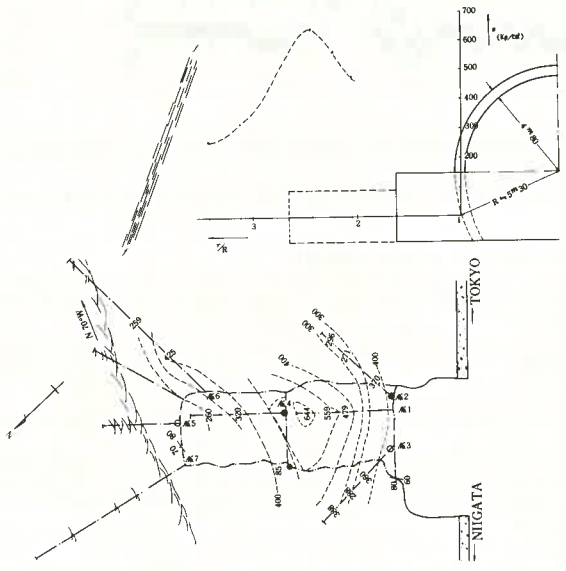

Fig. 6. The stress distribution at 138Km P.

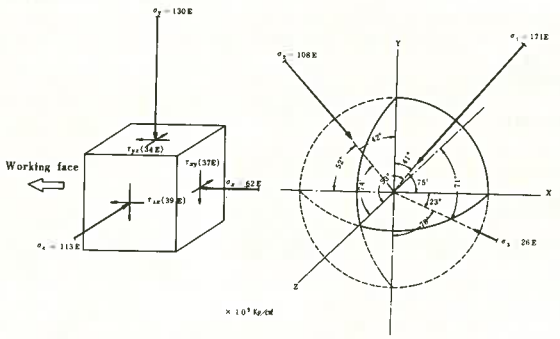

Fig. 7. Three dimensiomal analysis

velocities of elastic waves dropped to about 60% of those of original rocks. (see Fig. 8. and 9.)

The relations between compressive strength of cores and the velocties of longitudinal waves are shown in Fig. 10. by adopting logarithmic cordinates.(3)

The strength of the rock which has experienced rock-burst may be expressed by introducing a concept of deterioration coefficient expressed in terms of measured velocities of elastic waves as

$$\sigma c'adj=(\frac{Vp'}{Vp})^3\sigma c' < \sigma v=\rho gH$$

where,

Vp: Velocity of elastic waves before deterioration (no rock-brust)

Vp': Velocity of elastic waves after deterioration (rock-burst)

σv: Vertical stress

ρ: Specific gravity

g: Accelaration of gravity

H: Overburden of the tunnel

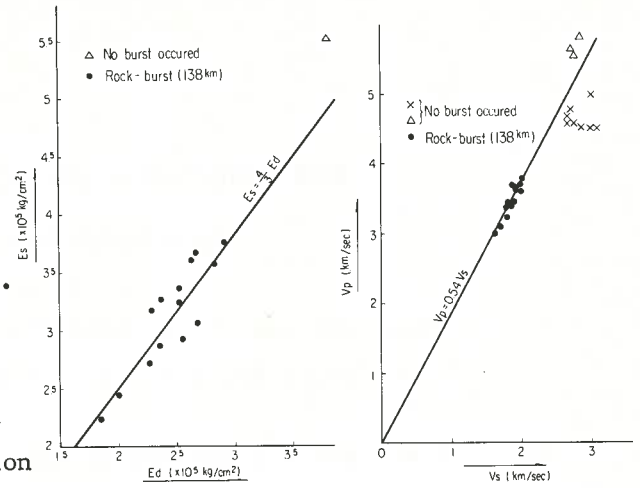

Fig. 8. (left) Relation between static and dynamic moduli of elasticity

Fig. 9. (right) Relation between velocities of primary and secondary waves.

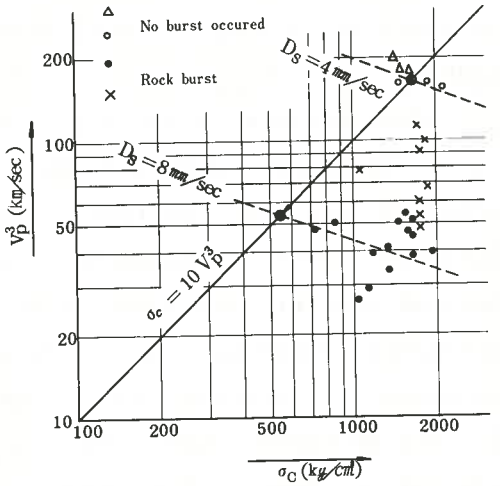

Fig. 10. Relation between compressive strength, velocity of elastic wave and driving speed of drifter.

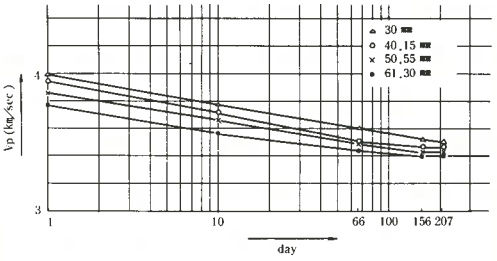

Fig. 11. Time historical changes in velocity of the longitndinal waves of core samples from rock-burst area.

4. Conclusion

The occurrence of rock-burst may be explained to be caused by the remakable concentration of compressive stress and decrease in compressive strength in the vicinity of tunnel excvation.

In actual job, workers were protected from possible injuries by unexpected rock-bursts by double wire netling supported with resin anchors.

(References)
(1) M.SHIMOKAWAUCHI On the full face excavation of the Mantarô Constracting section in the Dai-Shimizu-Tunnel, Proceedings of the 10th symposium on rock meckanics J.S.C.E (1976)
(2) K.SUZUKI Y.ISHIJIMA Theory and practice of rock-stress mesurement by bore-hole deformation method, jour. of the society of material seience, Japan Vol 17 No. 181 (1968)
(3) T.KIZAWA An attempt on rock classification for excavation purposes, Proceedings of the 4th symposium on rock mecamics in Japan (1973)

Rock Deformation Characteristics Revealed by a Borehole Load Tester

Toshiaki TAKEUCHI, Tateo SUZUKI, and Souichi TANAKA
Urawa Research Institute, OYO Corporation

The authors have accumulated the measurement data and examined them in order to develop the borehole load test into a comparatively easy in-situ method to measure mechanical properties of rock mass. In this paper the measured events are discussed based on the measurement results with addition of some considerations to their relation with the unique loading mechanism. Then, their relation with rock deformation and strength characteristics, and the applicability of the test is discussed.

Block diagram of the borehole load tester (Elastmeter 200) used by the authors is provided in Fig-1. The Elastmeter 200 is so designed as to send water or gas into its sonde assembly inserted into borehole and to detect the resultant displacement of borehole wall with the mechanism named Contract Balancer as shown in the figure. The theory of bellows mechanism is put into practical use in the Contract Blancer, which follows the changing cubic volume. Thus the balancer is so made that its sensors always move touching the inner face of the rubber tube of which shape follows the wall displacement. The movement thus detected by the sensors is conveyed to the differential transformer as that of the bellows. The sensors are installed in 6 radial directions near the center of the sonde assembly so as to measure the average displacement, avoiding the projecting expansion of the rubber

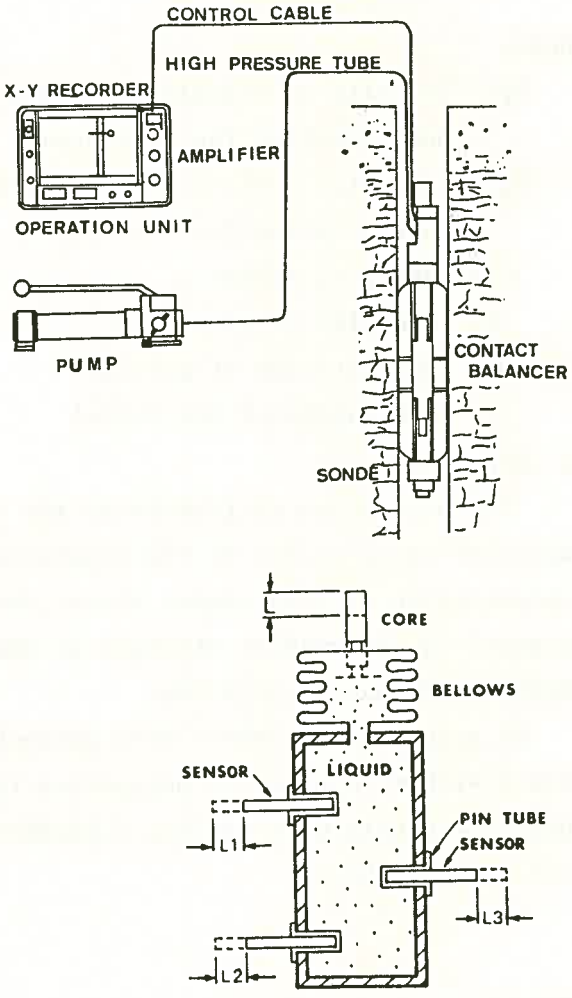

Fig-1 Block diagram of borehole load tester

tube at the both ends when pressure is given.

Strain distribution in the rock during the test is shown in Fig-2. A 66mm diameter hole was drilled in the rock block sample and wire strain gauges were installed in the radius direction outwards to obtain these data. In this chart theoretically computed strain distrubutions due to difference in Young's moduli are shown, as well as measured strain distribution. According to the chart the distribution of measured strains shows larger decrease in proportion to the distance than that of the theoretical. It means the displacement by the test is largely controlled by the deformation characteristics of the rock portion closely adjacent to the bore wall. Accordingly, the result teaches us the necessity of careful drilling not to hurt the wall face.

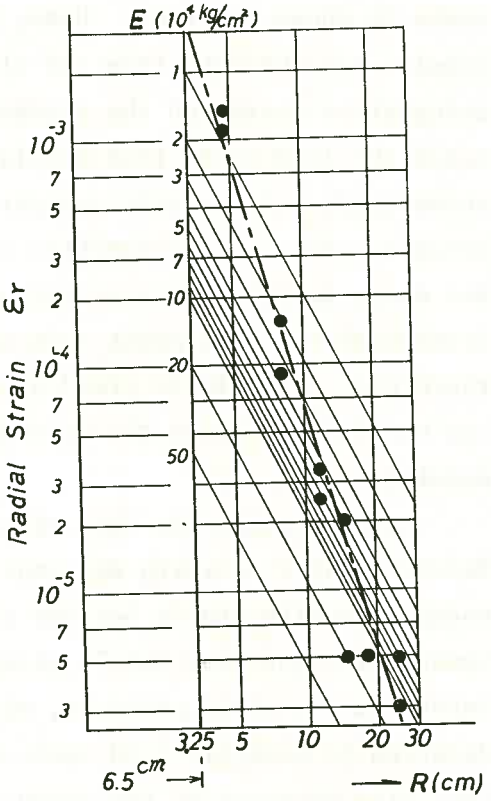

Fig-2 Strain distribution in the Rock

Fig-3 shows the relation between the virginal deformation coefficient of pressure-displacement curve and the elastic coefficient obtained from subsequent deformations through borehole load test and plate loading test respectively. According to the chart the borehole load test shows the ratio of the two coefficients as a whole to be nearly 2 and the degree of influence by rock relaxation, etc. seems to be contained little in the virginal deformation.

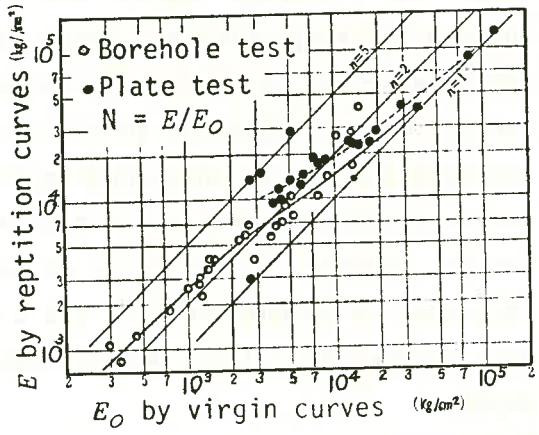

Fig-3 Differences in deformation characteristics due to plete and borehole test

Fig-4 shows the relation of the results obtained from plate loading test and borehole load test both of which were conducted at the same point. The trend of the chart apparently shows both deformation coefficients differ each other. In the borehole load test the circumference-direction stress works as tensile stress so that the tensile stress would be possible to generate fissures when the load is increased until the tensile stress exceeds the tensile strength of the rock. On the contrary, only compression force is applied to the rock in plate loading test and respective responses to the rock naturally differ.

The relation between the deformation modulus and yield pressure of various

rocks is shown in Fig-5. Here, the modulus was obtained from the virginal deformation curve and the pressure indicates the load where load displacement curve bends and the displacement suddenly becomes large. The connection of the two shows fairly good correlationship irrespective of different rock natute and, therefore, approximate yield pressure can be estimated from the deformation modulus.

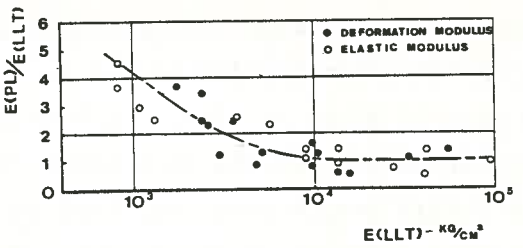

E(PL) : Deformation coefficient by plate loading test
E(LLT) : Deformation coefficient by inhole loading test

Fig-4 Relations between plate and borehole deformation test

Authors noted the data of a Neogene Tertiary layer of which deformation modulus remains stable because of the homogeneity and drew Mahr's circles regarding the yield pressure, which was detected by borehole load test, and the confining pressure by the overburden as σ_1 and σ_3 respectively as shown in Fig-6.

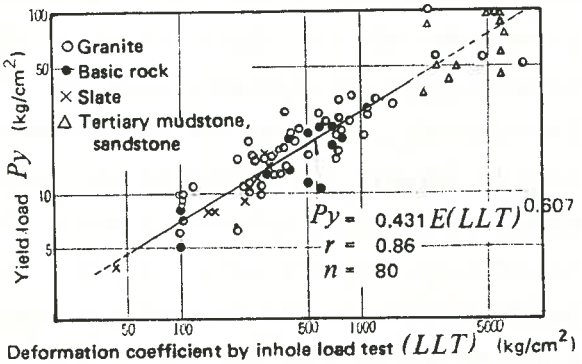

Fig-5 Relations between deformation coefficient and yield load

According to the chart, C and ϕ range from 5 through 7kg/cm^2 and 35° through 50° respectively. These values can be accepted as nearly appropriate for Neogene layer. Needless to mention, this approach results in only rough approximation instead of strict estimation. The result, however, proves to be an useful reference in comparison of C and ϕ of rock masses through the certain relation between respective yield point and depth.

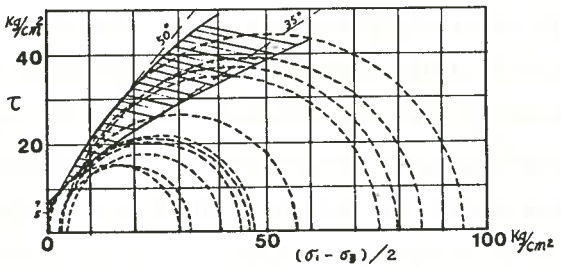

Fig-6 Estimation of Mohr's circles

References

(1) TAKEUCHI, T. SUZUKI, T. TANAKA, S. (1976): "A study of bore-hole lateral load tester and characteristics for deformation of rock" - Soils and Foundations, Vol. 24, No. 1, P35-41.

(2) TAKEUCHI, T. SUZUKI, T. TANAKA, S. (1977): "A study of measuring results for rock by bore-hole lateral load test" - Proc. of the 5th internal symposium of Rock Mechanics, P217-222.

(3) MIYAJIMA, K. OCHI, K. TAKEUCHI, T. SUZUKI, T. (1979): "Model experiment on characteristics of deformation of rocks by borehole load test" Proc. of the 12th symposium of Rock Mechanics, P96-100.

ACOUSTIC EMISSION ACTIVITY IN ROCK AT DEEPLEVEL COAL MINE

Yoshiteru WATANABE Iwao NAKAJIMA
Masayuki TAKEUCHI and Shota KAWAKURI
(Faculty of Engineering, Hokkaido University, Sapporo)

1. Introduction

The primary objective of this research is to clarify whether the acoustic emission technique is useful as a method for estimating the degree of instability of the rock structure surrounding underground working faces in deeplevel coal seam. In order to execute this objective the acoustic emission activity in the bed rocks surrounding faces in deeplevel(-700~900 m) coal mining operations such as hydraulic mining, drifting and relief boring was observed with sufficient sensitivity for practical use in Sunagawa Coal Mine and Yubari New Coal Mine from 1976 to 1977.

2. Observation method of acoustic emission

Fig.1 presents a block diagram of the acoustic emission monitoring system. In this diagram the detecting system consists of a basic 2-channel system, and included in the basic system are 2 vibration sensors and a tape recorder. The analyzing system, which accepts one input, consists of a totalyzer, distribution analyzer and energy processor.

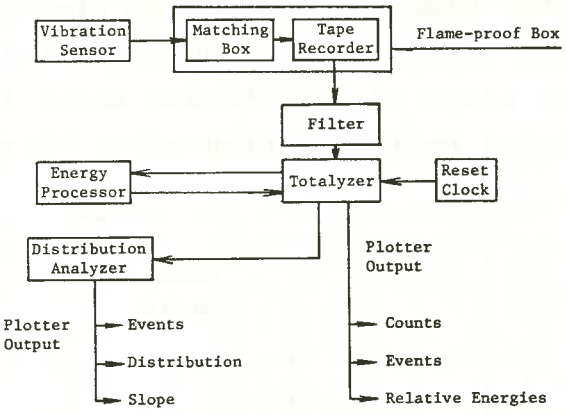

Fig.1 Block diagram of overall acoustic emission monitoring system.

These vibration sensors have a high sensitivity of 250 mV/g and a flat frequency response from 2 to 3000 Hz. They were cemented into the boreholes prepared in the solid rock around underground mining opening. The tape recorder placed in a flame-proof box were connected to the sensors with 2 conductor shielded cables, and these circuits were intrinsically safe. The data recorded underground were play back on the ground surface, and presented for the analysis of the

parameters associated with acoustic emission activity. The analyzing system processed the acoustic emission signals and provided a DC output of acoustic counts, events and relative energies.

3. Observational results

(1) Acoustic emission activity in hydraulic mining

At Noborikawa mining area in Sunagawa Coal Mine a hydraulic mining method has been applied to the coal seam of which the dip is about 70 degrees. Fig.2(a),(b) is the typical example of the observational results associated with acoustic emission activity during this hydraulic mining. In Fig.2(a) the bursts of acoustic emission are found sometimes besides much succesive acoustic emission. The curves such as accumulated counts, events and relative energies steepen rapidly corresponding to these bursts as shown in Fig.2(b). Such a burst of acoustic emission signifys the violent release of the strain energy stored in the rock mass surrounding working face in the process of caving. In fact the strain energy was released in the form of a coal burst when the slope of the frequency distribution of relative energies decreased.

(2) Acoustic emission activity in drifting

Fig.3 shows the acoustic emission activity of the vicinity of a face after blasting in drifting. The curves such as accumulated counts, events and relative energies steepen rapidly immediately after blasting and become flatter with the lapse of time. From this result it is found that the rock surrounding faces becomes the state of equilibrium while fracturing in the process of the stress redistribution after blasting.

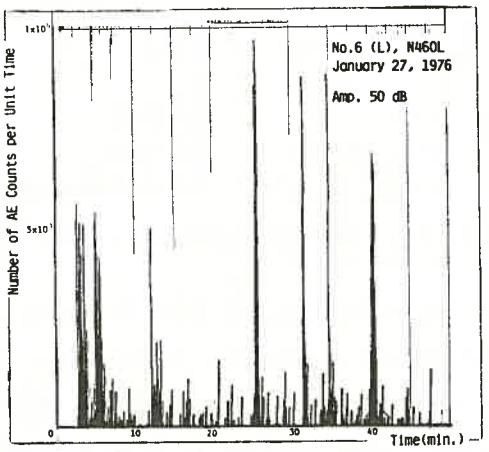

Fig.2(a) Number of AE counts per unit time during hydraulic mining.

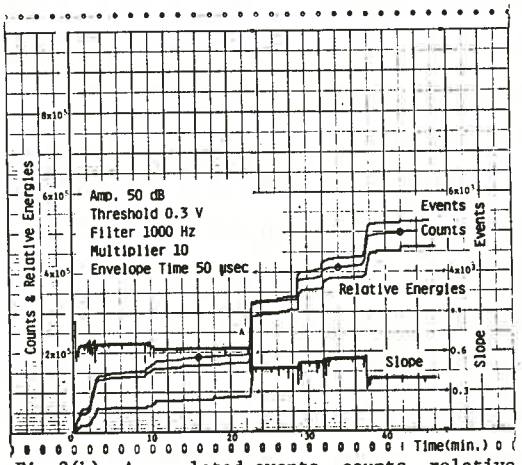

Fig.2(b) Accumulated events, counts, relative energies and slope during hydraulic mining.

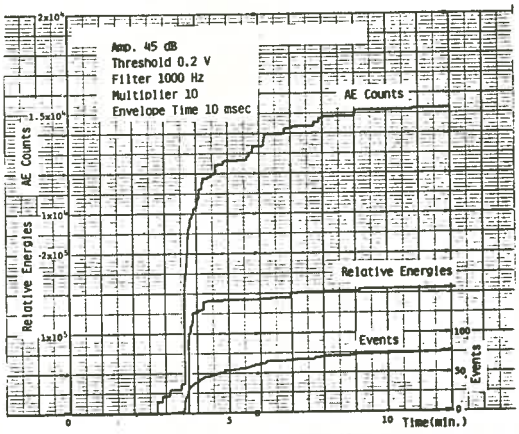

Fig.3 Accumulated AE counts, events and relative energies after blasting in drifting.

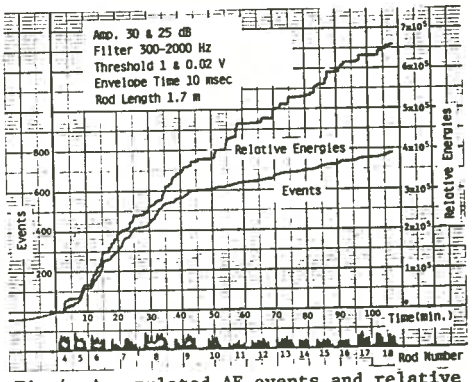

Fig.4 Accumulated AE events and relative energies in boring.

(3) Acoustic emission activity in boring

The observation of the acoustic emission activity in boring was carried out to asses the effects of the relaxation to a coal seam highly loaded. In this case the borehole of 30 m in depth was drilled by using a bit of 90 mm in diameter. Fig.4 shows the results obtained during this relief boring. Here, the acoustic emission activity is high in the former half and low in the latter half. This kind of observations was carried out several times and all results showed a high acoustic emission activity in an inner region 5 to 15 m away from face.

4. Concluding remarks

From the observational results above mentioned, the following conclusions can be drawn :

(1) The acoustic emission techniques are usefull as a method for estimating the mechanical state of the bed rock in deeplevel mining.

(2) The parameters associated with acoustic emission activity appear to be a factor indicative of the degree of instability of the rock surrounding working faces.

(3) In deeplevel mining the existence of highly stressed zone or geologically weak band can be presupposed from the degree of acoustic emission activity.

(4) A criterion for judgment on setting to the next working cycle safely can be obtained from the variation of the curves associated with the acoustic emission activity after blasting.

(5) The effects of the relaxation in a coal seam by boring can be assesed from the values of acoustic emission measurements.

ANALYSIS AND MEASUREMENTS OF BEHAVIOR OF ROCK AROUND UNDER-GROUND CAVITY IN THE PROCESS OF EXCAVATION

Minoru YOSHIDA, Senior Managing Director
The Kansai Electric Power Co., Inc.

1. Introduction

This paper deals with the results of studies on the theoretical deformation behavior of rocks and the actual measurements made during the underground cavity excavation at Okutataragi Pumped-Storage Hydro Project. This underground cavity has a room of 146,000 cubic meters; 24.9 meters wide 43.9 meters high and 133.4 meters long. The most important point for designing the underground large power station like this is to estimate the actual deformation precisely by calculations based on the properties of the rock obtained by repeated in-situ tests. In this paper, the calculation results are compared with the actual measurement records and effects of the rock strut which was used as the erection work base of turbine-generators and other components are also described.

2. Determination of the calculation constants and the analysis of the loose zone extent around the cavity.

The geological survey and the in-situ tests were conducted at the proposed location for the project and their results are as follows.

(1) The basic rock of the cavity consists of the hard phyolite, tuff and liparite-breccia. Quartz-porphyry and diabase intrude into them nearly vertically. The concept is shown in Fig. 1.

(2) The initial ground stress was surveyed by over-coring method at the adit 60 meters above the cavity arch. The measured value is 100kg/cm^2 horizontally and 50kg/cm^2 vertically.

(3) The shear tests were carried out at the proposed location of the cavity consisting of phyolite and Mohr's envelope equation as obtained is $\tau_R = 50 \sim 100 \pm 15$kg/cm^2. The angle of internal fricition is $45° \pm 15°$. For calculation purposes, the tensile strenghth of the rock is assumed $\sigma_t = 0.12\,\tau_R$.

(4) The loading tests were carried out at the same adit as for the initial stress tests. The secant modulus of the off-loading stage is 30,000 - 130,000kg/cm^2. In this analysis, the loading force equivalent to the excavation stage, the loosend zone by blasting, the poissons and modulus variation corresponding to the stress condition, and the shear deterioration are considerd as visco-elastic-plastic characters.
The calculation model and its constants are shown in Fig. 1.

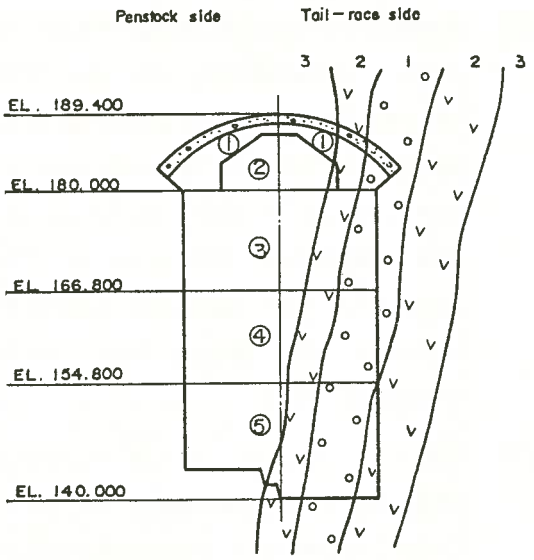

Table of rock characters around power house

Kind of rocks	1 Quartz — porphyry	2 Diabase	3 Rhyome	Concrete
Class	B	CH	B · CH	
E (kg/cm^2)	10 x 10^4	5 x 10^4	7 x 10^4	20 x 10^4
α	0.05	0.07	0.05	0.02
β (1/day)	20	10	70	10
Envelope	$\tau^2=(1-\sigma/\sigma_t)\times\tau_R^2$			
τ_R (kg/cm^2)	50	40	50	55
σ_t (°)	6	4.8	6	
μ	0.25	0.25	0.25	0.2
σ_t/τ_R	0.12	0.12	0.12	0.64
Damaged zone by blasting (1)	$E=4\times10^4$	2×10^4	3×10^4	
〃 (2)	$E=7\times10^4$	4×10^4	5×10^4	

Fig 1 Excavation model calculation constants

3. Measurement of the rock deformation around the cavity and the stress in the arch lining concrete.

In order to compare the actual deformation with the analytical calculation and to control the work during excavation, the rock deformeters were installed in such an arrangement as to observe changes with the time of the rock displacement at the cavity arch and side walls. Several concrete strain gauges and reinforcing bar strain meters were also buried in the arch concrete. The location of these instruments is shown in Fig. 2.

4. Comparison of the calculation results with the measured data.

Followings are disclosed.

(1) The comparison at the arch cavity is shown in Table 1. At the first stage of arch excavation, the arch crown was sinking, but after then rised by the force which pressed the arch abutment inside.

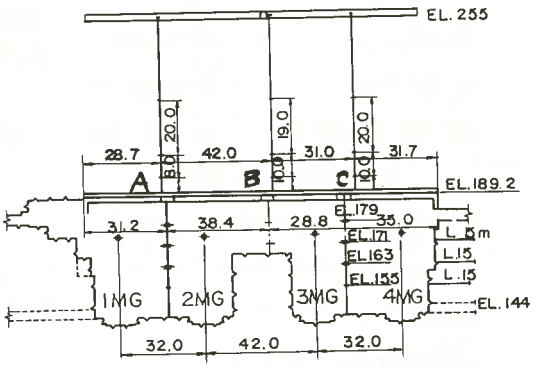

Fig 2 Disposition of rock deformeters

Longitudinal section Penstock side

(2) According to the progress of the cavity excavation, the measured stress of the arch crown and arch abutment grew to be compressive and at the time when the cavity excavation was completed, the growing stress had stopped. The measured upper fibre stress is smaller than the lower fibre stress. This means that the horizontal force is more eminent than the vertical load.

Table 1 Vertical displacement of cavity arch

	Value of calculation	Value of observation		
		A sec	Bsec (Rock strut)	Csec
Arch Crown	0.3 mm ~ 0.5 mm Rising	0.8mm rising after 0.7mm sinking	0.3 mm rising after 0.3 mm sinking	0.3 mm rising after 0.4 mm sinking

(3) The calculation result of the horizontal side wall displacement is shown in Fig.3. Calculation and measured value at a 30-meter depth are almost same, but at a 15-meter depth, they are different. It means that in a zone between 15 meters to 30 meters, the deformation of the rock is changeable due to the rigid body behavior by the prestressed rock bolts.

(4) As for the effects of rock strut, its B section showed the horizontal displacement less by 70 % and the arch stress less by 50 to 60 % than A and C sections.

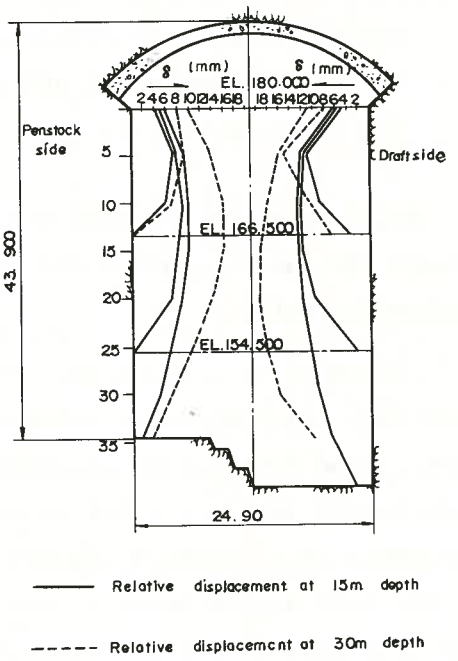

Fig 3 Progress of excavation and relative displacement of walls (by F. E. M)

(5) Upon designing the prestressed rock bolts, the slip circle calculation was carried out with a loose zone (a zone where poisson's ratio varies between 0.25 and 0.45) to obtain the inside horizontal slip force and the prestressed force was determined at a value enough to withstand such slip force. The location of rock bolts is given in Fig. 4. The prestress force is 35 ton per bolt at a maximum which is equivalent to 85 % of the allowable stress.

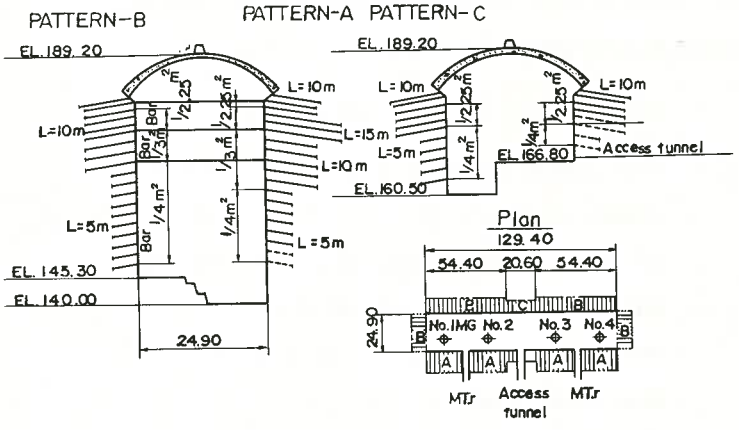

Fig 4 Disposition of prestressed steel bar.

STUDY ON DEVIATION OF BOREHOLE IN DEEP BORING

Tomio HORIBE, Tohoku University
Minoru USHIDA, Tohoku University
Kiyohiko OKUMURA, Tohoku University
Yung Tso SUNG, Atomic Energy Council, Rep. of China

The crooked-hole phenomenon is appeared frequently in deep boring, and it is generally accepted that the deviation of the borehole to the direction of "up-dip" side occurs in the drilling through the inclined boundary of layers, in case of the drilling from soft rock to hard one. In this investigation, the deviation of the borehole to the direction of "up-dip" side was observed after shifting to that of "down-dip" side primarily, i.e. so-called "dogleg phenomenon", when the bit drilled through the inclined boundary of layers. Moreover, not only the appearance of the drift angle but the three dimensional deflection of the orientation caused by the rotation of the bit was recognized.

An artificial rock sample in this experiment having the inclined boundary of two layers of different strengths caused by the ratio of contents of cement and pulverized limestone was made. The dimensions of this sample were 90cm in length, 30cm in width and 50cm in height. The compressive strengths of these soft and hard layers were 150kg/cm^2 and 290kg/cm^2, and the ratios of contents of cement, pulverized limestone and water were 1:1:0.9 and 1:0.2:0.5, respectively. The inclined angles of the boundary of layers were set as 15°, 30°, 45°, 60°, 75°, and these artificial rock samples were drilled from the upper layer of soft rock to the lower layer of hard rock.

The bit was a hard metal inserted non-coring type of 36mmϕ in diameter, 9mm in length as shown in Fig.1, set to the rod of 10.5mmϕ and 6.5mmϕ in outer and inner diameters and of 2000mm in length, then the rotation of the bit was 88r.p.m. and the thrusts for the penetration applied to the bit were 20kg, 30kg and 40kg in this experiment. The torque induced in the rod while drilling was recorded by the wireless telemeter using the foil strain gages sticked on the upper end of the rod.

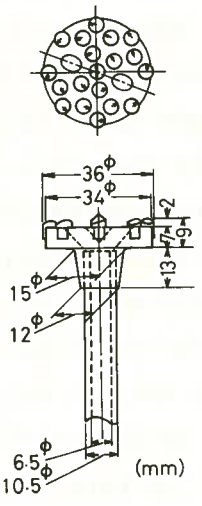

Fig.1 Detail of bit with inserted tips connected to rod

According to the results of the preliminary experiment, it was found that the less the circulating rate of water, the larger the degree of the deviation of the borehole became. Then, the drilling was proceeded under the

condition of the small amount of the circulating rate of water, i.e. 2 l/min. Also, the details of the crook of borehole were investigated by measuring the cast resin core which was made by means of the infusion of the polyester resin into the drilled borehole as shown in Fig.2.

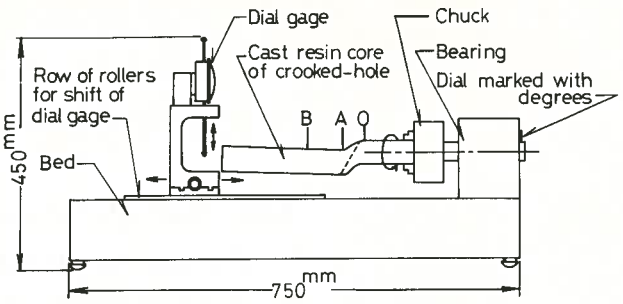

Fig.2 Measuring method of cast resin core of crooked-hole

Consequently, the followings were obtained within this experiment.

1. The smaller the clearance angle of tips of the bit was, the larger the drift angle of the borehole from vertical was.

2. Regarding the influences of the wearland of tips of the bit and of the thrust on the bit upon the drift angle of the crook, the tendency of the increase of the drift angle of the crook according as the widths of the wearlands of tips became larger was recognized, but this drift angle was decreased after reaching each maximum value with the excess wearland, shown in Fig.3. Moreover, the appearance of the maximum value of the drift angle was occurred at the smaller widths of the wearlands, in the case of lighter thrust compared with heavier, and the larger value of the maximum of the drift angle was obtained in the case of heavier thrust than lighter.

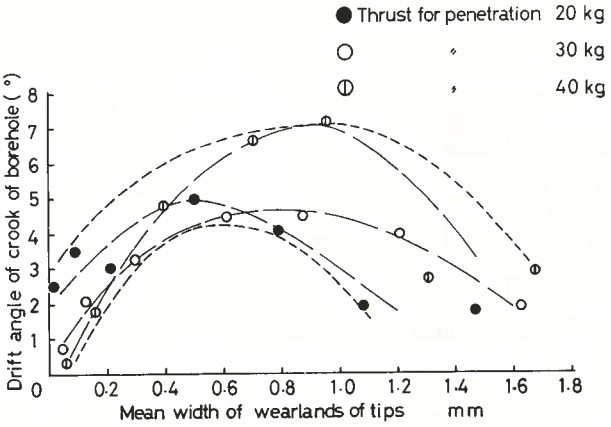

Fig.3 Relation of wearlands of tips to drift angle of crook

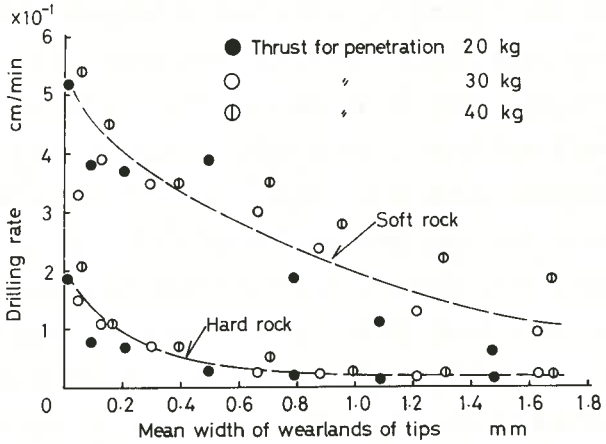

Fig.4 Relation of wearlands of tips to drilling rate

3. The relations between the both drilling rates of the soft and the hard rocks and the increase of the wearland of tips were shown in Fig.4. From this it was evident that the appearance of the maximum ratio of drilling rates of the soft and the hard rocks was occurred when the width of the wearlands of tips became at a certain value.

And a relation of the drift angle to the

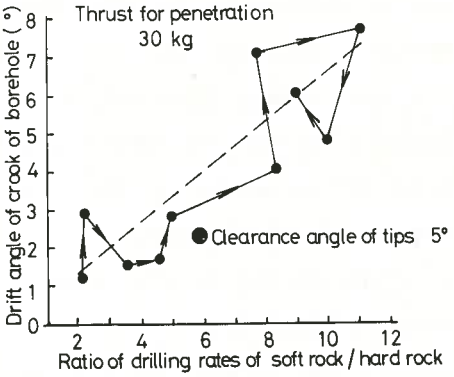

Fig.5 Example of relation of ratio of drilling rates to drift angle of crook

ratio of these rates of drilling was obtained in Fig.5. From this figure the behavior of the increase of the drift angle of the crook according as the ratio of drilling rates became larger was indicated, but this drift angle was decreased similarly after reaching the maximum value with the decrease of the ratio of drilling rates.

4. When the tips of the bit reached to the inclined boundary of layers, the increase of the torque induced in the rod was recognized. The relation of the rate of the torque increase at the boundary of layers to the drift angle of the crook was shown in Fig.6 and the appearance of the maximum value of the drift angle at a certain value of the rate of the torque increase was found.

5. When the bit drilled through the inclined boundary, the appearance of the horizontal shift of the borehole to the direction of the down-dip side along the soft rock caused by the difference of the drillability of the soft and the hard rocks previous to the crook to that of the up-dip side into the hard rock was recognized. It was the cause of the so-called "dogleg".

6. Because of the tendency to make the eccentric rotation of the bit through the boundary of layers, the considerable deflection of the orientation following the rotation of the bit was found. The values of this deflection angle were measured as more than 50° in this experiment.

7. In consequence of the change of the inclined angle of the boundary as 15°, 30°, 45°, 60°, 75° the drift angles showed different values at the larger widths of the wearlands of tips. And, at the inclined angle of 45° the drift angle reached even to the value of 10° when the thrust was 20kg as shown in Fig.7.

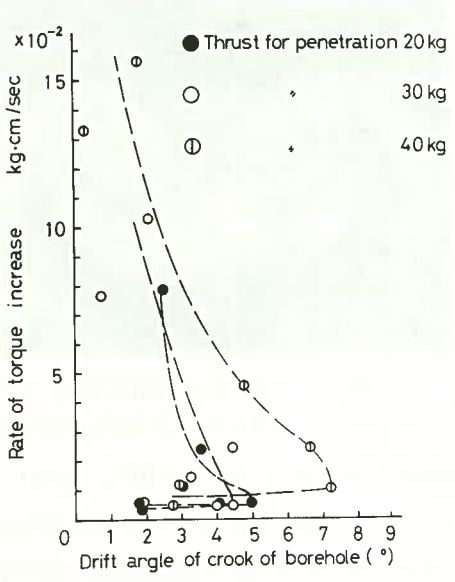

Fig.6 Relation of drift angle of crook to rate of torque increase

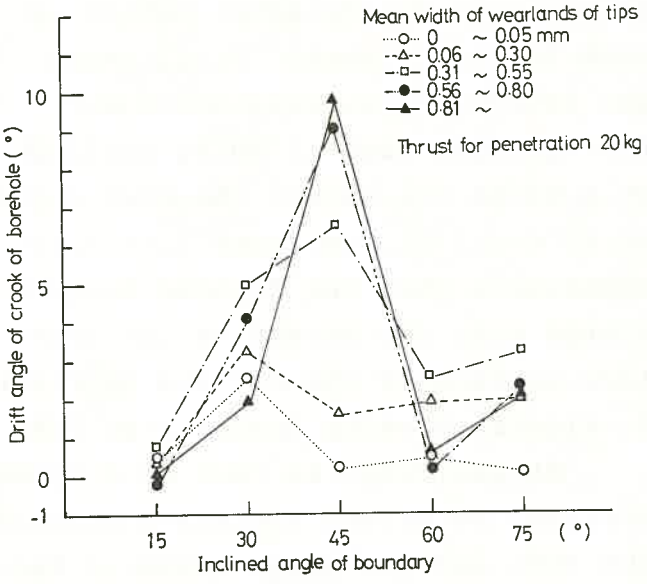

Fig.7 Relation of inclined angle to drift angle of crook

FUNDAMENTAL STUDIES ON MECHANICAL EXCAVATION OF ROCK WITH ROLLER CUTTERS

Michio KURIYAGAWA, National Research Institute for Pollution and Resources (NRIPR)
Shigeo MISAWA, NRIPR
Hirohide HAYAMIZU, NRIPR

In the mining industries including the development of oil and gas as well as geothermal heat and also in the tunnelling engineering, improvement in the techniques of mechanical excavation of rock is one of the most important problems. The present paper describes the results obtained from the theoretical and experimental investigations on the mechanism of failure of rock and from those on the excavation of rock by roller cutter.

1. Determination of the Force Acting Across the Contact Surface of the Bit and Rock

To investigate the mechanism of failure of rock caused by penetrating a wedge into rock, the stress state in the rock should first be clarified. The finite element method is applied to analyze the stress, but in advance of the analysis, the boundary condition on the contact surface of the rock and the bit should be determined. Photoelastic method is used in this purpose. Fig.1 shows the isochromatics obtained under the vertical load of 30 kg applied by a wedge bit having the nose angle of 90 deg.. It was found from this experiment that the fringes concentrated near the center of the contact surface of the bit and specimen.

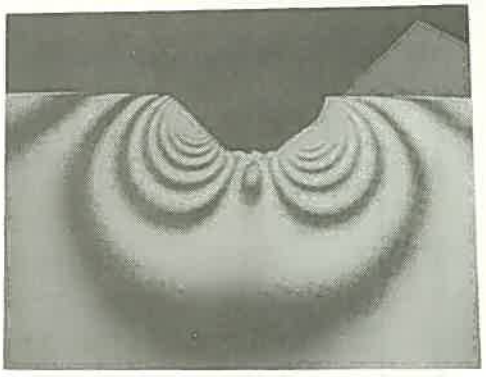

Fig.1 Isochromatics by Wedge Penetration

2. Elastic-plastic Analysis by FEM

Stress field in rock by a wedge penetration is non-linearly analyzed by direct iterative approach using the friction between the rock and the wedge measured beforehand and the Physical properties of rock. As the direction of the maximum compressive stress obtained by FEM may be considered that the stress directs toward the origin of the orthogonal coordinate system, O-xy, with the

surface of as the x-axis and the axis of symmetry as y-axis, the possible shear fracture trajectries are logarithmic spirals, if shear failure will occur at the constant angle of $\varphi = \frac{\pi}{4} - \frac{\phi}{2}$ from the minimum principal stress. Fig.2 shows the possible shear fracture paths at t_o= 4.5,6.0,7.5,9.0, 12.0 and 15.0, if the penetration depth is taken as unit length. The moment for fracture Ms and the moment against fracture Mr are given in Equ. (1)

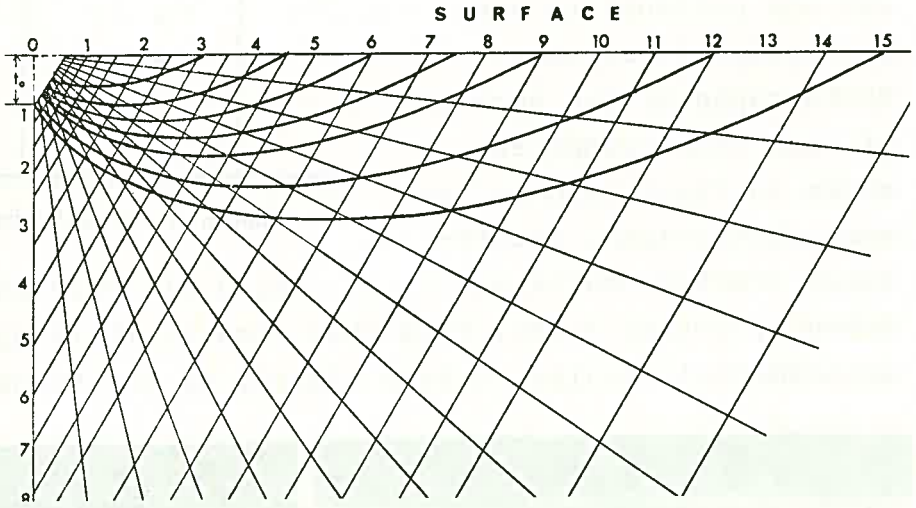

Fig.2 Possible Shear Fracture Paths

$$Ms = Sa \int_0^S \tau(x,y)\,d\xi \qquad (1)$$
$$Mr = Sa \int_0^S [\mu \sigma_n(x,y) + \tilde{c}]\,d\xi$$

The values of Ms and Mr on each trajectory can be calculated because the stress field in rock was already obtained by FEM. If we define Rm as the ratio of Ms to Mr, then it represents the parameter which shows the possibility of fracture. And it can be considered that the fracture occures when the value of Rm reached to 1. Thus the wedge force required to fracture rock, Pc, can be calculated by obtaining the wedge force which makes the value of Rm 1. In Table 1, the values of Pc for each rock are listed in case of wedge width of 20 mm and penetration depth of 1 mm.

Table 1. Comparison of fracture loads

Rock	Experiments	Theories
Sandy tuff	430 kg	520 kg
Andesite	624 kg	520 kg
Marble	1046 kg	920 kg

3. Bit Penetration Experiments

Experiments of the bit penetration into rock were conducted to compare the theoretical consideration with experiments. The apparatus used in the tests is illustrated in Fig.3. As shown in this figure, the load increases linearly with the penetration until chip is formed, whereupon the load decreases suddenly. In the-

se experiments, loading is stopped at this point and the part is cemented by resin. Then, the rock was cut and polished to see the state of fracture. Photographs of the section of each rock tested are shown in Fig.4. And in the same photographs, theoretical fracture paths are drawn by dotted lines. From this figure, it is apparent that the experimental results conform closely to the theoretical ones.

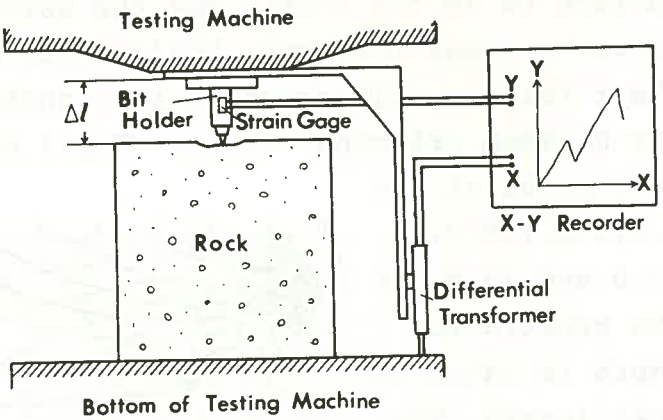

Fig.3 Bit Penetration Apparatus

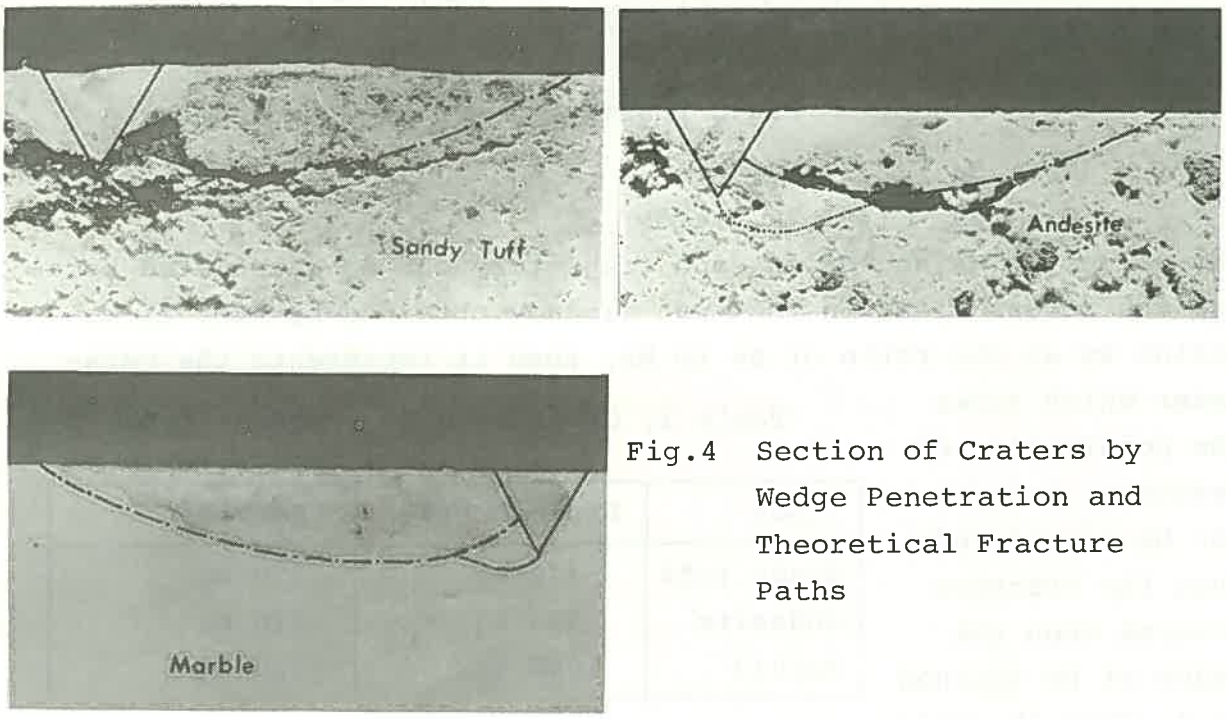

Fig.4 Section of Craters by Wedge Penetration and Theoretical Fracture Paths

As the load increases almost linearly with the penetration of bit, the load required for the chip formation can be obtained, if the crater depth is assumed to be 1 mm. On the other hand, the theoretical load was already obtained by FEM, and these results summerized in Table 1. In the aspect to the load required for chip formation, theoretical and experimental results agreed well.

PREDICTION OF GROUND VIBRATIONS FROM SUBMARINE OVERBURDEN BLASTING AND RESULTS OF THEIR MEASUREMENTS

Koichi SASSA, Kyoto University
Ichiro ITO, Kyoto University
Susumu NAGASAKA, Honshu-Shikoku Bridge Authority

1. Introduction

In planning a blasting close to buildings, one must predict the magnitude of vibration caused by a blasting. Vibrations from common types of blasting may be roughly predictable by using an experimental formula which has been derived from previous measurements. Honshu-Shikoku Bridge Authority planned a submarine overburden blasting. This type of blasting is an extremely special one, and this was the first trial in Japan. Therefore, prediction of the vibration from this particular blasting by the conventional method was very difficult for the sake of its speciality. Then, a numerical simulation was performed to predict the ground vibration. According to the results of this simulation, Honshu-Shikoku Bridge Authority designed and performed the submarine overburden blasting of this particular case in February, 1975. Ground vibrations were observed at several points. This paper shows the results of numerical simulation and comparison of those with the observed ones.

2. Site and Blasting Condition

Fig. 1 shows a geological section of the site along the line from the blasting point (7A) to the point of interest. Honshu-Shikoku Bridge Authority might be very care full for the ground vibration at the reclaimed ground. Because, there is a oil refining factory at about 400 m from the blasting point. Charge holes were drilled through layered sand and soil up to granite underneath it. Spacing of charge hole was 2 m. 20 kg GX-1 dynamite was loaded in each hole at 50 m below sea level, and 9 holes were fired under no free face condition, therefore, amount of explosive fired simultaneously

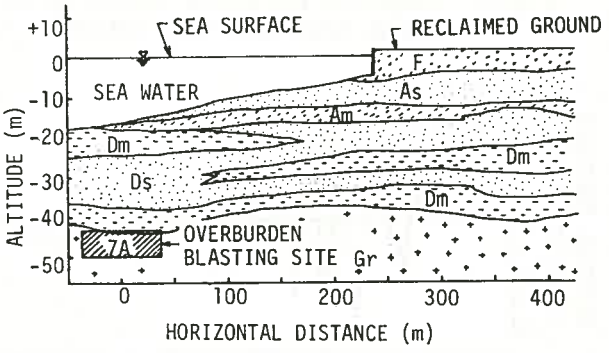

F : FILLED SAND, As : ALLUVIAL SAND,
Am : ALLUVIAL SOIL, Ds : DILUVIUM SAND,
Dm : DILUVIUM SOIL, Gr : GRANITE,

Fig.1 Geological section of the site

was 180 kg. This particular blasting is called as a submarine overburden blasting.

3. Numerical Simulation

Numerical simulation of this blasting was performed to predict ground vibration and shock wave in sea water. Computer program used for this simulation is a DAYS-2 Code which involves the finite difference approximation to the equation of motion in the Lagrangian coordinate system. In case of a simulation of explosion produced phenomena, in-put data for the simulation must be the detonation pressure of an explosive, therefore, the maximum size of a element composed the numerical model is controlled by the size of the explosive. In this simulation, three different size models were used. The first model was an axially symmetric model of which size was 5 m x 1.6 m consisting of 4.3 cm x 20 cm elements. In-put data of this model were detonation pressures those were applied to the elements at the position of the explosive. The stress condition around the charge hole which was computed by using the first model was used as the in-put data of the second model of which size was 16 m x 20 m. The size of the final model which was used for the computation of the ground vibration on the reclaimed ground was 160 m x 580 m, and the in-put data of

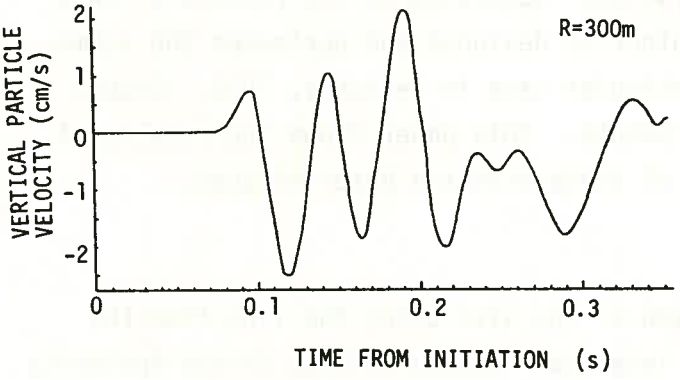

Fig.2 Computed particle velocity at 300 m from the shot point

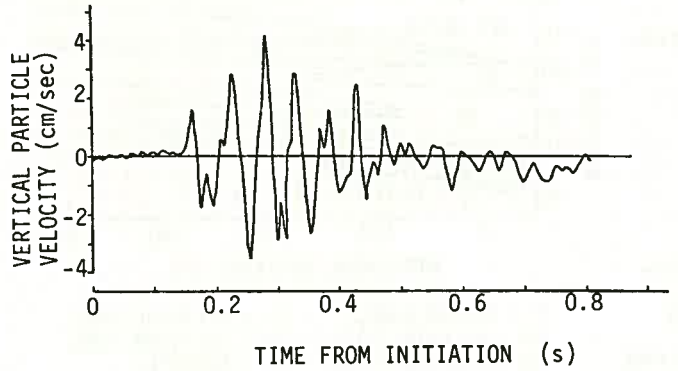

Fig.3 Particle velocity record observed at 340 m from the shot point

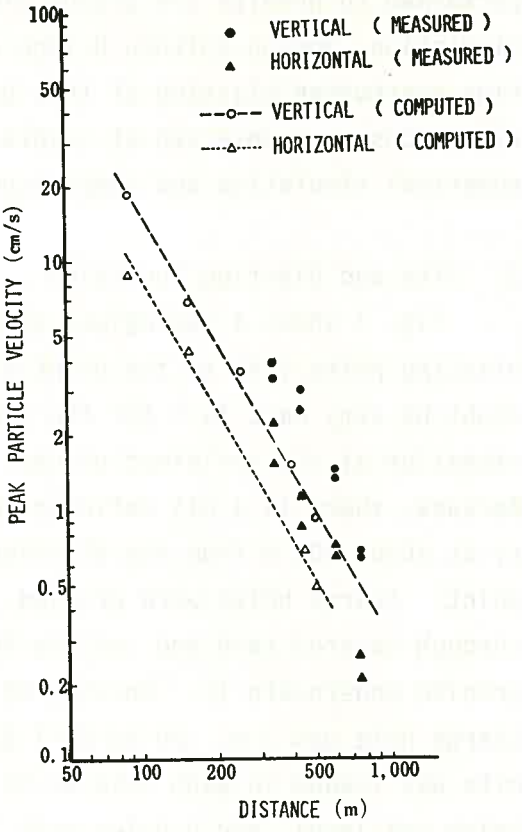

Fig.4 Comparison of measured peak particle velocities against computed ones

this model were derived from the stress condition computed by using the second model. Numbers of the element composed each model were 1000～1200. In order to get the values of various physical constants of the elements composed the model, characteristics of the geological materials in the site were measured by using both a seismic technique in-situ and a laboratory testing of core samples. As an example of the result of the simulation, Fig. 2 shows the computed particle velocity on the reclaimed ground at 300 m from the shot point.

4. Observed Ground Vibrations and Comparison of Those with Computed Ones

Ground vibrations on the reclaimed ground were observed at several points by using velocity pick-ups. Fig. 3 shows an example of the particle velocity record at 340 m from the shot point. Fig. 4 shows the observed peak particle velocities and the computed ones for comparison. As shown in Fig. 4 the amplitude of the ground vibration predicted from the simulation is about a half of the measured one, but the attenuation of the amplitude with distance and the ratio of vertical amplitude against horizontal one agree well. Furthermore, by comparing Fig. 2 and Fig. 3, it is recognized that the dominant frequency of the particle velocity obtained by the simulation agrees well with that of the observed one. On the whole, it may be considered that the results of this numerical simulation are reasonable. In order to discuss the validity of this numerical simulation, the amplitude of the ground vibration caused by this particular blasting was calculated by using an experimental formula which was derived from previous measurements of ground vibration caused by common types of blasting. This result showed that the amplitude estimated was 1/10～1/13 of the observed one. Therefore, the validity of this numerical simulation was verified.

References

K. SASSA and I. ITO : The Breakage and Stress Wave Caused by Detoantive Loading, Jour. of the Society of Material Science, Japan, Vol. 21, No. 221, pp. 123～129, 1972.

K. SASSA and I. ITO : On the Relation between the Strength of a Rock and the Pattern of Breakage by Blasting, Proc. of the 3rd ISRM Congress, 2-B, pp. 1501～1505, 1974.

K. SASSA, I. ITO and T. NARAHIRA : Numerical Simulation of Pressure Wave Caused by Submarine Blasting and Comparison of Those against Field Trials, Jour. of the Industrial Explosives Society, Japan, Vol. 38, No. 2, pp. 91～99, 1977.

K. SASSA, I. ITO and S. NAGASAKA : Prediction of Ground Vibrations from Submarine Overburden Blasting and Results of Their Measurements, Jour. of the Industrial Explosives Society, Japan, Vol. 38, No. 3, pp. 137～143, 1977.

ON THE ESTIMATION OF PERFORMANCE OF A PNEUMATIC ROCK-DRILL

Yoshio TAKAHASHI, Akita University
Zenjiro WATANABE, Akita University

1. INTRODUCTION

In order to increase the drilling efficiency,drilling tests must be carried out for various rocks by using a rock-drill. Since a drill must have enough power to crush various rocks, it is necessary to study on the performance of a pneumatic rock-drill.

In this study, the authors indicated that the performance index of non-dimensional quantity proposed by them made it possible to estimate the performance of a pneumatic rock-drill.

2. COMPARISON OF THEORETICAL AND EXPERIMENTAL VALUES FOR EACH PERFORMANCE VALUE

A theoretical equation[1] obtained by considering the equations of motion of the piston and the valve as well as the equations of continuity, state and energy of air was used for evaluating the performance of the drill.

Furthermore, a generally used TY-16 type drill was used as a testing drill for examining the effect of inlet air pressure on the performance of a pneumatic rock-drill with fully automatic valve.

The comparison of the theoretical and experimental values for each performance value is shown in Fig.1(a),(b),(c). According to these figures, the theoretical value is considered to be in good accordance with the experimental value except for an appreciable difference in the maximum pressure of rear-chamber(Pbmax). From the above results, the theoretical equation may be applicable for analysing the performance of a pneumatic rock-drill.

3. FACTORS AFFECTING THE NET THERMAL EFFICIENCY

In order to design a pneumatic rock-drill with better performance, the net thermal efficiency must be large as much as possible. The following functional form is obtained by the equation[2] for the net thermal efficiency.

$$\eta_t = f\ (\ Pi,\ Us,\ Qw,\ N,\ W,\ St,\ Ab\ ) \qquad (1)$$

where, η_t:net thermal efficiency, Pi:input air pressure, Us:blow-velocity of piston, Qw:inlet air consumption, N:number of blow, W:piston weight, St:piston stroke, and Ab:cross-sectional area of the rear-chamber in the cylinder.

Furthermore,it is necessary for the analysis of the performance of a pneumatic rock-drill to consider the physical property of rock under drilling.

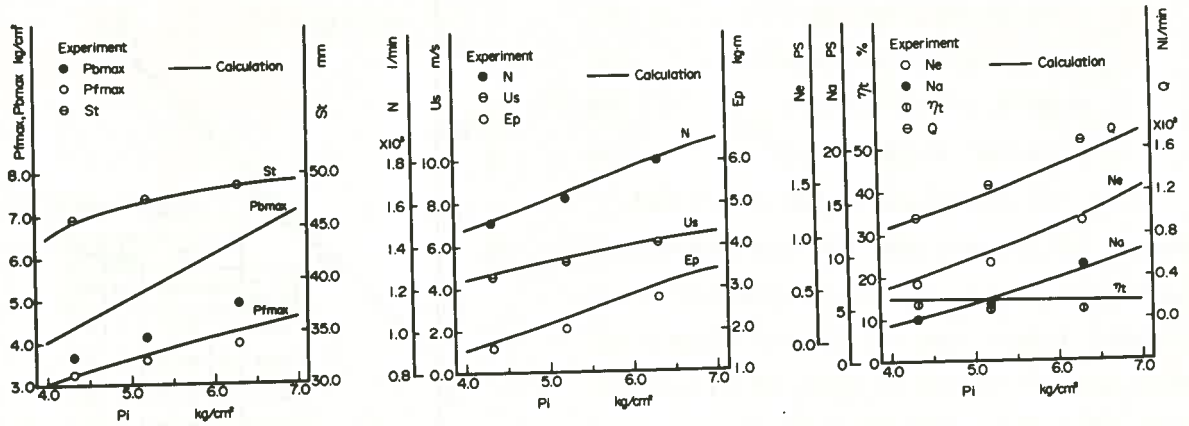

(a) (b) (c)

Fig.1 Comparison of theoretical and experimental values for each performance value

Thus, the effect of physical property of rock on the performance of the drill was also examined theoretically by introducing the parameters; the amount of penetration of bit(h) and the coefficient of restitution of rock(e), which were obtained by considering the drillability[3,4] of various rocks. Fig.2(a), (b),(c) show the calculated results. Especially, as is shown in Fig.2(c), the net thermal efficiency is not affected by the amount of penetration of bit, but greatly affected by the restitution of rock. Therefore, in case of rock-drilling, the coefficient of restitution of rock must be considered as a factor affecting the net thermal efficiency, and Eq.(1) must be modified to Eq.(2).

$$\eta_t = f\ (\ Pi,\ Us,\ Qw,\ N,\ W,\ St,\ Ab,\ e\ ) \qquad (2)$$

4. ESTIMATION OF THE PERFORMANCE OF A PNEUMATIC ROCK-DRILL

The following four non-dimensional quantities are obtained by applying the dimensional analysis to Eq.(2).

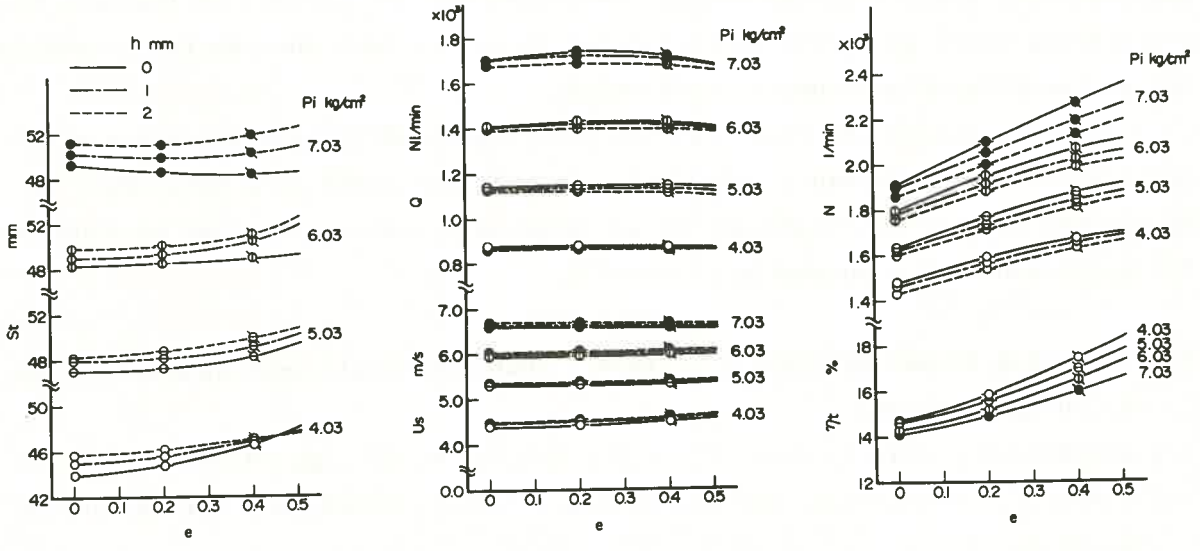

(a) (b) (c)

Fig.2 Relationship between coefficient of restitution of rock and each performance value (calculated values)

$$\Pi_1 = Pi \cdot St \cdot Us(1-e)/Qw \quad (3)$$

$$\Pi_2 = Pi^2 \cdot Us^2 \cdot Ab(1-e)/Qw^2 \quad (4)$$

$$\Pi_3 = Qw \cdot N/[Pi \cdot Us^2(1-e)] \quad (5)$$

$$\Pi_4 = Pi \cdot Us^2 \cdot W/[Qw^2(1-e)] \quad (6)$$

The relationships between the net thermal efficiency and the non-dimensional quantities, Π_1,Π_2,Π_3, are represented as straight lines, the values and slopes of which are different in case of different types of drills. On the other hand, as is shown in Fig.3, the net thermal efficiency increases almost straightly with increase of Π_4 independently of types of drill. Thus, in order to evaluate the net thermal efficiency, it is most appropriate to use Π_4 among four non-dimensional quantities. Hence, Π_4 is defined as the performance index(Ip). The X marks in Fig.3 correspond to the experimental values of TY-16 rock-drill. Furthermore, the solid line in this figure is obtained by applying the least square method to the theoretical values, and expressed in the following equation.

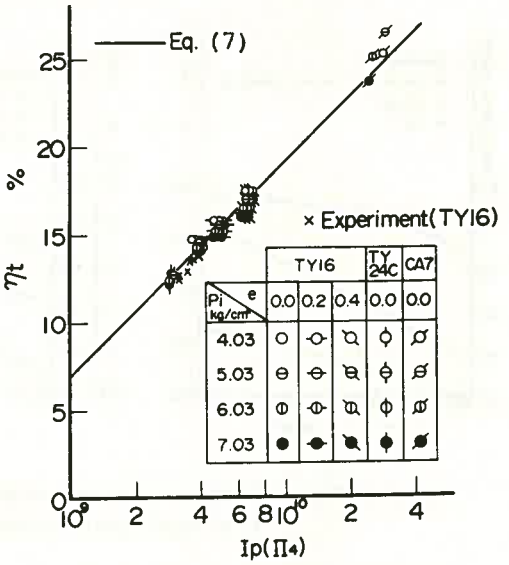

Fig.3 Relationship between net thermal efficiency and performance index

$$\eta_t = 12.25 \cdot \log Ip - 103.24 \quad (7)$$

5. CONCLUSION

(1) The results on the performance of the drill analysed by authors' theory well coincide with the experimental results.

(2) Among four non-dimensional quantities obtained by the dimensional analysis with respect to the factors affecting the net thermal efficiency, the performance index in Eq.(6) is considered to be the best measure for estimating the performance of a pneumatic rock-drill.

(3) Considering the fact that the net thermal efficiency increases with increase of the performance index, the sizes of the parts of a drill must be determined so that the index may be as large as possible, in order to improve the performance of a pneumatic rock-drill.

REFERENCES

[1] TAKAHASHI,Y. and WATANABE,Z., (1974), Jour.Min.Metall.Inst.Japan, Vol.90, No.1032, pp 91-96.

[2] HAYAMIZU,H., (1975), Jour. J.S.M.E., Vol.78, No.677, pp 341-46.

[3] SASAKI,K., YAMAKADO,N. and SHIOHARA,Z., (1957), Mining and Safety, Vol.3, No.9, pp 21-31.

[4] SASAKI,K., YAMAKADO,N. and SHIOHARA,Z., (1958), Jour.Min.Metall.Inst.Japan, Vol.74, No.846, pp 989-95.

PREDICTION OF DRILLABILITY OF ROCK FROM STAMP PENETRATION TEST

Shoichi TANAKA and Mitsuo SATO, University of Tokyo

Optimization of drilling operation and estimation of in-situ properties of rocks are basic problems in rotary drilling. The relationship between mechanical properties of rock and drillability of rock is considered a useful means to approach these problems. In this study, stamp penetration test (Shreiner hardness test) was selected for its similarity to bit tooth action on rock. Drilling rate test, stamp penetration test and compression test were carried out on the same block of rock to permit direct comparison of test results. All these test were carried out under atmospheric conditions.

1. Drilling rate test. Drilling rate tests were carried out on several rock samples with a ten ton bit test machine using a 95 mm soft type three cone bit. The drilling rate equation is expressed above some lower limit of bit weight as follows:

$$\frac{R}{N} = C\left(\frac{W}{D} - W_o\right)$$

where

R = drilling rate, cm/sec

N = rotating speed, rev/sec

W = bit weight, kg

D = bit diameter, cm

W_o = weight constant, kg/cm

C = drillability constant, cm^2/kg.

Specific drilling energy is defined as drilling energy divided by the volume of drilled rock. The specific drilling energy decreases with increased bit weight and approaches a certain minimum value, and then, if applied too much bit weight, increases again. This minimum value is considered as a parameter of the rock included an effect of the bit type used. The correlation between the drilling constant and the minimum specific drilling energy is shown in Figure 1. If the drilling data are measured at a given conditions, the specific drilling energy will be calculated and parameters of drilling equation will be reduced from the correlation like Figure 1. Properties of rock might be estimated by using after-mentioned correlations.

2. Compression test. Figure 2 shows the relation between the compressive strength and weight constant.

3. Stamp penetration test. In this test flat-faced cylindrical stamps of areas of 3, 5, 10 and 20 mm^2 respectively were used. For soft rocks 10 mm^2 stamps were used mainly, and for hard rocks 3 mm^2 stamps were used. Some examples of load-displacement curves are shown in Figure 3. Yield points and failure points of rocks are indicated by symbols of a and b respectively. Rocks are classified into two groups by post-yield behaviors. On rock E in Figure 3, the yield point coinsides with the failure point, and this rock is classified into an elastic failure type rock, and its plasticity coefficient equals to one. Other three rocks are classified into plastic failure type rocks, and their plasticity coefficients range from two to three. The plasticity coefficient is defined as a ratio of total work to elastic work required until rock failure. From failure point data, hardness and specific work of rocks are obtained. In this test, the specific work is defined as a value of work required to break rock divided by a volume of the stamp penetrated into the rock. The specific work is generally higher for plastic failure type rocks than for elastic failure rocks as shown in Figure 4. The hardness is obtained as the load at failure point divided by the area of stamp.

In this test, the stamp size affected the penetration at the yield

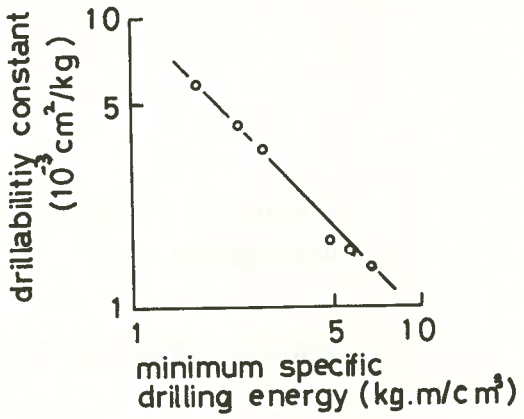

Fig 1 Correlation between drillability constant and minimum specific drilling energy.

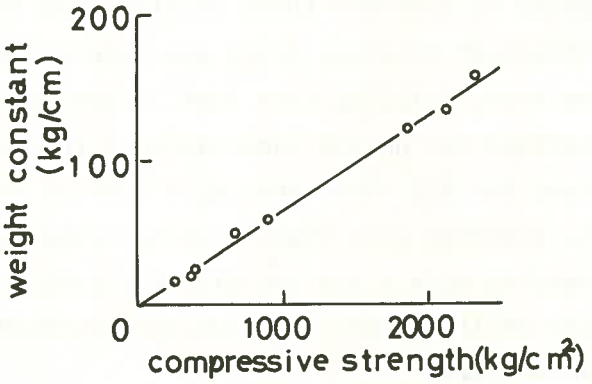

Fig 2 Correlation between compressive strngth and weight constant.

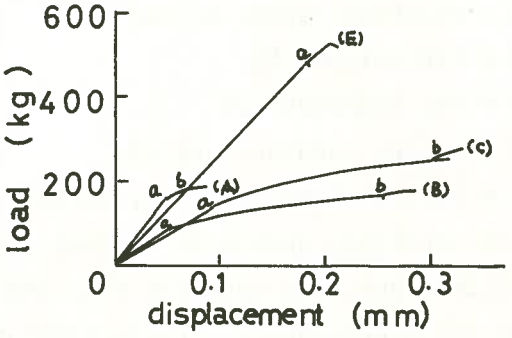

Fig 3 Examples of load-displacement curves with 10 mm^2 stamps.

point, and the penetration increased with increased size of stamp, but there was no positive effect of the stamp size on hardness and specific work. In general, parameters of stamp penetration test are defined for the stamp used, and, therefore, it seems advisable to select the range of the stamp size in making test.

There is a positive correlation between compressive strength and hardness, and the value of hardness is six to nine times as large as that of compressive strength compared in the same unit system. The correlation between the rock hardness and weight constant is shown in Figure 5. The correlation between the specific work and the drillability constant is shown in Figure 6. This figure has the similar shape to Figure 1. In Figure 6, however, the mode of failure affects definitely the position of the lines, since the specific work is affected by the failure mode as shown in Figure 4.

Above-mentioned correlations are, of course, applicable to this test conditions. These things, however, give hope that the stamp penetration test provides a means of prediction of drillability from mechanical properties of rocks, and also a means of estimation of rock properties from drilling data.

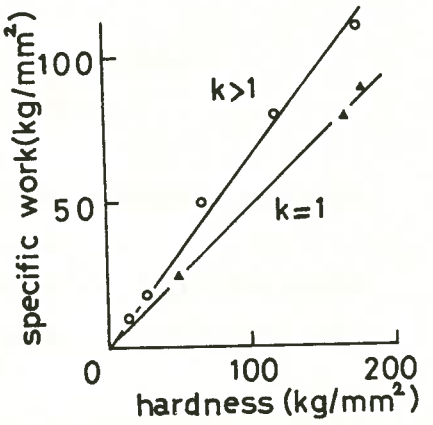

Fig 4 Relationship between hardness and specific work.
K = plasticity coefficient.

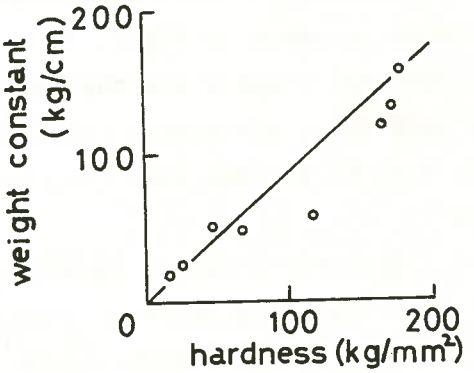

Fig 5 Correlation between hardness and weight constant.

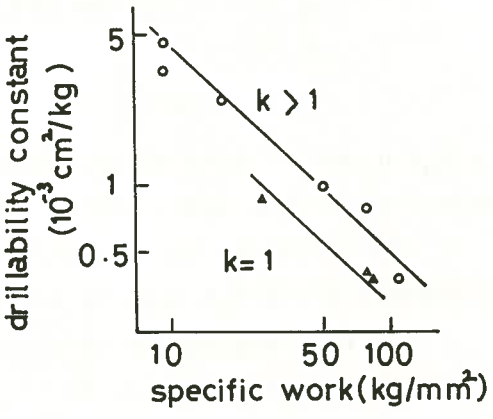

Fig 6 Correlation between specific work and drillability constant.
K = plasticity constant.

FRACTURING OF ROCK AT ELEVATED TEMPERATURE WITH BOREHOLE COOLING METHOD

Hirohide HAYAMIZU, National Research Institute for Pollution and Resources (NRIPR)
Hideo KOBAYASHI, NRIPR
Isao MATSUNAGA, NRIPR

The basic equations of linear elastics on problems of the thermal stress fracturing were investigated and laboratry experiments were carried out to make clear the fracturing mechanism.

1. Theoretical Consideration

Consider a vertical borehole(radius R_1) which is drilled into a hot dry rock mass as shown in Fig.1. It is postulated that the rock mass is homogeneous, and that elastic and thermal constants are not function of temperature. When cold water circulates the borehole, the temperature of rock mass(T_o°C) falls down to T°C and then the thermal stresses are initiated around the borehole.

The stress-strain equations are given by

$$\left.\begin{aligned}\sigma_r &= \lambda(\varepsilon_r+\varepsilon_\theta+\varepsilon_z)+2\mu\varepsilon_r+\sigma_r' \\ \sigma_\theta &= \lambda(\varepsilon_r+\varepsilon_\theta+\varepsilon_z)+2\mu\varepsilon_\theta+\sigma_\theta' \\ \sigma_z &= \lambda(\varepsilon_r+\varepsilon_\theta+\varepsilon_z)+2\mu\varepsilon_z+\sigma_z' \\ \tau_{rz} &= \mu\gamma_{rz}+\tau_{rz}'\end{aligned}\right\} \quad (1)$$

where

$$\left.\begin{aligned}\left.\begin{matrix}\sigma_r' \\ \sigma_\theta' \\ \sigma_z'\end{matrix}\right\} &= -(3\lambda+2\mu)\alpha T' \\ \tau_{rz}' &= -\mu\alpha z\frac{\partial T'}{\partial r}\end{aligned}\right\} \quad (2)$$

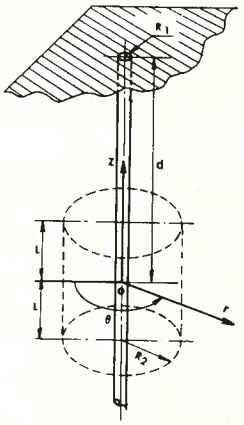

Fig.1.

u_r, u_θ, u_z are strains of each direction, α is the coefficient of linear thermal expansion, and μ and λ are Lame's parameter.

To calculate the thermal stresses around the borehole, the temperature difference $T'(=T-T_0)$ must be decided.

If the temperature of rock mass depends on r only, the equation of temperature field is given by

$$T = T_1 - (T_1-T_2)\log(r/R_1)/\log(R_2/R_1) \quad (3)$$

where T_1 is the temperature of the borehole wall ($r=R_1$) and T_2 the temperature of the boundary of $r=R_2$. If we think $R_2 \to \infty$, it is assumed that τ_{rz} and τ'_{rz} are zero.

Consider the thick hollow cylinder(radiuses R_1 and R_2, heigth 2L) in the

cubic specimen, so that the boundary condition of the experiments is as follows,

$$\sigma_r = 0 \ ; \ r = R_1, \ r = R_2$$
$$\sigma_z = 0 \ ; \ z = \pm L$$

While, the boundary condition of the hot dry rock mass(Fig. 1) is assumed as follows,

u_z(displacement of z direction) = 0 ; $z = \pm L$

u_r(displacement of r direction) = 0 ; $r = R_2$

Therefore we consider the plain stress condition for the case of experiments and the plain strain condition for the case of hot dry rock mass.

Using the equations of equilibrium and (1), (2) and (3), the equations of thermal stresses are given as (4) and (5) for each case.

Laboratory experiment:

$$\left.\begin{aligned} \sigma_r &= \frac{E\alpha(T_1 - T_2)}{2}\Phi_r \\ \sigma_\theta &= \frac{E\alpha(T_1 - T_2)}{2}\Phi_\theta \end{aligned}\right\} \quad (4)$$

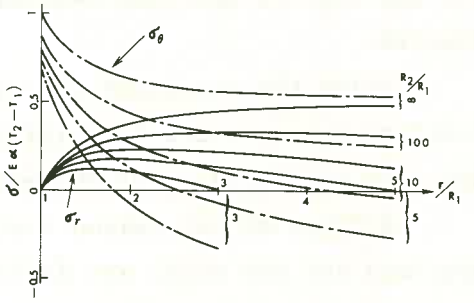

Fig.2

Hot dry rock mass

$$\left.\begin{aligned} \sigma_r &= \frac{E\alpha(T_1 - T_2)}{2(1-\nu)}\Phi_r \\ \sigma_\theta &= \frac{E\alpha(T_1 - T_2)}{2(1-\nu)}\Phi_\theta \\ \sigma_z &= \frac{E\alpha(T_1 - T_2)}{2(1-\nu)}\{\nu\Phi_r + \nu\Phi_\theta\} - E\alpha(T - T_2) \end{aligned}\right\} \quad (5)$$

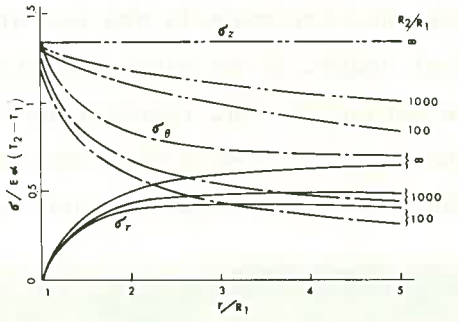

Fig.3

where E and ν are Young's modulus and Poisson's ratio of rock, respectively, and

$$\Phi_r = \log(r/R_1)/\log(R_2/R_1) - \left(1 - \frac{R_1^2}{r^2}\right) / \left(1 - \frac{R_1^2}{R_2^2}\right)$$

$$\Phi_\theta = \{\log(r/R_1)+1\}/\log(R_2/R_1) - \left(1 + \frac{R_1^2}{r^2}\right) / \left(1 - \frac{R_1^2}{R_2^2}\right)$$

The result of each case are shown in Figs.2 and 3. As is evident from Figs. 2 and 3, the radial stress σ_r is tensile stress, the tangential stress σ_θ shows the maximum value at the borehole wall($r=R_1$), and $\sigma_\theta \geq \sigma_r$ is valid near the borehole.

As the thermal stress is equal to or greater than the tensile strength of rock σ_t at the borehole wall, the vertical fracture will be created mainly by the tangential stress σ_θ in the experiments, if it is assumed that a fracting will first occur at this point.

3. Laboratry experiments

Cubic rock blocks of a side of 30 cm with the borehole of 6 cm in dia-

meter in the center were used for the laboratry fracturing experiments. The apparatus was shown Fig.4. The temperature of rock specimen was measured by the thermocouples on the borehle wall and at the depth 0.5 and 6 cm from the rock surface.

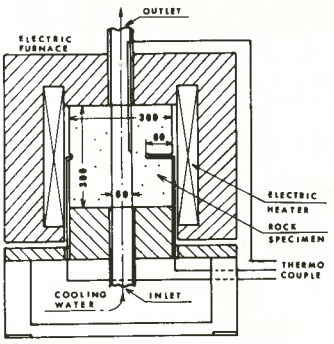

Fig.4

Fig.5 shows the two different modes of fracture. Inada granite (a) and Emochi andesite (b) were fractured by the tangential thermal stress σ_θ, while Kofu andesite((c),(d)) was fractured by the stresses, σ_r and σ_z, in addition to the stress σ_θ.

When the temperature difference between the surface of the borehole and the out side of specimen reached around 50°C for each specimen, the rapture occured.

Using the equations (4) and (5), the temperature difference required to initiate fracture are 27°C and 15°C for each experiment($R_2/R_1=5$) and the hot dry rock mass($R_2/R_1 \to \infty$) respectively.

Because of the reason that equations are simplifed and the shapes of the specimen and the model are different with each other, theoretical value somewhat differs from the experimental one.

From these consideration, we can estimate the temperature difference to make the fracture in the hot dry rock mass with the accurate enough for practical usage. If we superpose the rock pressure to the thermal stresses, it may be estimated that fracture by σ_θ would initiate in the hot dry rock mass at the depth of 5000 m when the temperature around the borehole was reduced about 440°C from the original rock temperature.

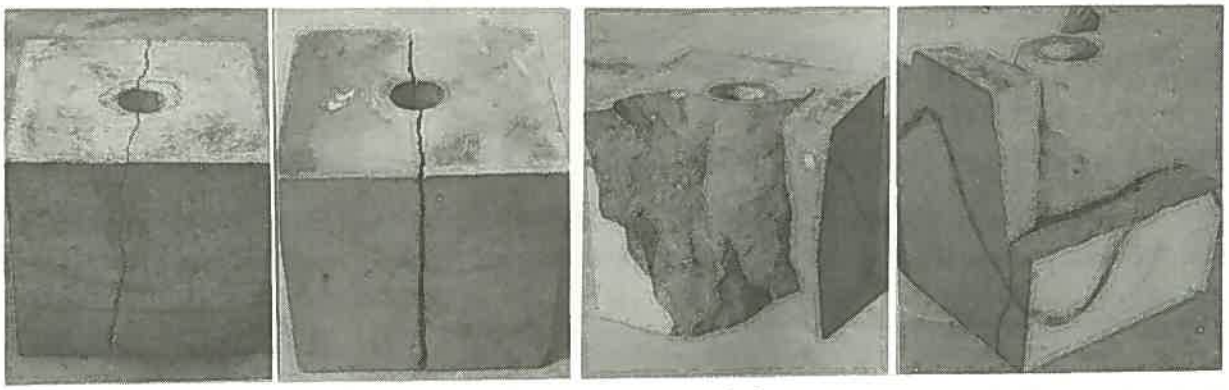

(a) (b) (c) (d)

Fig.5

STUDIES ON THE FRACTURING OF HOT DRY ROCKS BY HIGH SPEED WATER JETS
- Effects of rock temperature on the thermal fracturing of imitation rock specimen -

Hiroshi KIYOHASHI, Munesuke KYO and Wataru ISHIHAMA
Tohoku University

1. INTRODUCTION

As one of the new means of supplying energy, the development of geothermal energies stored in hot dry rocks without a hot water circulation system has also been studied in Japan. To extract the heat energy from such rocks, an artificial hot water circulation system must be created. Thus, it is necessary to develop methods for drilling and fracturing these hot dry rocks,to provide paths for the water. Theoretical studies on the heat extraction from fractured hot dry rocks (Ref. 1) and on the making of cracks in hot dry rocks by injecting high pressure water (Ref. 2,3) were carried out recently. But no one has reported how to drill holes for injecting water and extracting hot water or steam, or how to make cracks in such hot dry rocks in a designated direction.

High speed water jets have enormous hydraulic fracturing power and also impinging water jets having large heat transfer power are used in the cooling of high temperature bodies. In general, super high speed continuous or pulsed water jets (up to 3000 m/s) are needed for cutting hard rocks such as granite and basalt. But when the temperature of these rocks is high, it seems possible that they might become susceptible to cutting by relatively low speed continuous jets because of unsteady internal tensile thermal stresses induced near the rock surface by the high cooling power of these jets (Ref. 4).

The final objective of our studies is to investigate the applicability of a high speed water jet, whose fracturing ability is caused by the interactions between the thermal cracking and the hydraulic jet erosion, for drilling and fracturing of natural hot dry rocks. This paper describes a summary of our first stepped study (Ref. 5), which was carried out by using hot imitative dry rock specimens made of a castable fire-resistant material instead of natural high temperature rocks, on the effects of the temperature of the rock specimen on the drilling and fracturing patterns and on the efficiency, when water jet speed and standoff distance was kept constant at 70 m/s and 40 mm, respectively.

2. MATERIAL AND METHOD

Table 1 Physical properties of imitation rock specimens

Property	Temperature [°C]					
	15	200	400	600	800	1000
Apparent specific gravity [-]	1.61	1.60	1.54	1.51	1.49	1.51
True specific gravity [-]	2.62	2.62	2.73	2.76	2.77	2.77
Porosity [%]	38.6	38.9	43.6	45.3	46.2	45.5
Compressive strength [kgf/cm²]	66.4	93.8	55.2	57.3	46.1	43.9
Tensile strength by R.C.T.* [kgf/cm²]	9.17	12.0	6.53	5.75	6.54	6.54
Young's modulus [10^5 kgf/cm²]	3.70	5.39	1.46	1.35	1.16	1.70
Specific heat [kcal/kgf°C]	—	0.215	0.216	0.222	—	—
Thermal conductivity [kcal/mh°c]	0.172	0.179	0.231	0.296	(0.358)	—
Thermal diffusivity [10^{-4} m²/h]	—	5.20	6.94	8.83	—	—

* R.C.T. = Radial Compression Test

Imitation rock specimens (75 mm in diameter and 150 mm in length)were made of castable fire-resistant material (SiO_2:43 %, Al_2O_3:47 %, others:10 %, commercial name: "ASAHI CASTER-14F"). Table 1 shows the main physical properties of the imitation rock specimens tested at different temperatures. Compressive and tensile strengths and Young's modulus are the test results of gradually cooled specimens to room temperature.

The principal components of the experimental apparatus consisted of a water jet generator, test chamber, measuring apparatus and rock specimen heating furnace. Heating of the specimens was carried out in an electric furnace equipped with a programming temperature controller.

Experimental variables and conditions were as follows: The temperature of the specimens, θ, were normal temperature, 200, 400, 600, 800 and 1000 °C. Pressure of the water jet at nozzle exit, Ps, was at 25 Kg_f/cm^2 (2.45 MPa) corresponding to speed of the water jet at nozzle exit, Uo, 70 m/s. The temperature of the jet was almost equal to room temperature, 11-12 °C. The other fixed parameters were : nozzle diameter, Do, was 1.4 mm ; standoff distance, x, was 40 mm ; jet operation time, τ , was 10 s except an experiment to test the dependence of fracturing efficiency on τ ; the rate of increasing temperature was about 1.7 °C/min and the time of maintaining the certain tested temperature was over 100 min ; the number of specimens were five at each different condition.

3. RESULTS AND CONCLUSION

Experimental results indicated that the fracturing pattern of specimens varied characteristically with specimen temperature, θ. On the surface of a specimen struck by the water jet for 10 s, a cylindrical hole-shaped cavity with diameter of 3 to 5 mm at the jet stagnation point was observed in both cases of θ = 400 °C and $\theta \geq 800$ °C. A large crater-shaped cavity was observed at 600 °C. At θ = room temperature and 200°C, the surfaces of the specimens struck by the water jet were almost not damaged. In the present study the authors evaluated the fracturing efficiency by the maximum depth and the volume of the fractured cavity of the specimens. Figures 1 and 2 show dependences of the depth, l, and of the volume, v, of cavities fractured by the impinging water jet on specimen temperature, respectively. The tendency of curves showing the relation between l or v of cavities and θ was similar

to that of the boiling curve, having the maximum value at about 600 °C and the minimum at about 800 °C.

Referring to the effect of jet operation time, τ, on the depth, l, of the cavities fractured by the impinging water jet, l varied remarkably in τ at the beginning of impingement of the water jet; however, l reached nearly constant value at τ = 10 s when θ was 800 °C, as shown in Fig. 3.

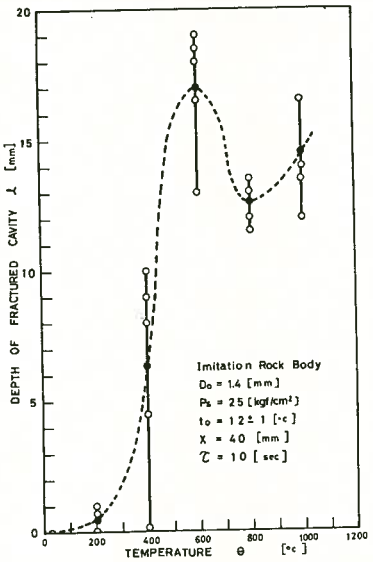

Fig. 1 Dependence of depth of cavity fractured by impinging water jet on specimen temperature.

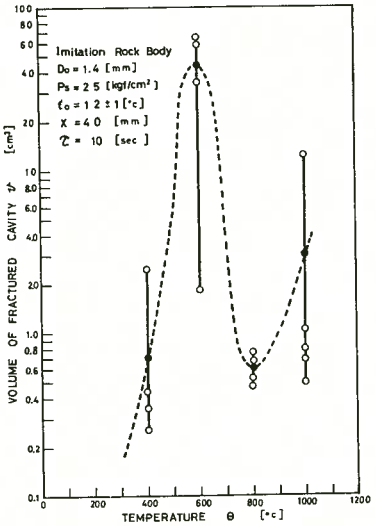

Fig. 2 Dependence of volume of cavity fractured by impinging water jet on specimen temperature.

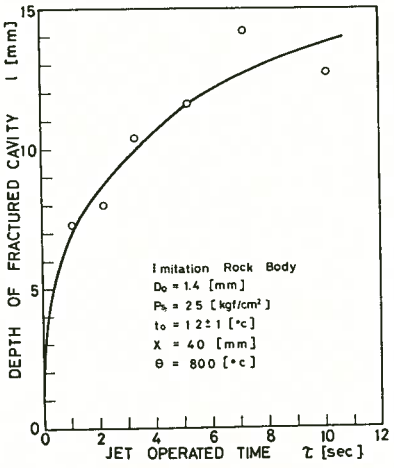

Fig. 3 Dependence of depth of cavity fractured by impinging water jet on jet operated time.

A model for the flow and the heat transfer with boiling of impinging water jets on a high temperature surface was proposed to explain the experimental results.

Some of the extended works of this study were reported already (Ref. 6,7), and now the authors are vigorously continuing the studies.

REFERENCES

1) Gringarten, A. C. et al: J. Geophys. Res., 80, 8 pp. 1120-1124. (1975).
2) Abe, H. et al: J. Geophys. Res., 81, 29 pp. 5335-5340. (1976).
3) Abe, H. et al:J. Geophys. Res., 81, 35 pp. 6292-6298. (1976).
4) Pritchett, H. W. et al: PB-244091, pp. 1-242. (1974).
5) Kiyohashi, H. et al: J. Min. & Metal. Inst. of Japan, 94, 1086 pp. 515-521. (1978). (In Japanese)
6) Kiyohashi, H. et al: ALTERNATIVE ENERGY SOURCES ed. by Veziroglu, T. N. : Vol. 6, pp. 2727-2745. Hemisphere Pub. Co., Washington. (1978).
7) Kiyohashi, H. et al: 4th Int. Symp. Jet Cutting Tech., BHRA, Vol. 1, pp. C2-7-C2-28. (1978).

ON THE METHOD OF COMBATING FLOOR LIFT BY FLOOR BOLTING

Zenjiro HOKAO, Tokyo University
Jisun YOON, Taisei Kiso Co. Ltd.

1. Introduction

A series of model experiments on the mechanisum of floor lift in coal mines were carried out in our laboratory, and some effects of several factors (depth of roadway, distance from roadway to upper coal seam etc.) to the floor lift were examined. Referring to the experimental results and todays Japanese coal mines conditions, we applied the floor bolting as one of the useful method of combating floor lift and the effect was demonstrated experimentally. The relations between length of bolt and effect of bolting were shown and discussed.

2. Dimensional analysis and properties of model material

In order to carry out a model study it is necessary to scale not only the geometrical factors but all the other independent parameters involved. As the results of dimensional analysis, we determined the scale factor as shown in Table 1.

In Table 2 figures are given for the compressive strength, tensile strength, cohesion and Young's modulus of rock together with the values required for the model material assuming a scale factor 1/40 2.3/2.6 = 1/45.2. To get a suitable model material of floor of road, the dry clay powder and water were mixed, and the relationship between the cohesion of model material and the water content was obtained experimentally. The roof and coal seam were modeled with the mixture of gypsum, sand and water.

3. Model construction

The essential features of the large size 40:1 model rig are as follows. The box which holds the model has internal dimensions 200 × 180 × 100cm and the height 150cm. The back, both sides and bottom plates of box are 6cm thick mild steel, while a front plate is a 1cm thick transparent plastic. In the box a model of road was constructed. Fig 1 shows the relation between the upper coal

Table 1. Some physical parameters, their dimensions and the model scale factors

PHYSICAL PARAMETERS	DIMENSIONS	SCALE FACTOR (a)	(b)*
acceleration	$[LT^{-2}]$	$a_g = a_L \cdot a_t^{-2}$	1
length	[L]	a_L	1/40
time	[T]	a_t	$1/\sqrt{40}$
density	$[ML^{-3}]$	a_ρ	2.3/2.6
stress	$[ML^{-1}T^{-2}]$	$a_\sigma = a_L \cdot a_\rho$	1/40 × 2.3/2.6
Young's modulus	$[ML^{-1}T^{-2}]$	$a_E = a_L \cdot a_\rho$	1/40 × 2.3/2.6
strength	$[ML^{-1}T^{-2}]$	$a_{\sigma_t} = a_L \cdot a_\rho$	1/40 × 2.3/2.6
cohesion	$[ML^{-1}T^{-2}]$	$a_{\sigma_c} = a_L \cdot a_\rho$	1/40 × 2.3/2.6
poisson ratio	[0]	a_ν	1
internal friction angle	[0]	a_γ	1

* Column (b) gives the scale factors employed in the present model work

Table 2. Compressive strength, tensile strength, cohesion and Young's modulus of rock and model material required

	ROCK	REQUIRED MODEL MATERIAL
compressive strength (kg/cm^2)	149	3.3
tensile strength (kg/cm^2)	13.6	0.3
cohesion (kg/cm^2)	6.3	0.14
Young's modulus (kg/cm^2)	5.6×10^4	1.2×10^3

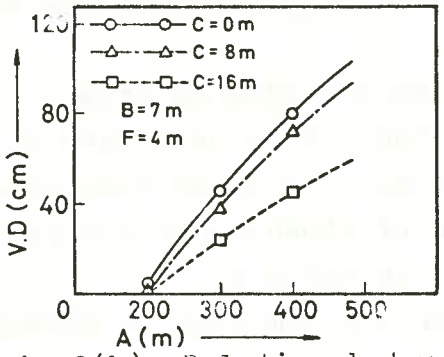

Fig 2(b). Relation between V.D and the depth

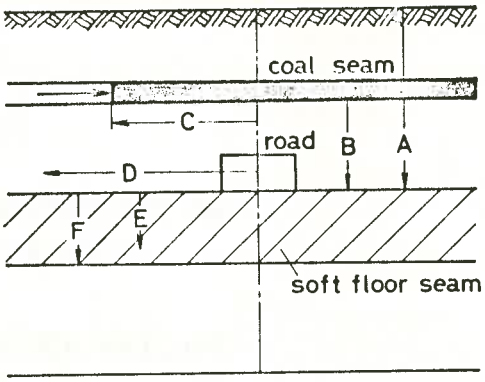

Fig 1. Nomen clature

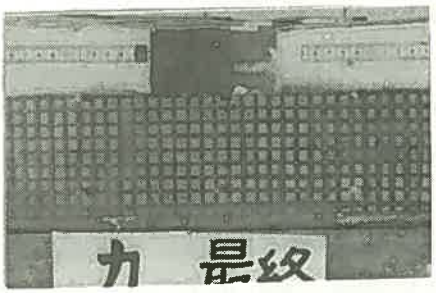

A = 200m

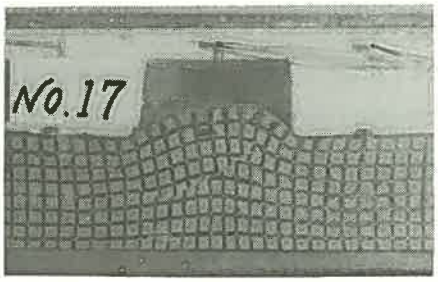

A = 300m

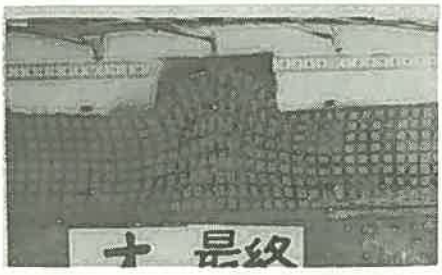

A = 400m

Fig 2(a) Floor lift of floor seam

seam, road and the soft floor seam. The face was advanced from the left to the direction of road. As the top loading system, 20 lever systems were applied.

4. Experimental results

On the floor model seam, many lines were drawn and the displacement of the cross points of these lines by the loading were measured.

Fig 2 shows the relation between the vertical displacement of floor surface of road and the depth. The vertical displacement will be increased very much according to the increment of the

depth.

Fig 3 shows the relation between the vertical displacement of floor surface of road, the distance between the upper coal seam and the road, and the depth. When the road is located beneath the coal seam about 20m and the depth is 600m, the vertical displacement is about 40cm.

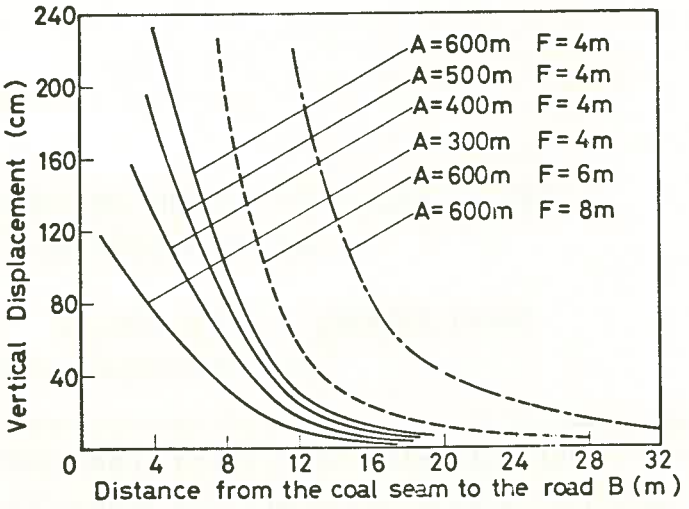

Fig 3. Relation between V.D and the depth and distance from the coal seam to the road

We tested the effect of floor bolting to the floor lift. In Fig 4 the floor bolting pattern were illustrated. We can see the good effect of bolting in Fig 5. When we apply the patter of bolting like Fig 4(a), the vertical displacement will be decreased from the 80cm in case of no bolting to about 20cm.

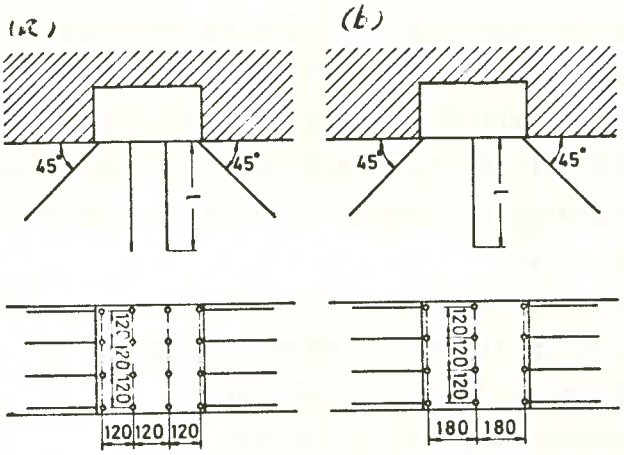

Fig 4. Bolting pattern

In Fig 5, the solid line shows the vertical displacement of a center of road at a point of 0.4m beneath of the floor surface, while the broken line 1.2m beneath. 'l' means the length of bolt and the effect of bolting will be increased with a increment of the bolting length. The diameter of bolt was 2mm in model.

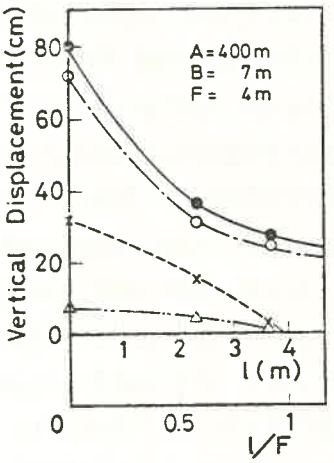

Fig 5. Effect of bolting

THE REINFORCE OF SUPPORT IN THE HEAVY EARTH PRESSURE ZONE AT THE MATSUMINE MINE

Yasuo KOTAKE, Yoji FUJII, Kazuhiro TSUMURA
Dowa Mining Co.,Ltd.

The Matsumine mine which commenced the operation in 1966 has produced nearly seven million tonnes of crude ore and occupies the leading position in the domestic copper production.

The Matsumine ore deposit,typical Kuroko(Black ore) type,consists of a few separated ore beds and lies 200 to 400 meters below the surface. These ore beds are in the argillized soft tuff that brings the extreme difficulties in keeping the openings standing up to the heavy and quick earth pressure.

At the Matsumine mine,approximately 14 kilometers of drifts are used for ore haulages and services. For supporting drifts and chutes, Matsumine generally used steel rib sets as shown by (a) and (c) in Fig. 1 .

However,the soft and swelling rocks in the heavy earth pressure extremely failed these steel supports and drifts became of no use in a few months. Under these circumstances,drifts were kept by repeating both the enlargement of narrowed openings and the renewal of supports. In spite of many times of the repair, openings became narrower ceaselessly due to the clayish and swelling rocks,as a matter of course the maintenance cost of drifts kept on rising.

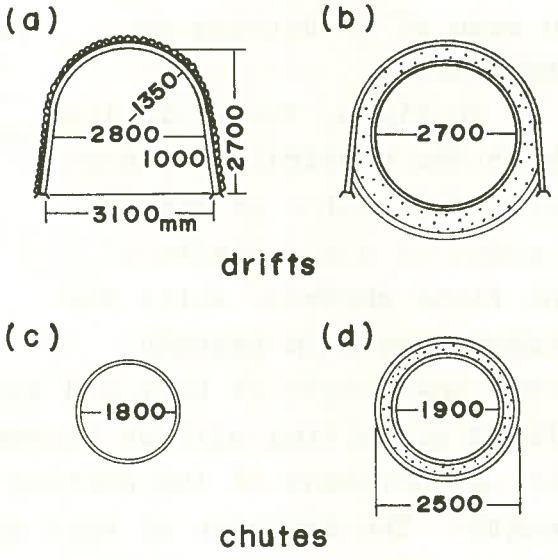

Fig.1 Steel rib sets and concrete lining

To improve the inefficiency in the maintenance of drifts, Matsumine crews employed tougher supports and modified the arrangement of drifts in bad grounds as follows.

(A) Concrete lining as shown by (b) and (d) in Fig.1 was applied to openings. Drifts were firstly driven with steel ribs and concrete was poured around heavy steel rings installed inside of ribs. By repeating this cycle — driving, installation of steel rings, concreting — , drifts with the solid support were constructed in bad grounds. Chutes were reinforced by tough liner which was composed of the concrete wall in a pair of circular steel plates.

By the reinforce of supports,the maintenance cost was substantially reduced in spite of the costly concreting.

(B) The arrangement of access drifts were modified as shown by (b) in Fig.2 . Horizontal drifts which need larger openings are positioned in hard rocks forming the foot wall. From access drifts up to the top of ore beds,chutes are constructed by mechanical raising. Ores are mined by means of undercut and fill stoping with artificial roof.

Formerly raising to the length of over fifteen meters was impossible in the heavy earth pressure zone because clayish and collapsible rocks were not competent enough to permit the openings to stand without the immediate installation of tough supports,no wonder it was one of the most dangerous and undesirable jobs in mining. On the ground of the above,access drifts were forced to be positioned at intervals of fifteen meters as shown by (a) in Fig.2 .

A few years ago,Matsumine crews developed a new type of the raise borer for the purpose of overcoming difficulties as mentioned earlier. This new machine is Blind up-hole raise borer with shield framing apparatus, which has taken the man out of the raise and enabled the safe and efficient raising to the length of over thirty meters even in the extremely bad grounds.

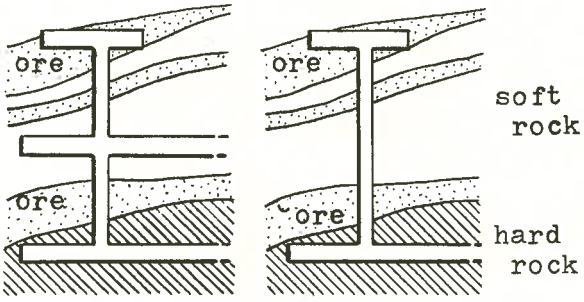

(a) Former (b) Present

Fig.2 Arrangement of access drifts and chutes

By modifying the arrangement of access drifts,the length of drifts passing in the heavy earth pressure zone was drastically decreased,which has contributed to reduce the maintenance cost of drifts.

The maintenance cost of drifts has decreased year by year as shown in Fig.3 .

The figure indicates that the maintenance cost in 1967 became

roughly one third of that in 1978.

As a result of many considerations, the Matsumine mine has not only reduced the maintenance cost of drifts but also enabled the development of high grade ores in the heavy earth pressure zone at the upper level, which has substantially improved the mine efficiency and prolonged the life.

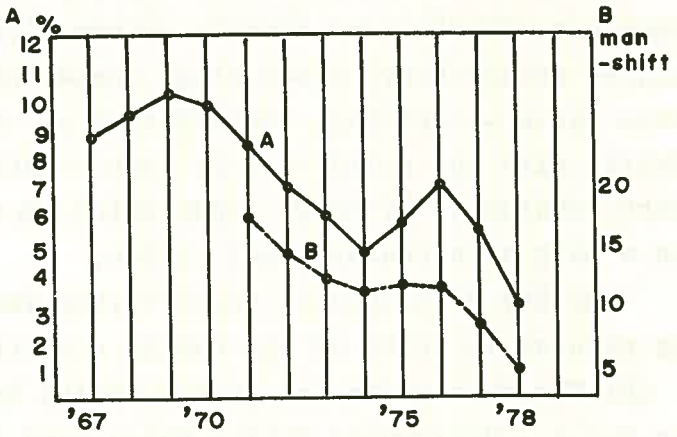

Fig.3 Drift maintenance cost

A. Ratio of the drift maintenance cost to the mining cost

B. Man-shift for the drift maintenance per one thousand tonnes of ore

ON THE ROOF SUPPORTING AT KAMIOKA MINE

- Especially about roof bolting and controlled blasting -

Nobukazu NANKO, Hiroshi KOMATSU, Mitsuhiro OHTA
and Takao HIRONAKA, Kamioka Mine,
Mitsui Mining & Smelting Co., Ltd.

1. Introduction

At Tochibora Mine, a mining section of Kamioka Mine, the roof supporting works become one of the most important problems at the point of view of safety and mining cost. Since a number of large mining machinery has been introduced for its trackless mining system and the size of drifts and inclines enlarged.

To solve this problem, the standardization of roof supporting works has been carried out. This report will introduce the standard of which is how to decide whether any supporting works require or not and the outline of the standardized roof supporting works including the smooth blasting system.

First of all, following items are taken into consideration.

(1) Based on the ground conditions and concerning data, how to decide the requirement of supporting works and how to choose the adequete roof supporting method.

(2) How to apply more roof bolts and how to standardize the roof bolting system.

(3) How to protect the weakening of rock～ by means of improvement of the blasting method and the shape of section of the drifts.

2. Standardization of the Roof Supporting Works

2.1 Selection Standard

Considering various experience following table 1 has been made as the Selection Standard of the supporting method in accordance with the rock conditions.

2.2 Roof Bolting

Since 1973, the resin anchor bolt has been introduced instead of former wedge-type roundbar rockbolt with a diameter of 19 mm. At present,

Table 1 Selection Standard of the Supporting Method in accordance with Rock Condition

General Condition of the Rock	Detailed Condition and Character of the Rock	Other Condition of the Rock (by Checking and Observation)	Other Condition of the Rock (by Boring Core)	Supporting Method
Solid and Compact Rock	(1) Without any fissure; with a few of tight fissure (2) With fissures but never cross each other ⟶ within a distance of 1.8m along the drift, number of fissure is less than 2 and no intersection	(1) Cut by the line connecting each blasting holes, Traces of drill holes are able to recognize on the roof and the wall after ordinary blasting (2) Rock repulses the hit by hammer or scalebar and no flat sound. No scale at all.	(1) Core recovery is more than 90% (2) Core is recovered completely as the cylindrical shape, and without any clayey fissure	No Supporting
Hard Rock, seemed to be with a pile of fissure	(1) Fresh and hard rock with a few number of clear fissure (2) With horizontal fissures (3) With fissures which may be broken down along the fissure surface (4) With fissures with water	(1) Many Traces of drill holes are remained on the roof and the wall after blasting. But some of them are fallen down by the effect of fissures. (2) If hit strongly by hammer or scalebar, flat sound and the massive scale comes out along fissures.	(1) Core recovery is 66 to 90% (2) 10～20 cm is not recovered within a drilling length of 1 m (3) Partially including clayey fissures	Direct Roof Bolting (Spot Bolting)
With a pile of fissure	(1) Within a distance of 1.8m along the drift, more than 2 fissures with thin clay including at least 1 big fissure among them (2) With a pile of fissure complicated (3) With a pile of fissure; or with loose rock partially	(1) A half of Traces of drill holes are remained, but other half is fallen down by the effect of fissures (2) If hit by hammer or scalebar, easily crushed along fissures and a many numbers of small scale comes out.	(1) Core recovery is 50～60% (2) Some core is broken as small pieces (5～10 cm size, breccia) within a drilling length of 30～50 cm. (3) With fault (4) Core recovery is less than 50% (5) Some core is broken as small pieces within a drilling length of 5～20 cm (6) Crushed zone with water	Direct Roof Bolting (Pattern Bolting) Indirect Roof Bolting (with Tie-Plate) Timber Support (Steel Frame Support for big size drift)
With a large number of fissures; or metamorphosed rock	(1) Intervals of rach fissures are less than 0.6m and including big fissures among them. (2) Loose methamorphosed rock with many joints (3) With many irregularly complicated fissures and joints	(1) After blasting, the wall and roof are shaped by the surface of crushed fissures (2) If hit by hammer or scalebar, roof and wall are easily fallen down (3) Supporting works must be done as soon		

nickedbar rockbolt with a diameter of 22 mm, length of 1 to 3 m, is adopted. This rockbolt is used to comfined with the resin (400 gr/cartridge, 0.7 m length, 22 mm diameter) as the resin anchor bolt. The bearing capacity of the resin anchor bolt is estimated as 17 ton considering a safety factor by the results of pulling test, and this value is much better than of the wedge type rockbolt which is about 10 ton.

Table 2 General Standard of the Roof Bolting Works

Roof Bolting Method	Purpose	Attention	Note
Direct Roof bolting (Spot bolting)	To protect preventively the occurrence of scale	(1) Observe carefully the condition of fissures and joints. (2) The bolting hole should penetrate more than 0.5m of solid rock at the bottom.	S : Supporting area of bolt (m^2) L : Length of bolt (m) Resin anchor bolt : S = 17/ (L - 0.5) x 3 Wedge type bolt : S = 10/ (L - 0.5) x 3
Direct Roof bolting (Pattern bolting)	To earn the effect of arch action (Bolting works are made with regular interval)	Bolting should be made radially from the center point of section of the drift.	W : Width of drift (m) L≧W/4 + 0.5 d1 : Interval of bolting cross the drift (m) 0.5L ≦ d1 ≦ 0.7L d2 : Interval of bolting along the drift (m) d2 = 1 ～ 2
Indirect Roof bolting (with tie-plate)	To support loose zone located in between roof bolts	Bolts and tie-plates should be strong enough and the interval of the bolts should be close enough to support the load of loose zone.	

3. Controlled Blasting (an Application of Smooth Blasting)

It is very important to avoid the weakening of the rock when develop drifts and stopes in order to save the supporting workes and the later transformation of the rock.

For the roof of drifts and stopes the smooth blasting method, and for the walls of vertical pillars the presplitting method is applied. These methods contribute to save mining cost.

3.1 Smooth Blasting (Cushion blasting) with Slurry Explosives

Standard drilling pattern of big section drift drilled by Mobile Jumbo is shown in Figure 1.

Charged holes are charged by ANFO. Smooth blasting holes are charged by slurry explosives.

At the drifting work, the ordinary blasting is made in advance and followed by smooth blasting. Each smooth blasting

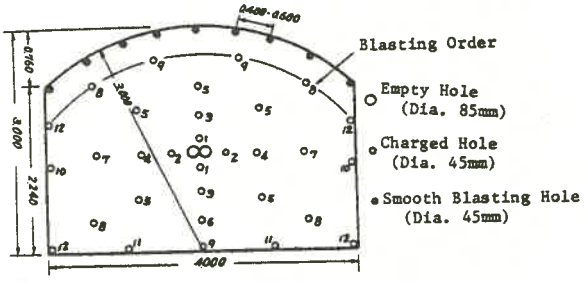

Fig. 1. Standard Drilling Pattern of Drift by Mobile Jumbo

Table 3 Specification of explosives

Items	Size & Weight of 1 Cartridge			Detonation velocity (m/sec)	Available energy (ℓ-kg/cm^2)
	Length (mm)	Diameter (mm)	Weight (g)		
S B dynamite	430	20	125	3,500 ~ 4,000	9,000
Slurry explosive	400	25	200	3,500 ~ 5,000	7,700

progress more or less an equivalent progressive distance of 1.5 ordinary blasting. Usually, the smooth blasting holes are blasted by simultaneous firing detonators at the same time when advanced ordinary holes are blasted.

A smooth blasting hole has a length of 2.5 m and is charged as shown in Figure 2. The weight of primer dynamite is 80 gr.

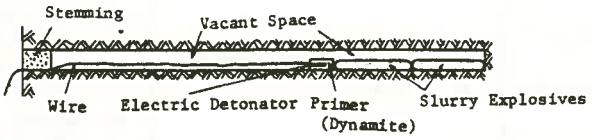

Fig. 2. Charging Method of Smooth Blasting Hole

3.2 Presplitting with Slurry Explosives

Presplitting is not so adequete to apply for drifting works as it is costly, but this method is successfully applied to keep the walls of vertical pillars and main underground chambers in good condition.

4. Conclusion

As the results of the series of abovementioned studies, following improvements has been carried out.

(1) Requirement of rock bolt for roof supporting increased about 50% compare with before. However, requirement of steel frames for timbering decreased 25 ~ 35%. So, total cost of roof supporting works is reduced considerably.

(2) The adoption of smooth blasting method has contributed not only saving the cost of roof supporting but reducing the explosive comsumption, about 15 percent.

THE STABILIZATION OF THE FRACTURED ZONE BY THE FAULT IN THE SEIKAN TUNNEL CONSTRUCTION

Yutaka MOCHIDA, Seikan Tunnel Construction Bureau
Japan Railway Construction
Public Corporation.

In the Seikan Undersea Tunnel, there were 10 Faults had been clear by presurveys in the Straits, in Fig-1.

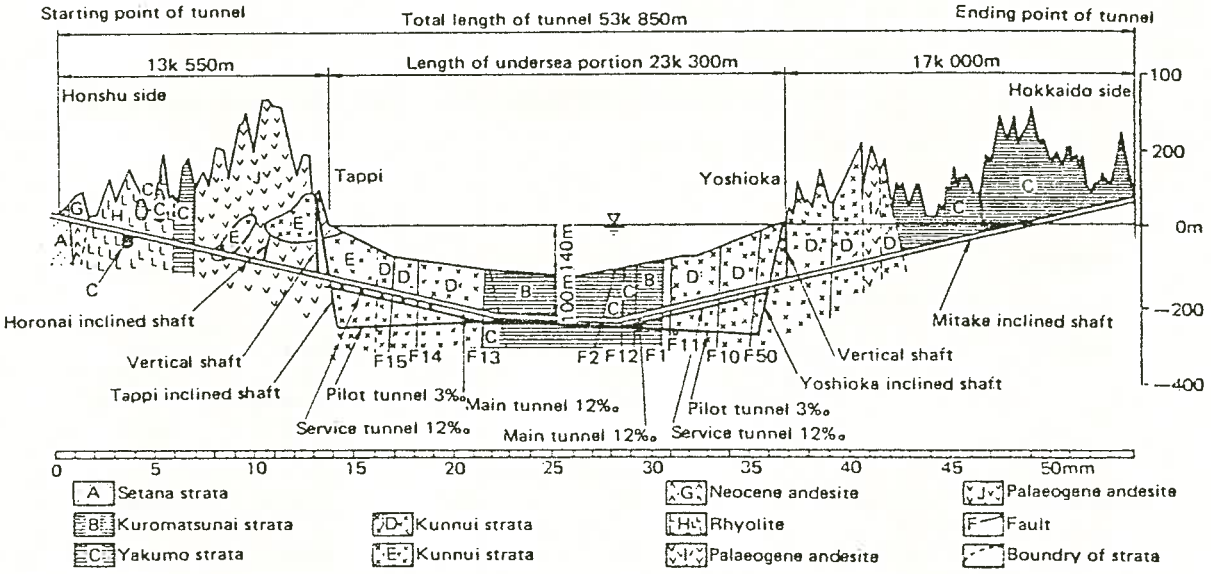

Fig. 1 Geological profile of Seikan tunnel

Now, the pilot tunnel and service tunnel have constructed through these all faults, the main tunnel finishes to excavate partly.

The faults have many kind of characters, the conditions of the faults is in general as follows.

1 In the vicinity of the faults, the ground is so weak and contains squeezing clay that earth pressure is large.
2 The rocks around the faults is so cracky and almost over-saturated by sea water.

To excavate the fractured zone by the faults, first, the grouting

is carried out around the tunnel as shown in Fig-2. The grouting zone is designed to be larger than the loosing zone resulted from excavation. Especially, in the fractured zone by the fault, the ground is so complicated that grouting zone is 4~6 times as large as excavated radius.

The grouting pressure is over 3 times as much as water pressure, the grouting holes are drilled at intervals of nearly 3 meters, quantity of grouting volume is very large compared with normal condition.

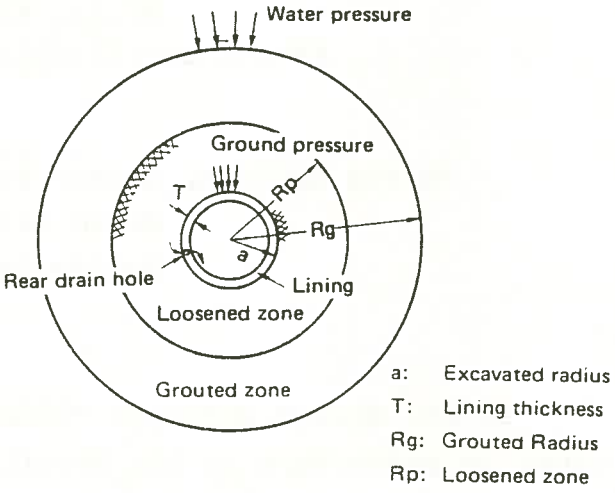

Fig. 2 Model diagram of grouting zone

Table-1 shows the grouting volume of the ground gushing water in Honshu, Hokkaido site.

Table 1 Summary of grouting records for no. 5 main tunnel in Yoshioka section and no. 4 main tunnel in Tappi section

Section	Tunnel	No. of grouting rounds	Required time, days	No. of grouting holes	No. of net grouting holes, m	Total amount of spring water, l/min
Yoshioka	No. 5 main tunnel	18	307	667	35 820.1	20 669.5
Tappi	No. 4 main tunnel	9	216	1097	66 082	87 192

Section	Volume of grout injected, m^3 LW No. 1 S 75%	Total LW	Total	Quantitative analysis Per round No. of grouting holes, hole/round	Time, day/round	Total length of grouting holes, m/round	Volume of grout injected, m^3/round
Yoshioka	6787.1	6787.1	6787.1	37.1	17.1	21.6	377.1
Tappi	6117.5	6117.5	6117.5	121.9	24.0	35.3	679.7

Total length of no. 4 main tunnel in Tappi section is 326.7 m and period of construction ranged from April, 1975, to end of July, 1978 (presently in progress).

Total length of no. 5 main tunnel in Yoshioka section is 388.1 m and period of construction ranged from June 1975, to end of July, 1978 (presently in progress).

Excavation method is short bench cut circular type or side drifts method, especially circular type with side medium drifts is adopted in bad ground in Fig-3. The shotcreting thickness 15~35^{cm} is carried out immediately after excavation and rock bolts. (the length 6^{m}, 1.0 ~1.8 bolts per m^2) The maximum earth pressure to the tunnel ever measured is about 300 t/m^2 near the faults.

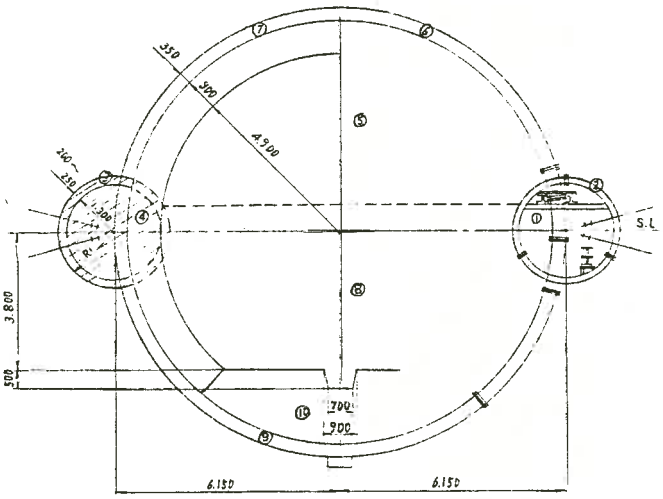

Fig. 3 Circular-type cross-section with side-drifts (upper half advancing after side-drifts concreted)

In the Seikan Tunnel, the stabilization of the fracutred zone caused by the faults is mainly obtained by the grouting, by means of enlarging the grouting zone water pressure is supported by the improved ground outside the tunnel.

ESTIMATE OF THE LOOSENED AND PLASTICALLY DEFORMED AREA AROUND THE OPENING

Kazuhiko IKEDA, Geological Measurements Co., Ltd.
and Takashi SAKURAI, RTRI, JNR.

Seismic survey is widely practiced as a method of geophysical surveys to determine the geological feature. The measuring results of seismic survey express the geological conditions as the distribution of seismic velocities.

To execute the same seismic test in tunnel is to discover the seismic velocities around the opening.

Loosened area around the opening appears to be lower velocity zone in contrast with the original rock-mass velocity.

There occurs loosened area around the opening even in the stiff rock mass excavation by blasting, release of the first stress stete, irregularity of the cutting plain, weathering and so on. Loosened depths measured by seismic tests are shown in Fig. 1 according to the width and height of the section. The horizontal axis in the figure is expressed by quasi-rockmass velocity, which is thought to be assessing some geological condition of the rock mass. Generally speaking, the seismic velocity of sound rock piece (V) indicates the hardness of the rock, on the other hand the rock-mass velocity (v) measured in tunnel indicates the condition of the rock mass. The authors defined the quasi-rockmass velocity to be the multiplied product of the fissuring coefficient v/V and the rock mass velocity v.

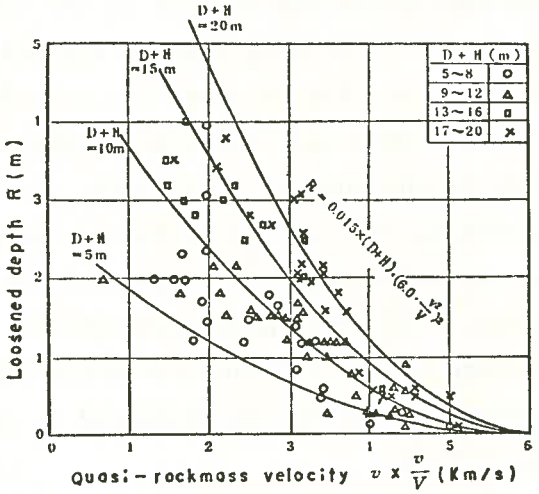

Fig. 1 Relation between loosened depth and seismic velocity

The loosened depth is experimentally expressed as following.

$$R = 0.05 \times (D + H)(6.0 - v \cdot v/V)^2 \quad \cdots\cdots\cdots (1)$$

where, R; loosened depth (m)

D; width of tunnel section (m)

H; height of tunnel section (m)

v, V; km/sec, dimensionless in

the express.

Ordinally seismic velocity of the most stiff rock mass scarecely overcomes more than 6.0 km/s and the fissuring coefficient is less than 1.0, so that the quasi-rockmass velocity does not reach to 6.0 km/s. The loosened depth depends on the magnitude of the quasi-rockmass velocity and the calculated value R by the expression (1) will show the standard of the loosened depth at the first step.

The loosened depths in circular openings excavated by R. T. M. (Rock Tunnelling Machine) are shown in Fig. 2. The measured data are not so match that the distinct difference depending on the section area is not found. The depth will be expressed as the expression (2), and it is about half value as compared to that by blasting method.

$$R = 0.06 \times (6.0 - v \cdot v/V)^2 \quad \cdots\cdots\cdots \quad (2)$$

During excavating such geological conditions as fault fractured zone, soft rocks or swelling rocks, the rock mass around the opening begins to squeeze to inward of the tunnel, and fairly large earth pressure acts on the support gradually. Fig.3 shows the plastically deformed and swelling depths measured by seismic tests. The recognition of plastic or swelling earth pressure depends on the occurence of deformation of support or bending of wooden lagging, magnitude of the pressure and existence of expansive clay minerals. Besides the residual or active orogenic force is existing, the loosened depth will be determined with the covering height (h), rock-mass strength and width of opening section as the expression (3).

$$R = \{0.3\ (D + H) + 3.0\} \times \sqrt{1.5 - x}$$

where, $x = v \cdot \frac{v}{V} \cdot \frac{1}{\log h}$

The rock mass around the opening starts to loose or deform plastically after excavation and it acts to the support to be earth pressure. The method and type of supporting must be applied according to the loosened area and the section size. Fig. 4 shows the relation of the loosened and plastically deformed depths to the support types used, distinguishing the section sizes and the presence of deformation or failure of the support. The each curved line ① to ④ according to the section size would show the maximum loosened depth beared by each support type.

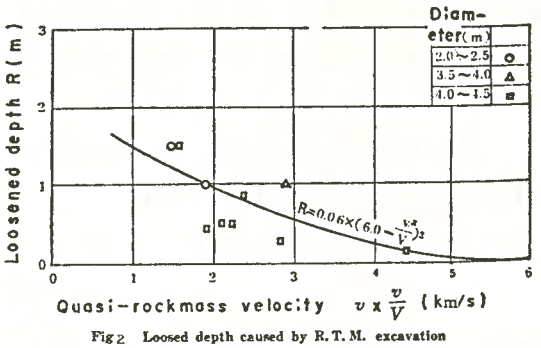

Fig 2 Loosed depth caused by R.T.M. excavation

The loosened depth discussing is measured by seismic test in tunnel and it is no more the width of the lower

velocity zone. On the other hand, the height of earth load proposed by Terzaghi and others is the calculated height of the dead weight above the tunnel crown. Therefore, some part in the loosened area is thought to act on support, and we must distinguish the loosened depth from the height of earth load. But the height calculated from the allowable stress of steel support used in SHINKANSEN section, for example, is nearly equal to the curved line ④. Namely the height of earth load is nearly equal to the maximum loosened depth. The reasons are thought as followings.

(1) the loosened depth is measured at side wall and it is smaller than that at crown

(2) some part of the actually loosened area may not be detected to be belonging to the lower velocity zone because of the lack of accuracy in seismic test.

Anyway, the estimated depth can be used as the height earth load at the stage of tunnel designing.

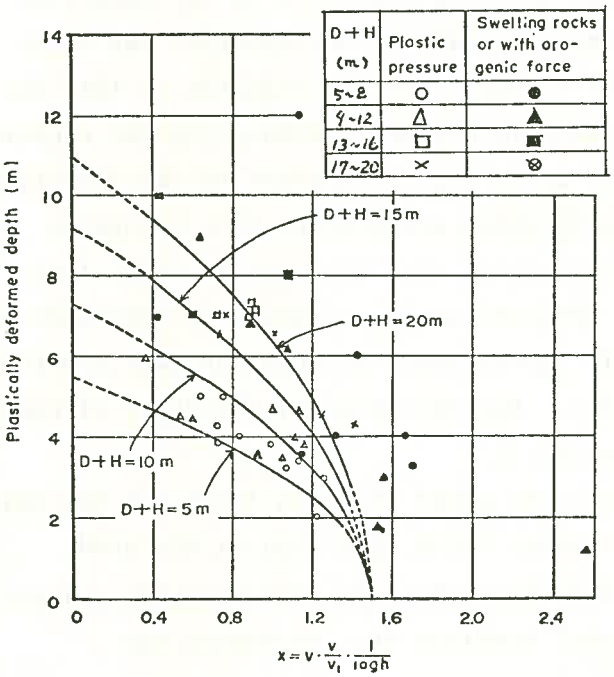

Fig. 3 Relation between plastically deformed depth and seismic velocity

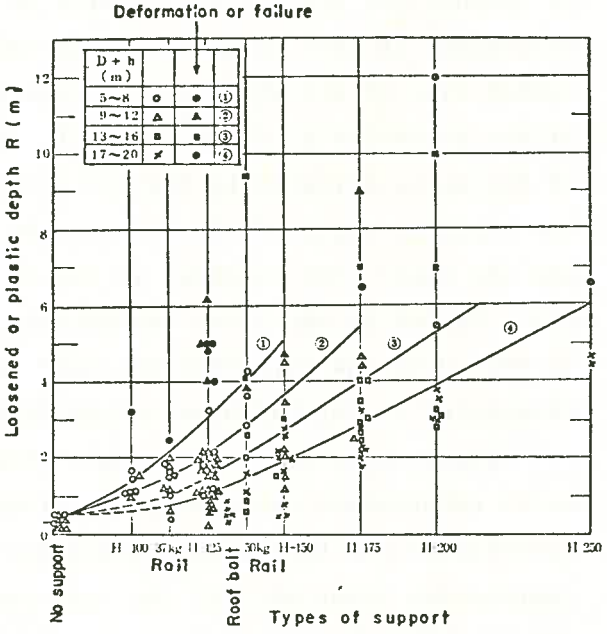

Fig. 4 Types of support according to loosened or plastic depth

STUDIES ON IN-SITU MEASUREMENTS FOR ESTIMATING STRENGTH OF ROCK MASS

Ryoji KOBAYASHI and Fumio SUGIMOTO
Faculty of Engineering, TOHOKU University

In this paper, it is described that the strength distribution of rock mass is obtained by shearing the rock between two parallel boreholes and that the crack distribution and the sonic velocity in rock mass are measured by a crack-detector.

For estimating the strength of rock mass, a borehole-type shear instrument as shown in Fig.1 has been designed. The procedures of the test using the shear instrument are as follows. The two parallel boreholes in the direction of up-and-down are closely drilled in the rock wall by the NX-bit. The shear instrument is then inserted in the lower borehole, and is adjusted so that the center line of the shear edge Ⓑ coincides with a line of connecting the centers of two boreholes as shown in Fig.1. The shear load is applied to the direction of the upper borehole by the two pistons Ⓓ which are pressed by a oil pump. The shear strength of the rock can be calculated from the applied shear load and the shear area as shown in Fig.2. From the shapes of the rock fragments as Fig.3 failed by the shear instrument, it is difficult to consider that the rock is failed in the direction of shear force. For this reason, the shear strength calculated is termed "shear strength index".

Fig.4 shows the relationship between the shear strength index and the uniaxial compressive strength for various rocks. From this figure, the good correlation can be recognized between the shear strength index and the uniaxial compressive strength, and the experimental equation that expresses the relationship is as follows;

$$Sc = 3.14\ Si \quad \text{------} \quad (1)$$

where Sc is the uniaxial compressive strength (kg/cm^2) and Si is the shear strength index (kg/cm^2).

In order to measure the sonic velocity and detect the cracks in rock mass, a crack-detector as shown in Fig.5 has been made in this study. The crack-detector is inserted into the NX-borehole and two probes of the crack-detector are pressed against the inner face of the borehole by the spring force. The sonic velocity of rock mass between the two probes is measured by an apparatus

for determining the ultrasonic wave velocity. Fig.6 shows the examples of the pulse wave patterr obtained on the model rock mass; that is, (A) shows the pulse wave pattern in the case of intact rock, (B) shows the pattern in the case of rock containing fine cracks, and (C) shows the pattern in the case of rock containing open cracks.

These in-situ tests were undertaken at 220 M.L. crosscut of Shakanai mine, AKITA prefecture. An example of in-situ measurement at Shakanai mine shows in Fig.7. In this figure, it is seen that the maximum value of sonic velocity is nearly equal to the velocity of rhyolite specimen which is collected from the rock mass, and that the shear strength index takes lower value in the rock containing cracks. The shear strength indexes are measured at 43 locations in the rock mass, and the probability in the cumulative distribution function of the shear strength index obtained from these tests is shown in Fig.8. It has been suggested by B.Košťák[1] that the probability of 11.5% in the cumulative distribution function of uniaxial compressive strength is equivalent to the pillar strength. If this suggestion is accepted, the shear strength index of rock mass is about 170kg/cm² as shown in Fig.8, and the compressive strength of rock mass is estimated to be about 530kg/cm² from equation (1).

Reference

1) B.Košťák ; Int. J. Rock Mech. Min. Sci. , Vol.8, pp.523-526.

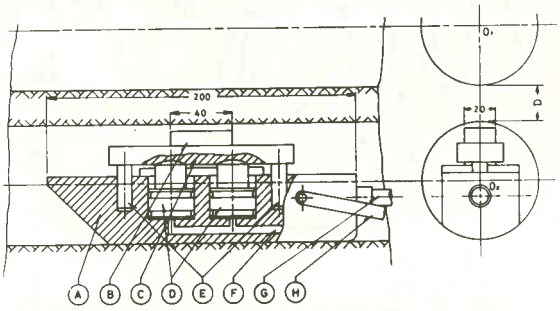

Fig.1-A Schematic diagram of borehole-type shear instrument.

Fig.1-B Photograph of borehole-type shear instrument.

Fig.3 Rock fragments failed by shear instrument.

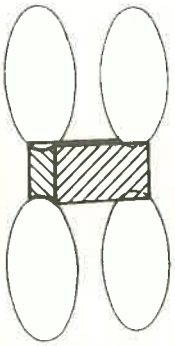

Fig.2 Shear area (oblique line)

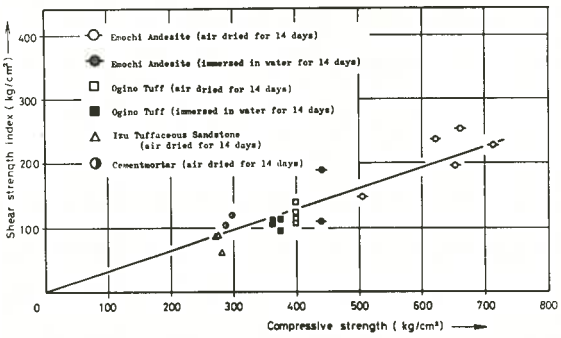

Fig.4 Relationship between shear strength index and uniaxial compressive strength for various rocks.

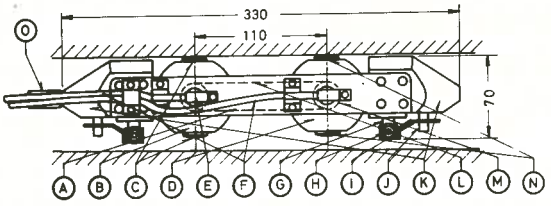

Fig.5-A Schematic diagram of crack-detector.

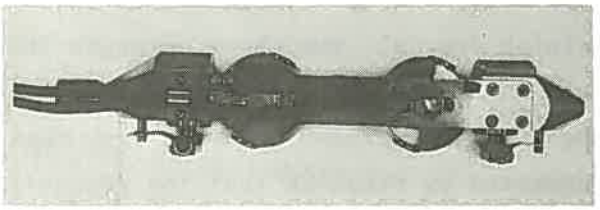

Fig.5-B Photograph of crack-detector.

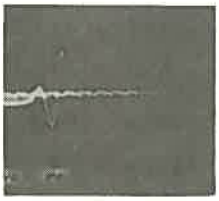

(A) Intact rock.

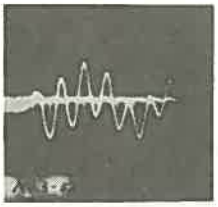

(B) Rock containing fine cracks.

(C) Rock containing open cracks.

Fig.6 Examples of pulse wave pattern in measurement using crack-detector.

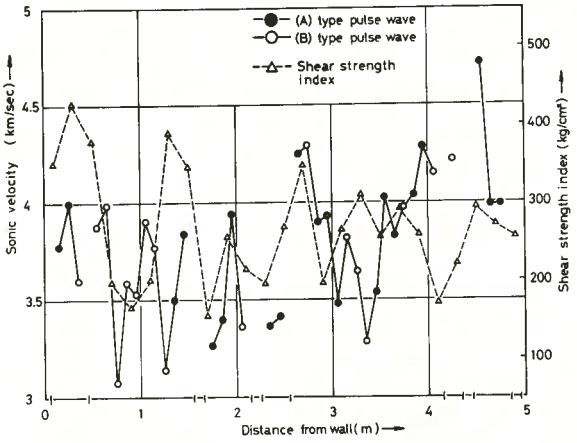

Fig.7 Example of in-situ measurement at Shakanai mine.

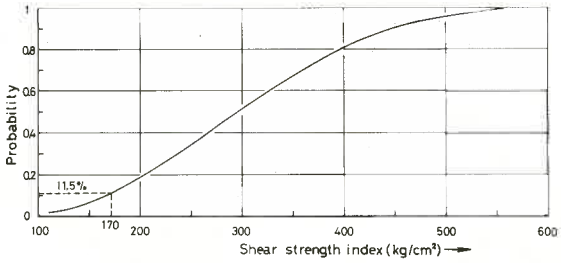

Fig.8 Probability in the cumulative distribution function of shear strength index at Shakanai mine.

COMPARISON OF BOREHOLE JACK AND PLATE BEARING TESTS

— Semi-hard or hard rocks —

Electric Power Development Co., Ltd. Eishin MITSUMUNE
Kawasaki Geological Engineering Co., Ltd. Makoto SATO
Kawasaki Geological Engineering Co., Ltd. Junichi MIYAGAWA

1. Introduction

It is one of the prime concerns to determine the optimum modulus of the rock mass for the design of structures in or on rocks. Several methods have been developed for this purpose. Among these, the method of plate bearing test is generally utilized for measuring the elastic properties of rock in-situ accurately. But this test is expensive to perform and difficult to do in water or at the places with some depth. These limitations have enhanced the increasing adoption of the borehole testing methods. In order to assess the applicability of the borehole jack test, both the borehole and plate bearing tests were conducted at a test gallery, and their comparisons are presented in this paper.

2. Site Conditions

The location is where the dam and the underground power house are planned to be constructed. The rocks at this site consists of the sandstone shale formation presumed to be the Mesozoic era and the diorite intruded into it, and they are unconformably covered by green tuff in the Tertiary. Here, only the sandstone shale formation silicified by the intrusion of the diorite is examined.

Values of P-wave velocity and uncofined compressive strengh are obtained from field and laboratory tests: for in-situ rock $Vpf=3.0 \sim 4.0$km/sec, for core specimens $Vpl=3.7 \sim 4.9$km/sec, $qu=350 \sim 500$kg/cm^2 .

3. Borehole Jack (High Pressure Type KKT)

The outline of borehole jack used in this investigation is given in Fig.1 and its geometry is summarized in Table 1. The applied pressure and diametral displacement are measured by the pressure

Table 1. Geometry of High Pressure Type KKT

body		loading plate		piston	max. contact pressure
o.d. (mm)	length (mm)	width (mm)	length (mm)	total travel (mm)	(kg/cm^2)
65	500	30	250	16	330

o.d. : outside diameter

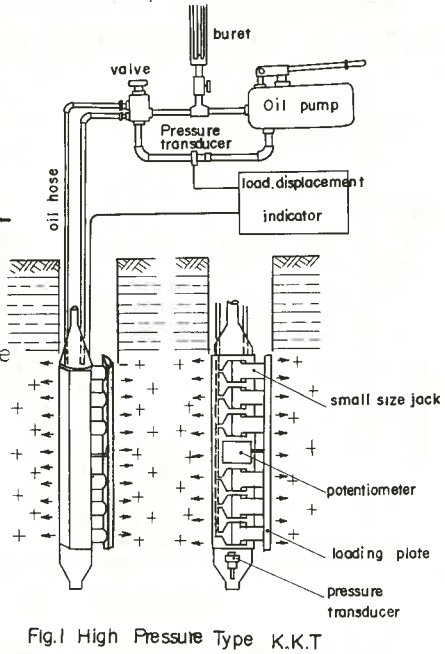

Fig.1 High Pressure Type K.K.T

transducer directly connected to the loading plate. Furthermore, the displacement can be measured by leading oil backward from the jack to the buret.

The typical curves of pressure vs. displacement for the borehole jack tests using repeated loading are shown in Fig.2. From this figure, the deformation modulus is obtained by the Goodman's equation as follows.

$$D_{I,II} = \Delta p / \Delta r \cdot d/2 \cdot \varphi(\nu, \beta) \qquad (1)$$

where Δr is half of the average diametral displacement for a given increment of pressure Δp and d is the borehole diameter. Values of $\varphi(\nu,\beta)$ are constants depending on the Poisson's ratio and the loading curvature.

4. Comparison of the Borehole Jack with the Plate Bearing Test

4-1. Differences in both the loading mechanisms

Before comparing the results of both tests, it is necessary to make clear the difference in loading mechanisms between the two tests. One of the major differences between the two is that in case of the plate bearing test, compressive stresses only act on the rocks, but in the borehole jack test high tensil stresses are found to be occured around the borehole wall. Goodman has investigated the influence of tensil stress about the Goodman-Jack similar to the KKT, and from his analytical results, it is concluded that even if corrections on tensil stresses were done, the maximum corrections of deformation modulus will never exceed 15%. Therefore, the results of the borehole jack tests were used without corrections for the difference in loading mechanisms.

4-2. Dependency of the deformation modulus on load

Generally, in case of the rock deformability, it is recognized; 1) a large residual displacement will be occured by repeated loading, 2) Dependency of rock deformability on load is predominated in the low stress level.

These facts are also recognized in the results measured by the KKT as shown in Fig.2. The deformation modulus for each increment of the pressure are

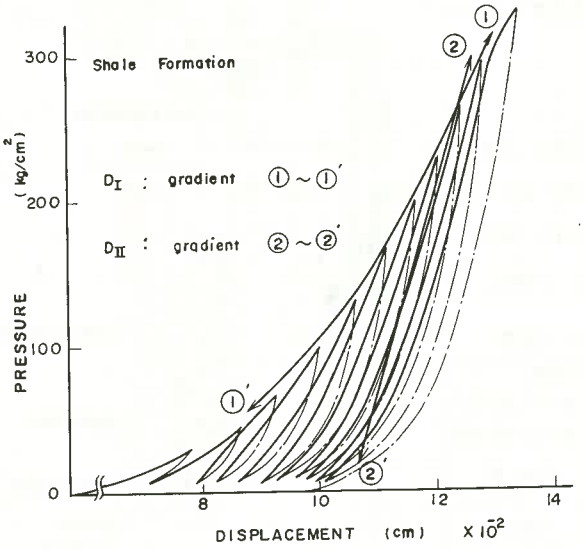

Fig.2 Pressure Displacement Curves With K.K.T

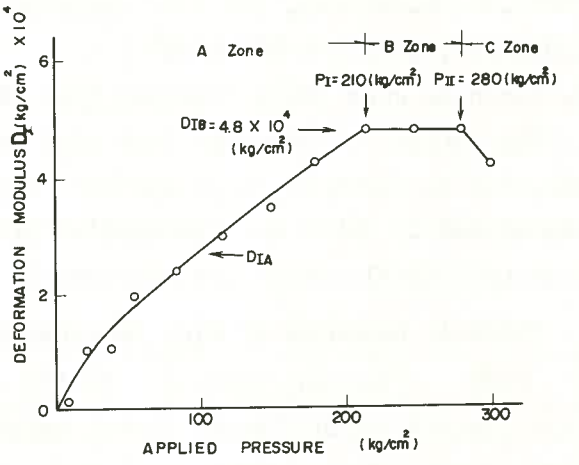

Fig.3 Dependency of Deformation Modulus D_I on load

plotted for the load (mean) in Fig.3. It is found that the modulus increases with increase in load to a certain stress level, but it reaches a constant value after it, as long as the rocks are not yielded. This tendency is common to all the results of the KKT for rock masses. In addition, the modulus results for the both tests were compared at the same stress level.

4-3. Influence of plate-rocks contact

When the roughness of the borehole wall is anticipated through the returned samples or visual observations (borehole camera, borehole television, etc.), it is necessary to examine the loading plate-borehole wall contact, before loading test will be carried out. The degree of contact between the two is confirmed using the pressure discrimination sheet.

4-4. Comparison between the two test data

The correlation between the two test data is shown in Fig.4. From this, it is obvious that the values of Dp/Dk vary with load. As the load increases, the value of Dp/Dk decreases and approaches a certain value. It is presumed that the value of Dp/Dk < 1 is attributed to the size effect, the difference in size of the loading area (the plate bearing A=700cm^2, the KKT A=75cm^2).

Then, as to 40kg/cm^2 considered to be the design load of general civil works, the results of Fig.4 are replotted as shown in Fig.5. The direct relation of Dp and Dk shows an equation as : Dp(40)=0.8 Dk(40) (2)

For reference, in case of 60kg/cm^2,

Dp(60)=0.5 Dk(60) (3)

In addition, the design data for the penstock and power house are to be obtained by the borehole jack tests and the related equation (2),(3).

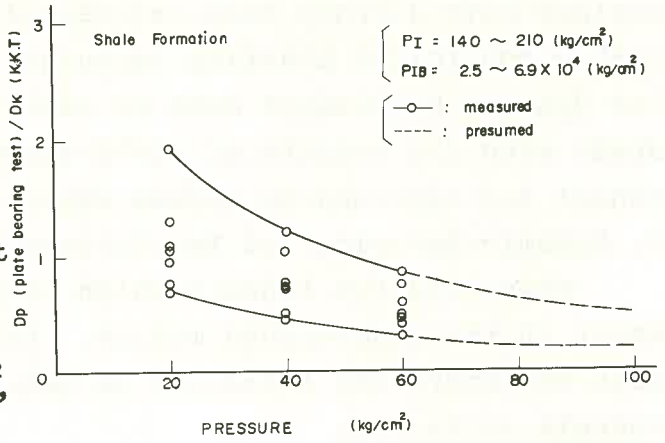

Fig. 4 Dependency of D_p/D_k on load

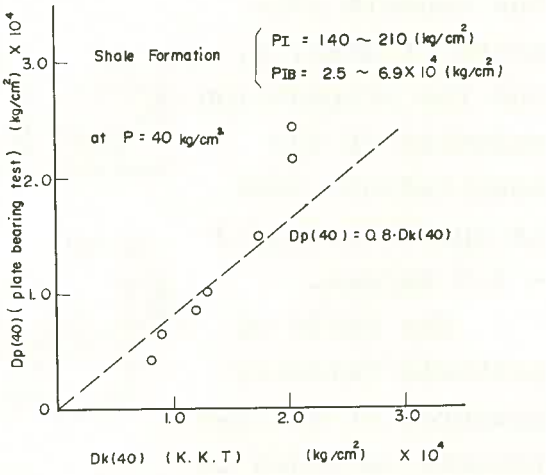

Fig. 5 Comparison of K.K.T and plate bearing test data. at P=40 kg/cm²

REFERENCES

1) R.E.Goodman, T.K.Van, andF.E.Heuze: "MEASUREMENT OF ROCK DEFORMABILITY IN BOREHOLES", Symposium on Rock Mechanics May 1968.

2) K.Miki, J.Miyagawa,: "ROCK DEFORMABILITY TEST BY BOREHOLE JACKS", Proceedings of The 11th Symposium on Rock Mechanics in Japan.

VIBRATIONAL CHARACTERISTICS OF TUNNEL AND SURROUNDING MEDIUM DUE TO ADJACENT BLASTING

Shunsuke SAKURAI, Kobe University
Yasutoshi KITAMURA, Kobe University

1. Introduction

When the construction works are conducted by blasting techniques, attention must be paid to blasting works, in order to avoid any serious damages on the adjacent structures. The dynamic response of underground structures like tunnels subjected to blasting excitation has not yet been fully understood, while the dynamic behaviours of the house-like structures constructed on the ground surface have already been extensively studied. In order to establish a controlled blasting technique to cause no damages on tunnel, its dynamic behaviours must be clearly understood. This paper deals with the results of field measurement on the vibrations of tunnel and surrounding medium caused by blasting operations.

2. Dynamic Behaviour of Two Unlined Tunnels[1)]

There are two tunnels which three-dimensionally cross each other in the underground medium. Both are under construction so that no liners are installed as yet. The clearance between the two tunnels is 29.7 m. The medium around the tunnels consists of granite, and the propagation velocity of the longitudinal wave is approximately 3 - 3.7 km/sec.

The ratio of particle velocity measured at the two tunnels is shown in Fig.1. The blasting operation is done at the face of Tunnel B. It can be seen that

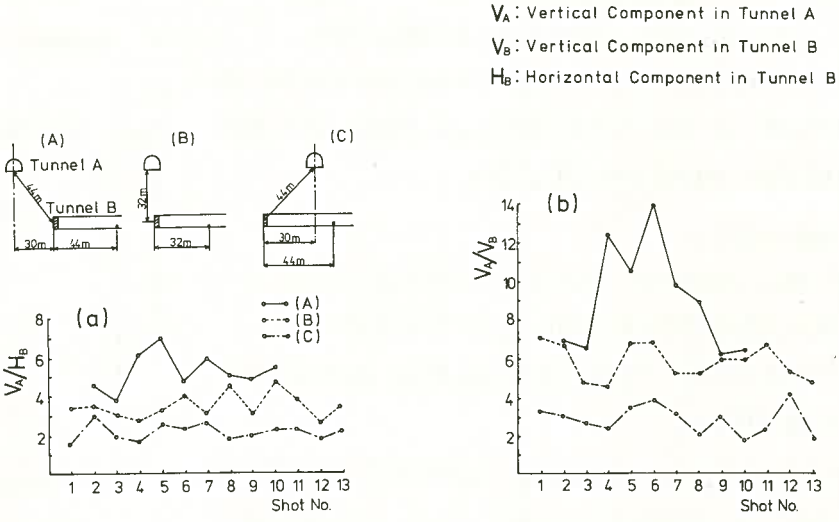

Fig.1 Ratio of particle velocities

the greater magnitudes of particle velocity appear at Tunnel A as the face of Tunnel B approaches the crossing point, compared with those obtained as the face leaves beyond the crossing. This means that the dynamic disturbances generated by blasting are mainly propagated in the direction of tunnel face progression rather than in the backward direction.

We assume the following relationship being valid among particle velocity v (cm/sec), charge weight W (gr) and distance r (m)

$$v = CW^{2/3} r^{-2.7}$$

where C is a coefficient depending on the method of blasting, nature of rock and type of charge. The value C back-calculated by using the measured particle velocities is plotted as a function of the angle between the tunnel axis and the direction to the measuring points, as shown in Fig.2. It is clearly understood that much energy is transmitted in the direction of tunnel face progression.

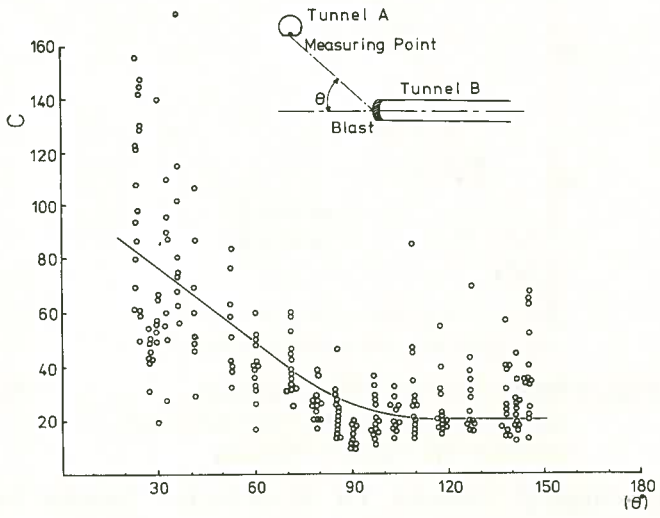

Fig.2 Orientation of energy propagation from blast zone

3. Relationship between Particle Velocity and Strain on Tunnel Lining[1)]

Experimental works have been conducted at two different sites where the concrete lined tunnels are located. Rocks around the tunnels are granite at Site-1 and liparite at Site-2. The propagation velocities of the longitudinal wave at Site-1 and -2 are in the range of 2 - 3 km/sec and 2.5 - 4 km/sec, respectively. The blasting operation is done at the distance of 10 - 100 m from the concrete lining.

The maximum values of particle velocity and strain at the internal surface of concrete lining are plotted in Fig.3, even though they occur at the different positions. It is interesting to know that there is a linear relationship between them. From this result the particle velocity for failure of the lining could be given on an assumption of tensile stress for failure of concrete.

4. Relationship between Vibrations of Tunnel and Ground Surface[2)]

Experimental works are conducted at a quarry under which a wa-

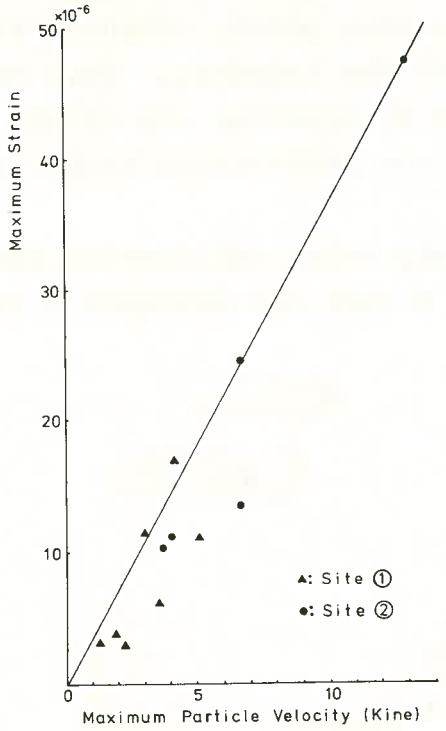

Fig.3 Relation between maximum particle velocity and maximum strain on tunnel lining

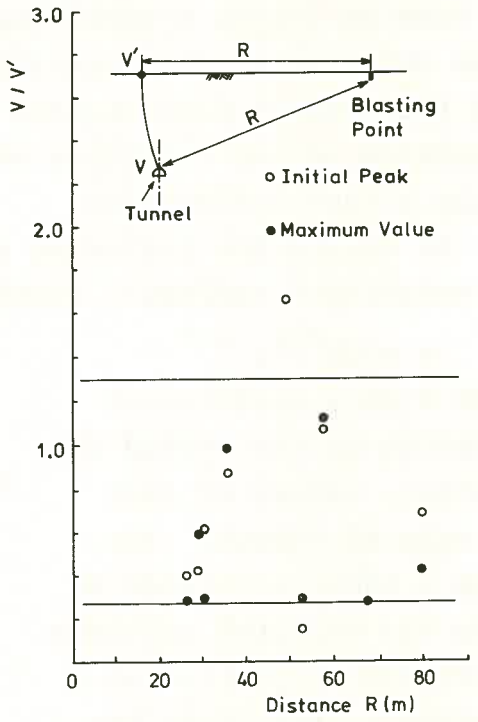

Fig.4 Ratio of maximum particle velocity of tunnel lining against one of ground surface

ter supply tunnel is located. There is no soil layer covering the ground surface. The medium consists of weathered granite and its propagation velocity of longitudinal wave is approximately 1.7 km/sec. The vibrations due to surface blastings are measured at both the tunnel and the ground surface. The results are shown in Fig.4. It is seen that the tunnel vibration is generally smaller than the vibration of ground surface.

5. Conclusions

In this study, all the results are discussed in terms of particle velocity, because that the failure of structure depends on the particle velocities in the range of the frequency of vibration caused by blasting. The results shown here must be very worthy in order to make a controlled blasting to avoid any serious damages on the adjacent structures like tunnel.

References

1. S. Sakurai and Y. Kitamura ; "Vibration of Tunnel due to Adjacent Blasting Operation", Proc. Int. Sympo. Field Measurements in Rock Mechanics, Zürich, 1977, pp.61 - 74.

2. S. Sakurai, Y. Kitamura and K. Yoshida ; "Vibrational Characteristics of Tunnel Lining and Surrounding Medium due to Adjacent Blasting (in Japanese)", Proc. 5th Japan National Symposium on Rock Mechanics, 1977, pp.169 - 173.

ELECTRICAL MEASUREMENT OF THE GROUTED ZONE IN THE GROUTING WORK

Eizaburo YOSHIZUMI, Tsuyoshi SUGANO
and Akira SAITO, Kyoto University

1. Introduction

In the grouting work,the evaluation of the grouted effects is generally concerned with next three matters:

(a) grouted zone and condition,
(b) mechanical characteristics,
(c) permeability.

The resistivity measuring test is used for the evaluation of (a) and supplies only complimentary materials to the evaluation of (b) and (c). However, when the mutual relations between (a)and (b) and also between (a) and (c) are previously given by the core test and so on, the data obtained by the resistivity measuring test are useful for the evaluation of (b) and (c). Further, the resistivity measuring test, which can measure and analyze a solid zone, makes it possible to evaluate the grouted effects three-dimensionally.

In this report, the authors suggest that the grouted effects can be successfully evaluated with the defined and proposed factor by the authors, which is named "Resistivity impregnation rate", obtained by the apparent resistivities before and after grouting by using the resistivity measuring test.

2. Resistivity measuring test

Fig.1 illustrates the planned zone to grout(g),the planned zone to measure (m),grouting bore hole(G) and measuring bore hole(M). In general, the investigation of the grouting mechanism is made under the assumption of axially symmetric condition. In the case of axially unsymmetric condition,the investigation has not almost been done by the reason

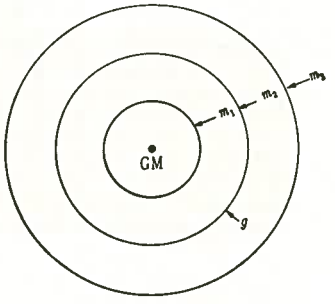

Fig.1 The planned zones and bore holes.

of measuring techniques.

The axially unsymmetric condition in Fig.1 can be measured and analyzed by using the electrode configurations where potential electrodes are arranged radially on the surface as shown in Figs.2(a) and (b) with "Sensitivity distribution" which is defined by the authors. Fig.3 shows, for example, the sensitivity distribution of CC(Bore hole) PP(Surface) solid electrode configuration.

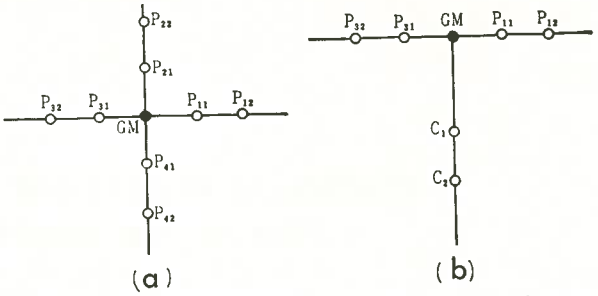

Fig.2 Electrode configurations and bore holes.
(a) Plan. (b) Cross-section.

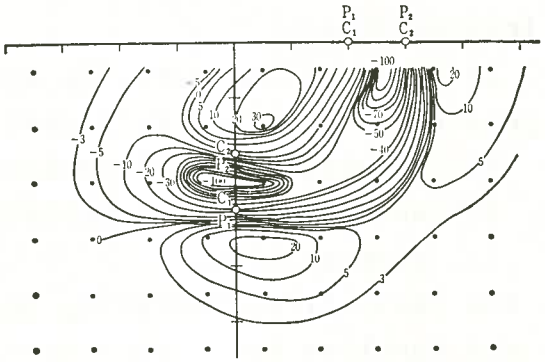

Fig.3 Sensitivity distribution of CC(Bore hole)PP(Surface) solid electrode configuration.

Here, "Resistivity impregnation rate", α_{res} ,is defined for arbitrary electrode configuration as

$$\alpha_{res} = \frac{\rho_{aw} - \rho_{ag}}{\rho_{ag}} \Big/ \frac{\rho_w - \rho_g}{\rho_g} ,$$

where ρ_{aw} and ρ_{ag} are the apparent resistivities before and after grouting, ρ_w and ρ_g are the resistivities of ground water and grout respectively.

In this report, the authors intend to explain the measured results of the grouting work in the sewerage works of the Magome Line in Tokyo by using this "Resistivity impregnation rate".

3. Grouting work in sewerage works of Magome Line in Tokyo

This work is made in order to improve the soft ground in which shield pipes are laid. Figs.4(a) and (b) illustrate the plan and

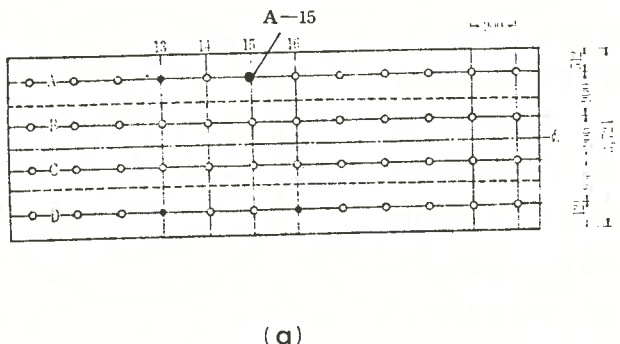

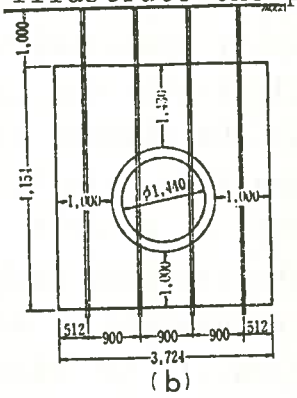

Fig.4 Plan and cross-section of grouting and measuring bore holes.
(a) Plan. (b) Cross-section.

the cross-section of the grouting bore holes and the measuring bore holes respectively. Here,the results of A-15 bore hole are explained.

Fig.5(a) shows the resistivity distribution before grouting,in which low resistivity zones L1 and L2 lie from measuring point 10 to 12 and high resistivity zones H1 and H2 from 4 to 8. Fig.5(b) shows the resistivity distribution after grouting,in which the resistivity decreased almost all over the zone. Fig.6 shows the

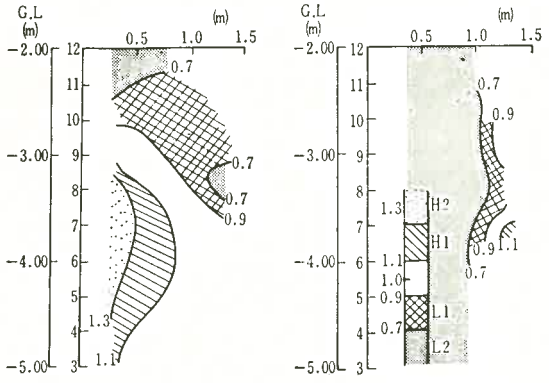

Fig.5 Resistivity distributions.
(a) Before grouting.
(b) After grouting.

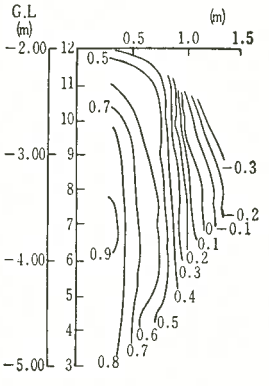

Fig.6 Resistivity impregnation rate stratigraphy.

resistivity impregnation rate stratigraphy obtained by Figs.5(a) and (b). In Fig.6,the rate of zone with the radius 66 cm. where is planned to grout is higher than 0.6, and then this suggests that the grouting work is done efficiently.

The authors wish to express thanks to the members of the chair of geophysical prospecting,Kyoto Univ. and Raito Kogyo Co.,Ltd..

References

E.Yoshizumi, T.Sugano and A.Saito; "Electrical measurement of the grouted zone in the grouting work", Journal of the Japanese Soceity of Soil Mechanics and Foundation Engineering,24,No.1, p.43-50(1976)

E.Yoshizumi and T.Sugano; "Sensitivity distribution of electrode configuration", Geophysical Exploration, Soceity of Exploration Geophysicists of Japan,25,No.1,p.27-33(1972)

ON THE MEASUREMENT OF THE GROUND WATER VELOCITY BY A SEISMOGRAPH

Kyoji SASSA, Kyoto University
Aritsune TAKEI, Kyoto University

1. Purpose

The purpose of this research is to develop the method to estimate the ground water velocity in one existing borehole, and thereby to detect the location of the ground water flow which exists in the state of vein due to beddings, faults and joints in a rocky slope. Almost existing boreholes are protected by Vinylchloride pipes in Japan. Some of the protective pipes have small holes such as four holes of ϕ =5 mm at every 20 cm, however, the ground water which flows into the borehole from their small holes has no steady direction, its flow is not uniform there and its velocity is too weak to measure. Therefore, it is nearly impossible to estimate the ground water velocity from the behavior of the water in the borehole. The method presented here is to hear the "sound" of the water flowing outside the borehole by a seismic detector, accordingly the movement of the water inside the borehole is not necessitated.

2. The apparatus and the method

The used apparatus consists of a seismic amplifier with a calibrator, a waterproofed seismic detector and a portable oscillograph. The characteristics of them are the followings. The seismic amplifier (OYO Corp. Japan): Magnification 80dB, Frequency 3-300 Hz, the attached calibrator oscillates the calibrating current of 0.01, 0.1, 1.0, 10 mV of 40 Hz (sine wave). The seimic detector(Geo Space Corp. USA): Type HS-J, 28 Hz, 215 ohms, the size of the detector (a basic unit was compactly waterproofed by us) is ϕ =25 mm, ℓ =30 mm. The method of measuring is illustrated in Fig.1, and its procedure is 1) Lower the detector into a borehole and keep it at a measured depth 2) Output of the detector is recorded in the oscillograph after the control of the attenuator and the gain 3) The comparable calibrating current is recorded at the same attenuation and gain by switching from the detector to the calibrator 4) The value of the output of the detector is

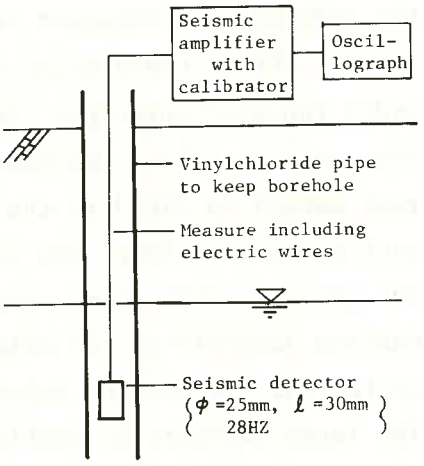

Fig.1 Measurement of the ground water velocity by a seismograph

estimated in comparison with the calibration.

3. The experimental study

We have done a experimental study to examine whether the output of a seismic detector in a protective pipe for borehole has an unique relation with the velocity of the ground water flowing outside the pipe or not. Fig.2 illustrates the equipment of the experiments. The ground water velocity in the channel was measured from the velocity of the dropped dyes between two points along the channel by a stopwatch. The results are shown in the lower line in Fig.3, it indicated that the output of the detector has an unique relation written in Fig.3 with the ground water velocity regardless of the grain size of the gravels. The range of this test was limited by the presence of noise and the capacity of water supply. The detected maximum seismic energy should be generated from the nearest collision, usually with the protective pipe. Therefore, when we set the pipe and the detector in open channels, we must obtain the similar relation in the wider range of velocity. The upper line (the water velocity was measured by a current meter) in Fig.3 is the results in open channels, both lines are parallel each other. However, the velocity in the open channels is about double that in the gravels at the same seismic output. It is due to the difference between the maximum velocity in the neighborhood of the pipe which was detected by the detector and the average velocity along the channel which was measured by dyes. The later velocity is smaller than the former velocity because of the meandering path of flow and the velocity - fluctuation along the path. Since the ground water velocity is conventionally defined as the average velocity between two points on the straight line, the lower line in Fig.3 is of practical usefull-

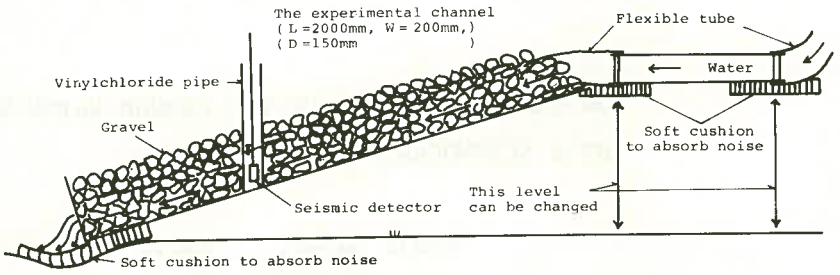

Fig.2 The equipment of the experiments

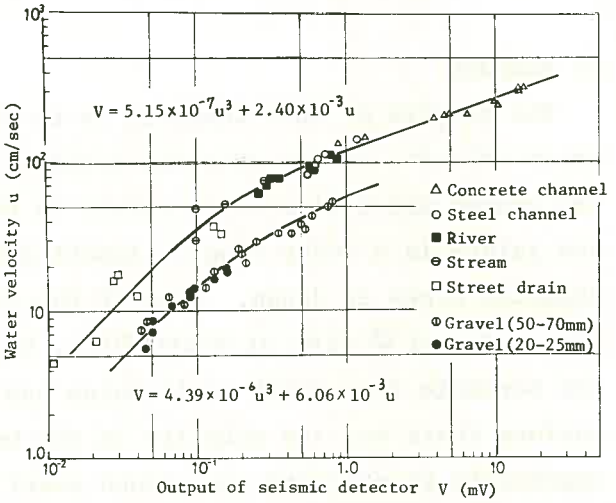

Fig.3 The results of the experiments

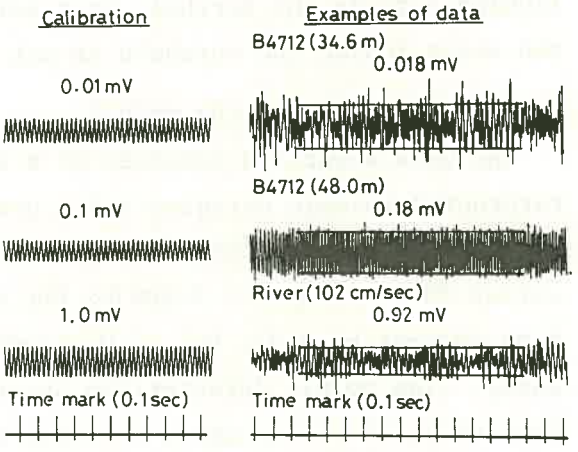

Fig.4 Examples of the measured data

ness. Therefore, we can say that the relation between the ground water velocity and the output of the detector varies between two lines in Fig.3 according to the degree of the meandering of flow and the fluctuation of velocity. Fig.4 is the samples of data. The shape of the waves depends on the state of flows, B4712(48.0m) is an example of the less disturbed flow, the other two are the case of the usual flows. The maximum output is decided to be the maximum value continuing constantly, the infrequent peak values are omitted because they may be noise or infrequent turbulent flows. The difference of the values of the output estimated by plural persons is within 20%. This value is of no practical problem in consideration with the measured data of Tig.5 & 6.

4. The application of it in the Kamenose landslide

In the Toge district of the Kamenose landslide of Osaka Prefecture, we applied this method to detect the path of the ground water flow. Fig.5 is the examples of the data and Fig.6 is the result plotted on the map. We can find the presence of the fast water flow like a stream and a clear path of the ground water flow in the marked arrow. The direction of this path agrees with one of two groups of the sheared zones formed by tectonic movements in this area, the water flow from B4659 to B 4656 was confirmed by the input of salt to B4659 and its detection at B4656 by the automatic record of the electric conductivity. In B4816, B4817 the ground water flows out of the protective pipe due to the artesian state. In B 4659 (after the covering water of 18-20m disappeared) and in B4622 we could hear the sound like a stream through their boreholes. On the other hand we could hear no sound in B4712 & B4656 where their ground water flows were confined. All of these facts endorses the result of Fig.6.

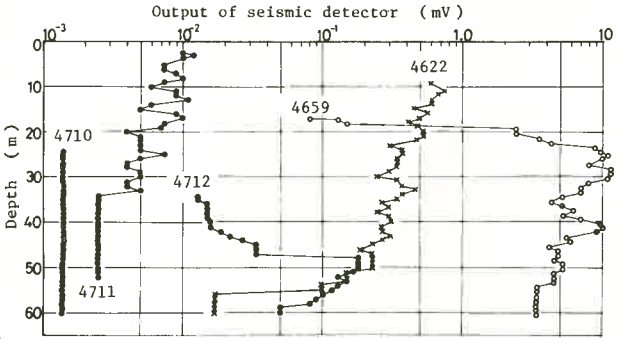

Fig.5 Examples of the measured data in the Kamenose landslide

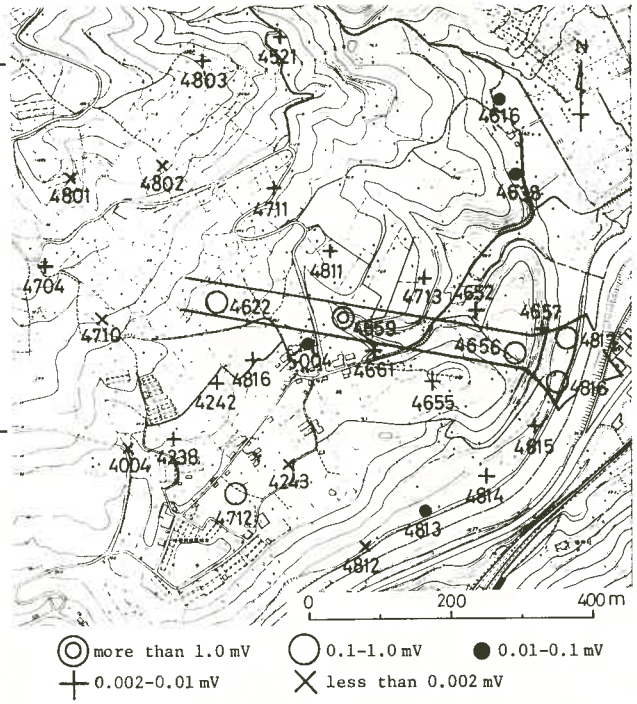

Fig.6 The results of the messurements in the Kamenose landslide

Finally we acknowledge a former postgraduate student Mr. D. Sakata for his helps, and also thank an assistant professor of Kyoto University Dr. S. Kobashi for his support.

PROPOSALS ON THE DECISION OF ROCK GRADES INTENDED FOR EVALUATING THE BEARING RESISTANCES OF DAM FOUNDATION ROCKS

Kokichi KIKUCHI, Kazuo SAITO and Kenichiro KUSUNOKI,
Central Research Institute of Electric Power Industry

1. Introduction

In this report, classification methods intended for the practical setting of rock grades are considered and collected data are summarized.

It mainly contains the arrangement of geologic factors as parameters of rock classification, consideration as to quantitative classification, and consideration on the correlation between the physical constants of rocks used for designing civil engineering structures, and geologic factors.

2. Selection and arrangement of qualitative classification factors

The authors considered it necessary to make classification factors as objective as possible, to eliminate individual differences involved in the decision of rock grades, and selected and discussed the geologic factors as classification factors, arranging them as shown in Table 1.

3. Correlation between rock grades and physical constants

3.1 Relations with static moduli of elasticity and moduli of deformation

Figures 1 and 2 show relations between rock grades on one hand and static moduli of elasticity and moduli of deformation on the other hand. They show remarkable correlativity existing between both.

3.2 Relation with cohesions

Figure 3 shows the measured values obtained from individual specimens of massive rocks, arranged in reference to shearing load and vertical load. It indicates that there is remarkable correlation between rock grades and the results of the shear test.

4. Consideration on quantitative classification

In an effort to have an objective decision method of rock grades, the authors tried to grasp rock grades quantitatively by measuring rock properties, using a Schmidt rock hammer and a simple elastic wave velocity measuring instrument. The results of the measurements shown in Figs. 4 and 5 indicate that the measurements of rebound based on Schmidt rock hammer and of velocity of elastic waves are effective for quantitative evaluation of bedrocks.

5. Conclusion

The authors do not think that bedrocks can be perfectly classified according to the above standard, since a bearing resistance of rock comprises various factors in complicated combinations. However, the authors are confident that they could realize, to some extent, the establishment of correlation with physical constants, which civil engineers earnestly desire.

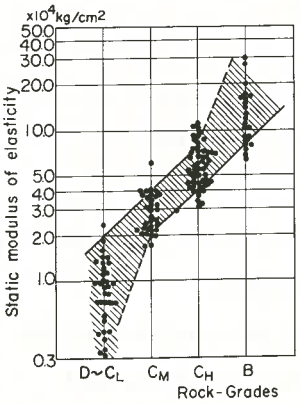

Fig.1 Relation between modulus of elasticity and Rock-Grades

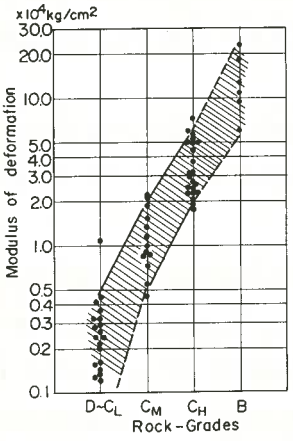

Fig.2 Relation between Modulus of deformation and Rock-Grades

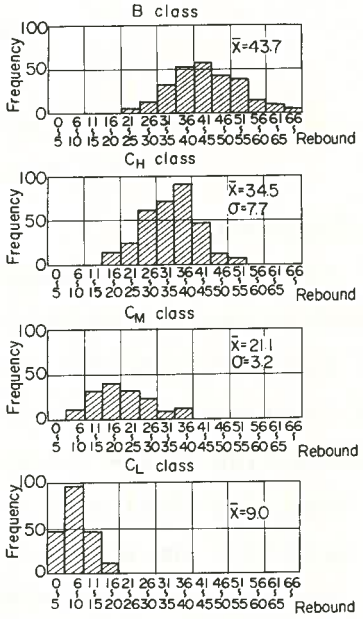

Fig.4 Relation between Rebound of Schmidt Rock Hammer and Rock-Grades

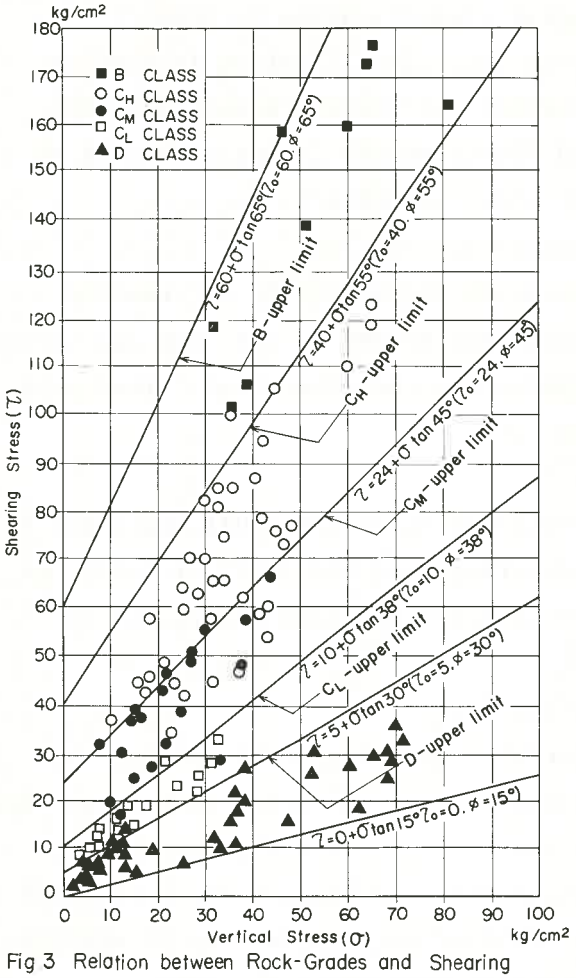

Fig 3 Relation between Rock-Grades and Shearing Strength

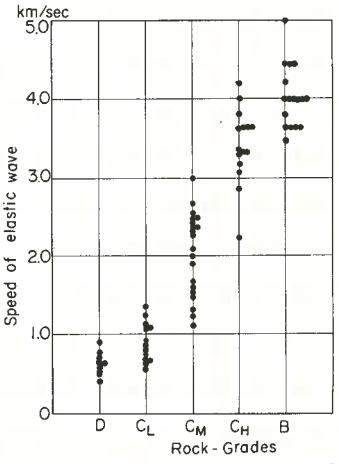

Fig.5 Relation between speed of elastic wave and Rock-Grades

Table 1 STANDARD OF ROCK GRADES (MASSIVE ROCKS)

Rock grade		Hard rocks	Medium hard rocks	Soft rocks	Static modulus of elasticity of rocks (kg/cm^2)	Modulus of deformation of rocks (kg/cm^2)	Cohesion of rocks (kg/cm^2)	Velocity of elastic wave of rocks (km/sec)	Rebound of Schmidt rock hammer *)
		As an approximate criterion, rocks of more than "800 to 1,000kg/cm²" in the unconfined compression strength of test pieces of fresh rocks are hard rocks. When hit by a rock hammer, they produce a metallic sound.	As an approximate criterion, rocks of "200 to 300kg/cm²" to "800 to 1,000kg/cm²" in the dry unconfined compression test of test pieces of rocks are medium hard rocks. When hit by a rock hammer, they produce a very tight sound, but generally do not produce a metallic sound. Of the rocks in this range, those rather soft may be depressed slightly on the surface, when hit by the spire of rock hammer.	As an approximate criterion, rocks of less than "200 to 300kg/cm²" in the dry unconfined compression test of test pieces of fresh rocks are soft rocks. When hit by a rock hammer, they produce a thick and loose sound, and may collapse. They are easily depressed on the surface, when hit by the spire of rock hammer.					
A		Very fresh in lighologic character. The rock-forming minerals of igneous rocks and the constituent grains of sedimentary rocks are not weathered and altered at all. Few joints are distributed. The rocks as a whole are very solid and densely hard.			80,000 or more	50,000 or more	40 or more	3.7 or more	36 or more
B		Fresh in lighologic character. The rock-forming minerals of igneous rocks and the constituent grains of sedimentary rocks are little weathered and altered. Joints are sparesely distributed, assuring close adhesion. The rocks as a whole are solid and densely hard.	Fresh in lighologic character. The constituent grains are quite free from secondary weathering and alteration. Fissures of joints, etc are little distributed. The rocks as a whole are solid and hard. In this case, those close to soft rocks which have the above properties may not belong to this class, but to C(u).						
C	CH	Almost fresh, solid and hard in lithologic character. Among the rock-forming minerals of igneous rocks, feldspars and colored minerals such as mica and amphibole may be slightly weathered and altered, and in sedimentary rocks, feldspars and colored minerals existing secondarily as constituent grains may be slightly weathered and altered. Joints are distributed considerably and joint walls are mostly weathered and altered, being discolored. Sometimes, weathered materials adhere thinly to joint walls. However, in general, the joints assure close adhesion. The rocks a whole are solid and hard.	Fresh in lighologic character. The constituent grains are free from secondary weathering and alteration. Joints are sparsely distributed, assuring close adhesion. The rocks as a whole are almost solid and hard. In this case, those close to hard rocks may belong to Class B.	Rocks of this class are close to medium hard rocks (about 150kg/cm² in the dry unconfined compression strength of fresh rocks). Fresh in lighologic character. Constituent grains are quite free from weathering and alteration, and joints are little distributed.	80,000 ∫ 40,000	50,000 ∫ 20,000	40 ∫ 20	3.7 ∫ 3	36 ∫ 27
	CM	Generally a little weathered and altered in lithologic character. In igneous rocks, feldspars and colored minerals excluding quartz are weathered, often being brown or reddish brown. In sedimentary rocks, feldspars and colored minerals existing secondarily as constituent grains are weathered and altered, often being brown or reddish brown as in case of igneous rocks. Joints are open and often hold clay or weathered materials. Rocks of this class often have many fine hair-like fissures. Therefore, when hit strongly by a rock hammer, they often collapse, being separated at the hair-like fissures. In addition, rocks which are fresh in lithologic character but have open joints distributed considerably to indicate cracky state are also included in this class.	Feldspars and colored minerals existing secondarily as constituent grains are mostly a little weathered and altered. The weathering is not so intensive, but since the rocks are medium hard, they give a little soft impression in absolute hardness. Joints are distributed considerably, and most of them are a little open. The joints are weathered and altered, being discolored, and often hold thin layers and weathered materials. Rocks of this class have hair-like fissures to some extent. Therefor, when hit by a rock hammer, they often collapse, being separated at the hair-like fissures.	Fresh in lighologic character. Constituent grains are free from secondary weathering and alteration Joints are little or sparsely distributed, assuring close adhesion. The rocks as a whole are little weathered, but since they are soft, they give soft impression in absolute hardness. In this case, those less than about "60 to 70kg/cm² in the dry unconfined compression strength do not belong to this class, but to C(1).	40,000 ∫ 15,000	20,000 ∫ 5,000	20 ∫ 10	3 ∫ 1.5	27 ∫ 15
	CL	Since the rock-forming minerals of igneous rocks or the constituent grains of sedimentary rocks are considerably weathered, the rocks as a whole are generally brown or reddish brown. Joints are open, and hold clay and weathered materials considerably. In rocks of this class, fine hair-like fissures are distributed remarkably, and weathering occurs along the fissures. Therefore, even if hit lightly by a rock hammer, they easily collapse or are depressed. In addition, rocks which are fresh in litholigic character but have open joints considerably distributed to indicate mansonry state are also included in this calss.	Constituent grains are weathered and altered, and the degree of consolidation is very low. Since the rocks are medium hard, they give considerably soft impression in absolute hardness. Joints are considerably distributed. The are open, and hold weathered materials and clay layer considerably. Rocks of this class are considerably weathered along hair-like fissures, and when hit lightly by a rock hammer, they collapse easily.	Constituent grains are a little weathered and altered, and the degree of consolidation is very low. The rocks as a whole give very soft impression in absolute hardness. When the rocks are hit by the spire of rock hammer, the spire often sticks in them.	15,000 or less	5,000 or less	10 or less	1.5 or less	15 or less
	D	The rock-forming minerals of igneous rocks or the constituent grains of sedimentary rocks are considerably weathered, and sandy and clayey portions are often seen. With rocks of this class, the distribution of joints is rather unclear.	Constituent grains are considerably weathered and altered, and the degree of consolidation is considerably low. They are often sandy and clayey. With rocks of this class, the distribution of fissures is rather unclear.	The degree of consolidation of constituent grains is very low, and most are sandy or clayey.					
Conformable rocks		(1) Igneous rocks such as plutonic rock, hypabyssal rock and volcanic rock (2) Sedimentary rocks such as sandstone, conglomerate, chert, schalstein, and pyroclastic rocks of the era before Mesozoic. However, slate and shale are excluded in principle. (3) Relatively massive gneiss, out of metamorphic rocks. However, crystalline schist is excluded. In addition, some of sedimentary rocks and pyroclastic rocks of Neogene period are hard rocks.	Most of sedimentary rocks (Mudstone, siltstone, sandstone and conglomerate) and pyroclastic rocks (tuff, tuff breccia, volcanic breccia, and welded tuff) of Tertiary before Miocene of Neogene. Some of pyroclastic rocks of Quaternary are medium hard rocks.	Most of sedimentary rocks (modstone, siltstone, sandstone and conglomerate) and pyroclastic rocks (tuff, tuff breaccia and volcanic breccia) of the era after Plicocene of Neogene. Some of pyroclastic rocks of Quaternary are soft rocks.					

*) Caution; These values of schmidt rock hammer shall not apply to the soft rocks comprising cohesive soil materials.

GEOLOGICAL STUDY ON COAL AND GAS OUTBURSTS IN HOKKAIDO COAL FIELD

Masuyuki UJIHIRA, Hokkaido University
Kiyoshi HASHIMOTO, Tohokugakuin University

1.Coal and gas outbursts occurrence in Hokkaido coal field

Hokkaido is one of the major coal producing districts in Japan as well as Kyushu. Fig.1 shows the places of six coal fields and a general picture of the occurrence of coal and gas outbursts in Hokkaido. From around 1927 through 1970, 540 times of outbursts had occurred in Hokkaido and nearly all of them had broken out in Ishikari coal field. Moreover, it will be noted that incidences of outbursts in Ishikari coal field are extremely concentrated in Sorachi coal field. Geologically, Ishikari coal field could be divided into two districts by Ponbetsu techtonic line. And northern half of it is named Sorachi coal field, while the other southern half of it is called Yubari coal field. In Sorachi coal field, 498 times of coal and gas outbursts had been recorded, but in Yubari coal field only 26 times of outbursts had occurred.

In the present paper, we would make a study on the geological causes why the outbursts are frequent in Sorachi coal field and why infrequent in Yubari coal field.

2.Geological views of Ishikari coal field

Fig.2 shows the general view of sediment before the time of intensive action of techtonic stress from eastern direction. Tab.1 gives the rate of sandstone in the sediment in Ishikari basin. The rate of sandstone in Sorachi basin is 30-60 % and that in Yubari basin is no more than 4-11 %. Standing on lithologic point of view, the sedimentary rocks in Sorachi coal field have higher strength than that of in Yubari coal field. Furthermore, regarding the terms of diagenesis, the time interval from the completion of sedimentation of Ishikari series to the time of intensive organic movement was $(31\pm2)\times10^6$ years and the interval from completion of sedimentation of Poronai series to that time was $(19\pm2)\times10^6$ years.Considering comparatively the diagenesis intervals of both sediments, rocks in Sorachi coal field have been harder than that of in Yubari coal

field at the very time of organic movement. It may be pointed out that the difference of hardness of both coal fields should have generated the structural difference.

Fig.3 shows the profiles of three districts in Ishikari coal field. As shown in these cross sections, northern part of Sorachi coal field where the outbursts occurred frequently has very complicated structure with many faults of various scale, while Yubari coal field where the outbursts were infrequent has generally overfolded structure.

3.Investigation of the fault in Ishikari coal field

Tab.2 gives the times of appearrance of faults per 100m drifting along coal seam. Both in Akabira and Sunagawa collieries where the outbursts have occurred frequently, the times of appearrance of faults is 3.3 and 3.48 respectively, however the times in 5 collieries in Yubari coal field is from 0.32 to 1.39.

Tab.3 gives the scale distribution of faults' throws of three collieries, Akabira, Horonai and Minamioyubari. In Akabira, not only there exist a lot of faults in high density, but also many faults that have large throw could be observed. In Horonai and Minamioyubari collieries, both values of the times of appearrance of faults and the rate of large throw faults are not so large as those in Akabira, and the fault whose throw is greater than 7 m couldn't be observed at all in investigated areas.

4.Complicated geological structure and gas outbursts

Fig.4 shows the drift driving state with inducer shot in Utashinai colliery having the most conspicuous geological disturbance in Sorachi coal field. The causes why the outbursts take place frequently in these districts may be estimated as follows.

(1).In a certain extent going along with various fault planes, fragile and weak coal which is abundant of cracks containing high pressure gas exists almost in every case. (2).In the area in which the coal seams have been divided into many irregular blocks by faults, it may be difficult to degas sufficiently on account of jamming of drilling rod and failure of borehole. (3). When the drift passes through large scale fault whose throw is larger than a height or width of heading, driving conditions may be very similar to those of cross cut reaches to coal seams, then the danger of outbursts may be increased. (4). Even though drift working is made along coal seam, many times, it is inevitable to drive through the foot or floor rocks. So practically, it may be impossible to adopt

other driving methods with much more slight impact except blasting. (5).In the drift driving through the rock by blasting, there may be many cases that the shock wave of strong blasting against rock propagates to fragile and weak coal site ahead of shot hole rears, and outbursts are apt to be induced.

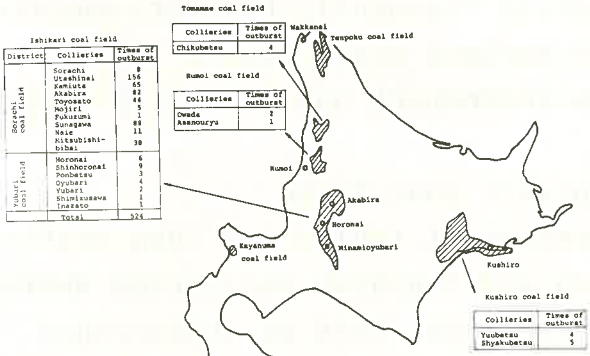

Fig.1 Coal and gas outbursts occurrence in Hokkaido coal field

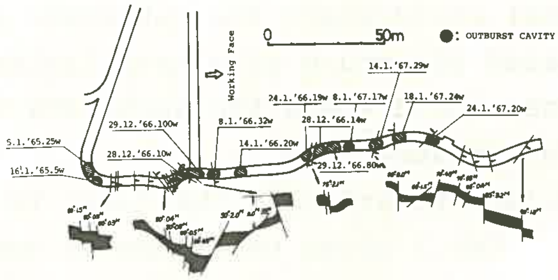

Fig.4 Example of drift driving in Utashinai colliery

Tab. 1 The rate of sand stone in the sediment in Ishikari basin

Sorachi coal field:

Series or formation \ Colliery	Ashibetsu [illegible]	Ashibetsu NO.1 shaft	Mojiri	Akabira	Sorachi	Toyosato	Utashinai	Mitsui-[illegible]	Mitsui-[illegible]	Sumitomo-[illegible]	Mitsubishi-[illegible]	Mitsui-bibai
Poronai series												
Ashibetsu formation	36	33								(190) 48		
Hiragishi formation	(327) 23	27	(121) 31						(251) 50	(267) 48	85	(54) 54
Ikushunbetsu formation	25	(391) 22	59						48	14	(142) 50	64
Akabira formation	37	34	(518) 19	30		34			63	50	(88) 44	(65) 44
Bibai formation	59	38	(167) 12	11	71	47	30	39	45	(162) 48	39	(85) 24
Wakanabe formation	(86) 50	(173) 41	(137) 37	(170) 42	(169) 52	16	24	21	57	54	85	(51) 62
Yubari formation	(162) 36	31	23	76	73	34		(191) 48	(441) 12	4[illegible]	44	65
Horokabetsu formation	13	16	5	(101) 23	(68) 0		37	35	(94) 48		67	
Noborikawa formation	(188) 39	57	39	53	59		56	46	53		50	
Total (thickness of sand stone) / (thickness of formations)	[illegible] / 329[illegible] m	913 / [illegible]	588 / [illegible]	535 / 1290	620 / 1033	318 / [illegible]	416 / [illegible]	542 / [illegible]	1001 / [illegible]	667 / [illegible]	798 / [illegible]	238 / 454
Total rate of sand stone	30	32	31	41	60	32	41	40	48	45	53	52

Yubari coal field:

Series or formation \ Colliery	Ponbetsu	Shinhoro	Horonai	Higashi-horonai	Manji	Yubari NO.1 shaft	Yubari NO.2 shaft	Heiwa	Shimizusawa
Poronai series	0	0	0	0	0	(150) 0	(150) 0	(150) 0	0
Ashibetsu formation									
Hiragishi formation									
Ikushunbetsu formation	49	49	32	37	(54) 31	(9) 88	(29) 100	(91) 48	(69) 74
Akabira formation									
Bibai formation									
Wakanabe formation					(112) 52	(149) 64	(126) 32	(174) 32	30
Yubari formation					(75) 16	(56) 28	(96) 28	(172) 37	50
Horokabetsu formation					(73) 0	(65) 0	(13) 0	(73) 0	
Noborikawa formation					(72) 65	(63) 46	(56) 52	(27) 56	
Total (thickness of sand stone) / (thickness of formations)	133 / 1371	103 / 1310	74 / 1330	51 / 1237	134 / 1486	150 / 1492	127 / 1570	177 / 1687	177 / 1548
Total rate of sand stone	10	8	6	4	9	10	8	10	11

Legend: Sedimentation itself had not been carried out; The sediment had been erosed; Data could not be supplied

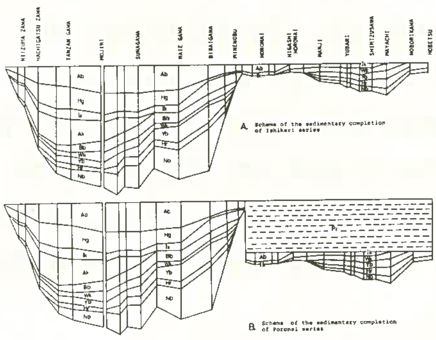

Fig.2 General view of sediments before the intensive organic movement in Ishikari coal field

Tab. 2 The times of appearrance of faults per 100 m drifting along coal seam in various collieries in Ishikari coal field

Sea level \ Colliery	Akabira	Sunagawa	Horonai	Yubari-shinniko	Shimizu-sawa	Minami-oyubari	Mayachi
+250 - +200 m	-	-	-	1.13	-	-	-
+200 - +100	-	-	-	0.84	-	-	-
+100 - 0	-	-	-	-	0.70	-	-
0 - -100	-	3.01	-	-	0.59	0.91	-
-100 - -200	-	3.47	-	-	0.86	1.50	0.60
-200 - -300	-	3.25	-	-	0.69	1.75	-
-300 - -400	4.85	3.72	-	-	0.99	-	-
-400 - -500	3.34	4.63	-	-	0.40	0.80	-
-500 - -600	3.81	-	0.43	-	-	-	-
-600 - -700	0.98	-	0.27	-	-	-	-
-700 - -800	-	-	0.36	-	-	-	-
-800 - -900	-	-	0.24	-	-	-	-
average	3.30	3.48	0.32	1.06	0.77	1.39	0.60
Total length of investigated road way	10.9km	45.5km	34.7km	6.9km	16.5km	15.4km	4.0km

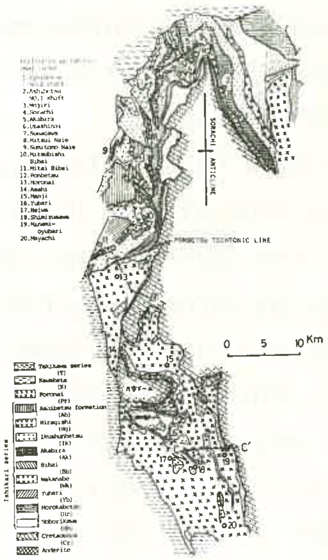

Fig.3 Geological map of Ishikari coal field

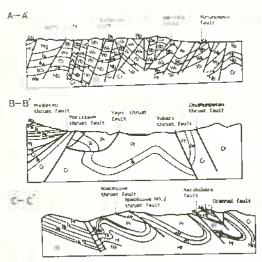

Cross sections of three districts

Tab.3 Scale distribution of fault's throw of three collieries

Colliery \ throw of fault (m)	0- 1	1- 2	2- 3	3- 4	4- 5	5- 6	6- 7	7- 8	8- 9	9-10	10-20	20-30	30-40	40-50	50-60	60-70	Total
Akabira	22.5	26.2	17.6	7.1	5.4	1.4	2.0	1.0	1.7	1.4	4.8	1.4	2.0	1.7	2.4	1.4	100 %
Horonai	53.6	22.7	10.0	9.2	0.9	0	3.6	0	0	0	0	0	0	0	0	0	100
Minamioyubari	50.5	29.8	13.3	2.8	1.8	1.8	0	0	0	0	0	0	0	0	0	0	100

Ⅲ LIST OF LITERATURE

Listed reports are picked up from nineteen journals, the names of which are printed on the preceding paper. The period for picking up the reports from these journals are limited from the beginning of 1970 to the end of 1978.

Symbols (A), (B), (C), (D), (E), (F), (G), (H) which can be seen at the end of each report, correspond to the items employed in Chapter II.

Ⅲ LIST OF LITERATURE

1. Soil Mechanics and Foundation Engineering (Journal of the Japanese Society of Soil Mechanics and Foundation Engineering)
   1) Yoshimasa KOBAYASHI: Rock Burst, Vol. 22, No. 2 (1974) p. 17-18 (B)
   2) Takeshi MITANI: Properties of Soft Rock and Construction in Soft Rock, Vol. 22, No. 6 (1974) p. 3-6 (A, H)
   3) Ryunoshin YOSHINAKA: Strength and Deformability of Soft Rock, Vol. 22, No. 6 (1974) p. 7-12 (A, C)
   4) Yasumasa FUKUMOTO, Toru YAMANOI: Disaster in Soft Rock Region --- Sliding ---, Vol. 22, No. 6 (1974) p. 21-27 (C)
   5) Masanori WATANABE, Seisuke MISAWA, Nobuyuki HASHIGUCHI: Excavation of Soft Rock by Machine --- Second Arikabe Tunnel ---, Vol. 22, No. 6 (1974) p. 29-35 (D)
   6) Takao TANEMURA, Tadahiro SHIROMOTO, Hirohisa ISOGAI: Mudstone used for Dam Construction Material --- Yamamura Dam, Mie Prefecture ---, Vol. 22, No. 6 (1974) p. 37-44 (A, H)
   7) Ryoichi SAKAMOTO, Hiroshi INUZUKA: Site Investigation for Hirato Ohashi Bridge, Vol. 22, No. 6 (1974) p. 41-51 (F)
   8) Keiji KOJIMA: Exploration Method of Soft Rock and Its Problems, Vol. 22, No. 6 (1974) p. 53-58 (F)
   9) Ikuo TOHNO, Tetsu NAKAYAMA: High Pressure Consolidation Test of Soft Rock, Vol. 22, No. 6 (1974) p. 59-65 (A)
   10) Hisato SHONO, Kiyoshi SASAKI, Shigenori FUJIWARA: Mechanical Properties of Undisterbed Sample of Weathered Granite, Vol. 23, No. 2 (1975) p. 19-24 (A, F)
   11) Noboru OKADA, Eiji OHYAMA: Field Measurement at Yamamura Dam and Its Application to Stability Analysis, Vol. 23, No. 3 (1975) p. 17-24 (F)
   12) Taizo FUKUDA: Investigation and Recording of Bored Cores of Rock Mass, Vol. 23, No. 4 (1975) p. 78-80 (F)
   13) Tsunemasa SIKI: Deposits and Sedimentary Rocks, Vol. 23, No. 7 (1975) p. 5-6 (F, H)
   14) Hayashi SUGAHARA: Creep Phenomenon of Soft Rock, Vol. 23, No. 12 (1975) p. 61-62 (A, F)
   15) Shunzo OKAMOTO: Rock Exploration and Designing, Vol. 24, No. 1 (1976) p. 3-6 (F, H)
   16) Ryunoshin YOSHINAKA, Toru ONODERA: Surface Roughness and Shear Strength of Rock Joint, Vol. 24, No. 1 (1976) p. 7-12 (C, F)
   17) Satoshi HIBINO, Mutsumi MOTOJIMA, Masao HAYASHI, Koichi GOTO: Behavior of Anisotropic Rock Masses during Excavation of Underground Cavity, Vol. 24, No. 1 (1976) p. 13-19 (C, H)
   18) Shosei SERATA, Toshihisa ADACHI, Yoshinori IWASAKI: Creep Deformation of Rock Mass in Underground Opening, Vol. 24, No. 1 (1976) p. 21-26 (C)
   19) Kazuya OHSHIMA: Creep Deformation of Loose Sandstone at Hirato Ohashi Bridge, Vol. 24, No. 1 (1976) p. 27-33 (C)

20) Toshiaki TAKEUCHI, Tateo SUZUKI, Soichi TANAKA: Borehole Loading Test for Rock Mass Deformability, Vol. 24, No. 1 (1976) p. 35-41 (C, F)
21) Eizaburo YOSHIZUMI, Tsuyoshi SUGANO, Akira SAITO: Electric Method to Determine Grouting Range of Rock Mass, Vol. 24, No. 1 (1976) p. 43-50 (E, F)
22) Chuichi FUJIWARA: Determination of Water Bearing Layer by Rock Exploration Boring, Vol. 24, No. 1 (1976) p. 51-57 (F, G)
23) Nobuhiro HAYASHI, Hiroto OCHI, Koji ISHIKAWA: Determination of Mechanical Properties of Rock Mass (Weathered Granite) by using Bore Hole Measurements, Vol. 24, No. 3 (1976) p. 7-14 (C, F)
24) Toshio OCHIAI: Application of RI Method to Rock Exploration, Vol. 24, No. 3 (1976) p. 41-48 (F, G)
25) Takeo YAMASHITA, Chuichi FUJIWARA: Application of Geophysical Methods to Rock Exploration, Vol. 24, No. 9 (1976) p. 51-58 (F, G)
26) Yasuo SHIRATORI: Rock Crushing by Electromagnetic Waves, Vol. 24, No. 10 (1976) p. 21-22 (D)
27) Hiroshi MORI: Rock PS Anchor, Vol. 24, No. 10 (1976) p. 72-73 (H)
28) Nobuo MIZUMOTO, Kenji MIYAHARA: Cutting and Embankment in Weathered Granite Region, Vol. 24, No. 12 (1976) p. 9-16 (H)
29) Masahiro ABE: Metamorphism and Alteration, Vol. 24, No. 12 (1976) p. 96 (H)
30) Shigeki NAGATOMO: Tunnel and Fault Zone, Vol. 25, No. 2 (1977) p. 1-6 (H)
31) Seiya IMANISHI: Properties of Faults and Fractured Zones, Vol. 25, No. 2 (1977) p. 7-11 (C, H)
32) Yutaka MOCHIDA: Stabilization of Fault Zone in Seikan Tunnel, Vol. 25, No. 2 (1977) p. 13-20 (C, H)
33) Ichiro HIRASAWA, Ichiro IMAMURA: Excavation of Non-cemented Water Bearing Layer in Haruna and Yamanaka Tunnels, Vol. 25, No. 2 (1977) p. 21-27 (D, G)
34) Shinichi TATEISHI, Hirobumi HATANAKA: Stabilization of Fractured Zone in Road Tunnel at Chubu District, Vol. 25, No. 2 (1977) p. 35-40 (C, H)
35) Mitsuo SHINTANI: Tunneling at Fault and Fractured Zone in Shin-Kobe Tunnel, Vol. 25, No. 2 (1977) p. 41-46 (H)
36) Hideo TAKAHASHI, Hajime WATANABE: Stabilization of Fractured Zone in Iwaya Dam, Vol. 25, No. 2 (1977) p. 47-55 (C, H)
37) Yoshihiko NISHIGAKI: Sliding of Fractured Zone in Osaka Formation, Vol. 25, No. 2 (1977) p. 57-62 (C, H)
38) Tatsuro TERAMOTO, Minoru KAWAMURA, Hiroshi AOTO, Kuniyasu RYOKE: Construction of Earth Tunnel adacent to Old Tunnel, Vol. 25, No. 2 (1977) p. 63-70 (H)

2. Journal of the Japan Society of Civil Engineers
1) Sadao ADACHI, Makoto HOSHINO, Norikura SAITO, Kazuo KOBAYASHI, Yoshio ISHIYAMA: Tunnel Construction in Expansive Ground, Vol. 59, Extra Number (1974) p. 37-47 (E, H)
2) Yasutaka TERADO: New Positioning of Grouting and Problems Involved in It, Vol. 59, No. 9 (1974) p. 57-59 (E)
3) Toshiro SHINOHARA: Judgement as to the Effect of Grouting on Bedrocks around High Pressure Tunnel, Vol. 59, No. 12 (1974) p. 26-32 (E)
4) Fujio MACHIDA: Investigation of Tunnel and the Effect of Tunnel Excavation onto Ground Surface, Vol. 60, Extra Number (1975) p. 43-53 (E, H)

3. Proceedings of the Japan Society of Civil Engineers
   1) Koichi AKAI, Hideo OTSUKI: Model Studies on the Stress Distribution and the Bearing Capacity of Soil Ground, No.223 (Mar. 1974) (B, C)
   2) Masayuki HORI: An Approximate Method for Analysing Earthquake Motions of an Inhomogeneous Elastic Layer, No.232 (Dec. 1974) p.71-85 (B, C)
   3) Takuo YAMAGAMI, Eiichi ODA: A Method of Analyzing Non-Darcy Flow Problems by Finite Elements, No.234 (Feb. 1975) (G)
   4) Akie ASADA, Fusayoshi KAWAKAMI: Consideration on the Characteristics of Seismics Motion in the Grounds, No.236 (Mar. 1975) (B, C)
   5) Yozo FUJINO, Motohiko HAKUNO: Characteristics of Elasto-Plastic Vibration of the Ground Due to Earthquakes, No.240 (Aug. 1975) p.1-9 (B, C)
   6) Kenichi MATSUOKA, Sumio NOMACHI: Stress Analysis of Multi-Layered Elastic Systems Subjected to Asymmetric Surface Shear, No.241 (Sep. 1975) p.1-12 (B, C)
   7) Jun YOKOTA: Studies on the Behavior of the Rock Foundation under Kurobe Dam, No.241 (Sep. 1975) p.67-80 (F, C)
   8) Kenzo TOKI, Tadanobu SATO: Non-Linear Harmonic Wave Propagration in a Layered Ground, No.247 (Mar. 1976) p.21-33 (H)
   9) Makoto KAMIYAMA: Stress and Strain in Ground during Earthquake, No.250 (Jun. 1976) p.9-23 (B)
   10) Tadashi NAKAGAWA, Masao HAYASHI, Hiroyasu NAKASA: Estimation of Spatial Geo-Stress Components in Rock Samples Using the Kaiser Effect of Acoustic Emission, No.258 (Feb. 1977) p.63-75 (B, C)
   11) Kouichi AKAI, Toshihisa ADACHI, Kouichi NISHI: Elasto-Plastic Behaviors of Soft Sedimentary Rock (Porous Tuff), No.271 (Mar. 1978) p.83-95 (G)

4. Proceedings of The Symposium on Rock Mechanics, the Japan Society of Civil Engineers
   1) Eizaburo YOSHIZUMI, Tsuyoshi SUGANO, Akira SAITO, Chugoro SATOH: The Electrical Prospecting at the Yoshioka Side of the Seikan Tunnel, 9th Symposium (Feb. 1975) p.1-5 (E)
   2) Soji YOSHIKAWA, Chugoro SATOH, Hakaru TAMURA, Hiroshi MOCHIZUKI: Seismic Prospecting in Seikan Tunnel, Hokkaido Side, 9th Symposium (Feb. 1975) p.6-10 (F)
   3) Keiji KOJIMA: Relation between Drillability and Some Properties of Soft Rock Foundation, 9th Sympoium (Feb. 1975) p.11-15 (D)
   4) Sang-chul KIM, Masanori SUYAMA, Hideo KITAGAWA: Fracture Mechanics Study on the Compression Test, 9th Symposium (Feb. 1975) p.16-20 (A)
   5) Mamoru YAMAGATA, Toshiaki TAKEUCHI: On some Characteristics of Deformation in a Granitic Ground, 9th Symposium (Feb. 1975) p.21-25 (C)
   6) Takashi YANAGIDANI, Osamu SANO, Makoto TERADA: The Observation of the Acoustic Emission in Rock-Like Materials, 9th Symposium (Feb. 1975) p.26-30 (B)
   7) Toshimasa KOBAYASHI, Tadashi HASHIMOTO, Yasuaki ICHIKAWA: Stability Analysis of a Submerged Cut Slope with Stress-path Dependence, 9th Symposium (Feb. 1975) p.31-35 (B)
   8) Ryunoshin YOSHINAKA, Toru ONODERA: Analytical Consideration in the Shear Strength of in-situ Granite, 9th Symposium (Feb. 1975) p.36-40 (F)

9) Shoichi HIKINO, Masahiro KAMIYA: Process of Rupture Observed in Rock Shear Test, 9th Symposium (Feb. 1975) p.41-45 (F, C)
10) Tadashi KANAGAWA, Masao HAYASHI, Satoshi HIBINO: Some Problems on the Measuring Methods of Natural Ground Pressure, 9th Symposium (Feb. 1975) p.46-50 (B)
11) Shunsuke SAKURAI, Yasutoshi KITAMURA, Kiyoshi MIYAGAWA: Blast Vibration at Tunnel Crossing, 9th Symposium (Feb. 1975) p.56-60 (F)
12) Kazuo SAITOH, Koichi KIKUCHI: An Application of Concrete Schmidt Hammer to Measurement on Rock Properties, 9th Symposium (Feb. 1975) p.61-65 (F)
13) Kokichi KIKUCHI, Kazuo SAITOH: A Proposed Method of the Classification of Rock Grade, in Connection with Bearing Resistance of Foundation Rock, 9th Symposium (Feb. 1975) p.66-70 (H)
14) Yuichi NISHIMATSU, Masaru SUZUKI, Masao AKIYAMA: The Development of Rock Machinability Testing System for Tunnel Boring, 9th Symposium (Feb. 1975) p.71-75 (D)
15) Masanori SUYAMA, Ryoji YUUKI, Hideo KITAGAWA: Fracture Mechanics Approach to the Strength of Rock as the Cracked Body, 9th Symposium (Feb. 1975) p.76-80 (C)
16) Tomoyuki AKAGI: On the Estimation of Viscoelastic Constant and Rock-Ground, 9th Symposium (Feb. 1975) p.81-85 (B, C)
17) Masao SATAKE, Hisataka TANO: On the Uniaxial Compressive Strength of Rocks with Artificial Single Slit, 9th Symposium (Feb. 1975) p.86-90 (A)
18) Tomio ITOH, Masayasu HISATAKE: Analysis of Ground Deformation Resulting from Tunnel Excavation, 9th Symposium (Feb. 1975) p.91-95 (B)
19) Toshiji NIWA, Shoichi KOBAYASHI, Masayasu OTSU: Stresses and Deformation Produced around Tunnel Excavation in Soft Rock, 9th Symposium (Feb. 1975) p.96-100 (B)
20) Koichi SASSA, Koichi HANASAKI, Ichiro ITOH: Numerical Simulation of Submarine Blasting, 9th Symposium (Feb. 1975) p.101-105 (E)
21) Mikio SHOJI, Nobuyuki OKABAYASHI, Harushige TANIMOTO, Takeshi SASAKI: Material Nonliner Finite Element Analysis by Newton-Raphson Method and Its Application to Underground Excavating Space, 9th Symposium (Feb. 1975) p.106-110 (B)
22) Yutaka NAKAZAWA, Seishi OKUZONO, Tadanori SHIMADA: Study on Weathering Characteristics of Cut Slopes in the Tomei Expressway and the Chuo Expressway, 9th Symposium (Feb. 1975) p.111-115 (E)
23) Takeshi MITANI, Takeo KAWAI: On a new Drilling Equipment with a Retractable Bit and Wire Line System, 9th Symposium (Feb. 1975) p.116-120 (D)
24) Kenji NAKAO: On the Excavation by the Method of Large Scale Under-water-Drilling and Blasting, 9th Symposium (Feb. 1975) p.121-125 (D)
25) Takeo WADA: Actual Results of Mini-John Shield Tunnelling Machine, 9th Symposium (Feb. 1975) p.126-130 (D)
26) Toshio KIMURA: Deformation Styles of Rocks Produced by Earth Movements, 9th Symposium (Feb. 1975) p.131-135 (D)
27) Soji YOSHIKAWA, Chugoro SATOH, Hiroshi MOCHIZUKI: Seismic Prospecting in Tunnels Using Boreholes, 10th Symposium (Feb. 1976) p.1-5 (F)

28) Kazuo SAITO, Kokichi KIKUCHI: Comparision between Rock-Grades and Physical Properties Measured by a New Seismic Timer, 10th Symposium (Feb. 1976) p.6-10 (F)
29) Kokichi KIKUCHI, Kazuo SAITO, Daiei INOUE, Yuji KANAORI: Quantitative Estimation and Analysis of Joint Distribution in a Basement Rock, 10th Symposium (Feb. 1976) p.11-15 (H, F)
30) Takehiko NIWA: Structural Behavior of the Kurobe Dam Especially, the Deformation of the Foundation Rock, 10th Symposium (Feb. 1976) p.21-25 (C)
31) Yuichi NISHIMATSU, Masao AKIYAMA: Mechanical and Geomerical Similarities of Rock Cutting, 10th Symposium (Feb. 1976) p.26-30 (D)
32) Ryunoshin YOSHINAKA, Toru ONODERA: Strength and Dilatancy of Artificially Granulated Granite --- As a Model of Fissured Rock Mass ---, 10th Symposium (Feb. 1976) p.31-35 (B)
33) Shunsuke SAKURAI, Yasutoshi KITAMURA, Kohzo YOSHIDA: Tunnel Vibration from Adjacent Blasting, 10th Symposium (Feb. 1976) p.41-45 (E)
34) Yoshiji NIWA, Shoichi KOBAYASHI, Takuo FUKUI, Takashi YANAGIDANI, Masayasu OTSUKA: Some Considerations on Acoustic Emission due to Rock Burst, 10th Symposium (Feb. 1976) p.46-50 (B)
35) Ryoji KOBAYASHI, Naohiro OTSUKA: On Rock Noise during Failure Process in Compression, 10th Symposium (Feb. 1976) p.51-55 (A)
36) Toshiaki TAKEUCHI: On some Characteristics of Deformation on Rocks used by Borehole Load Test, 10th Symposium (Feb. 1976) p.56-60 (F)
37) Ryoji KOBAYASHI: In Situ Method for Determing Rock Strength by Shearing Rock between Two Parallel Boreholes, 10th Symposium (Feb. 1976) p.61-65 (F)
38) Hisataka TANO, Masao SAKATA: Consideration on the Strength of Brittle Materials with Crack, 10th Symposium (Feb. 1976) p.76-80 (A)
39) Satoshi HIBINO, Hiroya KOMADA, Toshihide TOKUE, Mutsumi MOTOJIMA, Hideki NAGASHIMA: Estimation of Surface Settlement Induced by Tunnelling in a Soft Ground, 10th Symposium (Feb. 1976) p.91-95 (B)
40) Yoshihiro KITAHARA: A Contribution to the Problem of Excavation of Slope, 10th Symposium (Feb. 1976) p.96-100 (B)
41) Minoru SHIMOGOCHI: On the Full Face Excavation of the Mantarodani Constructing Section in the Dai-Shizu-Tunnel, 10th Symposium (Feb. 1976) p.101-105 (D)
42) Nobutoshi INABA, Shigeru TAKAMURA: Novel Blade Shield Practiced in the Boso Water-Way Project, 10th Symposium (Feb. 1976) p.106-110 (D)
43) Toshitaka INOUE, Yasuo KOIDE: Tunnel Excavation through Swelling Mud Stone Accompanied with Spring Water, 10th Symposium (Feb. 1976) p.111-115 (D)
44) Ryunoshin YOSHINAKA, Tadashi YAMABE: Mechanical Properties of Some Japanese Mudstone Obtained by CD Triaxial Compression Test, 11th Symposium (Feb. 1978) p.1-5 (A)
45) Takeshi ITO, Tomio HORIBE: A Basic Study on Swelling Rock Mass Behavior with Montmorillonite, 11th Symposium (Feb. 1978) p.6-10 (A, C)
46) Toshitaka INOUE, Hiroshi AOTO: On the Prediction Technique of Ground Pressure at Tunnel Excavation in Swelling Mudstone, 11th Symposium (Feb. 1978) p.11-15 (F)

47) Ryuichi OKAMOTO, Hayashi SUGAHARA: Deformability Tests of Rock Masses by Thin Flatjacks in Slot, 11th Symposium (Feb. 1978) p.16-20 (F)
48) Atsushi WATANABE: Relations between Semi-Strength and Yield Strength by Borehole Jack Test in Rocks, 11th Symposium (Feb. 1978) p.21-25 (F)
49) Eishin MATSUMUNE, Makoto SATO, Junichi MIYAGAWA: Consideration on Jack Test in Gallary and Borehole --- Semi-Hard or Hard Rocks ---, 11th Symposium (Feb. 1978) p.26-30 (F)
50) Kozo MIKI, Junichi MIYAGAWA: Rock Deformability Test by Borehole Jacks, 11th Symposium (Feb. 1978) p.31-35 (F)
51) Yoshihiro KITAHARA, Hiroshi ITO, Toshihide TOKUE, Mutumi MOTOJIMA: Experimental and Numerical Investigation on the Pulling-out Resistance of Transmission Tower Footing (Long-Anchor Type), 11th Symposium (Feb. 1978) p.36-40 (F)
52) Ryunoshin YOSHINAKA, Hitoshi NISHIMAKI: Finite Element Analysis of Bearing Capacity and Load-Displacement Behavior of a Foundation on Soft Rock, 11th Symposium (Feb. 1978) p.41-45 (C)
53) Ryuichi IIDA, Isao SHIBATA, Tadashi NISHIOKA, Kozo SAITO: Rock Deformation Tests and the Characteristics of the Strain Distributions in Rock Masses, 11th Symposium (Feb. 1978) p.46-50 (F, C)
54) Shojiro HATA, Chikaosa TANIMOTO, Koh KIMURA: Field Measurement and Consideration on Deformability of the Izumi-Layers, 11th Symposium (Feb. 1978) p.51-55 (A)
55) Hayashi SUGAHARA: Experimental Studies of Compressive Stress and Elastic Wave Velocities in Rocks, 11th Symposium (Feb. 1978) p.56-60 (A)
56) Tadashi KANAGAWA, Masao HAYASHI, Yoshihiro KITAHARA: Method of Estimation of Geo-Stress in Rocks Using the Kaiser Effect of Acoustic Emission and Some Considerations, 11th Symposium (Feb. 1978) p.61-65 (B)
57) Toshiro ISOBE, Yuusaku TOMINAGA: Estimation of Destruction Time of Rock under Creep Test, 11th Symposium (Feb. 1978) p.66-70 (A)
58) Tomoyuki AKAGI: Some Consideration about Creep Rupture of Soils and Rocks, 11th Symposium (Feb. 1978) p.71-75 (C)
59) Hisataka TANO, Masao SATAKE: Experimental Study on the Mechanism of Fracture and Deformation of Brittle Materials by Models, 11th Symposium (Feb. 1978) p.76-80 (C)
60) Masayasu INOUE, Michito OHMI, Yasushi TAKASU: Experimental Studies on Slope Rupture, 11th Symposium (Feb. 1978) p.81-85 (C)
61) Ryoji KOBAYASHI, Osamu KAWAZUMI, Masao HIRAI, Toshihiro OKITSU, Masayuki KOSUGI: Scale Model Tests of Rock Movement Caused by Excavating Roadway, 11th Symposium (Feb. 1978) p.86-90 (D)
62) Kunio WATANABE, Kuniaki SATO: On Some Stochastic Properties of Cracks and These Applications to the Permeability in Rock Masses, 11th Symposium (Feb. 1978) p.91-95 (G)
63) Hiroya KOMADA, Masao HAYASHI: Evaluation of Underground Containment of Fission Radioactive Gases Caused at the Hypothetical Accident of Underground Nuclear Power Station, 11th Symposium (Feb. 1978) p.96-100 (G)

64) Toshihide TOKUE, Mutsumi MOTOJIMA, Yoshihiro KITAHARA: A Consideration about Influences of Residual Strength and Stress Path of Stability of Excavated Slopes, 11th Symposium (Feb. 1978) p.101-105 (C)
65) Toshikazu KAWAMOTO, Naoki TAKEDA: Displacement Behavior of Rock Slope with Considering the Shear Failure, 11th Symposium (Feb. 1978) p.106-110 (C)
66) Satoshi HIBINO, Masao HAYASHI, Mutsumi MOTOJIMA: Dependence of the Behavior of Rock Masses on the Shape of a Cavity during Underground Excavation, 11th Symposium (Feb. 1978) p.111-115 (F)
67) Yuichi NISHIMATSU, Tsutomu YAMAGUCHI: A Computer Modelling of Caving around Tunnel near to the Surface, 11th Symposium (Feb. 1978) p.116-120 (C)

5. Journal of the Mining and Metallurgical Institute of Japan
1) Ryoji KOBAYASHI: Studies on Crack Distribution and Sonic Velocity Change in Rocks, Vol.90, No.1031 (Jan. 1974) p.21-26 (A, C)
2) Takatoku SHIMOTANI, Umetaro YAMAGUCHI: Elastic Wave Propagation in Calcite Crystal and Limestone --- Studies for the Microstructure of Rock and It's Mechanical Properties (1st Report) ---, Vol.90, No.1032 (Feb. 1974) p.85-90 (A)
3) Yoshio TAKAHASHI, Zenjiro WATANABE: Studies on Performances of Air Rock-Drill of Automatic Valve Type --- Basic Studies on the Performance of Air Rock-Drills (2nd Report) ---, Vol.90, No.1032 (Feb. 1974) p.91-96 (D)
4) Noriyasu MORI, Toshiro ISOBE, Ikuro KAMEDA: Measurements of Seismic Waves caused from Underground Extraction of Coal Seams (1st Report), Vol.90, No.1033 (Mar. 1974) p.167-173 (C, E)
5) Noriyasu MORI, Toshiro ISOBE, Ikuro KAMEDA: Measurements of Seismic Wave caused by Underground Extraction of Coal Seams (2nd Report), Vol.90, No.1034 (Apr. 1974) p.231-236 (C, E)
6) Zenjiro HOKAO: On Development of New Type Thermodrills using Air, Vol.90, No.1034 (Apr. 1974) p.237-242 (D)
7) Ryuzo MASUMURA, Hiroshi ARAI, Hiroshi SUZUKI: On Development of Deep Deposit at Shinyama Pit, Kamaishi Mine, Vol.90, No.1035 (May 1974) p.273-277 (H)
8) Tsuyoshi NAKAO, Tadao NAGAHIRO: On Block-Shrinkage Mining at Yanahara Mine, Vol.90, No.1035 (May 1974) p.299-304 (H)
9) Ikuro KAMEDA, Toshiro ISOBE, Noriyasu MORI: Some Statistical Properties of Rock Noises --- Measurements of Seismic Waves Caused by Underground Extraction of Coal Seams (3rd Report) ---, Vol.90, No.1036 (June 1974) p.393-397 (C, E)
10) Yoshio HIRAMATSU, Yukitoshi OKA, Yoshiaki MIZUTA, Toshiaki SAITO, Katsuhiko SUGAWARA: The Deformation Behaivior of Rocks after Failure and a Consideration about the Mechanism of Burst of Pillars, Vol.90, No.1036 (June 1974) p.399-404 (A, B, C)
11) Shigeo NAKAJIMA: Development of the Super Dynamic SD-Type High Speed Mining System, Vol.90, No.1037 (July 1974) p.455-460 (H)
12) Kazuhiko SATO, Shigenori KINOSHITA: On the Compression Tests of Rock by the Split Hopkinson Bar Method, Vol.90, No.1038 (Aug. 1974) p.527-532 (A)

13) Yusaku TOMINAGA, Shigenori KINOSHITA: Stress Interference between an Elliptical Coal Face and a Circular Drift in the Elastic Rock, Vol. 90, No. 1038 (Aug. 1974) p. 533-538 (B, C)
14) Masuyuki UJIHIRA, Kiyoshi HASHIMOTO: Geological Study on the Outburst of Gas and Coal in Hokkaido Coal Field, Vol. 90, No. 1039 (Sep. 1974) p. 589-594 (H)
15) Zenjiro HOKAO, Jisun YUUN: Scale Model Experimental Studies on Roadway Swelling in Coal Mines, Vol. 90, No. 1040 (Oct. 1974) p. 635-640 (C)
16) Atsushi FUKUSHIMA, Shigenori KINOSHITA: The Study on Volumetric Deformation of Rock --- Dilatancy and Fracture of Rocks Under Uniaxial Compression (1st Report) ---, Vol. 90, No. 1041 (Nov. 1974) p. 699-704 (A, B, C)
17) Atsushi FUKUSHIMA, Shigenori KINOSHITA: Elasto-Plastic Properties of Rock in Post-Failure Region --- Dilatancy and Fracture of Rocks Under Uniaxial Compression (2nd Report) ---, Vol. 90, No. 1042 (Dec. 1974) p. 769-774 (A, B, C)
18) Yuji ISHIJIMA, Tatsuhiko GOTO, Shigenori KINOSHITA: A Basic Study on the Cylindrical Shaped Moulded Gage for the Measurement of Stress in Rock, Vol. 91, No. 1043 (Jan. 1975) p. 5-12 (B)
19) Hirohide HAYAMIZU, Shigeo MISAWA, Michio KURIYAGAWA, Saburo TAKAOKA: A Study on the Frictional Resistance on a Cutting Tool, Vol. 91, No. 1044 (Feb. 1975) p. 55-59 (D)
20) Yoshiteru WATANABE, Masaru SUZUKI, Yuichi NISHIMATSU, Masao AKIYAMA, Satoru MIWA: On the Development of a Portable Rock Machinability Tester for Tunnel Boring, Vol. 91, No. 1044 (Feb. 1974) p. 61-66 (D)
21) Naohiko NAKAJIMA, Takeo FUKAZAWA: The Mining Plan of Open-Pit by Computer Model, Vol. 91, No. 1046 (May 1975) p. 174-181 (H)
22) Akiyoshi OTSUKI, Hitoshi MAIE, Nitaro SATO: The Mining Method With Artificial Mortar Roof Reinforced by Pre-placed Captimbers, Vol. 91, No. 1046 (Apr. 1975) p. 224-233 (H)
23) Atsushi YOSHIDA, Shotaro TAN, Hironori KANNO: On Development of Inclined Drift and Fill Mining (IDF), Vol. 91, No. 1046 (Apr. 1975) p. 233-239 (H)
24) Tadashi NISHIDA, Nobuhiro KAMEDA: On the Mechanism of Caving-in due to Mining at a Shallow Depth (2nd Report), Vol. 91, No. 1047 (May 1975) p. 323-328 (C)
25) Kazuhiko SATO, Shigenori KINOSHITA: On the Effect of Strain Rate on the Compressive Strength of Rocks, Vol. 91, No. 1048 (June 1975) p. 385-390 (B, C)
26) Yoshio HIRAMATSU, Kaoru ISHIHARA, Jinji MAEBASHI, Yoshiaki MIZUTA, Yukitoshi OKA, Norio ICHISUGI, Kusuo SAKAI, Shigeru OGASAWARA: Observation of Bumps in Besshi Copper Mine, Vol. 91, No. 1050 (Aug. 1975) p. 513-519 (B, C)
27) Yusaku TOMINAGA, Toshiro ISOBE: Stress Concentration around a Circular Drift Situated Near to an Elliptical Goaf in the Elastic Rock, Vol. 91, No. 1051 (Sep. 1975) p. 567-571 (B)

28) Ryoji KOBAYASHI, Fumio SUGIMOTO: On Mechanical Behaviour of Rocks during Failure Precess in Compression, Vol.91, No.1052 (Oct. 1975) p.647-652 (A, B, C)
29) Yuichi NISHIMATSU, Noboru OKUBO, Yukihisa HIRASAWA: The Rock Cutting with Roller Cutters, Vol.91, No.1052 (Oct. 1975) p.653-658 (D)
30) Tomio HORIBE, Minoru USHIDA, Yung Tso SUNG, Kiyohiko OKUMURA: Mechanism of Crook of Borehole and Influence of Circulating Rate of Water --- Study on Deviation of Borehole in Deep Boring (1st Report) ---, Vol.91, No.1053 (Nov. 1975) p.709-712 (D)
31) Kazuo OTSUKA, Hiroshi MIYAKOSHI, Hiroshi SATO: Studies on Surface Reaction of Coal --- The Surface Area-pore Size Distribution ---, Vol.91, No.1054 (Dec. 1975) p.759-764 (H)
32) Yukitoshi OKA, Yoshio HIRAMATSU, Toshiaki SAITO, Katsuhiko SUGAWARA: The Observation Equations Obtained from Three-dimensional Stress Analysis and Some Examples of Stress Determination by This Method --- Stress Determination in Rock from Strains on Borehole Bottoms by the Stress Relief Technique (1st Report) ---, Vol.92, No.1055 (Jan. 1976) p.1-6 (B, C)
33) Yuichi NISHIMATSU, Koji MATSUKI: A Computer Simulation of the Failure Process of Rock in Compression, Vol.92, No.1055 (Jan. 1976) p.13-18 (A, B, C)
34) Mamoru ABE, Tokumi SAITO: Effect of Water Content in Cracks on the Elastic Wave Velocity in Rock, Vol.92, No.1056 (Feb. 1976) p.73-78 (A)
35) Yoneji NISHIDA, Yasuhiko TAKEDA, Hisaaki KUROSAWA, Yoji MIZUMA: On Reinforce of Artificial Roof and Thick Filling by the Utilization of Properties of Flotation Tailings of Converted Slag and Granulated Slag of Flush Smelting Furnace, Vol.92, No.1058 (Apr. 1976) p.222-226 (H)
36) Takumi KIMURA: The Mining Method of Weak Deposit at Hosokura Mine, Vol.92, No.1058 (Apr. 1976) p.226-230 (H)
37) Satoshi USUI: Drifting in High Temperature Rock Masses, Vol.92, No.1058 (Apr. 1976) p.230-235 (H)
38) Masataka MURAHARA, Bunsaku HASHIMOTO, Yoshikazu HAGIWARA: Application of Laser Holography to Measurement of Poisson's Ratio and Young's Modulus of Rock, Vol.92, No.1059 (May 1976) p.333-338 (A)
39) Kazuhiko SATO, Shigenori KINOSHITA: Griffith Locus in Compression, Vol.92, No.1060 (June 1976) p.409-414 (A, C)
40) Tomio HORIBE, Minoru USHIDA, Yung Tso SUNG, Kiyohiko OKUMURA: On Influence of Clearance Angle & Wear of Bit and Thrust Affecting to Crook of Borehole --- Stúdy on Deviayion of Borehole in Deep Boring (2nd Report) ---, Vol.92, No.1061 (July 1976) p.477-482 (D)
41) Kazuhiko SATO, Shigenori KINOSHITA: Transient Phenomena in Compressive Failure, Vol.92, No.1061 (July 1976) p.483-489 (A, C)
42) Zenjiroo HOKAO, Soohei SHIMADA: On Thermal Characteristics in Cutting Rocks by Thermodrill, Vol.92, No.1062 (Aug. 1976) p.531-535 (A, D)
43) Masayuki TAKEUCHI, Shigenori KINOSHITA: The In-situ Stress Measurements in the Yubari New Colliery, Vol.92, No.1063 (Sep. 1976) p.595-600 (B, F)
44) Takazo KAWAGUCHI, Koichi SASSA, Ichiro ITO: Fundamental Studies on Estimation of Strength of In-situ Rock, Vol.92 (Oct. 1976) p.657 (A, B, F)

45) Zenjiro HOKAO, Jisun YUUN: On the Effect of Roadway Depth to Swelling --- Experimental Study on Roadway Swelling in Coal Mines (1st Report) ---, Vol. 92, No. 1064 (Oct. 1976) p. 663-668 (C)
46) Michio KURIYAGAWA, Shigeo MISAWA, Hirohide HAYAMIZU: Fracture of Rock by Bit Penetration --- Stress Analysis by Comparison of Photo-elastic Method and Finite Element Method (1st Report) ---, Vol. 92, No. 1064 (Oct. 1976) p. 669-674 (D)
47) Zenjiro HOKAO, Jisun YOON: On the Effect of Distance from Roadway to Upper Coal Seam and Thickness of Weak Floor to Floor Lift --- Experimental Study on Roadway Lift in Coal Mines (2nd Report) ---, Vol. 92, No. 1065 (Nov. 1976) p. 707-711 (C)
48) Hidekichi YOKOYAMA, Mamoru ABE, Atsushi HASEBE: On the Vibration Characteristics of Subsoil Layers --- Study on the Vibration of Subsoil Layers (1st Report) ---, Vol. 92, No. 1066 (Dec. 1976) p. 779-783 (H)
49) Koji MATSUKI, Yuichi NISHIMATSU: The Correlation between the Fracture Propagation and the Stress- Strain Diagram of Rocks in Compression --- A Computer Simulation of the Failure Process of Rock in Compression (2nd Report) ---, Vol. 92, No. 1066 (Dec. 1976) p. 785-790 (A, C)
50) Masuyuki UJIHIRA, Kiyoshi HASHIMOTO: A Study on the Outburst of Gas and Coal --- On the Geological Structure Conditions and Back Effect of Blasting ---, Vol. 92, No. 1066 (Dec. 1976) p. 791-796 (H)
51) Michio KURIYAGAWA, Shigeo MISAWA, Hirohide HAYAMIZU: Fracture Mechanism of Rock by the Penetration of the Wedge --- Fracture of Rock by Bit Penetration (2nd Report) ---, Vol. 92, No. 1066 (Dec. 1976) p. 797-802 (D)
52) Munehiro KITAOKA, Seiji TANAKA, Ken-ichro KUSUNOKI, Gensuke ENDO: Mechanical Properties of Ohya Tuyy --- Correspondence of Experimental Results of In-situ and Laboratory Tests, and Effects of Rock Texture on Mechanical Properties ---, Vol. 93, No. 1067 (Jan. 1977) p. 1-6 (A, F)
53) Ryoji KOBAYASHI, Mitsumasa FURUZUMI: Study on Elastic Wave Velocity of Rocks during Failure Process in Compression, Vol. 93, No. 1067 (Jan. 1977) p. 7-11 (A, B, C)
54) Tatsuhiko GOTO, Yoji ISHIZIMA, Shigenori KINOSHITA, Niheiji ODA: Effectiveness of Relief Boring in Case of Akabira Colliery --- Field Tests and Some Results ---, Vol. 93, No. 1068 (Feb. 1077) p. 75-81 (B, C, D, E, F)
55) Yuichi NISHIMATSU, Koji MATSUKI: The Failure of Borehole-Wall Considered from the Point of View of Linear Fracture Mechanics (1st Report), Vol. 93, No. 1069 (Mar. 1977) p. 185-191 (A, B, C)
56) Yasuo KOTAKE, Yoji FUJII, Kazuhiro TSUMURA: The Reinforce of Support in the Heavy Earth Pressure Zone at the Matsumine Mine, Vol. 93, No. 1070 (Apr. 1977) p. 238-241 (B, C, E)
57) Nobukazu NANKO, Hiroshi KOMATSU, Hisashi YONEDA, Minoru TATSUTANI: The Operation Result of Raise Borer (BM-100, Koken) at Kamioka Mine, Vol. 93, No. 1070 (Apr. 1977) p. 262-268 (D)

58) Yukitoshi OKA, Makio KATAGIRI, Makoto TERADA, Shoichiro GOCHO, Kazuo KURODA, Kazuo KOMUKAEMORI, Koji NAKANO: Prediction on the Drainage Control by the Mine Sealing (1st Report) --- Studies on the Technique to Prevent the Pollution at Closed Mines (1) ---, Vol. 93, No. 1071 (May 1977) p. 353-357 (G)
59) Zenjiro HOKAO, Jisun YOON: On the Method of Combating Floor Lift by Floor Boltong --- Experimental Studies on Floor Lift in Coal Mines Roadway (3rd Report) ---, Vol. 93, No. 1071 (May 1977) p. 359-363 (C)
60) Kazuo ASO, Katsushige KAN: The Damping Effect of Surrounding Water on the Lateral Vibration of Rod --- Lateral Vibration of Rod in Off-shore Boring (4th Report) ---, Vol. 93, No. 1071 (May 1977) p. 365-369 (D)
61) Tokumi SAITO, Mamoru ABE, Hidekichi YOKOYAMA: Relationship between Rock Texture and Variation of Longtudinal Wave Velocity with Saturation in Rock, Vol. 93, No. 1072 (June 1977) p. 417-422 (A)
62) Yuichi NISHIMATSU, Seisuke OKUBO, Koji MATSUKI, Shozo KOIZUMI: The Failure of Borehole- Wall Considered from the Point of View of Linear Fracture Mechanics (2nd Report), Vol. 93, No. 1074 (Aug. 1977) p. 561-566 (A, B, C)
63) Zenjiro WATANABE, Katsumi SAKAKIDA, Takeo SAGA: A Study of Tool Wear in Rock Cutting --- On the Profile of Worn Edge in Case of the Small Depth of Cut (1st Report) ---, Vol. 93, No. 1074 (Aug. 1977) p. 567-571 (D)
64) Zenjiro HOKAO, Sohei SHIMADA: On the Development of Small Thermo-drills and the Thermal Drilling Rate, Vol. 93, No. 1075 (Sep. 1977) p. 615-620 (D)
65) Hirohide HAYAMIZU, Hideo KOBAYASHI, Isao MATSUNAGA: Fracturing of Rock at Elevated Temperature with Borehole Coolong Method, Vol. 93, No. 1077 (Nov. 1977) p. 863-868 (A, B, C)
66) Yusaku TOMINAGA, Toshiro ISOBE: Study on Rock Fracture Condition in the Case of Stress Concentration due to an Elliptical Inclusion, Vol. 93, No. 1078 (Dec. 1977) p. 939-944 (B, C)
67) Yoshio HIRAMATSU, Hikeun LEE, Yukitoshi OKA: Deformation Behaviors of Rocks under Uniaxial Tension and Comression Tests, Vol. 83, No. 1078 (Dec. 1977) p. 945-949 (A, B, C)
68) Hikeun LEE, Yoshio HIRAMATSU, Yukitoshi OKA: Deformation and Failure Behaviors of Rocks Inferred from Results of Tension, Compression and Bending Tests, Vol. 94, No. 1079 (Jan. 1978) p. 11-16 (A, B, C)
69) Michio KURIYAGAWA, Shigeo MISAWA, Hirohide HAYAMIZU: Fracture Mechanism of Rock by Roller Cutter --- Mechanical Fracture of Rock by Cutter (3rd Report) ---, Vol. 94, No. 1079 (Jan. 1978) p. 17-24 (D)
70) Yoshio TAKAHASHI, Zenjiro WATANABE: On the Evaluation of the New Thermal Efficiency of the Air Rock-Drill --- Basic Studies on the Performance of Air Rock-drill (5th Report) ---, Vol. 94, No. 1079 (Jan. 1978) p. 25-29 (D)
71) Michio KURIYAGAWA, Shigeo MISAWA, Hirohide HAYAMIZU, Naoki KANEKO: Fracture Mechanism of Rock at Elevated Temperature by Wedge Bit and Roller Cutter --- Mechanical Fracture of Rock by Cutter (4th Report) ---, Vol. 94, No. 1080 (Feb. 1978) p. 69-76 (D)

72) Katsuhiko KANEKO, Hiroyuki INOUE, Koichi SASSA, Ichiro ITO: Experimental and Theoretical Studies on the effect of the Progress of Breakage in Rock on Elastic Wave Propagation Velocity --- Studies on the effect of the Progress of Breakage in Rock on Elastic Wave Propagation (1st Report) ---, Vol. 94, No. 1080 (Feb. 1978) p. 77-83 (A, C)
73) Yoshiaki MIZUTA, Hikeun LEE, Yukitoshi OKA, Yoshio HIRAMATSU, Shoji OGINO: The Method of Elasto-Plastic Analysis for Underground Excavation in Consideration of the Post-Failure Properties of Rocks, Vol. 94, No. 1081 (Mar. 1978) p. 151-156 (B, C)
74) Michito KIFUNE: A Improvement of Mining System at Toyoha Mine, Vol. 94, No. 1082 (Apr. 1978) p. 226-229 (H)
75) Norio TANAKA, Naotake KUROSAKI: Blasting Method at Kamaishi Mine, Vol. 94, No. 1082 (Apr. 1978) p. 229-233 (D)
76) Nobukazu NANKO, Hiroshi KOMATSU, Mitsuhiro OHTA, Takao HIRONAKA: On the Roof Supporting at Kamioka Mine --- Especially about Roofsupporting and Controlled Blasting ---, Vol. 94, No. 1082 (Apr. 1978) p. 239-242 (B, C, D, E)
77) Hiroyuki INOUE, Katsuhiko KANEKO, Koichi SASSA, Ichiro ITO: The Attenuation of the Wave due to the Progress of Breakage in Rocks --- Studies on the Effect of the Progress of Breakage in Rocks on Elastic Wave Propagation (2nd Report) ---, Vol. 94, No. 1083 (May 1978) p. 323-328 (A, C)
78) Ryoji KOBAYASHI, Koji MATSUKI, Tadashi HAYASAKA: Fundamental Studies on Rock Burst --- On Rupture Behaviors of Rock Caused by Rapid Reduction of Confining Pressure in Triaxial Compression Test ---, Vol. 94, No. 1084 (June 1978) p. 379-383 (A, B, C)
79) Yuichi NISHIMATSU, Yukitoshi OKA, Keiji KOJIMA, Yoneji NISHIDA, Masanori OCHIISHI: On the Failure and Displacement of Concrete Plug for Sealing in the Pit Mouth of Closed Mine (1st Report) --- Studies on the Technique to Prevent the Pollution at Closed Mines (3) ---, Vol. 94, No. 1084 (June 1978) p. 385-390 (B, C)
80) Koichi SASSA, Eiji KIKUOKA, Jun RI, Ichiro ITO: Emissive Mechanism of Blast Noise Caused by Quarry Blasting, Vol. 94, No. 1085 (July 1978) p. 457-461 (D)
81) Tomio HORIBE, Minoru USHIDA, Yung Tso SUNG, Kiyohiko OKUMURA, Tokumi SAITO: Relation of Inclined Angle of Boundary to Crook of Borehole --- Study on Deviation of Borehole in Deep Boring (3rd Report) ---, Vol. 94, No. 1085 (July 1978) p. 463-467 (D)
82) Tadakazu KONDO: A Theory of Gas Outburst on the Basis of the Various Field Observations and its Verification by an Experimental Study, Vol. 94, No. 1085 (July 1978) p. 469-474 (H)
83) Hiroshi KIYOHASHI, Munesuke KYO, Wataru ISHIHARA: Effects of Rock Temperature on the Thermal Fracturing of an Imitation Rock Specimen --- Studies on the Fracturing of Hot Dry Rock by High Speed Water Jets ---, Vol. 94, No. 1086 (Aug. 1978) p. 515-521 (A, C)
84) Makoto IHARA, Kikuo MATSUI: A Study of Roadway Closure --- Linear Analysis by the FEM ---, Vol. 94, No. 1087 (Sep. 1978) p. 581-586 (B, C)

85) Yoji ISHIJIMA, Shigenori KINOSHITA, Toshio ISOBE, Koji SAITO: Interpretation of Field Phenomena Observed in the Vicinity of a Fault Zone in Terms of a Mechanical Model, Vol. 94, No. 1087 (Sep. 1978) p. 587-592 (B, C)

6. Journal of the Society of Materials Science, Japan
   1) Koji NAKAGAWA: A Study on Fracture Condition of Rock-like Materials in Compression, Vol. 23, No. 246 (Mar. 1974) p. 242-248 (A, C)
   2) Kiyoo MOGI: Rock Fracture and Earthquake Prediction, Vol. 23, No. 248 (May 1974) p. 320-331 (C, H)
   3) Ichiro ITO: Rock Breakage Caused by Explosion of Explosives, Vol. 23, No. 248 (May 1974) p. 332-340 (D)
   4) Minoru YOSHIDA: Analysis and Measurements of Behaviors of Rock around Under-ground Cavity in the Process of Excavation, Vol. 23, No. 248 (May 1974) p. 341-348) (C, F)
   5) Ken-ichi HIRASHIMA, Yoshiji NIWA: Stresses and Deformations around Two or More Pressure Tunnels in Elastic Rock Masses, Vol. 23, No. 248 (May 1974) p. 349-354 (B)
   6) Shunsuke SAKURAI, Yoshiteru YOSHIMURA: The Maximum Pressure Acting on Tunnel Lining Installed in Viscoelastic Orthotropic Underground Medium, Vol. 23, No. 248 (May 1974) p. 355-360 (B)
   7) Yoshiji NIWA, Shoichi KOBAYASHI, Tadaaki MATSUMOTO: Transient Stresses Produced around Tunnels by Traveling Waves, Vol. 23, No. 248 (May 1974) p. 361-367 (B)
   8) Koichi AKAI, Toshihisa ADACHI, Nobuo TABUSHI: Mechanical Properties of Soft Rock in Terms of Effective Stress, Vol. 23, No 248 (May 1974) p. 368-373 (A)
   9) Yuichi NISHIMATSU, Koji MATSUKI, Shozo KOIZUMI: The Failure Process of Rock in Compression, Vol. 23, No. 248 (May 1974) p. 374-379 (A)
   10) Yoshio HIRAMATSU, Yukitoshi OKA, Hidebumi ITO, Yutaka TANAKA: The Correlation of the Rock Stress Measured in situ and the Tectonic Stress Inferred from Geological and Geophysical Studies, Vol. 23, No. 248 (May 1974) p. 380-386 (B, F, H)
   11) Izuo OZAWA: Observations on Secular Changes of the Crustal Movements in a Tunnel at Otsu, Vol. 23, No. 248 (May 1974) p. 387-391 (F)
   12) Yoshio HIRAMATSU, Kiyoshi OKADA, Yukitoshi OKA, Wataru KOYANAGI, Yoshiaki MIZUTA: Designing and Constructing a Stiff Testing Machine and the Deformation Characteristics of Various Kinds of Concrete, Vol. 24, No. 260 (May 1975) p. 447-454 (A, C)
   13) Atsushi FUKUSHIMA, Shigenori KINOSHITA: A Progressive Failure Model of Rocks in Uniaxial Compression, Vol. 24, No. 263 (Aug. 1975) p. 741-746 (A, C)
   14) Katsuhiko KANEKO, Ichiro ITO: Study on Microfracture Produced in Rocks, Vol. 26, No. 285 (June 1977) p. 503-509 (A, C)
   15) Shoichi KOBAYASHI: Applications of Acoustic Emission to Rock Mechanics, Vol. 27, No. 293 (Feb. 1978) p. 118-128 (A, F)
   16) Toshikazu KAWAMOTO, Toshiaki ISHII: Experimental Study on Deformation Characteristics of Rock-like Materials, Vol. 27, No. 293 (Feb. 1978) p. 129-135 (A, C)

17) Takashi YANAGIDANI, Osamu SANO, Makoto TERADA, Ichiro ITO: The Fracture Behavior of the Granodiorite under Uniaxial Compression, Vol. 27, No. 293 (Feb. 1978) p. 136-141 (A)
18) Koji MATSUKI, Yuichi NISHIMATSU, Shozo KOIZUMI: Acoustic Emission and Failure Process of Rocks under Compression, Vol. 27, No. 293 (Feb. 1978) p. 142-147 (A)
19) Kiyoo MOGI, Kansaku IGARASHI, Hiromine MOCHIZUKI: Deformation and Fracture of Rocks under General Triaxial Stress States --- Anisotropic Dilatancy ---, Vol. 27, No. 293 (Feb. 1978) p. 148-154 (A)
20) Naoichi KUMAGAI, Sadao SASAJIMA, Hidebumi ITO: Long-term Creep of Rocks (Results with Large Specimens Obtained in about 20 Years and Those with Small Specimens in about 3 Years), Vol. 27, No. 293 (Feb. 1978) p. 155-161 (A)
21) Koichi AKAI, Yuzo OHNISHI, Hiroaki MIZOBE: Bearing Capacity of Weathered Rock Mass Determined by Graphical Solution of Pole Trail Method, Vol. 27, No. 293 (Feb. 1978) p. 162-168 (B, C)

7. Proceedings of the National Symposium on Rock Mechanics, Japan
1) Tokumi SAITO, Mamoru ABE: Study on Variation of Longitudial Wave Velocity with Saturation in various Rock Types, 5th Symposium (Feb. 1977) p. 1-6 (A)
2) Michito OHMI, Masayasu INOUE: Experimental Studies of the Propagation of Elastic Waves in Rocks under Uniaxial Compression, 5th Symposium (Feb. 1977) p. 7-12 (A)
3) Kyoji SASSA, Daizo SAKATA: Measurement of the Ground Water Velocity Using Seismic Detector, 5th Symposium (Feb. 1977) p. 13-18 (G)
4) Ryunoshin YOSHINAKA, Tomoari AWA: Water Retention and Mechanical Properties of Mudstones, 5th Symposium (Feb. 1977) p. 19-24 (A)
5) Keiji KOJIMA, Yasusuke SAITO, Hiroto OCHI: Softening of Muddy Soft Rock and the Evaluation of Mechanical Test Values, 5th Symposium (Feb. 1977) p. 25-29 (A)
6) Munehiro KITAOKA, Gensuke ENDO, Kazuo HOSHINO: Influence of Moisture on the Mechanical Properties of Soft Rocks --- Especially on the Strength ---, 5th Symposium (Feb. 1977) p. 31-36 (C)
7) Takakoto SHIMOTANI, Umetaro YAMAGUCHI: Experimental Studies of Strength and Crystal Grains for Crystalline Limestones, 5th Symposium (Feb. 1977) p. 37-42 (A)
8) Kiyoo MOGI, Hiromine MOCHIZUKI: Deformation and Fracture of Rocks under General Triaxial Stress State --- Anisotropic Dilatancy ---, 5th Symposium (Feb. 1977) p. 43-48 (C)
9) Hidefumi ITO, Sadao SASAJIMA: Creep Tests of Rocks Measured by Making Use of Interference Fringes of Light --- Experimental Results Obtained for the First 2 Years ---, 5th Symposium (Feb. 1977) p. 49-54 (A, C)
10) Hisataka TANO, Masao SAKATA: Consideration on the Mechanism of Fracture Initiation and Propagation of Brittle Materials, 5th Symposium (Feb. 1977) p. 55-59 (A, C)
11) Makoto TERADA, Takashi YANAGIDANI, Osamu SANO, Ichiro ITO: Fracture Behavior of Class II Type-Rock, 5th Symposium (Feb. 1977) p. 61-66 (A, C)

12) Yuichi NISHIMATSU, Seisuke OKUBO: A Computer Simulation of the Failure Process of Rock by the Finite Element Method, 5th Symposium (Feb. 1977) p.67-72 (A, C)
13) Masayasu INOUE, Michito OHMI, Takeshi NAGAO: Study on the Relation between Crusing Strength and Some Physical Properties of Common Rocks, 5th Symposium (Feb. 1977) p.73-79 (A, C)
14) Minoru SHIMOKAWACHI: An Investigation from Rock-Burst Phenomenon in Dai-Shimizu Tunnel, 5th Symposium (Feb. 1977) p.78-84 (B)
15) Yoshiji NIWA, Takuo FUKUI, Masayasu OTSU, Minoru SHIMOGOCHI: A Study of Rock Burst Mechanism, 5th Symposium (Feb. 1977) p.85-90 (B)
16) Yutaka TANAKA, Ryohei NISHIDA: Generation Mechanism of Rock Bursts and Microearthquakes Induced by Water-Injection into a Deep Abandoned Mine, 5th Symposium (Feb. 1977) p.91-96 (B)
17) Koji MATSUKI, Yuichi NISHIMATSU, Shozo KOIZUMI: Acoustic Emission and Failure Process of Rocks under Compression, 5th Symposium (Feb. 1977) p.97-102 (A, C)
18) Tadashi KANAGAWA, Masao HAYASHI, Hiroyasu NAKASA: Estimation of Spatial Geo-Stress Components in Rock Samples Using the Kaiser Effect of Acoustic Emission, 5th Symposium (Feb. 1977) p.103-108 (B)
19) Yoshiteru WATANABE, Iwao NAKAJIMA, Masayuki TAKEUCHI, Shota KAWAKURI: Acoustic Emission Activity in Rock around Underground Coal Mine Excavation, 5th Symposium (Feb. 1977) p.109-114 (B)
20) Toshiro ISOBE, Noriyasu MORI, Kazuhiko SATO, Ikuro KAMEDA, Takashi GOTO: Measurement of Rock Fracturing Noises Induced by Underground Coal Mining, 5th Symposium (Feb. 1977) p.115-120 (B)
21) Kokichi KIKUCHI, Kazuo SAITO, Daiei INOUE, Yuji NAKAORI: A Method for the Analysis of Characteristics of Joint Distribution in Foundation Rock, 5th Symposium (Feb. 1977) p.121-126 (F)
22) Ryunoshin YOSHINAKA, Ryokichi HAMAJIMA, Hitoshi NISHIMAKI: Consideration in Size Effect on Settlement of Foundation, 5th Symposium (Feb. 1977) p.127-132 (F)
23) Koichi AKAI, Yuzo OHNISHI, Hiroaki MIZOBE: Bearing Capacity of Weathered Rock Mass, 5th Symposium (Feb. 1977) p.133-138 (C)
24) Toshihisa ADACHI, Koichi NISHI, Kazuyoshi FUJIMOTO: Constitutive Equations and Long Term Strength-Deformation Characteristics of Soft Sedimentary Rocks, 5th Symposium (Feb. 1977) p.139-144 (C)
25) Satoshi HIBINO, Masao HAYASHI, Mutsumi MOTOJIMA: Measurement and Prediction of Behavior of Anistropic Rock Masses during Underground Excavation Works, 5th Symposium (Feb. 1977) p.145-150 (B)
26) Kazuhiko IKEDA, Seisuke MISAWA: Actual Results and Future Prospect about Tunnel Boring Machine in Japan, 5th Symposium (Feb. 1977) p.151-155 (D)
27) Soji YOSHIKAWA, Yoshimasa KOBAYASHI, Chugoro SATOH, Hiroshi MOCHIZUKI: Seismic Prospecting in Tunnels Using various Waves, 5th Symposium (Feb. 1977) p.157-162 (F)
28) Kazuhiko IKEDA, Takashi SAKURAI: Measuring Results and Estimated of Loosened Area around Tunnel Opening, 5th Symposium (Feb. 1977) p.163-167 (B)

29) Shunsuke SAKURAI, Yasutoshi KITAMURA, Kohzo YOSHIDA: Vibrational Characteristics of Tunnel Lining and Surrounding Medium due to Adjacent Blasting, 5th Symposium (Feb. 1977) p.169-173 (D, H)
30) Koichi SASSA, Ichiro ITO, Susumu NAGASAKI: Prediction of Ground Vibrations from Submarine Overburden Blasting and Results of Their Measurements, 5th Symposium (Feb. 1977) p.175-180 (D, H)
31) Yoji ISHIJIMA, Shigenori KINOSHITA: Measurement of Rock Disturbance Induced by the Mining Activities in the Steep Coal Mine --- A Case History of Noborikawa Pit of Sunagawa Coal Mine ---, 5th Symposium (Feb. 1977) p.181-186 (F)
32) Yukitoshi OKA, Yoshio HIRAMATSU, Yoshitomi KAMEOKA: Investigations into the Method of Determining Rock Stress by the Stress Relief Technique Accompanied by Applications of the Method Obtained, 5th Symposium (Feb. 1977) p.187-192 (F)
33) Sakuro MURAYAMA, Yutaka MOCHIDA, Toshihisa ADACHI, Yoshinori IWASAKI, Minoru SAKAMOTO: Field Measurement to Monitor the Stability of Under Ground Cavity at Seikan Tunnel, 5th Symposium (Feb. 1977) p.193-198 (F)
34) Kazuo SAITO, Kokichi KIKUCHI, Kenzo KIHO: An Application of Concrete Schmidt Hammer to Measurements on Rock Properties, 5th Symposium (Feb. 1977) p.199-204 (F)
35) Kyoji SASSA, Keizen HIURA, Kiyoshi OGAWA: On the New In-Situ Shear Test Pabijast and the Result of Traial Test, 5th Symposium (Feb. 1977) p.205-210 (F)
36) Keizen HIURA, Kyoji SASSA, Kiyoshi OGAWA: Weathering and Joint Effect on Experimental Studies of Shearing, 5th Symposium (Feb. 1977) p.211-216 (F)
37) Toshiaki TAKEUCHI, Tateo SUZUKI, Soichi TANAKA: A Study of Results of the Rock Measurement by Borehole Load Tester of Granite, 5th Symposium (Feb. 1977) p.217-221 (F)
38) Hisashi OHSHIMA, Yukikazu YANAKA, Koji ISHIKAWA, Tetsuo SHIBATA: In-Situ Creep Testing of Weathered Granite, 5th Symposium (Feb. 1977) p.223-228 (F)
39) Ryoji KOBAYASHI: Studies on In-Situ Measurements for Estimating Strength of Rock Mass, 5th Symposium (Feb. 1977) p.229-234 (F)
40) Eizaburo YOSHIZUMI, Kazutoshi KOJIWARA, Bunkoku RA: A Study on the Results of Grouting on the Rock Foundation, 5th Symposium (Feb. 1977) p.235-239 (E)

8. Hydro Electric Power (Electric Power Civil Engineering No.154~)
1) Seizo MIMURA, Hiroshi YAMASHITA: Outline of Design and Execution Planning of Underground Power Station and Waterway Structures in Shin-Takasegawa Development Works, No.130 (May 1974) p.3-19 (A, B, C, D, F, G, H)
2) Masaomi TAKEGAWA, Shinichi MIYAZAKI: Design and Execution Works of Okutataragi Power Station, No.132 (Sep. 1974) p.10-33 (A, B, C, F)
3) Ikuo ADACHI, Kenji NAKAMURA: Prevention of Cave-in by Grout Rock Bolts in an Existing Headrace, No.133 (Nov. 1974) p.25-30 (E)
4) Toshio HAGIWARA, Kiyoshi KISHI: Geology of Kashiwazaki Kariwa Nuclear Power Site, No.136 (May 1975) p.49-61 (A, C, E, F, G, H)

5) Noboru IWASA, Seishi KUNIHISA: Investigation Works for Owatari Power Station, No. 137 (July 1975) p. 3-9 (A, B, C, E, H)
6) Yoichi MIMAKI, Shozo KATANO, Minoru KAMIJO: Rock Burden of Penstock in Shin-takasegawa Power Station, No. 138 (Sep. 1975) p. 3-14 (A, C, F, H)
7) Takeyasu USHIDA, Mosayasu ADACHI, Isamu USUDA: Grouting of Waterway Tunnel in Okutataragi Power Station, No. 139 (Nov. 1975) p. 23-34 (A, B, E, F)
8) Yukio TAKAHASHI: Execution Works of Main Underground Structures in Ohira Power Station, No. 143 (July 1976) p. 3-17 (E)
9) Kokichi KIKUCHI: A Method of Engineering Geology Investigation for Developing Pumped-Storage Site, No. 143 (July 1976) p. 66-80 (A, B, C, E, F, H)
10) Kokichi KIKUCHI, Kazuo SAITO: Consideration on Concrete Schmidt Hammer in the Measurements of Rock Properties and its Application, No. 145 (Nov. 1976) p. 47-53 (A, F)
11) Toshikazu KAWAMOTO, Shunichi KADOTA: An Analysis of Seepage Flow in Cracky Bedrocks, No. 147 (Mar. 1977) p. 7-16 (A, E, G)
12) Kokichi KIKUCHI, Kazuo SAITO: Examination of Rock Grades for the Purpose of Bearing Resistance Estimation in Dam Foundation Rocks, No. 147 (Mar. 1977) p. 50-62 (A, F, H)
13) Yoshiyuki MIYATA: Examination of Grouting in Foundation Rocks Supporting Takase Dam (The First Report), No. 149 (July 1977) p. 20-34 (A, F, G)
14) Hiroya KOMADA: An Analysis of Stability for Seepage Flow of Fill Dam, No. 154 (May 1978) p. 40-49 (A, G)
15) Kokichi KIKUCHI, Kazuo SAITO, Kenichiro KUSUNOKI: Examination on Quantitative Estimation of Characteristics of Joint Distribution in Foundation Rocks, No. 154 (May 1978) p. 50-59 (A, H)
16) Kenzo AOKI, Hiroshi BANDO, Takeo HAMURO: Non-blasting Excavation Process in the Extension Works of Nuclear Power Station, No. 154 (May 1978) p. 66-83 (D)
17) Giichi FUJIWARA: Dynamic Deformation Characteristics of Bedrocks by the Dynamic Jack Test Method, No. 144 (Nov. 1976) p. 71-76 (A, B, C, F)

9. Large Dams
1) Isao SHIBATA: Grouting of Soft Rocks (Grouting of Dam Foundation Rocks), No. 68 (June 1974) p. 4-26 (E)
2) Toshio FUJII: Grouting of Firm Rock Foundation ---Mainly on Nagawado Dam (Grouting of Dam Foundation Rocks) ---, No. 68 (June 1974) p. 26-44 (E)
3) Ryuichi OKAMOTO: Geological Problems of Dam with Soft Rock Foundation, No. 75 (Mar. 1976) p. 20-29 (H)
4) Nobuyuki KUMAKAWA: A Method of Analyzing the Permeability of Dam Subsurface, No. 78 (Dec. 1976) p. 29-40 (G)
5) Seiken OGATA: Characteristics of Landslide Sites in View of Geological Structure, No. 80 (June 1977) p. 29-40 (C)
6) Masatora WATARI: Dam Filling and Landslide, No. 80 (June 1977) p. 41-53 (G)

7) Akio ONAGA: Safety Management of Fill Dam ---Some Views on the Stability Analysis and the Results of Observation ---, No. 80 (Sep. 1977) p. 1-11 (G)
8) Masao HAYASHI: Consideration on the Improvement of Stability of Fill Dam Foundation, No. 83 (Mar. 1978) p. 1-22 (E)
9) Yoshinori NAKANO: Crack Occurrence in Abutment by Dam Construction, No. 83 (Mar. 1978) p. 23-31 (C, G)
10) Yoshiyuki MIYATA: Design and Execution Works of Takase Dam Foundation, No. 83 (Mar. 1978) p. 32-49 (E)
11) Kazuo GOMI: Design and Execution Works of Miho-Dam, No. 83 (Mar. 1978) p. 83-108 (E)
12) Yoshinobu MACHINO, Tokie KAWASHIMA: Design of Taketoshi Dam for Setose Hydraulic Power Station, No. 84 (June 1978) p. 26-34 (E)
13) Seizo TAKEBAYASHI, Kenji NISHIMURA, Akio KURITA: Geological Features and Grouting of Managawa Dam Foundation, No. 85 (Sep. 1978) p. 1-20 (E)

10. Zishin, Journal of the Seismological Society of Japan
1) Kiyohiko YAMAMOTO, Kinichiro KUSUSE, Tomowo HIRASAWA: Frequency Distribution of Microfractures in Rock Samples under Cyclic Loading Tests, Vol. 30, No. 4 (1977) p. 477-486 (A)

11. Zisubeli (Landslides)
1) Bungo TAMADA: Studies on the Dynamical Properties of Landslide Face and Their Soil Tests, Vol. 10, No. 4 (1974) p. 4-11 (A)
2) Akira IWAMATSU, Masaki HATTORI, Shoichi NISHIDA: Landslide and Mechanical Properties of Rocks ---An Example of Yamanaka Anticline, Niigata, Japan ---, Vol. 11, No. 1 (1974) p. 13-20 (A, H)
3) Bungo TAMADA: Studies on the Dynamical Properties of Landslide Face and Their Soil Tests, Vol. 11, No. 1 (1974) p. 37-40 (A)
4) Hiroyuki NAKAMURA, Kiyobumi SHIMIZU: Soil Tests for Determination of Shear Strength along the Slide Surface, Vol. 15, No. 2 (1978) p. 25-32 (A)

12. Engineering Geology
1) Mamoru SUZUKI, Zensuke YOSHIDA, Tsuguo TAKEBAYASHI: On Geology and Swelling Earth Pressure of the Mineoka Tunnel, Kamogawa, Chiba Prefecture, Japan, Vol. 15, No. 1 (1974) p. 1-13 (A, B)
2) Michio OMI, Masayasu INOUE: On the change of Elastic Wave Velocities and Uniaxial Compressive Strength of Sandstone and Andesite by Condition of Drying, Vol. 15, No. 1 (1974) p. 14-22 (A)
3) Kunitake HAYASHIDA, Kenji MIYAHARA: Structure of Weathered Granitic Rocks and its Engineering Significance, Vol. 15, No. 2 (1974) p. 47-57 (A, F)
4) Ryunoshin YOSHINAKA, Masami FURUTA: Joint Shear Strength of Granite, Vol. 15, No. 2 (1974) p. 58-68 (A)
5) Yoshiro HAYASHIDA, Takeshi YAMADA: On the Mineral Compositions and the Physical Properties of Mudstones of Kobe Group, Vol. 15, No. 3 (1974) p. 1-6 (A)

6) Toshiaki TAKEUCHI, Takeshi GOTO: An Estimation of the Rock Quality for the Excavation by Using Reflection Loggings, Vol. 15, No. 3 (1974) p. 7-12 (F)
7) Keiji KOJIMA, Shoichi TANAKA, Mitsuo SATO, Yasusuke SAITO: How to get Geotechnical Informations making Use of Submarine Drills --- Development of Investigation Methods with a Simple Device, Vol. 15, No. 3 (1974) p. 13-26 (F)
8) Ryoki NAKANO: On the Mechanism of Squeezing Rock Pressure of Mudstone on Tunnel Support in Relation to the Case History of Noshiro Tunnel, Vol. 15, No. 3 (1974) p. 27-43 (A, C, F)
9) Takayoshi SUEHIRO, Keizo KUWAHARA: On the Characteristics of Hard Clay in Yabakei Formation, Vol. 16, No. 1 (1975) p. 1-8 (A)
10) Nobuhiko OBARA, Koreya NAKAMURA: An Estimation of the Penetrating Depth of Weathering Penomenon in Mountainous Districts by Way of Vegetation Analysis, together with Significance for Engineering Geology, Vol. 16, No. 1 (1975) p. 9-16 (A, H)
11) Ryunoshin YOSHINAKA, Hiroyuki ISHII: Effect of Surface Condition and Intensity of Normal Stress on Joint Shear Strength of Granite, Vol. 16, No. 2 (1975) p. 21-32 (A)
12) Yasunori OTSUKA, Toru ONODERA: Anisotropy of Rocks and Effect of Water Absorption, Vol. 16, No. 3 (1975) p. 12-17 (A)
13) Yoshiro HAYASHDA: On the Swelling Behaviours of the Artificially Crushed Tertiary Mudstones, Vol. 16, No. 3 (1975) p. 18-26 (A)
14) Yoshinao HORI: Geology and In-Situ Stress in the Shin-takase-gawa Underground Powerhouse, Vol. 16, No. 4 (1975) p. 19-26 (B)
15) Michio OMI, Tetsuji KANAZAWA, Masayasu INOUE: Physical Properties of Weathered Andesite, Vol. 17, No. 1 (1976) p. 1-9 (A)
16) Sadazi NODA, Shogo MATSUKI, Hiroshi IIJIMA: On the Modification of Geological Structure of Damsite and Geotechnical Analysis by the Finite Element Method, Vol. 17, No. 3 (1976) p. 100-104 (H)
17) Keiji MIYAJIMA: Engineering Geology of Ohnaruto Bridge Foundation, Vol. 17, No. 4 (1976) p. 153-167 (A, H)
18) Tomio TANAKA, Masami FURUTA: On the Rock Mass Shear Strength by In-Situ Block Shear Tests, Vol. 18, No. 1 (1977) p. 1-12 (C)
19) Yoshiro HAYASHIDA: Some Investigation on the Weathering of the Nonsilicified Mudstone of Izumi Group, Vol. 18, No. 3 (1977) p. 125-130 (A)
20) Seiken OGATA: Quantitative Characterization of Distribution Parameters of Joints in Rock Mass, Vol. 19, No. 1 (1978) p. 12-20 (F)
21) Kunitake HAYASHIDA: On an Anisotropic Effect to the P-wave Velocity affected by the Sheeting Joint in the Weathered Granitic Rocks and its Analysis, Vol. 19, No. 1 (1978) p. 21-29 (F)

13. Tunnels and Underground
1) Masashi WATANABE, Shozo IMAI: Introductory Lecture on Underground Power Station (1) - (4) --- Lecture Series ---, Vol. 5, No. 2-5 (1974) (H)
2) Kazuhiko IKEDA, Hiroshi OHSHIMA, Masatsugu ISHII: Groundwater Inflow within Tunnel and Drying-up of Rivers and Water Wells, Vol. 6, No. 4 (1975) p. 41-47 (G)
3) Ryoki NAKANO: Real State of Expansive Ground, Vol. 6, No. 10 (1975) p. 15-21 (C, H)

4) Satoshi HIBINO: Excavation in Heterogeneous Rock Mass, Vol.7, No.6 (1976) p.37-43 (D)
5) Yasuo TOKI, Keiji SHIRAI, Ichiriki IIZUKA: Model Experiment Considering Interaction between Tunnel and Ground, Vol.8, No.5 (1977) p.7-15 (C, H)
6) Ikuo MURAKAMI, Hiroshi OSHIMA, Masao TSUKAMOTO: Water Inflow and Drought of Tanna Tunnel, Vol.8, No.10 (1977) p.41-47 (G)
7) Shogo MATSUO, Tetsuo YABE: Geologic Survey for Undersea Tunnels, Vol.8, No.11 (1977) p.7-14 (F)
8) Michiro KURIYAGAWA: Prospects to Underground Oil Storage Project, Vol.9, No.1-5 (1978) (H)
9) Keiji SHIRAI: Introductory Lecture on Rock Blasting (1) - (6) --- Lecture Series ---, Vol.9, No.2-8 (1978) (D, H)
10) Tetsu MITANI, Takayuki IWAI: Classification of Rock Mass for Tunnelling, Vol.9, No.3 (1978) p.7-19 (H)

14. Journal of Japanese Society of Irrigation, Drainage and Reclamation Engineering
1) Takemasa ITO, Takeshi YOSHIDA: On the Foundation Treatment of Kakobo Disaster Dam, Vol.43, No.9 (1975) p.21-26 (E)
2) Isao SUGII, Yasunori SAWADA: On the Foundation Treatment of Futaba Dam, Vol.44, No.11 (1976) p.11-20 (E)
3) Ryoki NAKANO: On the Design of Water Tunnels in Relation with the Type and Magnitude of Rock Load, Vol.42, No.3 (1974) p.147-152 (H)
4) Toshio SAWADA, Takashi UCHIDA, Kazunori HASEGAWA: The Safety Analysis of Fill Dam with Highway on its Dam-Crest, Vol.59 (1975) p.45-52 (E)
5) Takenobu FUJIKAWA, Seiich GIBO: On the Determination of Residual Strength by Stress Analysis of Failure Surface, Vol.57 (1975) p.33-38 (E)

15. The Journal of the Geological Society of Japan
1) Yukio IKEDA, Toshihiko SHIMAMOTO: Numerical Experiments on the Viscous Bending Folds, Vol.80, No.2 (1974) p.65-74 (C)
2) Kenshiro OTSUKI, Masayuki EHIRO, Toru KAWAKAMI, Nobu KITAMURA: Effects of Interstitial Water on the Mechanical Properties of Rocks, Vol.80, No.9 (1974) p.391-395 (A)
3) Toshihiko SHIMAMOTO: The Finite Element Analysis of the Deformation of a Viscous Spherical Body Embedded in a Viscous Medium, Vol.81, No.4 (1975) p.255-267 (C)
4) Kazukuni KIMIYA: Tensile Strength as a Physical Scale of Weathering in Granitic Rocks (1), Vol.81, No.6 (1975) p.349-364 (A)
5) Mitsuhiro TORIUMI: A Dynamic Aspect of Metamorphic Differentiation, Vol.81, No.8 (1975) p.505-511 (H)
6) Ikuo TOHNO: Diagenesis and Mechanical Characteristics of Sediments --- Relation Between Arrangement of Grain and Unconfined Compressive Strength of Quaternary Southern Kanto ---, Vol.81, No.9 (1975) p.547-558 (A)
7) Daigoro HAYASHI: Rising of a Granitie Mass as an Incompressible Newtonian Fluid, Vol.81, No.12 (1975) p.769-782 (C, H)

8) Hiroaki KOMURO, Kisaburo KODAMA, Yukinori FUJITA: Numerical Analysis on the Mechanism of the Collapse Basin Formation due to Local Uplift in the Green Tuff Orogenesis, Vol.83, No.5 (1977) p.277-288 (H)

16. Earth Science
    1) Keiji MIYAJIMA: A Trial of Rock Slope Stability Analysis and Some Geological Considerations in Shikoku, Vol.28, No.1 (1974) p.11-21 (C, H)
    2) Shuichiro YOKOTA: Viscosity Ratio between Bronitic Rocks and Paleozoic Sedimentary Rocks inferred from the Difference of Uplift Rate of the Basement Rock Body, Vol.30, No.6 (1976) p.336-346 (H)

17. Journal of the Geodetic Society of Japan
    1) Tsuneo YAMAUCHI: On the Elastic After-effect Associated with Earthquake, Vol.21, No.2 (1975) p.75-80 (C, H)
    2) Yoichiro FUJII: Vertical Crustal Movement and Pilatancy Associated with the Itō Earthquake Swarm in 1930, Vol.22, No.3 (1976) p.139-148 (C, H)
    3) Yukio HAGIWARA: Tidal Groundwater-Related Gravity Change in a Seaside Area, Vol.23, No.1 (1977) p.25-35 (C, H)

18. Journal of the Japanese Association of Petroleum Technologists
    1) Kazuo INAMI, Kazuo HOSHINO: Compressibility and Compaction of Clastic Sedimentary Rocks, Vol.39, No.6 (1974) p.357-365 (A)
    2) Kazuo HOSHINO, Kazuo INAMI: Comparative Study on Strength in Sedimentary Basins and it's Bearing to Petroleum Geology, Vol.39, No.6 (1974) p.366-374 (A, H)
    3) Shoichi TANAKA, Mitsuo SATO: Measurement of Rock Properties with Stamp Penetration Method and their Relationship to Rock Drilling, Vol.40, No.2 (1975) p.90-98 (A, D)
    4) Kazuo HOSHINO, Kazuo INAMI: Mechanical Properties of Rocks under High Pressure and it's Bearing to Petroleum Geology in Amakusa and Northwestern Kyushu, Vol.40, No.5 (1975) p.236-245 (A, H)
    5) Kazuo INAMI: Mechanical Properties of Carbonate Rocks, Vol.42, No.6 (1977) p.397-401 (A)

19. Geophysical Exploration
    1) Tokumi SAITO, Mamoru ABE, Shoichi KUNORI: Study on Weathering of Volcanic Rocks (1), Vol.27, No.1 (1974) p.3-15 (A, H)
    2) Tokumi SAITO, Mamoru ABE, Shoichi KUNORI: Study on Weathering of Volcanic Rocks (2), Vol.27, No.1 (1974) p.16-26 (A, H)
    3) Tokumi SAITO, Mamoru ABE, Shoichi KUNORI: Variation of Elastic Wave Velocity with Satulation in Igneous Rocks (2), Vol.27, No.3 (1974) p.103-110 (A)
    4) Yasumasa HATTORI, Takuji SUGIMOTO: A Statistical Study on the Longitudinal Wave Velocities for Various Rocks in Japan (1), Vol.28, No.1 (1975) p.3-12 (A)
    5) Yasumasa HATTORI, Takuji SUGIMOTO: A Statistical Study on the Longitudinal Wave Velocities for Various Rocks in Japan (2), Vol.28, No.2 (1975) p.43-56 (A)

6) Tokumi SAITO, Mamoru ABE, Shoichi KUNORI: Relationship between Elastic Wave Velocity and Pore System of Weathered Igneous Rocks, Vol. 28, No. 3 (1975) p. 95-105 (A, H)
7) Michito OMI, Masayasu INOUE: On the Variation of Propagation Velocity of Elastic Waves in Water Saturated Porous Rocks (2), Vol. 28, No. 5 (1975) p. 199-209 (A)
8) Tokumi SAITO, Mamoru ABE: Variation of Elastic Wave Velocity with Saturation in Crystalline Limestones (1), Vol. 29, No. 2 (1976) p. 149-158 (A)
9) Hiroshi SUETOMI, Shigetosi KURIHARA: Grid Analysis of the Velocity Distribution of the Base-Rock, Vol. 29, No. 4 (1976) p. 237-250 (F, H)
10) Yutaka OHTA, Noritoshi GOTO: Estimation of S-Wave Velocity in Terms of Characteristic Indices Soil, Vol. 29, No. 4 (1976) p. 251-261 (A, F, H)
11) Tokumi SAITO, Mamoru ABE, Hidekichi YOKOYAMA: Variation of Elastic Wave Velocity with Saturation in Crystalline Limestones (2), Vol. 30, No. 2 (1977) p. 70-80 (A)
12) Michito OMI, Michio OKA, Atsuo HIRATA, Masayasu INOUE: On the Variation of Propagation Velocity of Elastic Waves in Water Saturated Porous Rocks (3), Vol. 30, No. 6 (1977) p. 303-311 (A)